ADAPTIVE FINITE ELEMENT METHODS FOR PARABOLIC INTERFACE PROBLEMS

by

Tanushree Ray

DEPARTMENT OF MATHEMATICS
INDIAN INSTITUTE OF TECHNOLOGY GUWAHATI
GUWAHATI-781039, INDIA

January, 2021

TH-2911_136123010

TH-2911_136123010

ADAPTIVE FINITE ELEMENT METHODS FOR PARABOLIC INTERFACE PROBLEMS

A thesis submitted

in partial fulfillment of the requirements

for the degree of

DOCTOR OF PHILOSOPHY

by

Tanushree Ray

(Roll No.: 136123010)

DEPARTMENT OF MATHEMATICS

INDIAN INSTITUTE OF TECHNOLOGY GUWAHATI

GUWAHATI-781039, INDIA

January, 2021

TH-2911_136123010

TH-2911_136123010

CERTIFICATE

It is certified that the work contained in this thesis entitled **"Adaptive finite element methods for parabolic interface problems"** by **Tanushree Ray (136123010)**, a student of the Department of Mathematics, Indian Institute of Technology Guwahati, for the award of the degree of Doctor of Philosophy has been carried out under my supervision. The contents of this thesis, in full or in parts, have not been submitted to any other Institute or University for the award of any degree or diploma.

January, 2021

Prof. Rajen Kumar Sinha
Professor
Department of Mathematics
Indian Institute of Technology Guwahati
Assam, India

TH-2911_136123010

Dedicated

To

my Grandparents and Parents

TH-2911_136123010

Acknowledgements

First and foremost, I would like to express my sincere appreciation and gratitude to my thesis supervisor Prof. R. K. Sinha, who led me into this inspiring Finite Element field. His constant guidance, support, and encouragement have helped me during my long research work journey. I learn not only mathematics but also so many life lessons from him. His integrity, enthusiasm, and patience always inspire me to complete my work. It is truly an honor to have studied under him these years. Furthermore, my fathomless gratitude goes to Rupa Ma'am for her affection, which gave me a homely feeling during my IIT Guwahati stay.

I extend my thanks to the doctoral committee members Prof. D. C. Dalal, Prof. N. Srinivasan, and Dr. B. Deka for their insightful comments and suggestions on my work. I am grateful to the Indian Institute of Technology (IIT) Guwahati for providing the opportunity, facility during my Ph.D. tenure. I am most thankful to the Ministry of Human Resource Development, Government of India, for providing me financial assistance for the completion of my thesis work. I am also blessed to have some courses taught by Prof. S. N. Bora, Prof. D. C. Dalal, Prof. B. K. Sarma, and Prof. A. Saikia during my course work in the Ph.D. program.

I express my sincere thanks to the Head, Department of Mathematics, IIT Guwahati, for providing me with the necessary support and facilities for my research work. I take this opportunity to thank all the faculty members and the staff members, Department of Mathematics, for their support and assist in various ways during my long research period.

I take this opportunity to convey my gratitude to the Teacher-in-Charge (present and former), all the teachers, and colleagues of Dinhata College, West Bengal.

During my research work, I have been encouraged and helped by many friends, with them, I spent many memorable moments at IIT Guwahati. I take this opportunity to thank all of them. Additionally, I thank all my seniors, juniors, and research scholars of the Department of Mathematics, IIT Guwahati.

TH-2911_136123010

I am highly indebted to all my family members, especially my father, Mr. Harikanta Ray, mother, Mrs. Chapala Karjee Ray, and sister Satabdi Ray, for their constant love, encouragement, and inspiration throughout my life. Words can never be enough to express my most profound sense of gratitude towards them. The endless thanks go to my late grandparents, to whom this dissertation is dedicated, for their blessings. I take this opportunity to thank my fiancé Mohan who always encouraged and supported me to complete this most challenging journey.

Besides all my well-wishers who have helped me knowingly and unknowingly in the successful completion of this work, my heartfelt gratitude goes to them.

Tanushree Ray

TH-2911_136123010

Abstract

The main objective of this thesis is to study adaptive finite element methods (AFEMs) for parabolic interface problems in a bounded convex polygonal domain in $\mathbb{R}^2$. Interface problems arise in a wide variety of applications in science and engineering such as material sciences and fluid dynamics when two or more distinct materials or fluids with different conductivities or densities or diffusions are interacting across the interface. Due to the discontinuity of the coefficients along the interface, the analytic solutions are rarely available for the interface problems. Therefore, the numerical approximation is the only way to proceed with such problems. Even if the solution is smooth in each individual subdomain, the global regularity of the solution of such problem is very low. As a result, it is very challenging to achieve higher order accuracy in the finite element method (FEM). Therefore, much attention has been paid in the recent years to the study both theory and numerics of time-dependent interface problems. It is known that AFEMs are widely used numerical techniques to enhance the accuracy and efficiency of the finite element method. The key to the success of AFEMs relies on the *a posteriori* error analysis, which provides error indicators for the design of adaptive algorithms. The adaptive method reduces the computational efforts and ensures higher density nodes in a particular area of the given domain where the solution is very difficult to approximate.

This thesis investigates *a posteriori* error analysis and develop adaptive algorithms for various FEMs for solving parabolic interface problems. More precisely, AFEMs for the conforming FEM, non-conforming FEM, immersed FEM, non-conforming immersed FEM for linear parabolic interface problems have been analyzed. Lastly, an extension to the semilinear parabolic interface problem using the conforming finite element method is considered and analyzed. For all these methods, new error indicators are introduced and adaptive algorithms are presented. Our first problem focuses on the linear parabolic interface problems with nonzero flux jump across the interface using conforming finite elements. A residual-based *a posteriori* error estimate for the fully discrete approximation is considered and analyzed. Both global upper and local lower bounds for the error are derived. Among the crucial technical tools used in the analysis include the Cauchy-Schwarz inequality, the approximation properties of the Clément interpolation operator, the properties of bubble functions, and energy arguments. An adaptive space-time algorithm is presented using the derived error indicators. Numerical

TH-2911_136123010

results are displayed to study the performance of the error estimators. Our next attempt is to investigate an adaptive immersed finite element method for parabolic interface problems with nonzero flux jump. The interface is assumed to be smooth, and the finite element meshes do not lie on the interface. We derive both upper and lower bounds for the error using energy arguments. A space-time adaptive algorithm is provided and supportive numerical results are presented. Our next focus is on residual-based *a posteriori* error estimation for nonconforming finite element approximation to the parabolic interface problem. The reliability of the estimator is analyzed without using the Helmholtz decomposition. We derive both upper and lower bounds for the error. The representation of the error equation, the approximation properties of the modified Clément interpolation operator, the trace inequality, and energy arguments are key ingredients used in the analysis. Numerical results are presented to demonstrate the behavior of the derived estimators. Next, we turn our attention to the *a posteriori* error analysis and adaptive mesh refinement for the parabolic interface problem using nonconforming immersed finite element method. The residual-based *a posteriori* error estimates are derived using energy arguments. Both upper and lower bounds for the error are established. A space-time adaptive algorithm is proposed and numerical results are provided.

Finally, we extend our analysis for the linear case to treat the semi-linear parabolic interface problems. The residual-based *a posteriori* error analysis for the fully discrete backward Euler method is presented. Our strategy is to avoid solving the nonlinear system by considering a modified linearized fully discrete scheme. The properties of the Clément interpolation operator and energy arguments are used to derive an upper bound for the *a posteriori* error. The bubble function technique is used to derive *a posteriori* lower bound for the error. A space-time adaptive algorithm is presented using the derived estimators. Numerical results are provided to illustrate the behavior of the derived estimators.

TH-2911_136123010

Contents

TH-2911_136123010

TH-2911_136123010

TH-2911_136123010

TH-2911_136123010

NOMENCLATURE

AFEM	Adaptive finite element method
AIFEM	Adaptive immersed finite element method
PDE	Partial differential equation
FDM	Finite difference method
FEM	Finite element method
IFE	Immersed finite element
PIP	Parabolic interface problem
$\mathbb{N}$	The set of natural numbers
$\mathbb{R}$	The set of real numbers
$\mathbb{R}^+$	The set of positive real numbers
$\mathbb{R}^d$	The d-th dimensional Euclidean space
$\bar{A}$	The closure of a set $A \subset \mathbb{R}^2$
Ω	Bounded convex polygonal domain in $\mathbb{R}^2$
$\partial\Omega$	Lipschitz boundary of Ω
Ω_1, Ω_2	Subdomains of Ω
$\partial\Omega_1 := \Gamma$	Boundary of Ω_1, i.e., interface
u	The exact solution of the PIP
β	Diffusion coefficient
f	Forcing term
u_0	Initial function
g	Interface function
$[v]$	Jump of a quantity v across the interface Γ
$\mathbf{n}$	Unit outward normal to the interface Γ
$D^\alpha\phi$	One of the partial derivative of order $\lvert\alpha\rvert$ of $\phi : \mathbb{R}^d \to \mathbb{R}$
$C^m(\overline{\Omega})$	Space of functions with m times continuously differentiable in $\overline{\Omega}$

TH-2911_136123010

$C_0^m(\Omega)$	Space of all $C^m(\Omega)$ functions with compact support in Ω
$C_0^\infty(\Omega)$	Space of all infinitely differentiable functions with compact support in Ω
$\text{supp}(v)$	Support of a function v
$L^p(\Omega)$, $1 \leq p \leq \infty$	The standard Lebesgue space of order p over the measurable set Ω
$\|\cdot\|_{L^p(\Omega)}$	Norm on $L^p(\Omega)$
$(\cdot,\cdot)$	Standard $L^2(\Omega)$ inner product on Ω
$\langle\cdot,\cdot\rangle$	The scalar product of the space $L^2(\Gamma)$
$W^{m,p}(\Omega)$	Standard Sobolev space of order (m,p) over a measurable set Ω
$\|\cdot\|_{W^{m,p}(\Omega)}$	Norm on $W^{m,p}(\Omega)$
$H^m(\Omega), m \in \mathbb{N}$	Hilbert space $W^{m,2}(\Omega)$
$\|\cdot\|_{H^m(\Omega)}$	Norm on $H^m(\Omega)$
$H_0^1(\Omega)$	Space of functions in $H^1(\Omega)$ that vanish on the boundary of Ω
$L^p(0,T;\mathbf{B})$	The standard Bochner space with $\mathbf{B}$ is a Banach space $(1 \leq p \leq \infty)$
$\|\cdot\|_{L^p(0,T;\mathbf{B})}$	Norm on $L^p(0,T;\mathbf{B})$
α_0	Continuity constant for $a(\cdot,\cdot)$
α_1	Coercivity constant for $a(\cdot,\cdot)$
$\mathcal{T}^n$	Shape regular discretization of $\overline{\Omega}$ for the fully discrete finite element approximation
$\mathcal{T}_\Gamma^n$	Set of all interface triangles
$\mathcal{T}^n \setminus \mathcal{T}_\Gamma^n$	Set of non-interface triangles
S^n	The conforming finite element space associated with the triangulation $\mathcal{T}^n$
$\mathcal{E}^n$	Set of all interior edges of the triangles in $\mathcal{T}^n$
$\mathcal{E}_\Gamma^n$	Set of all interface edges of the triangles in $\mathcal{T}_\Gamma^n$
$\mathcal{E}^n \setminus \mathcal{E}_\Gamma^n$	Set of all interior edges of non-interface triangles in $\mathcal{T}^n \setminus \mathcal{T}_\Gamma^n$
$\mathcal{E}_i^n, (i = 1, 2)$	Set of all edges of a triangle in $\mathcal{T}_i^n$
Ω_e	The collection of two triangles sharing the common edge e in $\mathcal{E}^n$

TH-2911_136123010

K	Triangle (closed)
$\text{diam}(K)$	Longest side of K
h_K	$\text{diam}(K)$
h_e	Length of an edge e
k_n	Time-step size
Ω_T	$\Omega \times (0, T]$ with $T < \infty$
$\partial\Omega_T$	$\partial\Omega \times [0, T]$
$\mathbb{P}_1(K)$	The space of polynomials of degree at most 1 over K
$\|\|\|\cdot\|\|\|_\Omega$	The energy norm on the domain Ω
$a(\cdot, \cdot)$	Bilinear form corresponding to the elliptic operator
R^n	The interior (element) residual for the fully discrete approximation
J_e^n	The interior jump residual for the fully discrete approximation
ω_K	Patch of a triangle K in $\mathcal{T}^n$
ω_e	Patch of an edge in $\mathcal{T}^n$
$U_h(t)$	Continuous, piecewise linear approximation in time of $u(t)$
$\mathcal{P}_K(\phi)$	Mean value of a given function ϕ on a given measurable set K
$\text{meas}(K)$	The measure of K
Π^n	The Clément-type interpolation operator corresponding to the finite element space S^n
$\Omega_{\Gamma,e}$	The collection of two triangles sharing the common edge e intersecting the interface Γ
$\|\cdot\|_{k_n,\Omega}$	The weighted norm of $H^1(\Omega)$ with parameter k_n
$\text{osc}(\phi, \mathcal{T}^n)$	The oscillation of any function $\phi \in L^2(\Omega)$ over $\mathcal{T}^n$
$\eta^n_{1,\text{time}}$	Time error indicator for the conforming FEM
$\eta^n_{1,\text{space}}$	Space error indicator for the conforming FEM
$\eta^n_{1,e}$	Local space error indicator for the conforming FEM

TH-2911_136123010

$\eta^n_{2,\text{time}}$	Time error indicator for the conforming IFE method
$\eta^n_{2,\text{space}}$	Space error indicator for the conforming IFE method
$\eta^n_{2,K}$	Local space error indicator for the conforming IFE method
$\mathcal{T}^n_h$	Space-time shape regular discretization of $\overline{\Omega}$ for nonconforming FEM
$\mathcal{N}^n_h$	The set of all vertices of the triangulation $\mathcal{T}^n_h$
$\mathcal{E}^n_h$	The set of all edges of the triangulation $\mathcal{T}^n_h$
$\mathcal{N}^n_{h,i}$	The set of all interior vertices in the triangulation $\mathcal{T}^n_h$
$\mathcal{N}^n_{h,b}$	The set of all vertices on the boundary $\partial\Omega$ in $\mathcal{T}^n_h$
$\mathcal{E}^n_{h,i}$	The set of all interior edges in the triangulation $\mathcal{T}^n_h$
$\mathcal{E}^n_{h,b}$	The set of all edges on the boundary $\partial\Omega$
m_e	The mid-point of the edge e
$S^n_{h,nc}$	The nonconforming finite element space associated with $\mathcal{T}^n_h$
$H^1(\mathcal{T}^n)$	The broken Sobolev space with respect to $\mathcal{T}^n_h$
$a_h(\cdot,\cdot)$	The broken bilinear form corresponding to the bilinear form $a(\cdot,\cdot)$
$\{\phi\}_e$	The average of a function ϕ over an edge e
$J^n_{\sigma,e}$	The numerical flux jump for the nonconforming FEM
$J^n_{u,e}$	The numerical solution jump for the nonconforming FEM
Π^n_h	The modified Clément-type interpolation operator corresponding to the finite element space $S^n_{h,nc}$
φ_e	The nodal basis function of $S^n_{h,nc}$ which takes value 1 at m_e and 0 at mid-points of other edges
$\mathcal{N}^n_K$	The set of three vertices of a triangle K
$\mathcal{E}^n_K$	The set of three edges of a triangle K
$\eta^n_{R_K,K}$	The element residual indicator for the nonconforming FEM
$\eta^n_{J_\sigma,K}$	The edge flux jump indicator for the nonconforming FEM
$\eta^n_{J_u,K}$	The edge solution jump indicator for the nonconforming FEM

TH-2911_136123010

$\eta^n_{3,\text{space}}$	Space error indicator for the nonconforming FEM
$\eta^n_{3,K}$	Local space error indicator for the nonconforming FEM
$\eta^n_{3,\text{time}}$	Time error estimator for the nonconforming FEM
ω^n_z	Patch of a triangle K in $\mathcal{T}^n_h$
$\mathcal{E}^n_z$	Patch of an edge in $\mathcal{T}^n_h$
$\mathcal{N}^n_\vartheta$	The set of all interface intersecting points whose vertex patches are not quasi-monotone in $\mathcal{T}^n_h$
τ	Sub-triangles formed by joining the mid-points of the edges of a triangle K
$\mathcal{T}^n_{\frac{h}{2}}$	The refined triangulation of $\mathcal{T}^n_h$
$\mathcal{N}^n_{\frac{h}{2}}$	The set of all vertices of $\mathcal{T}^n_{\frac{h}{2}}$
$\mathcal{N}^n_{\frac{h}{2},i}$	The set of all interior vertices of $\mathcal{T}^n_{\frac{h}{2}}$
$\mathcal{N}^n_{\frac{h}{2},b}$	The set of all vertices on the boundary $\partial\Omega$
$\mathcal{E}^n_{\frac{h}{2},i}$	The set of all interior edges of $\mathcal{T}^n_{\frac{h}{2}}$
$\mathcal{E}^n_{\frac{h}{2},b}$	The set of all edges on the boundary $\partial\Omega$
$S^n_{\frac{h}{2},\mathcal{G}}$	The finite element space associated with the triangulation $\mathcal{T}^n_{\frac{h}{2}}$
$\mathcal{I}^n_{\frac{h}{2}}$	The interpolation operator on $S^n_{h,\mathcal{G},nc}$
$\omega^n_{z,\tau}$	The set of all elements $\tau \in \mathcal{T}^n_{\frac{h}{2}}$ with atleast one vertex in $\mathcal{N}^n_\vartheta$
$\bar{\eta}^n_{J_u,K}$	The modified numerical solution jump indicator of $\eta^n_{J_u,K}$
$\bar{\eta}^n_{3,K}$	The modified local space error indicator for the nonconforming FEM
$\bar{\eta}^n_{3,\text{space}}$	The modified space error estimator for the nonconforming FEM
$J^n_{\nu,e}$	Jump of the tangential derivative of the numerical solution along the edge e
$\nabla^\perp$	The formal adjoint operator of the curl operator in two dimension
I^n_h	The quasi-interpolation operator on $S^n_h(\Omega)$
$\eta^n_{4,\text{time}}$	Time error estimator for the nonconforming IFE method
$\eta^n_{4,\text{space}}$	Space error estimator for the nonconforming IFE method

TH-2911_136123010

$\eta^n_{4,K}$	Local space error indicator for the nonconforming IFE method
$\eta^n_{5,\text{time}}$	Time error indicator for the conforming FEM correspnding to the semilinear PIP
$\eta^n_{5,\text{space}}$	Space error indicator for the conforming FEM correspnding to the semilinear PIP
$\eta^n_{5,e}$	Local space error indicator for the conforming FEM correspnding to the semilinear PIP
$C_{I,j}, j \in \{1,\ldots,6\}$	Interpolation constants
C_L	Lipschitz constant

TH-2911_136123010

List of Figures

TH-2911_136123010

TH-2911_136123010

भारतीय प्रौद्योगिकी संस्थान गुवाहाटी • Indian Institute of Technology Guwahati •

TH-2911_136123010

List of Tables

TH-2911_136123010

TH-2911_136123010

1 Introduction

The adaptive finite element method (AFEM) is a fundamental and attractive strategy in modern computational science and engineering to approximate the solution of a partial differential equation (PDE). The main purpose of this thesis is to study AFEMs for solving parabolic interface problems (PIPs). More explicitly, *a posteriori* error analysis and adaptive algorithms for conforming finite element method, followed by conforming immersed finite element (IFE) method, non-conforming finite element method, non-conforming IFE method for linear PIPs and conforming finite element method for semilinear PIPs are considered and analyzed in the thesis. This chapter introduces the model problems, some necessary notations, and preliminary materials for subsequent use in this dissertation. It also entails a brief survey of the relevant literature and the motivational background for the present work. The organization of the thesis is outlined in the last section of this chapter.

1.1 The Model Equation

Interface problems are often referred as differential equations with discontinuous coefficients. The discontinuity of the coefficients occurs when the medium consists of two or more different materials. A typical example of an interface problem is the heat equation in two different materials with varying heat conductivities. In this section, we briefly discuss the model equations to be considered in this thesis.

Let Ω be a bounded convex polygon in $\mathbb{R}^2$ with Lipschitz boundary $\partial\Omega$. Further, let $\Omega_1 \subset \Omega$ be an open domain with boundary $\Gamma = \partial\Omega_1 \subset \Omega$. The interface Γ divides the domain Ω into two subdomains Ω_1 and $\Omega_2 = \Omega \backslash \Omega_1$. We consider the following linear PIPs of the form

$$\frac{\partial u}{\partial t} - \nabla \cdot (\beta(x)\nabla u) = f(x,t) \quad \text{in } \Omega_T \tag{1.1}$$

TH-2911_136123010

with the given initial and boundary conditions

$$u(x,0) = u_0(x) \quad \text{in} \quad \Omega; \qquad u = 0 \quad \text{on} \quad \partial\Omega_T \tag{1.2}$$

and jump conditions across the interface Γ

$$[u] = 0, \quad \left[\beta \frac{\partial u}{\partial \mathbf{n}}\right] = g(x,t), \tag{1.3}$$

where $\Omega_T = \Omega \times (0,T]$ and $\partial\Omega_T = \partial\Omega \times [0,T]$, $T < \infty$. Here the symbol $[v]$ denotes the jump of a quantity v across the interface Γ, i.e., $[v](x) = v_1(x) - v_2(x)$, $x \in \Gamma$ with $v_i(x) = v(x)|_{\Omega_i}$, $i = 1, 2$; $\mathbf{n}$ denotes the unit outward normal to the boundary $\partial\Omega_1$ and ∇ denotes the spatial gradient. Further, we assume that the discontinuous coefficient β is positive and piecewise constant on each subdomain, i.e.,

$$\beta(x) = \beta_i \quad \text{for} \quad x \in \Omega_i, i = 1, 2.$$

The forcing term $f(x,t)$, the initial function $u_0(x)$ and the flux jump $g(x,t)$ are real valued functions and the regularity requirement on these functions to be specified later. In this thesis, for some problems, we assume the interface Γ either to be of the polygonal type (see, Figure 1.1(a)) or class C^2 (see, Figure 1.1(b)), and the forcing term f is a nonlinear function.

Interface problems occur in many applications such as fluid dynamics, electrodynamics, material sciences, solid mechanics, bio-medical and chemical engineering and so on. The study of PIPs is motivated by the models of heat conduction in different material conductivity [71], heat-mass transfer problem [69], viscoplasticity and plasticity with hardening as well as perfect plasticity [25], transport of a dissolved species in two-phase incompressible flow problems [92], eddy current in electromagnetic field theory [7, 80, 81], water flow in porous media with a source at the interface [82], electrokinetic flows [19] and references therein. Moreover, in [92], the case $[u] = 0$ and $[\beta \frac{\partial u}{\partial \mathbf{n}}] = 0$ models the transport of a dissolved species in two-phase incompressible flow problems. The existence and uniqueness of the solutions for the elliptic and parabolic interface problems are inspected by numerous authors, see Babuška [8], Chen and Zou [32], Gilberg and Trudinger [53], Girault and Raviart [54], Hackbusch [61], Kellogg [70] and references therein. Further, we refer to Ladyženskaja [71] and Lumer and Weis [80] for the existence and uniqueness results for general interface problems.

Due to the discontinuity of the coefficient β along the interface Γ, the solution u usually has a low global regularity even if the coefficients are smooth in each subdomain. Because of the low global regularity of the solution, it is very challenging to achieve

TH-2911_136123010

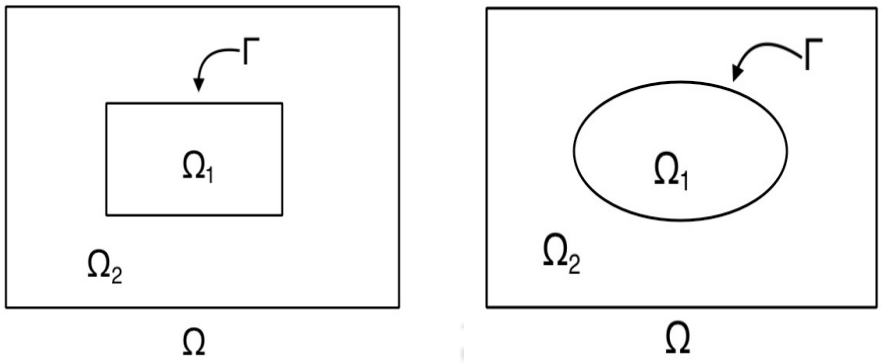

(a) (b)

Figure 1.1: Domain Ω, its subdomains Ω_1, Ω_2 and interface Γ.

higher-order accuracy by finite element methods. AFEMs are the best suited for these kinds of problems for accuracy enhancement, and their theoretical and computational studies have paid much attention to time-dependent problems. Since the AFEM is based on the *a posteriori* error estimates, therefore, it has become very interesting and challenging to study a posteriori error analysis for interface problems. Therefore, an attempt has been made in this thesis to investigate *a posteriori* error analysis and adaptive meshing procedure using various space-time discretization for the PIPs. The adaptive meshing procedure technique initiates a high mesh generation only around the interface where it is needed whereas generates coarse mesh where the solution is smooth enough.

1.2 Notations and Preliminaries

In this section, we shall introduce some standard notations and recall some useful inequalities which will be frequently used in this thesis. All functions considered here are real valued. For this purpose, we assume that Ω is a polygonal domain in $\mathbb{R}^d$ with boundary $\partial\Omega$. Let $x = (x_1, x_2, \ldots, x_d)$ be a d-tuple with $dx := dx_1 dx_2 \ldots dx_d$. Let $\alpha = (\alpha_1, \alpha_2, \ldots, \alpha_d)$, where $\alpha_i \geq 0$, $i = 1, \ldots, d$, are integers and we denote $|\alpha| := \sum_{i=1}^{d} \alpha_i$. Then, the $|\alpha|^{th}$ order partial derivatives of v defined on Ω is denoted by $D^\alpha v$ and is given by

$$D^\alpha v := \frac{\partial^{|\alpha|} v}{\partial x_1^{\alpha_1} \partial x_2^{\alpha_2} \ldots \partial x_d^{\alpha_d}}.$$

TH-2911_136123010

The support of a function v on Ω is denoted by supp v and is defined by

$$\text{supp } v := \overline{\{x \in \Omega : v(x) \neq 0\}}.$$

Thus, we say that v has a compact support in Ω if supp v is a compact set in Ω.

Now we introduce the following well-known function spaces for frequently use in our analysis. For any integer $m > 0$, let $C^m(\overline{\Omega})$ denote the space of m times continuously differentiable functions on $\overline{\Omega}$. Let $C_0^m(\Omega)$ be the space of all $C^m(\Omega)$ functions with compact support in Ω and let $C_0^\infty(\Omega)$ denote the space of all infinitely differentiable functions with compact support in Ω.

For a Lebesgue measurable set $\Omega \subset \mathbb{R}^d$ and $1 \leq p \leq \infty$, the Lebesgue space $L^p(\Omega)$ denotes the linear space of equivalence classes of measurable functions v on Ω such that $\|v\|_{L^p(\Omega)} < \infty$, where

$$\begin{aligned} \|v\|_{L^p(\Omega)} &:= \Big(\int_\Omega |v(x)|^p dx\Big)^{\frac{1}{p}}, \quad 1 \leq p < \infty, \\ \|v\|_{L^\infty(\Omega)} &:= \text{ess } \sup_{x\in\Omega} |v(x)| < \infty, \quad p = \infty. \end{aligned}$$

In particular, when $p = 2$, $L^2(\Omega)$ denotes the Hilbert space with respect to the norm induced by the inner product $(v, w) = \int_\Omega v(x)w(x)dx$.

We now introduce the notations of Sobolev spaces. Let m be a positive integer and $1 \leq p \leq \infty$. The Sobolev space $W^{m,p}(\Omega)$ is defined as a linear spaces of functions (or equivalence class of functions) in $L^p(\Omega)$ such that all distributional derivatives upto order m are also in $L^p(\Omega)$, i.e.,

$$W^{m,p}(\Omega) := \Big\{v \in L^p(\Omega) \mid D^\alpha v \in L^p(\Omega) \quad \text{for all } 0 \leq |\alpha| \leq m\Big\}$$

with norms

$$\|v\|_{W^{m,p}(\Omega)} := \left(\sum_{0\leq|\alpha|\leq m} \|D^\alpha v\|^p\right)^{\frac{1}{p}}, \quad 1 \leq p < \infty,$$

and

$$\|v\|_{W^{m,\infty}(\Omega)} := \max_{0\leq|\alpha|\leq m} \|D^\alpha v\|, \quad p = \infty.$$

For $p = 2$, the space $W^{m,2}(\Omega)$ is denoted by $H^m(\Omega)$ with the norm $\|\cdot\|_{W^{m,2}(\Omega)} = \|\cdot\|_{H^m(\Omega)}$ and the semi-norm $|\cdot|_{W^{m,2}(\Omega)} = |\cdot|_{H^m(\Omega)}$. Clearly, for $m = 0$, $L^2(\Omega) = H^0(\Omega)$ and $\|\cdot\|_{L^2(\Omega)} = \|\cdot\|_{H^0(\Omega)}$.

The Sobolev space $H^m(\Omega)$ is a Hilbert space with the norm induced by the inner product defined by

$$(v, w)_m := \sum_{0\leq|\alpha|\leq m} \int_\Omega D^\alpha v D^\alpha w \qquad \forall v, w \in H^m(\Omega).$$

TH-2911_136123010

The space $H_0^m(\Omega)$ is also defined as the closure of $C_0^\infty(\Omega)$ in the H^m-norm. In addition, let $H_0^1(\Omega)$ be a subspace of $H^1(\Omega)$ whose elements vanish on the boundary $\partial\Omega$ of Ω, where the boundary values are to be interpreted in the sense of trace[1].

In the subsequent chapters, we shall also use the following spaces. For a given Banach space $\mathbf{B}$ and $1 \le p \le \infty$, we define the standard Bochner spaces $L^p(0,T;\mathbf{B})$ as

$$L^p(0,T;\mathbf{B}) = \left\{ v : (0,T) \to \mathbf{B} \mid v(t) \in \mathbf{B} \text{ for a.e. } t \in (0,T) \text{ and } \int_0^T \|v(t)\|_{\mathbf{B}}^p dt < \infty \right\}$$

equipped with the norms

$$\begin{aligned} \|v\|_{L^p(0,T;\mathbf{B})} &:= \left(\int_0^T \|v(t)\|_{\mathbf{B}}^p dt \right)^{\frac{1}{p}}, \qquad 1 \le p < \infty, \\ \|v\|_{L^\infty(0,T;\mathbf{B})} &:= \text{ ess } \sup_{t\in(0,T)} \|v(t)\|_{\mathbf{B}} < \infty, \qquad p = \infty. \end{aligned}$$

Further, the space $H^1(0,T;\mathbf{B})$ consists of all measurable functions $v : (0,T) \to \mathbf{B}$ for which

$$\|v\|_{H^1(0,T;\mathbf{B})} := \left(\int_0^T \left\{ \|v(t)\|_{\mathbf{B}}^2 + \|\tfrac{\partial v}{\partial t}\|_{\mathbf{B}}^2 \right\} dt \right)^{\frac{1}{2}} < \infty.$$

For more detailed discussion on Sobolev spaces, one may refer to Adams [1], Adams and Fourier [2], Dautray and Lions [39] and Grisvard [56].

Some useful inequalities. We recall the following well known inequalities from Hardy *et al.* [63].

Young's inequality: If a, b are non-negative integer and $\varepsilon > 0$, then

$$ab \le \frac{a^2}{2\varepsilon} + \frac{\varepsilon b^2}{2}.$$

Hölder's inequality: Let $p > 1$ and q be such that $\frac{1}{p} + \frac{1}{q} = 1$. Then, for any numbers $a_i, b_i \in \mathbb{R}$, $i = 1, 2, \ldots, d$,

$$\sum_{i=1}^d |a_i b_i| \le \left(\sum_{i=1}^d |a_i|^p \right)^{\frac{1}{p}} \left(\sum_{i=1}^d |b_i|^q \right)^{\frac{1}{q}}.$$

In particular, for $p = q = 2$, the above inequality is known as Cauchy-Schwarz inequality in $\mathbb{R}^d$.

In terms of integral form, the Hölder's inequality is stated as follows:
Let $1 \le p, q \le \infty$ be such that $\frac{1}{p} + \frac{1}{q} = 1$. Let $v, w : \Omega \to \mathbb{R}$ be Lebesgue measurable functions. Then

$$\|v\, w\|_{L^1(\Omega)} \le \|v\|_{L^p(\Omega)} \|w\|_{L^q(\Omega)}.$$

[1]The trace is a continuous bounded linear operator $\gamma : H^1(\Omega) \to L^2(\partial\Omega)$ with $\gamma(u) = u|_\gamma$.

TH-2911_136123010

In particular, for $p = q = 2$, the above inequality is known as the Cauchy-Schwarz inequality in the integral form which will be used frequently.

Weak formulation of the problem. For the purpose of finite element approximation, we first write the weak formulation of the problem (1.1)-(1.3) which may be stated as follows : For $t \in (0, T)$, find $u(t) \in H_0^1(\Omega)$ such that

$$\begin{aligned} \left(\frac{\partial u}{\partial t}, \phi\right) + a(u, \phi) &= (f, \phi) + \langle g, \phi \rangle \quad \forall \phi \in H_0^1(\Omega), \\ u(0) &= u_0, \end{aligned} \tag{1.4}$$

where the bilinear form $a(\cdot, \cdot) : H_0^1(\Omega) \times H_0^1(\Omega) \to \mathbb{R}$ is defined by

$$a(v, w) = (\beta \nabla v, \nabla w) \quad \forall v, w \in H_0^1(\Omega)$$

and $\langle \cdot, \cdot \rangle$ denotes the scalar product for the space $L^2(\Gamma)$. Further, we assume that the bilinear form $a(\cdot, \cdot)$ is continuous and coercive on $H_0^1(\Omega)$, i.e., there exist constants $\alpha_0, \alpha_1 > 0$ such that

$$|a(v, w)| \leq \alpha_0 \|v\|_{H^1(\Omega)} \|w\|_{H^1(\Omega)} \quad \forall v, w \in H_0^1(\Omega), \tag{1.5}$$

and

$$a(v, v) \geq \alpha_1 \|v\|^2_{H^1(\Omega)} \quad \forall v \in H_0^1(\Omega). \tag{1.6}$$

1.3 Background and Motivation

This section describes a brief account of the relevant literature pertaining to the theory and numerics of the interface problems and explains the motivation of the present study. Interface problems arise in a wide variety of applications in science and engineering such as material sciences and fluid dynamics when two or more distinct materials or fluids with different conductivities or densities or diffusions are interacting across the interface. Due to the discontinuity of the coefficients along the interface, the analytic solutions are rarely available for the interface problems. Therefore, the numerical approximation is the only way to proceed with such problems. There are several numerical methods in the literature designed for interface problems such as finite difference methods (FDMs), finite element methods (FEMs), and adaptive finite element methods (AFEMs). We first give a brief survey of the literature concerning FDMs and FEMs for elliptic and parabolic interface problems.

FDMs for interface problems. There have been several considerable efforts to solve interface problems using FDMs, see [6, 15, 67, 72, 73, 76, 79] and the references

TH-2911_136123010

quoted therein. In [73], LeVeque has introduced an immersed interface method with second-order accuracy for the elliptic interface problem using a uniform rectangular grid. Li *et al.* in [76] have considered an elliptic interface problem in polar coordinates and transformed the interface problem with a non-smooth or discontinuous solution to a problem with a smooth solution. Then, a second-order finite difference scheme was introduced for the elliptic interface problem in polar coordinates. In [79], the authors have used a first-order finite difference scheme for an elliptic interface problem to control the boundary conditions across an interface. The resulting linear system is symmetric and it is the same as the one obtained for the standard Poisson equation in the absence of interface. Further, this method has been extended to achieve second-order accuracy for the elliptic interface problem in [67]. Akrivis *et al.* in [6] has developed an implicit finite difference scheme for the one-dimensional heat equation with a stationary interface to obtain second-order accuracy in space and time. The convergence of the finite difference scheme for two-dimensional PIPs has been studied by Bojović in [15]. We refer to [73, 74] and references cited therein for a detailed discussion on FDMs for interface problems.

FEMs for interface problems. FEM is a very powerful numerical technique for finding an approximate solution of partial differential equations over a given domain. The advantage of FEMs is that it can handle easily the complex geometry of the domain, non-linear material properties, and general boundary condition and it has a solid theoretical foundation in contrast to FDMs. The error analysis of FEM is classified into two types namely, *a priori error analysis* and *a posteriori error analysis*.

A priori error analysis: The *a priori* error analysis of elliptic interface problems has been first studied by Babuška in [8]. The author of [8] has converted the problem to an equivalent minimization problem and obtained a sub-optimal order error estimate in the H^1-norm using FEM. Later, it has been studied rigorously by many authors Barrett and Elliot [12], Bramble and King [16], Chen and Zou [32], Nielsen [85], Cai *et al.* [21] and references cited therein. The authors of [12] have derived the convergence of the finite element solution to the true solution at an optimal rate in both H^1 and L^2-norms on each subdomain. Subsequently, the authors of [16] have approximated the smooth domain by a polygonal domain and transferred the boundary data to the polygonal boundaries. Then, the discontinuous Galerkin FEM is applied to the perturbed problem and optimal order accuracy is obtained for rough and smooth boundary data for the non-homogeneous second-order elliptic interface problems. The authors of [32, 85] have studied the convergence of FEM with reasonable regularity assumption on the true solution. In [32], Chen and Zou have proved an almost optimal order of convergence in both the H^1 and L^2-norms using piecewise linear elements. Whereas the author of [85]

TH-2911_136123010

has shown an optimal order of convergence in the H^1-norm for elliptic interface problem in the presence of arbitrary small ellipticity. The error analysis is carried out with the assumption that the interface triangles follow exactly the actual interface Γ. In [21], Cai *et al.* have studied the discontinuous Galerkin FEM for a bounded polygonal domain in $\mathbb{R}^2$ and derived a quasi-optimal *a priori* error estimates under the assumption that the solutions are only in $H^{1+\epsilon}(\Omega)$ with $\epsilon \in (0, 1)$. Further, we also refer to [12, 72] for *a priori* error estimates of elliptic interface problems and the references quoted therein.

Till now, the literature described above is about the elliptic interface problems. We now present some relevant literature on the *a priori* error analysis of parabolic interface problem (1.1)-(1.3). The first work in this direction was due to Chen and Zou in [32]. They have studied the fully discrete backward Euler approximation and obtained nearly optimal order estimates in both the L^2 and H^1-norms with low global regularity of the solution. Some new *a priori* estimates of the solutions to the elliptic and parabolic interface problems have been derived in [68] which explicitly contain the discontinuous coefficients and the jumps of coefficients across the interface. Subsequently, Sinha and Deka in [98] have proposed a new isoparametric type of discretizations. They have analyzed both semi-discrete and fully-discrete backward Euler approximations and obtained the optimal order of convergence in the $L^2(H^1)$ and $L^2(L^2)$ norms. The same authors have extended their work to obtain optimal order of convergence in the $L^\infty(H^1)$ and $L^\infty(L^2)$-norms in [101] with piecewise linear elements.

Usually, the standard finite element method for interface problems use the body-fitted meshes to achieve an optimal or almost optimal convergence (cf. [60, 98, 101]). But it is technically difficult to construct good body-fitted meshes for problems involving geometrically complicated interfaces. To overcome this difficulty, a new finite element method known as immersed finite element (IFE) method was introduced first in [75]. The basic idea of the IFE method is to modify the basis functions which satisfy the natural jump conditions across the interface. The details regarding IFE method for elliptic and parabolic interface problems, we refer to [12, 16, 55, 58, 59, 62, 64, 72, 74, 77, 78, 99, 109, 111] and the references cited therein.

Next, we turn our attention to the semilinear PIPs in the *a priori* framework, i.e., when the forcing term f of (1.1)-(1.3) is a function of x, t and u. The study of the semilinear interface problem is motivated by modeling of mass transfer of substances through semipermeable membranes. These problems occur in many applications such as in chemical and biomedical engineering, e.g., modeling of electrokinetic flows, cellular signal transduction, and solute dynamics across arterial walls (see [19, 24]). Feng and Shen in [51] have introduced the existence, uniqueness, and regularity of the solution

TH-2911_136123010

of the semilinear parabolic interface problems. The authors of [100] have derived an optimal energy-norm error estimates for both semilinear elliptic and parabolic interface problems. We refer to [33, 102, 103] and references therein for the finite element error analysis of semilinear parabolic problems without interface whereas to Jovanović and Vulkov [69], Peterseim [88], Wei *et al.* [107] and references quoted therein for further works on *a priori* error analysis of interface problems.

In *a priori* error analysis we derive an error bound of the form

$$\|u - U_h\|_\chi \leq C(u, \text{data})h^r, \tag{1.7}$$

where u is the exact solution of the problem and U_h be its finite element approximation. In the above, $C(u, \text{data})$ is a positive constant depends on the exact solution u and given data, h denotes the maximum mesh size, r measures the order of convergence of approximation of the exact solution by its finite element solution and $\|\cdot\|_\chi$ denotes a specified norm. In general, the estimate (1.7) is not realistic because the exact solution is unknown for most of the problems. Moreover, the estimate (1.7) provides the asymptotic rates of convergence as the mesh size $h \to 0$. As the right-hand side can be estimated prior to computing U_h, the error analysis is called *a priori* error analysis. Further, we observe that *a priori* error estimate does not provide quantitative information about the size of the actual error which brings to a new error estimation technique to quantify the error known as *a posteriori* error estimation technique.

A posteriori error analysis. An *a posteriori* error analysis leads to a bound for the error in terms of the finite element solution U_h, data of the given problem and the mesh parameter h, i.e.,

$$\|u - U_h\|_\chi \leq \eta(U_h, \text{data})h^r,$$

where the estimator $\eta(U_h, \text{data})h^r$ is a computable quantity which reduces with optimal order with respect to the mesh parameter h. The main concept of *a posteriori* error analysis is to provide techniques for the automatic choice of discretization leading to efficient approximation algorithms. In recent years, this technique attracts many researchers because of its ability to control the error in the quantity with physical interest. Basically, *a posteriori* error estimation is an essential tool for the design of adaptive algorithms to control and minimize the error. Many researchers have proposed and analyzed a variety of different *a posteriori* error estimates for parabolic problems such as residual-based, recovery-based and hierarchic bases error estimators. In residual-based error estimates, various residual quantities such as element and jump residuals are used to bound the error. Whereas in recovery-based error estimates, a gradient recovery (postprocessing) operator is applied to the finite element solution and compared with the gradient of the

TH-2911_136123010

exact solution to estimate the error. Also, *a posteriori* error estimates have been derived based on the use of hierarchic bases or equilibrated residuals. In this thesis, we shall consider only residual-based *a posteriori* error estimates.

We now present a brief survey of literature concerning *a posteriori* error analysis for elliptic and parabolic PDEs. The research on *a posteriori* error analysis for FEMs for one-dimensional elliptic boundary value problems dates back to late 1970's. The pioneering work of Babušska and Rheinboldt [9] was devoted to *a posteriori* error estimation technique. In particular, we refer to Babuška and Rheinboldt [10], Eriksson and Jhonson [46], Dörfler and Rumpf [45], Verfürth [105, 106], Bernardi and Verfürth [13], Ainsworth and Oden [5], Rannachar [91], Berrone [14], Cai *et al.* [21] and references cited therein. The first significant work towards the *a posteriori* error analysis of the parabolic problem has been provided by Eriksson and Jhonson in [47, 48, 49]. The authors have used the analysis of linear dual problems of the corresponding error equations to derive the *a posteriori* error estimates. These *a posteriori* error estimates require H^2 regularity assumption on the associated elliptic operator. Without using this regularity assumption, Picasso in [90] has derived an *a posteriori* error estimate using energy method. The energy method is a more adaptable technique for the finite element error analysis because it is directly based on the variational formulation of the problem. More importantly, the energy method applies to less regular solutions than the duality method whereas the latter yields a better rate in the case of regular solutions. Verfürth in [106] has demonstrated optimal order estimate in the $L^2(H^1)$-norm and sub-optimal estimate in the $L^\infty(L^2)$-norm for parabolic problem by using the energy argument. The authors of [13] have derived the *a posteriori* error bounds in the H^1-norm for elliptic interface problems. Berrone in [14] has investigated a residual-based *a posteriori* error estimate for the PIPs. The authors of [21] have used discontinuous Galerkin method to study both the residual and recovery-based *a posteriori* error estimates for elliptic interface problems. Recently, Sen Gupta and Sinha in [96, 97] have studied *a posteriori* error analysis for the linear PIPs. The authors have considered the problem on a polygonal subdomain of the domain Ω and derived *a posteriori* upper bound in the $L^\infty(L^2)$-norm using elliptic reconstruction approach.

AFEMs for interface problems. AFEMs for the numerical solution of PDEs have been active research themes in the past decades. They are indispensable while solving a particularly challenging class of problems having low regularity solution. An *a posteriori* error estimate provides important feedback for the design of adaptive algorithms. AFEM reduces the computational efforts and ensures higher density of nodes in a certain area of the given domain where the solution is very difficult to approximate. If further

TH-2911_136123010

refinement is implemented then *a posteriori* error estimator is used as a guide to show how the refinement might accomplish most efficiently. In recent years, the AFEM has attracted many researchers to solve interface problems because it is able to control the error in the quantity of physical interest.

The main objective of this thesis to study AFEMs for the PIPs of the form (1.1)-(1.3). To start with, we now present a brief account of the literature concerning the AFEM for elliptic and parabolic problems. The pioneering work of Babuška and Rheinboldt [11] has provided an adaptive meshing procedure for the FEM based on the *a posteriori* error estimates. There are several kinds of literature on AFEMs available for elliptic and parabolic problems. We refer to Picasso [90], Verfürth [106], Chen and Feng [29] for the *a posteriori* error analysis and adaptive mesh refinement technique of parabolic problem using energy argument. In [90], Picasso has derived an optimal order residual-based *a posteriori* error estimate in the $L^2(H^1)$-norm. Chen and Feng [29] have studied an AFEM for a linear parabolic problem and derived both a global upper and local lower bounds for the error using the energy method. They have proved the convergence of the adaptive algorithm that reduces the error indicators below any given tolerance in a finite number of iteration steps. Nicaise and Soualem [84] have considered nonconforming finite element approximation of the heat equation and derived *a posteriori* error bounds for the error, where the spatial residual error indicator is based on the jumps of normal and tangential derivatives of the nonconforming approximation and a time residual indicator is based on the jump of broken gradients at each time step. Recently, Chen *et al.* in [30] have derived *a posteriori* error estimates based on the adaptive immersed finite element method for parabolic problems in time-variable domains. For AFEMs based on energy argument for nonlinear partial differential equations arising from physical and industrial processes, one may refer to the work of Morin, Nochetto, and Seibert [83] and their references.

We now turn our attention to present a state-of-art of the current research on AFEM for elliptic and parabolic interface problems. The research on *a psoteriori* error estimates and adaptive strategies for elliptic interface problems have been investigated by numerous authors [22, 23, 28, 31, 94] and references cited therein. In [94], Schmidt and Siebert have derived *a posteriori* error estimates and developed an adaptive algorithm for elliptic interface problems. The authors of [28] have derived both upper and lower bounds for linear elliptic problems with discontinuous coefficients and presented adaptive algorithms. Cai and Zhang in [22] have introduced a new recovery-based *a posteriori* error bounds for the conforming linear finite element approximation to the elliptic interface problems. Eventually, the same author in [23] have derived robust residual and recovery-

TH-2911_136123010

based *a posteriori* error estimates for interface problems with flux jump $\left[\beta\frac{\partial u}{\partial \mathbf{n}}\right] = g$. In particular, the adaptive immersed finite element method for elliptic interface problems can be found in Chen *et al.* [31]. Based on the idea of [28] an adaptive algorithm is presented in [31].

Though several adaptive strategies have been proposed in the context of both elliptic and parabolic non-interface problems and elliptic interface problems, the literature seems lack concerning AFEM for PIPs. In the context of PIPs, Berrone has investigated a residual-based *a posteriori* error estimates for PIPs in [14]. Assuming the quasi-monotonicity condition on the diffusion coefficients both upper and lower bounds are derived in the $L^2(H^1)$-norm. Further, the author has used the idea of a bubble function technique to derive the lower bound. Our first problem in this thesis is to investigate an AFEM for PIPs with nonhomogeneous flux jump. More explicitly, an attempt has been made to extend the work of [29] from linear parabolic problems to PIPs with $\left[\beta\frac{\partial u}{\partial \mathbf{n}}\right] = g(x,t)$, where $g \neq 0$ across the interface. We have used the continuous, piecewise linear functions for the approximation of the spatial variable, whereas an implicit backward Euler method is considered for the time discretization. Both upper and lower bounds for the error to the problem (1.1)-(1.3) are derived. Some new error indicators are introduced and the global upper bound (Theorem 2.3.1) is derived in terms of the estimators which contains the time error indicator $\eta^n_{1,time}$, the space error indicator $\eta^n_{1,space}$, (see, (2.15)) and data approximation errors. Further, a lower bound (Theorem 2.3.2) for the local error in terms of the space error indicator is established using the coarsening strategy of [29]. A space-time adaptive algorithm (Algorithm 2.4.1) is provided using these estimators based on the error equidistribution strategy which reduces the error indicators below any given tolerance within a finite number of steps. The refinement procedure includes both the space and time-step size modifications for the adaptive algorithm. Numerical experiments are provided to support our theoretical results.

The second problem of this thesis deals with an adaptive immersed finite element method (AIFEM) for the approximation of PIP (1.1)-(1.3). The proposed method is based on the residual-based *a posteriori* error estimates. The main advantage of the IFE method is that it can use interface independent meshes and hence structured or even cartesian meshes can be used to solve problems with nontrivial interface geometry. The relevant literature in this direction can be found in Chen, Xiao and Zhang [31], Chen, Wu and Xiao [30] and the references cited therein. In [31], Chen *et al.* have proposed an AIFEM for elliptic and Maxwell interface problems with singularity, where the interface is assumed to be of arbitrary shape. They have extended the idea of AFEM of [9]. The

TH-2911_136123010

authors of [30] have worked on AIFEM for parabolic problems in time-variable domains. To the best of the author's knowledge there seems to be no literature on AIFEM for PIPs. In the second problem, we generalize the work of [31] to the time dependent interface problems. More precisely, we investigate an AIFEM for PIPs with nonzero flux jump. We assume that the interface is independent of time and the finite element mesh whose vertices do not necessarily lie on the interface. Both a global upper bound (Theorem 3.3.1) and a local lower bound (Theorem 3.3.2) for the error to the problem (1.1)-(1.3) are established using energy method. An adaptive algorithm is provided and a numerical experiment is presented to demonstrate the behavior of the adaptive algorithm for the proposed method.

Our next objective is to study a residual-based *a posteriori* error estimation for nonconforming finite element approximation to the PIP (1.1)-(1.3). The research works on *a posteriori* error estimation using nonconforming finite element have been extensively analyzed by Anisworth [4], Cai *et al.*[20], Cai and Zhang [22], Dari *et al.*[37, 38] and Schieweck [93]. The Helmholtz decomposition is a necessary tool for obtaining the reliability bound for the nonconforming elements. Ainsworth [4] has constructed an equilibrated estimator without Clément type interpolation and observed that the error bounds depend on the diffusion coefficients. Due to the lack of the error equation, Dari *et al.* in [38] have investigated the reliable bound for the residual-based error estimate for the Poisson equation through Helmholtz decomposition of the true error. There are several interesting research work [66, 93] that approached differently despite using Helmholtz decomposition in the nonconforming finite element analysis. The authors of [20] have derived the reliability of the estimators for the elliptic interface problems by a new and direct approach without using Helmholtz decomposition and the quasi-monotone assumption. *A posteriori* error estimates for a nonconforming finite element discretization of the heat equation (for non-interface) has been investigated by Nicaise and Soualem in [84] and derived the efficiency and reliable bounds for the error using Helmholtz decomposition. We wish to emphasize the fact that the degrees of freedom for the conforming linear element is the nodal values at vertices of triangles. However, for the nonconforming linear element, the degrees of freedom are nodal values at the middle points of edges of triangles and that each middle point is shared by at most two triangles, which is a key advantage for the nonconforming linear element for AFEM. It is also possible to construct a modified Clément-type interpolation satisfying the desired properties without the quasi-monotonicity assumption.

In this context, though there are several works on *a posteriori* error estimation for nonconforming finite element approximation for both elliptic interface problems and

TH-2911_136123010

parabolic problems, but a lack of interest has been seen for the PIPs. Therefore, an effort has been made in this thesis to extend the analysis of [20] for elliptic interface problem to a linear PIP (1.1)-(1.3) using nonconforming finite elements. Our analysis does not involve the Helmholtz decomposition while analyzing the reliability of the estimator. The constant involved in the estimators are independent of the jump of the diffusion coefficient across the interface, and the quasi-monotonicity assumption on the diffusion coefficient is relaxed. The reliability bound of the estimator consists of the element residual, the edge flux jump, and the edge solution jump. We derive both a global upper bound (Theorem 4.3.1) and a local lower bound (Theorem 4.3.2) for the error. The key technical tools used in deriving the upper bound include the representation of the error equation (Lemma 4.3.2), Lemma 4.3.3 and Lemma 4.3.4. The local efficiency bound is established using the coarsening strategy of Chen and Feng [29] and it is uniformly with respect to the jump of the diffusion coefficient. Numerical results illustrating the behavior of the estimators are provided.

Our next aim is to study *a posteriori* error estimation and adaptive mesh refinement for the problem (1.1)-(1.3) using non-conforming IFE method. The basic idea of the IFE method is to locally modify basis functions on interface triangles to fit the interface jump condition (1.3). The finite element mesh and local mesh refinement do not need to fit the interface. Wu *et al.* in [108] have proposed an adaptive mesh refinement technique for elliptic interface problems using the nonconforming IFE method. Therefore, motivated by the discussion in [13] and Wu *et al.*[108], we generalize the adaptive mesh refinement technique of elliptic interface problems to the PIPs (1.1)-(1.3) using nonconforming IFE methods. New error indicators (5.16)-(5.17) are provided to control the error due to non-body fitted mesh. For the adaptive mesh refinement procedure, the residual-based *a posteriori* error estimates are derived using the energy method. We have established a residual-based global upper bound (Theorem 5.3.1) which is bounded by the element residual and the jump residual. A lower bound (Theorem 5.3.2) for the local error in terms of the space error indicator is also derived. A space-time adaptive algorithm is reported for the proposed method.

Finally, we now turn our attention to the study of AFEM for the semilinear PIPs. The forcing term $f(x,t,u)$ is assumed to satisfy the Lipschitz condition with respect to the third argument, i.e., there exists a constant $C_L > 0$ such that

$$|f(x,t,w_1) - f(x,t,w_2)| \leq C_L|w_1 - w_2| \quad \forall w_1, w_2 \in \mathbb{R}. \tag{1.8}$$

The goal of this work is to extend our AFEM for the linear PIPs to the semilinear PIPs. To discretize the problem in time we have considered the implicit backward Euler

TH-2911_136123010

approximation and the standard piecewise linear finite elements for the approximation of the space variable. We have derived *a posteriori* error estimates based on the energy argument and an adaptive algorithm for the proposed problem with nonzero flux jump is constructed. While deriving *a posteriori* error estimates using the standard finite element method, the main disadvantage is that one has to solve a nonlinear system of algebraic equations at each time steps due to the presence of $f^n(U_h^n)$ in (6.8). To avoid this difficulty, we consider a linearized modification of the fully discrete approximation (6.10) replacing the term $f^n(U_h^n)$ by $f^n(U_h^{n-1})$. An *a posteriori* global upper bound (Theorem 6.3.1) as well as local lower bound (Theorem 6.3.2) for the error are obtained. Numerical results are shown to illustrate the performance of the derived estimators. We refer to the recent work of [95] for *a posteriori* error estimate for semilinear PIPs.

1.4 Organization of the Thesis

This thesis consists of seven chapters and it is structured as follows.

Chapter 1 introduces the model problem and provides some useful notation and preliminary materials to be used in this thesis. It also contains a brief survey of the relevant literature and the motivation for the present study.

Chapter 2 considers an AFEM for the fully discrete finite element approximation for the linear PIP (1.1)-(1.3). The continuous piecewise linear elements are employed for the space discretization and the backward Euler scheme is used to approximate the time derivative. We derive a residual based *a posteriori* error estimate in the $L^2(0,T;H^1(\Omega))$-norm using the energy method. Both global upper and local lower bounds for the error for the problem (1.1)-(1.3 are established. Using the derived error indicators an adaptive algorithm is presented and a numerical example is reported to illustrate the theoretical analysis.

Chapter 3 is devoted to the AIFEM for the fully discrete finite element approximation for the linear PIP (1.1)-(1.3). The space-time immersed finite element discretization is introduced where the finite element mesh does not follow the actual interface. A global upper bound and a local lower bound for the error in terms of the error indicators are derived using energy method. Numerical experiments are performed to implement the proposed adaptive algorithm.

In Chapter 4, we study a residual based AFEM for the problem (1.1)-(1.3) using nonconforming finite elements. We first describe the nonconforming linear finite element discretization and then derive both upper and lower bounds for the error in terms of the error indicators. The proposed *a posteriori* error analysis does not involve the Helmholtz decomposition while analyzing the reliability of the estimator. A space-time adaptive

TH-2911_136123010

algorithm is prescribed using the derived estimators. Numerical results are provided to demonstrate the effectiveness of the estimators.

In Chapter 5, we investigate *a posteriori* error estimation and adaptive mesh refinement for the problem (1.1)-(1.3) using nonconforming IFEs. The nonconforming IFE discretization is introduced and new error indicators are provided to control the error due to non-body fitted mesh. The residual-based *a posteriori* error estimates are derived using energy argument. A global upper bound for the error is estimated using the energy technique and a lower bound for the error in terms of the local error indicators is derived. An adaptive algorithm for the proposed method is provided and the numerical results are presented.

Chapter 6 addresses an AFEM for a semilinear PIP with nonzero flux jump. For the fully discrete approximation, we have considered the implicit backward Euler approximation in time and the standard piecewise linear finite elements for the space variable. Our strategy is to avoid solving the nonlinear system by considering a linearized fully discrete scheme. The global upper bound for the error is shown to be bounded by the element residual and interior jump residual whereas a lower bound for the error in terms of the local error indicator is established. An adaptive algorithm is supplied for the proposed method. Numerical results are presented to illustrate the performance of the derived error indicators.

Finally, in Chapter 7, we discuss the critical evaluation of the results provided in this thesis. This chapter winds up with brief information for the scope of future investigations.

For clarity of presentation we have repeatedly mentioned the equation (1.1)-(1.3) and the relevant preliminary materials at the beginning of each chapter. The pictorial representation of this thesis is displayed as follows.

TH-2911_136123010

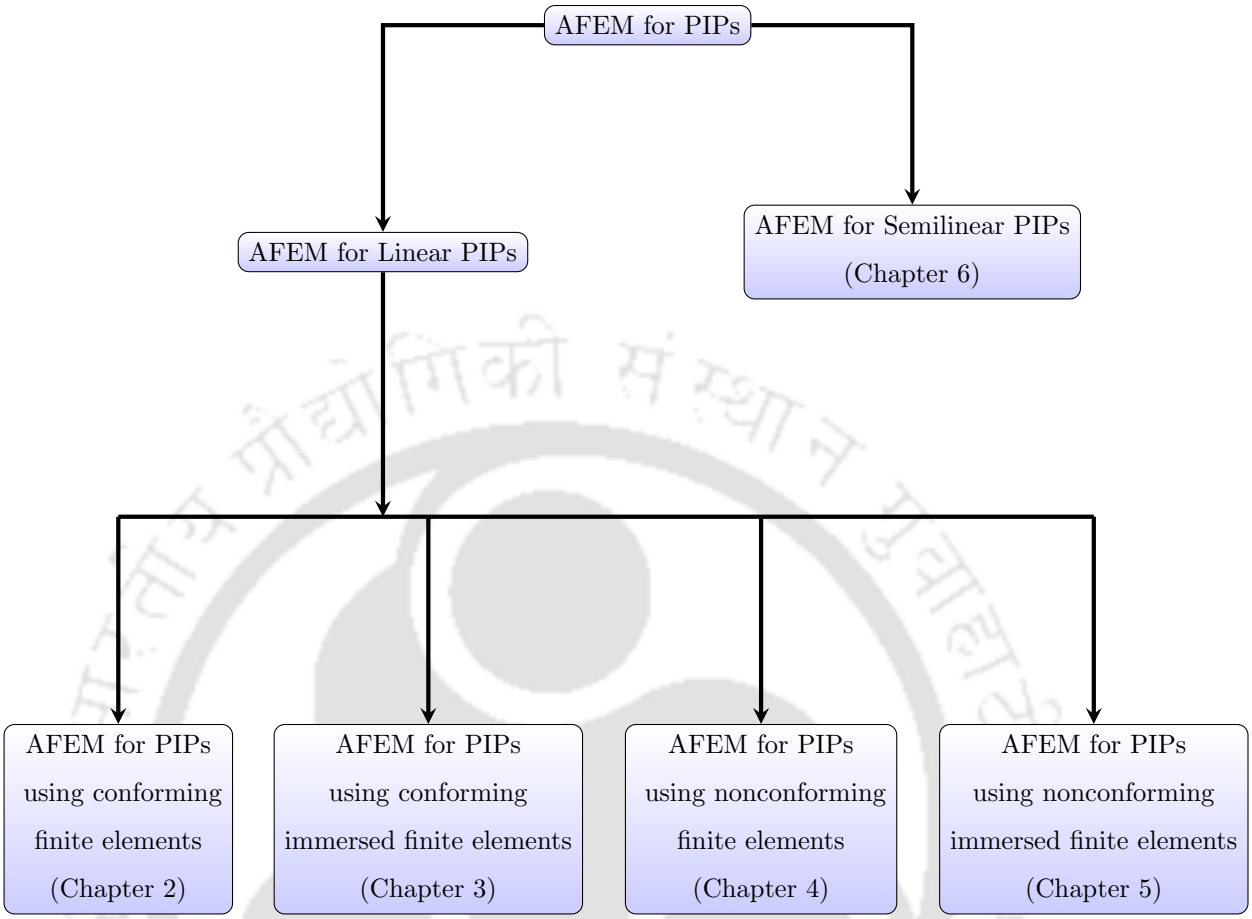

TH-2911_136123010

2

An AFEM for PIPs with Nonzero Flux Jump

In this chapter, we study an AFEM for solving the linear PIPs with nonzero flux jumps in a two-dimensional convex polygonal domain. We use continuous, piecewise linear functions for the approximation of the spatial variable whereas the backward Euler method is employed for the time discretization. An upper bound of the error is derived in terms of the error indicators. A lower bound for the local error in terms of the space error indicator is also obtained. We use the energy method to derive these *a posteriori* error estimates. An adaptive algorithm is provided using derived error indicators. A numerical experiment is presented to support the theoretical results.

2.1 Introduction

To begin with, we first recall the following linear parabolic interface problem of the form:

$$\frac{\partial u}{\partial t} - \nabla \cdot (\beta(x)\nabla u) = f \quad \text{in } \Omega_T, \tag{2.1}$$

with prescribed initial and boundary conditions

$$u(x,0) = u_0(x) \quad \text{in} \quad \Omega; \qquad u = 0 \quad \text{on } \partial\Omega_T, \tag{2.2}$$

and jump conditions across the interface Γ

$$[u] = 0, \quad \left[\beta \frac{\partial u}{\partial \mathbf{n}}\right] = g, \tag{2.3}$$

where $\Omega_T = \Omega \times (0,T]$ and $\partial\Omega_T = \partial\Omega \times [0,T]$ with $T < \infty$. Here Ω is a bounded convex polygonal domain in $\mathbb{R}^2$ with Lipschitz boundary $\partial\Omega$. Further, $\Omega_1 \subset \Omega$ is an open domain with polygonal boundary $\partial\Omega_1 := \Gamma$. The interface Γ divides Ω into two subdomains Ω_1 and $\Omega_2 = \Omega \backslash \Omega_1$. The symbol $[v]$ is the jump of a quantity v across the

TH-2911_136123010

interface Γ, i.e., $[v](x) = v_1(x) - v_2(x)$, $x \in \Gamma$ with $v_i(x) = v(x)|_{\Omega_i}$, $i = 1, 2$. The symbol $\mathbf{n}$ denotes the unit outward normal to the boundary $\partial\Omega_1$ and ∇ denotes the spatial gradient. Here u, f and g are real valued functions of x and t only. The initial data u_0 is assumed to be smooth and

$$f \in L^2(0, T; L^2(\Omega)) \text{ and } g \in L^2(0, T; L^2(\Gamma)).$$

Further, we assume that the discontinuous coefficient β is positive and piecewise constant on each subdomain, i.e.,

$$\beta(x) = \beta_1 \quad \text{for} \quad x \in \Omega_1; \quad \beta(x) = \beta_2 \quad \text{for} \quad x \in \Omega_2.$$

As a first step towards finite element approximation of (2.1)-(2.3), we recall the bilinear form $a(\cdot, \cdot) : H_0^1(\Omega) \times H_0^1(\Omega) \to \mathbb{R}$ defined by

$$a(v, w) \;=\; (\beta(x)\nabla v, \nabla w) \quad \forall v, w \in H_0^1(\Omega).$$

We assume that the bilinear form $a(\cdot, \cdot)$ is continuous and coercive on $H_0^1(\Omega)$, i.e., there exist constants $\alpha_0, \alpha_1 > 0$ such that

$$|a(v, w)| \le \alpha_0 \|v\|_{H^1(\Omega)} \|w\|_{H^1(\Omega)} \quad \forall v, w \in H_0^1(\Omega), \tag{2.4}$$

$$\text{and} \qquad a(v, v) \ge \alpha_1 \|v\|^2_{H^1(\Omega)} \quad \forall v \in H_0^1(\Omega). \tag{2.5}$$

Then the weak formulation of (2.1)-(2.3) is read as follows: Find $u : [0, T] \to H_0^1(\Omega)$ such that

$$\begin{aligned} \left(\frac{\partial u}{\partial t}, \phi\right) + a(u, \phi) &= (f, \phi) + \langle g, \phi\rangle_\Gamma \quad \forall \phi \in H_0^1(\Omega), \\ u(0) &= u_0, \end{aligned} \tag{2.6}$$

where $\langle \cdot, \cdot \rangle_\Gamma$ denotes the scalar product of the space $L^2(\Gamma)$. We shall use the notation $\langle \cdot, \cdot \rangle$ instead of $\langle \cdot, \cdot \rangle_\Gamma$ in the rest of the analysis of this chapter.

For purely parabolic problems, residual-based *a posteriori* error estimation for the backward Euler approximation and adaptive refinement procedure have been studied by Picasso [90], Verfürth [106], and Chen and Feng [29]. The authors of [90, 106] have obtained optimal order estimates in the $L^2(H^1)$-norm and suboptimal order estimates in the $L^\infty(L^2)$-norm. In [29], the authors have proved that the adaptive iteration in each single time step terminates within finitely many iterations and the space-time error is always bounded by the given tolerance. The authors of [29, 90, 106] have used the energy method to derive *a posteriori* error estimates. For parabolic problems with

TH-2911_136123010

discontinuous coefficients, Berrone [14] has derived upper and lower bounds for the error under some quasi-monotonicity assumption on the diffusion coefficients. Recently, Sen Gupta and Sinha [96, 97] have established *a posteriori* upper bound of the error for parabolic interface problems with homogeneous flux jump. One important ingredient used in [96, 97] is the elliptic reconstruction technique which is quite similar to the role played by an elliptic projection operator for recovering optimal *a priori* error estimates for finite element method to parabolic problems.

In this chapter, an attempt has been made to extend the AFEM for linear parabolic problem to the linear PIP (2.1)-(2.3) with nonzero flux jump. The discretization is done using adaptive finite elements in space combined with the implicit Euler scheme in time. The conforming finite element spaces are piecewise linear functions over a simplicial triangulation of the domain Ω. We derive both upper and lower bounds for the error. The upper bound of the error consists of an indicator for the initial error, indicators for the temporal error and the spatial error, indicators for the data approximation error, and the local error indicator. A lower bound for the local error in terms of the space error indicator is established using the coarsening strategy of Chen and Feng [29]. The space mesh and time step size adaption are carried out simultaneously to control the error in the approximation of the problem. The technical tools used in our analysis involve interpolation approximation properties, Cauchy-Schwarz inequality, Young's inequality, properties of bubble function, and energy argument.

The organization of this chapter is as follows. In Section 2.2, we describe the space-time finite element discretization for the problem (2.1)-(2.3). A global upper bound and a local lower bound for the error between the discrete solution and the solution of the continuous problem is derived in Section 2.3. In Section 2.4, we present a space-time adaptive algorithm based on the error equidistribution strategy. Numerical results are provided to validate the usefulness of the derived estimators in Section 2.5. Finally, we give some concluding remarks in the last section.

2.2 Space-Time Discretization

In this section, we introduce the space-time finite element discretization of the domain for the fully discrete approximation of (2.1)-(2.3) and the finite element space for our analysis.

Let $\{(t_{n-1}, t_n]\}_{n=1}^N$ be a partition of $[0, T]$ with N number of subintervals with time-step size $k_n = t_n - t_{n-1}$. At each time level $n = 0, 1, \ldots, N$, let $\mathcal{T}^n$ be a regular triangulation of the domain Ω. We divide the triangulation $\mathcal{T}^n$ into three set of triangles. At time t_n, let $\mathcal{T}_\Gamma^n$ denote the set of interface triangles, and let $\mathcal{T}_1^n$ and $\mathcal{T}_2^n$ be the set of

TH-2911_136123010

non-interface triangles corresponding to Ω_1 and Ω_2, respectively such that $\mathcal{T}^n \setminus \mathcal{T}_\Gamma^n = \mathcal{T}_1^n \cup \mathcal{T}_2^n$, where

$$\begin{aligned} \mathcal{T}_\Gamma^n &= \{K \in \mathcal{T}^n : K \cap \Gamma^n \neq \emptyset\}, \\ \mathcal{T}_i^n &= \{K \in \mathcal{T}^n : K \subset \Omega_i\} \quad \text{for } i = 1, 2. \end{aligned}$$

We make the following assumptions on the triangulation $\mathcal{T}^n$ (cf. [18, 34]):

(A1) If $K_1, K_2 \in \mathcal{T}^n$ and $K_1 \neq K_2$ then either $K_1 \cap K_2 = \emptyset$ or $K_1 \cap K_2$ share a common edge or a common vertex.

(A2) Each triangle K is either in $\mathcal{T}_1^n$ or in $\mathcal{T}_2^n$ or intersects the interface Γ^n at most two vertices.

(A3) The triangulations $\mathcal{T}^n$ and $\mathcal{T}^{n-1}$ are said to be compatible if one is the local refinement by admissible refinement procedure of the other and satisfy the shape regularity condition.

Set $\Omega_\Gamma = \cup_{K \in \mathcal{T}_\Gamma^n} K$ and $h_K = \text{diam}(K) \ \ \forall K \in \mathcal{T}^n$. Let $\mathcal{E}^n$ be the collection of all interior edges e of the triangle $K \in \mathcal{T}^n$ with length h_e. We now divide $\mathcal{E}^n$ into three sets $\mathcal{E}_1^n$, $\mathcal{E}_2^n$ and $\mathcal{E}_\Gamma^n$, where $\mathcal{E}_\Gamma^n$ denotes the set of all edges belonging to the interface Γ^n and $\mathcal{E}_i^n$ denotes the set of all edges of triangle $K \in \mathcal{T}_i^n$, for $i = 1, 2$. Let Ω_e be the collection of two triangles sharing the common side $e \in \mathcal{E}^n$.

For $1 \leq n \leq N$, let S^n denote the finite element space corresponding to the triangulation $\mathcal{T}^n$ and be defined by

$$S^n = \{v \in H_0^1(\Omega) : v|_K \in \mathbb{P}_1(K) \quad \forall K \in \mathcal{T}^n\},$$

where $\mathbb{P}_1(K)$ is the space of polynomials of degree less than or equal to 1 over K. The fully discrete approximation of the exact solution $u(t)$ at $t = t_n$ in S^n is denoted by U_h^n. For any continuous function φ defined in $(t_{n-1}, t_n]$, let $\varphi^n = \varphi(\cdot, t_n)$ and $\bar{\varphi}^n = \frac{1}{k_n} \int_{t_{n-1}}^{t_n} \varphi(\cdot, t) dt$.

To discretize the problem (2.6), we use the continuous piecewise linear finite element space for the approximation of spatial variable and the time discretization employs the backward Euler method. Let U_h^0 be the suitable approximation of u_0 in S^0 over the initial mesh $\mathcal{T}^0$.

The fully discrete approximation to the weak form (2.6) reads: Given $U_h^0 \in S^0$, for $1 \leq n \leq N$, find $U_h^n \in S^n$ such that

$$\left(\frac{U_h^n - U_h^{n-1}}{k_n}, v \right) + a(U_h^n, v) = (\bar{f}^n, v) + \langle \bar{g}^n, v \rangle \quad \forall v \in S^n. \tag{2.7}$$

TH-2911_136123010

2.3 A Posteriori Error Analysis

This section concerns *a posteriori* error analysis for the fully discrete approximation to the problem (2.1)-(2.3). We derive a global upper bound in terms of error indicators and a local lower bound for the error in terms of the space error indicator.

In the context of the fully discrete case, we will have two residual functions associated with (2.6), namely the interior residual and the jump residual.

The interior residual R^n is defined as

$$R^n := \bar{f}^n - k_n^{-1}(U_h^n - U_h^{n-1}) \tag{2.8}$$

and the jump residual J_e^n across $e \in \mathcal{E}^n$ is defined as

$$J_e^n := \begin{cases} [\beta(x)\nabla U_h^n]_e \cdot \mathbf{n}_e, & \text{if } e \in \mathcal{E}^n \setminus \mathcal{E}_\Gamma^n, \\ \bar{g}^n - [\beta(x)\nabla U_h^n]_e \cdot \mathbf{n}_e, & \text{if } e \in \mathcal{E}_\Gamma^n, \end{cases} \tag{2.9}$$

respectively, where $[\beta(x)\nabla U_h^n]_e \cdot \mathbf{n}_e = \big(\beta(x)\nabla U_h^n|_{K_1} - \beta(x)\nabla U_h^n|_{K_2}\big) \cdot \mathbf{n}_e$, $e = \partial K_1 \cap \partial K_2$ and $\mathbf{n}_e$ denotes the unit outer normal vector to e points from K_2 to K_1. Using integration by parts formula, we have

$$\begin{aligned} a(U_h^n, \phi) &= \sum_{K \in \mathcal{T}^n} \int_K \nabla \cdot (\beta(x)\nabla U_h^n)\phi \, dx - \sum_{e \in \mathcal{E}^n} \int_e J_e^n \phi \, ds \quad \forall \phi \in H_0^1(\Omega) \\ &= -\sum_{e \in \mathcal{E}^n} \int_e J_e^n \phi \, ds \quad \forall \phi \in H_0^1(\Omega). \end{aligned} \tag{2.10}$$

Following [35], we recall the local interpolation properties for the Clément interpolation operator in the context of a fully discrete approximation.

Lemma 2.3.1. *Let $\Pi^n : H_0^1(\Omega) \to S^n$ be the Clément interpolation operator. Then, for $\phi \in H_0^1(\Omega)$, we have*

$$\|\phi - \Pi^n\phi\|_{L^2(K)} + h_K\|\nabla(\phi - \Pi^n\phi)\|_{L^2(K)} \leq C_{I,1}h_K\|\nabla\phi\|_{L^2(\omega_K)}, \tag{2.11}$$

$$\|\phi - \Pi^n\phi\|_{L^2(e)} \leq C_{I,2}h_e^{\frac{1}{2}}\|\nabla\phi\|_{L^2(\omega_e)}, \tag{2.12}$$

where ω_K and ω_e denote the patch of triangles and edges in $\mathcal{T}^n$, respectively. Here the constants $C_{I,1}, C_{I,2}$ depend only on the minimum angle of the mesh $\mathcal{T}^n$, $n = 1, \ldots, N$.

TH-2911_136123010

2.3.1 An Upper Bound

To derive an *a posteriori* upper bound, we first introduce the following notations. For any time $t \in (t_{n-1}, t_n]$, let $U_h : [0,T] \to H_0^1(\Omega)$ be a continuous piecewise linear approximation in time of $u(t)$ defined by

$$U_h(t) = l_n(t)U_h^n + l_{n-1}(t)U_h^{n-1}, \quad 1 \le n \le N, \tag{2.13}$$

where $l_n(t)$ and $l_{n-1}(t)$ are the Lagrange hat functions given by

$$l_n(t) = \frac{t - t_{n-1}}{k_n} \quad \text{and} \quad l_{n-1}(t) = \frac{t_n - t}{k_n}, \quad \text{for } t \in (t_{n-1}, t_n].$$

Now, we prove the main result of this chapter in the following theorem.

Theorem 2.3.1. *Let u be the exact solution of (2.1)-(2.3) and let U_h be its approximation defined by (2.13). Then, there exists a constant $C > 0$ such that for $1 \le m \le N$, we have*

$$\begin{aligned} \frac{1}{2}\|u^m - U_h^m\|^2_{L^2(\Omega)} \;+\; \sum_{n=1}^{m}\int_{t_{n-1}}^{t_n} |||u - U_h^n|||^2_{\Omega} dt \;\le\; \|u_0 - U_h^0\|^2_{L^2(\Omega)} + \sum_{n=1}^{m} k_n \eta^n_{1,time} \\ + \; C\sum_{n=1}^{m} k_n \eta^n_{1,space} + 4\left(\sum_{n=1}^{m}\int_{t_{n-1}}^{t_n} \|f - \bar{f}^n\|_{L^2(\Omega)} dt\right)^2 \\ + \; 4\left(\sum_{n=1}^{m}\int_{t_{n-1}}^{t_n} \|g - \bar{g}^n\|_{L^2(\Gamma)} dt\right)^2, \end{aligned} \tag{2.14}$$

where the constant C depends on the minimum angle of meshes $\mathcal{T}^n$, $n = 1, 2, \ldots, m$, and the coefficient $\beta(x)$; and the time error indicator $\eta^n_{1,time}$ and the space error indicator $\eta^n_{1,space}$ are given by

$$\eta^n_{1,time} = \frac{1}{3}|||U_h^n - U_h^{n-1}|||^2_{\Omega}, \qquad \eta^n_{1,space} = \sum_{e \in \mathcal{E}^n} \eta^n_{1,e} \tag{2.15}$$

with the local error indicator $\eta^n_{1,e}$ is defined as

$$\eta^n_{1,e} \;=\; \frac{1}{2}\sum_{K \in \Omega_e} h_K^2 \|R^n\|^2_{L^2(K)} + h_e \|J_e^n\|^2_{L^2(e)} + h_e \|\bar{g}^n\|^2_{L^2(e)}. \tag{2.16}$$

Proof. For any $\phi \in H_0^1(\Omega)$ and $v \in S^n$, we have from (2.7)

$$\left(\frac{U_h^n - U_h^{n-1}}{k_n}, \phi\right) + a(U_h^n, \phi) = (\bar{f}^n, \phi) + \langle \bar{g}^n, v\rangle - (R^n, \phi - v) + a(U_h^n, \phi - v). \tag{2.17}$$

TH-2911_136123010

Using (2.6), (2.13) and (2.17), for all $t \in (t_{n-1}, t_n]$ and $v \in S^n$, we find that

$$\begin{aligned}\left(\frac{\partial(u-U_h)}{\partial t}, \phi\right) + a(u-U_h^n, \phi) &= (f-\bar{f}^n, \phi) + \langle g, \phi\rangle - \langle \bar{g}^n, v\rangle \\ &\quad + (R^n, \phi - v) - a(U_h^n, \phi - v).\end{aligned}$$

Substituting $\phi = u - U_h \in H_0^1(\Omega)$ and $v = \Pi^n \phi \in S^n$ in the above equation, we obtain

$$\begin{aligned}&\frac{1}{2}\frac{d}{dt}\|u-U_h\|^2_{L^2(\Omega)} + \frac{1}{2}|||u-U_h^n|||^2_\Omega + \frac{1}{2}|||u-U_h|||^2_\Omega \\ =\ & \frac{1}{2}|||U_h - U_h^n|||^2_\Omega + (f-\bar{f}^n, u-U_h) + \langle g, (u-U_h)\rangle - \langle \bar{g}^n, \Pi^n(u-U_h)\rangle \\ &+ (R^n, (u-U_h) - \Pi^n(u-U_h)) + \sum_{e\in\mathcal{E}^n}\int_e J_e^n\big((u-U_h) - \Pi^n(u-U_h)\big)ds, \qquad (2.18)\end{aligned}$$

where we have used the identity

$$a(u-U_h^n, u-U_h) = \frac{1}{2}|||u-U_h^n|||^2_\Omega + \frac{1}{2}|||u-U_h|||^2_\Omega - \frac{1}{2}|||U_h - U_h^n|||^2_\Omega.$$

Now integrating (2.18) in time t from 0 to t_*, for any $t_* \in (t_{m-1}, t_m]$ with $t_n \wedge t_* = \min(t_n, t_*)$, we have

$$\begin{aligned}&\frac{1}{2}\|(u-U_h)(t_*)\|^2_{L^2(\Omega)} + \frac{1}{2}\sum_{n=1}^m \int_{t_{n-1}}^{t_n\wedge t_*}\Big(|||u-U_h^n|||^2_\Omega + |||u-U_h|||^2_\Omega\Big)\,dt \\ &= \frac{1}{2}\|u_0 - U_h^0\|^2_{L^2(\Omega)} + \frac{1}{2}\sum_{n=1}^m\int_{t_{n-1}}^{t_n}|||U_h-U_h^n|||^2_\Omega\,dt + \sum_{n=1}^m\int_{t_{n-1}}^{t_n}(f-\bar{f}^n, u-U_h)\,dt \\ &\quad + \sum_{n=1}^m\int_{t_{n-1}}^{t_n}\big(\langle g, (u-U_h)\rangle - \langle \bar{g}^n, \Pi^n(u-U_h)\rangle\big)\,dt \\ &\quad + \sum_{n=1}^m\int_{t_{n-1}}^{t_n}\langle R^n, (u-U_h) - \Pi^n(u-U_h)\rangle\,dt \\ &\quad + \sum_{n=1}^m\int_{t_{n-1}}^{t_n}\sum_{e\in\mathcal{E}^n}\int_e J_e^n\big((u-U_h) - \Pi^n(u-U_h)\big)\,ds\,dt \\ &:= \frac{1}{2}\|u_0 - U_h^0\|^2_{L^2(\Omega)} + I_1 + I_2 + I_3 + I_4 + I_5. \qquad (2.19)\end{aligned}$$

Now we need to estimate the terms $I_i, i = 1, \ldots, 5$ separately. For I_1, using (2.13) we have

$$\begin{aligned}I_1 &= \frac{1}{2}\sum_{n=1}^m\int_{t_{n-1}}^{t_n}\Big(\frac{t_n - t}{k_n}\Big)^2|||U_h^n - U_h^{n-1}|||^2_\Omega\,dt \\ &= \frac{1}{2}\sum_{n=1}^m\frac{k_n}{3}|||U_h^n - U_h^{n-1}|||^2_\Omega = \frac{1}{2}\sum_{n=1}^m k_n\eta^n_{1,\text{time}}. \qquad (2.20)\end{aligned}$$

TH-2911_136123010

For I_2, an application of the Cauchy-Schwarz inequality yields

$$\begin{aligned} I_2 &\leq \sum_{n=1}^{m}\int_{t_{n-1}}^{t_n} \|f-\bar{f}^n\|_{L^2(\Omega)}\|u-U_h\|_{L^2(\Omega)}\,dt \\ &\leq \frac{1}{8}\max_{0\leq t\leq t_*}\|u-U_h\|^2_{L^2(\Omega)} + 2\left(\sum_{n=1}^{m}\int_{t_{n-1}}^{t_n}\|f-\bar{f}^n\|_{L^2(\Omega)}\,dt\right)^2. \end{aligned} \tag{2.21}$$

Again, we use the Cauchy-Schwarz inequality for the term I_3 to have

$$\begin{aligned} I_3 &\leq \sum_{n=1}^{m}\int_{t_{n-1}}^{t_n} |\langle g-\bar{g}^n,(u-U_h)\rangle|\,dt \\ &\quad+\sum_{n=1}^{m}\int_{t_{n-1}}^{t_n} |\langle \bar{g}^n,(u-U_h)-\Pi^n(u-U_h)\rangle|\,dt \\ &\leq \sum_{n=1}^{m}\int_{t_{n-1}}^{t_n} \|g-\bar{g}^n\|_{L^2(\Gamma)}\|u-U_h\|_{L^2(\Gamma)}dt \\ &\quad+\sum_{n=1}^{m}\int_{t_{n-1}}^{t_n}\sum_{e\in\mathcal{E}_\Gamma^n}\|\bar{g}^n\|_{L^2(e)}\|(u-U_h)-\Pi^n(u-U_h)\|_{L^2(e)}dt. \end{aligned} \tag{2.22}$$

Application of Young's inequality to the first term and the Clément approximation property (2.12) to the second term of right hand side of (2.22) yields

$$\begin{aligned} I_3 &\leq 2\left(\sum_{n=1}^{m}\int_{t_{n-1}}^{t_n}\|g-\bar{g}^n\|_{L^2(\Gamma)}dt\right)^2 + \frac{1}{8}\max_{0\leq t\leq t_*}\|u-U_h\|_{L^2(\Omega)} \\ &\quad+C_{I,2}\sum_{n=1}^{m}\int_{t_{n-1}}^{t_n}\sum_{e\in\mathcal{E}_\Gamma^n} h_e^{\frac{1}{2}}\|\bar{g}^n\|_{L^2(e)}\|\nabla(u-U_h)\|_{L^2(\omega_e)}dt. \end{aligned} \tag{2.23}$$

For I_4 and I_5, using the Cauchy-Schwarz inequality and (2.11)-(2.12) we obtain

$$\begin{aligned} I_4 &\leq \sum_{n=1}^{m}\int_{t_{n-1}}^{t_n}\sum_{K\in\mathcal{T}^n}\|R^n\|_{L^2(K)}\|(u-U_h)-\Pi^n(u-U_h)\|_{L^2(K)}dt \\ &\leq C_{I,1}\sum_{n=1}^{m}\int_{t_{n-1}}^{t_n}\sum_{K\in\mathcal{T}^n} h_K\|R^n\|_{L^2(K)}\|\nabla(u-U_h)\|_{L^2(\omega_K)}dt, \end{aligned} \tag{2.24}$$

and

$$\begin{aligned} I_5 &\leq \sum_{n=1}^{m}\int_{t_{n-1}}^{t_n}\sum_{e\in\mathcal{E}^n}\|J_e^n\|_{L^2(e)}\|(u-U_h)-\Pi^n(u-U_h)\|_{L^2(e)}dt \\ &\leq C_{I,2}\sum_{n=1}^{m}\int_{t_{n-1}}^{t_n}\sum_{e\in\mathcal{E}^n} h_e^{\frac{1}{2}}\|J_e^n\|_{L^2(e)}\|\nabla(u-U_h)\|_{L^2(\omega_e)}dt. \end{aligned} \tag{2.25}$$

TH-2911_136123010

Together all the above estimates (2.20)-(2.25) and (2.19), we have

$$\begin{aligned}
&\frac{1}{2}\|(u-U_h)(t_*)\|^2_{L^2(\Omega)} + \frac{1}{2}\sum_{n=1}^{m}\int_{t_{n-1}}^{t_n\wedge t_*}\Big(|||u-U_h^n|||^2_\Omega + |||u-U_h|||^2_\Omega\Big)dt\\
\leq\ & \frac{1}{2}\|u_0-U_h^0\|^2_{L^2(\Omega)} + \frac{1}{2}\sum_{n=1}^{m}k_n\eta^n_{1,time} + \frac{1}{4}\max_{0\leq t\leq t^*}\|u-U_h\|^2_{L^2(\Omega)}\\
+\ & 2\left(\sum_{n=1}^{m}\int_{t_{n-1}}^{t_n}\|f-\bar f^n\|_{L^2(\Omega)}dt\right)^2 + 2\left(\sum_{n=1}^{m}\int_{t_{n-1}}^{t_n}\|g-\bar g^n\|_{L^2(\Gamma)}dt\right)^2\\
+\ & \sum_{n=1}^{m}\int_{t_{n-1}}^{t_n}\left(C\sum_{e\in\mathcal{E}^n}\left(\frac{1}{2}\sum_{K\in\Omega_e}h_K^2\|R^n\|^2_{L^2(K)} + h_e\|J_e^n\|^2_{L^2(e)} + h_e\|\bar g^n\|^2_{L^2(e)}\right)\right)^{\frac{1}{2}}|||u-U_h|||_\Omega dt\\
\leq\ & \frac{1}{2}\|u_0-U_h^0\|^2_{L^2(\Omega)} + \frac{1}{2}\sum_{n=1}^{m}k_n\eta^n_{1,\text{time}} + \frac{1}{4}\max_{0\leq t\leq t^*}\|u-U_h\|^2_{L^2(\Omega)}\\
+\ & 2\left(\sum_{n=1}^{m}\int_{t_{n-1}}^{t_n}\|f-\bar f^n\|_{L^2(\Omega)}dt\right)^2 + 2\left(\sum_{n=1}^{m}\int_{t_{n-1}}^{t_n}\|g-\bar g^n\|_{L^2(\Gamma)}dt\right)^2\\
+\ & \sum_{n=1}^{m}\int_{t_{n-1}}^{t_n}C^{\frac{1}{2}}\Big(\eta^n_{1,\text{space}}\Big)^{\frac{1}{2}}|||u-U_h|||_\Omega dt
\end{aligned}$$

with $C = \max\{C^2_{I,1}, C^2_{I,2}\}$. For the last term on the right hand side of the above inequality, we apply Young's inequality to obtain

$$\begin{aligned}
&\frac{1}{2}\|(u-U_h)(t_*)\|^2_{L^2(\Omega)} + \frac{1}{2}\sum_{n=1}^{m}\int_{t_{n-1}}^{t_n\wedge t_*}\Big(|||u-U_h^n|||^2_\Omega + |||u-U_h|||^2_\Omega\Big)dt\\
\leq\ & \frac{1}{2}\|u_0-U_h^0\|^2_{L^2(\Omega)} + \frac{1}{2}\sum_{n=1}^{m}k_n\eta^n_{1,\text{time}} + \frac{1}{4}\max_{0\leq t\leq t^*}\|u-U_h\|^2_{L^2(\Omega)}\\
&+ 2\left(\sum_{n=1}^{m}\int_{t_{n-1}}^{t_n}\|f-\bar f^n\|_{L^2(\Omega)}dt\right)^2 + 2\left(\sum_{n=1}^{m}\int_{t_{n-1}}^{t_n}\|g-\bar g^n\|_{L^2(\Gamma)}dt\right)^2\\
&+ \frac{C}{2}\sum_{n=1}^{m}\int_{t_{n-1}}^{t_n}\eta^n_{1,\text{space}}dt + \frac{1}{2}\sum_{n=1}^{m}\int_{t_{n-1}}^{t_n}|||u-U_h|||^2_\Omega dt.
\end{aligned}$$

Finally, taking maximum over $t_* \in [t_{m-1}, t_m]$, using the fact $\|(u-U_h)(t_m)\|^2_{L^2(\Omega)} \leq \|(u-U_h)(\bar t)\|^2_{L^2(\Omega)}$, where $\|(u-U_h)(\bar t)\|^2_{L^2(\Omega)} = \max_{t_*\in[t_{m-1},t_m]}\|(u-U_h)(t_*)\|^2_{L^2(\Omega)}$ and the standard kickback argument, the desired inequality (2.14) follows. This completes the rest of the proof. □

Remark 2.3.1. In Theorem 2.3.1, at the n-th time-step, $\eta^n_{1,time}$ (the time discretization error), $\int_{t_{n-1}}^{t_n}\|f-\bar f^n\|_{L^2(\Omega)}dt$ and $\int_{t_{n-1}}^{t_n}\|g-\bar g^n\|_{L^2(\Gamma)}dt$ (the data approximation errors) can be reduced by reducing time-step size k_n.

TH-2911_136123010

Remark 2.3.2. *Let $P^n : L^2(\Omega) \to V_0^n$ be the L^2 projection operator. The coarsening errors involving $U_h^{n-1} - P^n U_h^{n-1}$ which appeared in Eriksson and Johnson [47], are not present in our a posteriori error estimates. They are hidden in the space error term $\|h^2 R^n\|^2_{L^2(\Omega)}$ and the time error indicator $|||U_h^n - U_h^{n-1}|||_\Omega$, where $h := h_K$ on each $K \in \mathcal{T}^n$.*

2.3.2 A Lower Bound

In this section, we derive a lower bound for the local error indicator which is crucial for the refinement procedure.

To begin this section, we consider the following auxiliary problem. Let $U_*^n \in H_0^1(\Omega)$ be the solution of

$$\left(\frac{U_*^n - U^{n-1}}{k_n}, \phi\right) + a(U_*^n, \phi) \;=\; (\bar{f}^n, \phi) + \langle \bar{g}^n, \phi\rangle \quad \forall \phi \in H_0^1(\Omega). \tag{2.26}$$

The purpose of introducing (2.26) is essentially to control the error between U_h^n and U_*^n, not between U_h^n and the exact solution $u^n = u(x, t_n)$ for fixed time-step size k_n by adapting the mesh $\mathcal{T}^n$. This facts play a crucial role in deriving lower bound for the space error indicator.

We now need the following notations. For any $K \in \mathcal{T}^n$ and $\phi \in L^2(\Omega)$, we define

$$\mathcal{P}_K \phi = \frac{1}{|K|} \int_K \phi \, dx,$$

the average of ϕ over the triangle K. For any $n = 1, 2, \ldots$, we choose the constant

$$\hat{\mathcal{C}}_n \;=\; \max_{K \in \mathcal{T}^n} \left\{ \frac{h_K^2}{k_n} : h_K = \mathrm{diam}(K) \right\}. \tag{2.27}$$

The crucial part is to handle the oscillation of the residual R^n which changes at each refinement stage. Define the oscillation of any function $\phi \in L^2(\Omega)$ over the mesh $\mathcal{T}^n$ by

$$\mathrm{osc}(\phi, \mathcal{T}^n) \;=\; \left(\sum_{K \in \mathcal{T}^n} h_K^2 \|\phi - \mathcal{P}_K \phi\|^2_{L^2(K)} \right)^{\frac{1}{2}} \tag{2.28}$$

and the weighted norm $\|\cdot\|_{k_n,\Omega}$ of $H^1(\Omega)$ with the parameter $k_n > 0$ by

$$\|\phi\|_{k_n,\Omega} \;=\; \left(\frac{1}{k_n} \|\phi\|^2_{L^2(\Omega)} + |||\phi|||^2_\Omega \right)^{\frac{1}{2}}. \tag{2.29}$$

From [104], we now recall the properties of the bubble functions which are crucial for the analysis of the lower bound.

TH-2911_136123010

The following theorem shows that a local lower bound for the error is bounded in terms of the space error indicator.

Theorem 2.3.2. *Let U_h^n and U_*^n be the solutions of (2.7) and (2.26), respectively. Then, for $n = 1, 2, \ldots, m$, we have*

$$\begin{aligned} \eta_{1,e}^n &\leq C_{1,8}\hat{\mathcal{C}}_n \sum_{K\in\Omega_e} \left\{ \frac{1}{k_n}\|U_*^n - U_h^n\|_{L^2(K)}^2 + |||U_*^n - U_h^n|||_K^2 \right\} \\ &\quad + C_{1,7} \sum_{K\in\Omega_e} h_n^2 \|R^n - \mathcal{P}_K R^n\|_{L^2(K)}^2 + C_{1,6} h_e \|\bar{g}^n\|_{L^2(e)}^2, \end{aligned} \tag{2.30}$$

where the constants $C_{1,i}$ $(i = 6, 7, 8)$ depend only on the minimum angle of meshes $\mathcal{T}^n$, $n = 1, 2, \ldots, m$, and the coefficient $\beta(x)$.

Proof. The proof follows the idea of Verfürth [104]. For any $K \in \mathcal{T}^n$, let $\psi_K = 27\lambda_1\lambda_2\lambda_3$ be the element bubble function, where λ_i $(i = 1, 2, 3)$ are the barycentric coordinate functions. Using the properties of the bubble function, we have the following inf-sup relation:

$$\inf_{v_h\in\mathbb{P}_1(K)} \sup_{\varphi_h\in\mathbb{P}_1(K)} \frac{\int_K v_h\varphi_h\psi_K}{\|\varphi_h\|_{L^2(K)}\|v_h\|_{L^2(K)}} \geq \gamma_0,$$

where the constant $\gamma_0(> 0)$ depends only on the minimum angle of triangle $K \in \mathcal{T}^n$. Let $\varphi^n \in \mathbb{P}_1(K)$ be a function such that $\|\varphi^n\|_{L^2(K)} = 1$. Since $\psi_K = 0$ on ∂K and $U_h^n \in \mathbb{P}_1(K)$, we have $\langle \bar{g}^n, \psi_K\varphi^n\rangle = 0$ on ∂K and $a(U_h^n, \psi_K\varphi^n) = 0$ over K. Taking $v_h = \mathcal{P}_K R^n$ in the inf-sup relation and using (2.26) we obtain

$$\begin{aligned} \gamma_0\|\mathcal{P}_K R^n\|_{L^2(K)} &\leq \int_K (\mathcal{P}_K R^n)\psi_K\varphi^n \, dx \\ &= \int_K (\mathcal{P}_K R^n - R^n)\psi_K\varphi^n \, dx + \int_K \left(\bar{f}^n - \frac{U_h^n - U_h^{n-1}}{k_n}\right)\psi_K\varphi^n \, dx \\ &= \int_K (\mathcal{P}_K R^n - R^n)\psi_K\varphi^n \, dx + \int_K \left(\frac{U_*^n - U_h^n}{k_n}\right)\psi_K\varphi^n \, dx \\ &\quad + a(U_*^n - U_h^n, \psi_K\varphi^n). \end{aligned} \tag{2.31}$$

An application of the Cauchy-Schwarz inequality, inverse estimate $|||\psi_K\varphi^n|||_K \leq C_{1,1}h_K^{-1}$, and (2.31) to have

$$\gamma_0\|\mathcal{P}_K R^n\|_{L^2(K)} \leq \|\mathcal{P}_K R^n - R^n\|_{L^2(K)} + \frac{1}{k_n}\|U_*^n - U_h^n\|_{L^2(K)} + C_{1,1}h_K^{-1}|||U_*^n - U_h^n|||_K.$$

By the definition of $\hat{\mathcal{C}}_n$ in (2.27), it gives

$$\gamma_0\|\mathcal{P}_K R^n\|_{L^2(K)} \leq \|\mathcal{P}_K R^n - R^n\|_{L^2(K)}$$

TH-2911_136123010

$$+ C_{1,1}\hat{\mathcal{C}}_n^{\frac{1}{2}} h_K^{-1}\left\{\frac{1}{k_n}\|U_*^n - U_h^n\|_{L^2(K)}^2 + |||U_*^n - U_h^n|||_K^2\right\}^{\frac{1}{2}}. \tag{2.32}$$

Therefore, using (2.32), we obtain

$$\begin{aligned} h_K^2\|R^n\|_{L^2(K)}^2 &\leq h_K^2\ \|\mathcal{P}_K R^n - R^n\|_{L^2(K)}^2 + h_K^2\ \|\mathcal{P}_K R^n\|_{L^2(K)}^2 \\ &\leq \left(1 + 1/\gamma_0^2\right) h_K^2\ \|R^n - \mathcal{P}_K R^n\|_{L^2(K)}^2 \\ &\quad + \frac{C_{1,1}^2}{\gamma_0^2}\,\hat{\mathcal{C}}_n\left\{\frac{1}{k_n}\|U_*^n - U_h^n\|_{L^2(K)}^2 + |||U_*^n - U_h^n|||_K^2\right\} \\ &\leq C_{1,5}\ h_K^2\ \|R^n - \mathcal{P}_K R^n\|_{L^2(K)}^2 \\ &\quad + C_{1,5}\,\hat{\mathcal{C}}_n\left\{\frac{1}{k_n}\|U_*^n - U_h^n\|_{L^2(K)}^2 + |||U_*^n - U_h^n|||_K^2\right\}, \end{aligned} \tag{2.33}$$

where the constant $C_{1,5} = \max\left\{\left(1 + 1/\gamma_0^2\right), C_{1,1}^2/\gamma_0^2\right\}$.

Let $\psi_e = 4\lambda_1\lambda_2$ be the edge bubble function for any edge $e \in \mathcal{E}^n$, where λ_1, λ_2 are the barycentric coordinate functions associated with the nodes of e. Set $\psi^n = J_e^n\psi_e \in H_0^1(\Omega)$. Since J_e^n is constant on $e \in \mathcal{E}^n$, using the property $\|\phi\|_{L^2(e)} \leq C_{1,2}\|\psi_e^{\frac{1}{2}}\phi\|_{L^2(e)}$, (2.26) and integration by parts, we conclude that

$$\begin{aligned} \|J_e^n\|_{L^2(e)}^2 &\leq C_{1,2}\int_e J_e^n\psi^n dx \\ &= -C_{1,2}\sum_{K\in\Omega_e}\int_K \beta(x)\nabla U_h^n\cdot\nabla\psi^n dx \\ &= C_{1,2}\sum_{K\in\Omega_e}\int_K \beta(x)\nabla(U_*^n - U_h^n)\nabla\psi^n dx - C_{1,2}\sum_{K\in\Omega_e}\int_K R^n\psi^n dx \\ &\quad - C_{1,2}\int_{e;\partial K\cap\Gamma^n\neq\emptyset}\bar{g}^n\psi^n dx. \end{aligned}$$

By the Cauchy-Schwarz inequality, it follows that

$$\begin{aligned} \|J_e^n\|_{L^2(e)}^2 &\leq C_{1,2}\Bigg(\sum_{K\in\Omega_e}\|\nabla(U_*^n - U_h^n)\|_{L^2(K)}\|\nabla\psi^n\|_{L^2(K)} \\ &\quad + \sum_{K\in\Omega_e}\|R^n\|_{L^2(K)}\|\psi^n\|_{L^2(K)} + \|\bar{g}^n\|_{L^2(e)}\|\psi^n\|_{L^2(e)}\Bigg). \end{aligned} \tag{2.34}$$

Now, utilizing the fact $\|\nabla\psi^n\|_{L^2(K)} \leq C_{1,3}\ h_e^{-\frac{1}{2}}\|J_e^n\|_{L^2(e)}$, $\|\psi^n\|_{L^2(K)} \leq C_{1,4}\ h_e^{\frac{1}{2}}\|J_e^n\|_{L^2(e)}$ for all $K \in \Omega_e$, and $\|\psi^n\|_{L^2(e)} \leq C_{1,4}\ \|J_e^n\|_{L^2(e)}$ for all edge e in Ω_e in (2.34), it gives

$$h_e\|J_e^n\|_{L^2(e)}^2 \leq C_{1,2}C_{1,3}\sum_{K\in\Omega_e} h_e^{\frac{1}{2}}\|\nabla(U_*^n - U_h^n)\|_{L^2(K)}\|J_e^n\|_{L^2(e)}$$

TH-2911_136123010

$$+ C_{1,2}C_{1,4}\sum_{K\in\Omega_e} h_e^{\frac{3}{2}}\|R^n\|_{L^2(K)}\|J_e^n\|_{L^2(e)} + C_{1,2}C_{1,4}h_e\|\bar{g}^n\|_{L^2(e)}\|J_e^n\|_{L^2(e)}. \tag{2.35}$$

Again, applying the Young's inequality in (2.35), we have

$$\begin{aligned} h_e\|J_e^n\|^2_{L^2(e)} &\leq C_{1,6}^{\frac{1}{2}}\Bigg(\sum_{K\in\Omega_e}|||U_*^n - U_h^n|||_K^2 + \sum_{K\in\Omega_e} h_e^2\|R^n\|^2_{L^2(K)} + h_e\|\bar{g}^n\|^2_{L^2(e)}\Bigg)^{\frac{1}{2}} \\ &\quad\times\Big(h_e\|J_e^n\|^2_{L^2(e)}\Big)^{\frac{1}{2}}, \end{aligned}$$

which leads to

$$h_e\|J_e^n\|^2_{L^2(e)} \leq C_{1,6}\Bigg(\sum_{K\in\Omega_e}|||U_*^n - U_h^n|||_K^2 + \sum_{K\in\Omega_e} h_e^2\|R^n\|^2_{L^2(K)} + h_e\|\bar{g}^n\|^2_{L^2(e)}\Bigg), \tag{2.36}$$

where the constant $C_{1,6} = \max\big\{C_{1,2}C_{1,3}, C_{1,2}C_{1,4}\big\}$.

Finally, altogether (2.16), (2.33) and (2.36) now leads to

$$\begin{aligned} \eta_{1,e}^n &= \frac{1}{2}\sum_{K\in\Omega_e} h_K^2\|R^n\|^2_{L^2(K)} + h_K\|J_e^n\|^2_{L^2(e)} \\ &\leq C_{1,7}\sum_{K\in\Omega_e} h_K^2\|R^n - \mathcal{P}_K R^n\|^2_{L^2(K)} + C_{1,6}h_e\|\bar{g}^n\|^2_{L^2(e)} \\ &\quad + C_{1,8}\hat{\mathcal{C}}_n\sum_{K\in\Omega_e}\left\{\frac{1}{k_n}\|U_*^n - U_h^n\|^2_{L^2(K)} + |||U_*^n - U_h^n|||_K^2\right\}, \end{aligned}$$

where the constants $C_{1,7} = (\frac{1}{2} + C_{1,6})C_{1,5}$ and $C_{1,8} = \max\{(\frac{1}{2} + C_{1,6})C_{1,5}, C_{1,6}\}$. This completes the rest of the proof. □

Remark 2.3.3. *Taking summation over all edges $e \in \mathcal{E}^n$, we have from (2.30)*

$$\begin{aligned} \eta_{1,space}^n &= \sum_{e\in\mathcal{E}_n}\eta_{1,e}^n \\ &\leq C_{1,7}\sum_{e\in\mathcal{E}^n}\sum_{K\in\Omega_e} h_K^2\|R^n - \mathcal{P}_K R^n\|^2_{L^2(K)} + C_{1,6}\sum_{e\in\mathcal{E}_\Gamma^n} h_e\|\bar{g}^n\|^2_{L^2(e)} \\ &\quad + C_{1,8}\hat{\mathcal{C}}_n\sum_{e\in\mathcal{E}_n}\sum_{K\in\Omega_e}\left\{\frac{1}{k_n}\|U_*^n - U_h^n\|^2_{L^2(K)} + |||U_*^n - U_h^n|||_K^2\right\} \\ &= 2C_{1,7}\ osc(R^n, \mathcal{T}^n)^2 + 2C_{1,8}\hat{\mathcal{C}}_n\|U_*^n - U_h^n\|^2_{k_n,\Omega} + C_{1,6}\sum_{e\in\mathcal{E}_\Gamma^n} h_e\|\bar{g}^n\|^2_{L^2(e)}, \end{aligned} \tag{2.37}$$

where the oscillation of residual $osc(R^n, \mathcal{T}^n)$ and the weighted norm $\|U_*^n - U_h^n\|_{k_n,\Omega}$ are defined in (2.28) and (2.29), respectively.

TH-2911_136123010

2.4 Adaptive Algorithm

In this section, we provide a space-time adaptive algorithm for the problem (2.1)-(2.3) based on the error equidistribution strategy ([29, 94]). In this strategy the time discretization error is equally distributed to each time interval $(t_{n-1}, t_n]$, $n = 1, \ldots, N$. Let ϵ_{time} be the total tolerance for the time discretization. This tolerance allowed for the part of *a posteriori* error estimate in (2.14), i.e.,

$$\begin{cases} \displaystyle\sum_{n=1}^{N} k_n \eta_{1,\text{time}}^n + 4\left(\sum_{n=1}^{N}\int_{t_{n-1}}^{t_n} \|f-\bar{f}^n\|_{L^2(\Omega)}dt\right)^2 \\ \qquad + 4\left(\displaystyle\sum_{n=1}^{N}\int_{t_{n-1}}^{t_n} \|g-\bar{g}^n\|_{L^2(\Gamma)}dt\right)^2 \leq \epsilon_{\text{time}}. \end{cases} \tag{2.38}$$

Now, (2.38) can be achieved by adjusting the time-step size k_n such that the following relations hold:

$$\begin{cases} \eta_{1,\text{time}}^n \leq \dfrac{\epsilon_{\text{time}}}{3T}, \qquad \dfrac{1}{k_n}\displaystyle\int_{t_{n-1}}^{t_n} \|f-\bar{f}^n\|_{L^2(\Omega)}dt \leq \dfrac{\sqrt{\epsilon_{\text{time}}}}{2\sqrt{3}T}, \\ \dfrac{1}{k_n}\displaystyle\int_{t_{n-1}}^{t_n} \|g-\bar{g}^n\|_{L^2(\Gamma)}dt \leq \dfrac{\sqrt{\epsilon_{\text{time}}}}{2\sqrt{3}T}. \end{cases} \tag{2.39}$$

In order to control the time-step size at each time step t_n, for any given $\delta_{\text{time}} \in (0,1)$, we have

$$\begin{cases} \eta_{1,\text{time}}^n \leq \delta_{\text{time}}\dfrac{\epsilon_{\text{time}}}{3T}, \qquad \dfrac{1}{k_n}\displaystyle\int_{t_{n-1}}^{t_n} \|f-\bar{f}^n\|_{L^2(\Omega)}dt \leq \dfrac{\sqrt{\delta_{\text{time}}\epsilon_{\text{time}}}}{2\sqrt{3}T}, \\ \dfrac{1}{k_n}\displaystyle\int_{t_{n-1}}^{t_n} \|g-\bar{g}^n\|_{L^2(\Gamma)}dt \leq \dfrac{\sqrt{\delta_{\text{time}}\epsilon_{\text{time}}}}{2\sqrt{3}T}. \end{cases} \tag{2.40}$$

Let ϵ_{space} be the tolerance related to the space discretization and it is allowed for the part of the *a posteriori* error estimate in (2.14). Then, for each time step n, the stopping criterion for mesh adaptation reads

$$\eta_{1,\text{space}}^n \leq \frac{\epsilon_{\text{space}}}{T}. \tag{2.41}$$

This stopping criteria is appropriate for mesh refinements but not for mesh coarsening.

Remark 2.4.1. *A coarsening error indicator for our problem can be used and it is based on the result stated as follows, see [29, Theorem 3.1]:*

With given $U_h^{n-1} \in S^{n-1}$ and $k_n > 0$, let $\mathcal{T}_H^n$ be the coarsening of the mesh $\mathcal{T}^n$. Let $U_H^n \in S_H^n$ and $U_h^n \in S^n$ be the solutions of the discrete problem (2.7) over meshes $\mathcal{T}_H^n$ and $\mathcal{T}^n$, respectively. Then the following error estimate

$$\|U_*^n - U_H^n\|_{k_n,\Omega}^2 \leq \|U_*^n - U_h^n\|_{k_n,\Omega}^2 + \|U_h^n - I_H^n U_h^n\|_{k_n,\Omega}^2 \tag{2.42}$$

TH-2911_136123010

holds, where $I_H^n : C(\bar{\Omega}) \to S_H^n$ *is the standard linear interpolation operator and the weighted norm* $\|\cdot\|_{k_n,\Omega}$ *is defined in (2.29).*

Define the coarsening error indicator

$$\eta_{1,coarse}^n = \frac{1}{k_n}\|I_H^n U_h^n - U_h^n\|_{L^2(\Omega)}^2 + |||I_H^n U_h^n - U_h^n|||_\Omega^2. \tag{2.43}$$

It is to be noted that $\eta_{1,coarse}^n$ *does not depend on* U_H^n*, the solution of the coarsened problem. Using this indicator, one can coarsen only once, without checking whether* U_H^n *satisfies some stopping criterion such as (2.41).*

The following algorithm incorporates this idea and presents for one single time step (cf., [29, 94]).

Algorithm 2.4.1 (Space and time adaptive algorithm)**.** Given tolerances ϵ_{time}, ϵ_{space} and ϵ_{coarse}, parameters $\gamma_1 \in (0,1)$, $\gamma_2 > 1$ and $\delta_{\text{time}} \in (0,1)$. Let U_h^{n-1} be the computed value from the previous time-step at t_{n-1} with the time step size k_{n-1} and the mesh $\mathcal{T}^{n-1}$.

Step 1: $\mathcal{T}^n := \mathcal{T}^{n-1}$, $k_n := k_{n-1}$, $t_n := t_{n-1} + k_n$
solve the fully discrete problem (2.7) for U_h^n on $\mathcal{T}^n$
compute the error estimates on $\mathcal{T}^n$

Step 2: while (2.39) is not satisfied do
{
$k_n := \gamma_1 k_n$, $t_n := t_{n-1} + k_n$
solve the fully discrete problem (2.7) for U_h^n on $\mathcal{T}^n$
compute the error estimates on $\mathcal{T}^n$
}
end while

Step 3: while ($\eta_{1,\text{space}}^n > \frac{\epsilon_{\text{space}}}{T}$) do
{
refine $\mathcal{T}^n$ to produce a modified mesh $\hat{\mathcal{T}}^n$
solve the fully discrete problem (2.7) for U_h^n on modified mesh $\hat{\mathcal{T}}^n$
compute error estimates on $\hat{\mathcal{T}}^n$
while (2.39) is not satisfied do
{
$k_n := \gamma_1 k_n$, $t_n := t_{n-1} + k_n$
solve the fully discrete problem (2.7) for U_h^n on $\hat{\mathcal{T}}^n$

TH-2911_136123010

compute error estimates on $\hat{\mathcal{T}}^n$

} end while

} end while

Step 4: if $(\eta^n_{1,\text{coarse}} \leq \frac{\epsilon_{\text{coarse}}}{T})$

coarsening $\mathcal{T}^n$ to produce a modified mesh $\check{\mathcal{T}}^n$

solve the fully discrete problem for U^n_h on $\check{\mathcal{T}}^n$

Step 5: if (2.40) is satisfied then

{ $k_n := \gamma_2 k_n$ }

end

Remark 2.4.2. *The role of the first three steps in Algorithm 2.4.1 is to reduce the time-step size and refine the mesh such that the time and space error indicators become smaller than the respective tolerances. To achieve this we first reduce the time-step size so that the time error estimator is below the prescribed tolerances while keeping the mesh unchanged. In step* 5*, if the time error indicator is much smaller than the tolerance, then the time-step size is coarsened by a factor* $\gamma_2 > 1$.

2.5 Numerical Experiment

In this section, we present the results of a numerical experiment to illustrate the performance of the estimators obtained in Theorem 2.3.1 and 2.3.2 for the problem (2.1)-(2.3) with nonzero flux jump across the interface. We consider two test problems to validate our theoretical results. For both the examples, we consider two different choices of the discontinuous coefficients β: (i) $\beta_1 = 1, \beta_2 = 10$, and (ii) $\beta_1 = 1, \beta_2 = 100$. The bisection algorithm is used to generate the refined meshes. We take the parameters $\gamma_1 = 0.5, \gamma_2 = 2$, $\delta_{time} = 0.5$ in Algorithm 2.4.1. All the constants involved in the estimators are taken as 1. The tolerances $\epsilon_{time}, \epsilon_{space}$ are chosen to be equal, say, ϵ, and $\epsilon_{coarse} = 0.5\epsilon$. We compute the energy error $Err := \left(\sum_{n=1}^{N} k_n |||u - U^n_h|||^2_\Omega\right)^{1/2}$ and the effectivity index of *a posteriori* error estimate which is defined as eff. index $= \eta_{1,1}/Err$, where the error estimator $\eta_{1,1}$ is given by

$$\begin{aligned}\eta^2_{1,1} &= \sum_{n=1}^{N} k_n(\eta^n_{1,time} + \eta^n_{1,space} + \eta^n_{1,coarse}) + 4\left(\sum_{n=1}^{m}\int_{t_{n-1}}^{t_n} \|f - \bar{f}^n\|_{L^2(\Omega)}\right)^2 \\ &\quad + 4\left(\sum_{n=1}^{m}\int_{t_{n-1}}^{t_n} \|g - \bar{g}^n\|_{L^2(\Gamma)}\right)^2.\end{aligned}$$

All computations are carried out using the software FreeFEM++ (cf. [65]).

TH-2911_136123010

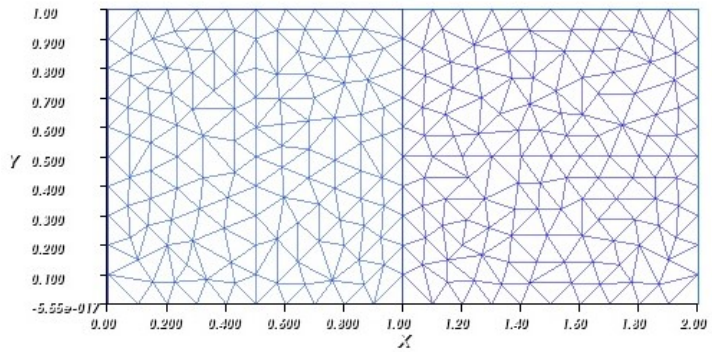

Figure 2.1: The uniform mesh of the numerical domain Ω with mesh size $h = 0.1$.

Example 2.1. In the first example, we take the computational domain $\Omega = (0, 2) \times (0, 1)$ and the final time $T = 0.1$. The interface Γ occurs at $x = 1$ which divides Ω into two subdomains such that $\Omega_1 = (0, 1) \times (0, 1)$ and $\Omega_2 = (1, 2) \times (0, 1)$. We select the functions f and g such that the exact solution of (2.1)-(2.3) is chosen as

$$u(x, y, t) = \begin{cases} e^{\sin t} \sin(\pi x) \sin(\pi y) & \text{in } \Omega_{1,T}, \\ -e^{\sin t} \sin(2\pi x) \sin(\pi y) & \text{in } \Omega_{2,T}, \end{cases}$$

where $\Omega_{1,T} = \Omega_1 \times [0, 0.1]$, $\Omega_{2,T} = \Omega_2 \times [0, 0.1]$.

Table 2.1: The degrees of freedom (DOF), the error estimator $\eta_{1,1}$, the energy error (Err) and the effectivity index (eff. index) for each step of adaptive mesh generation at the final time $T = 0.1$ with tolerance $\epsilon = 0.019$.

β	DOF	$\eta_{1,1}$	Err
$\beta_1 = 1$	988	0.219011	0.069592
$\beta_2 = 10$	2064	0.112026	0.040766
	4110	0.054817	0.023802
$\beta_1 = 1$	982	0.711163	0.069816
$\beta_2 = 100$	2038	0.362030	0.040764
	4090	0.176404	0.023882

TH-2911_136123010

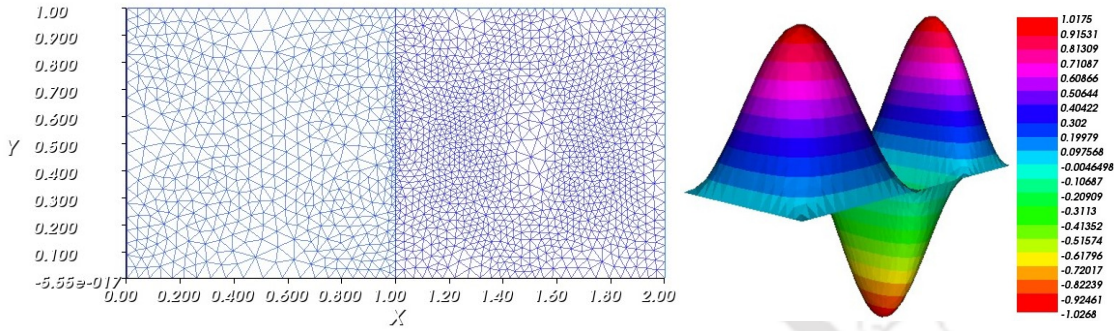

Figure 2.2: An adaptive mesh and the corresponding discrete solution at step 1.

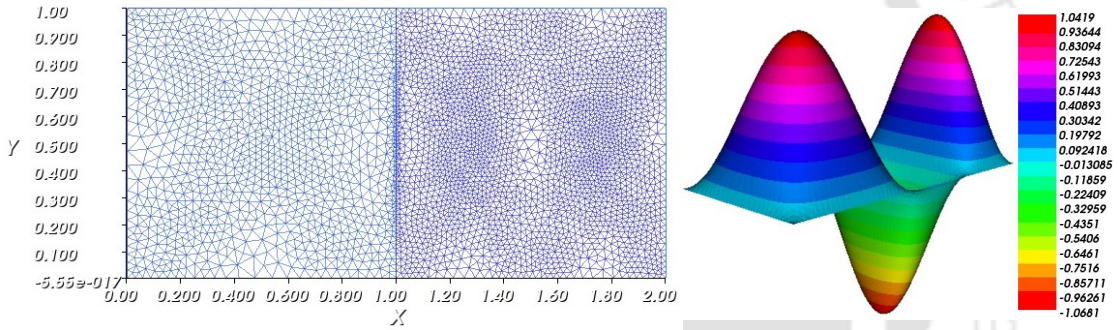

Figure 2.3: An adaptive mesh and the corresponding discrete solution at step 2.

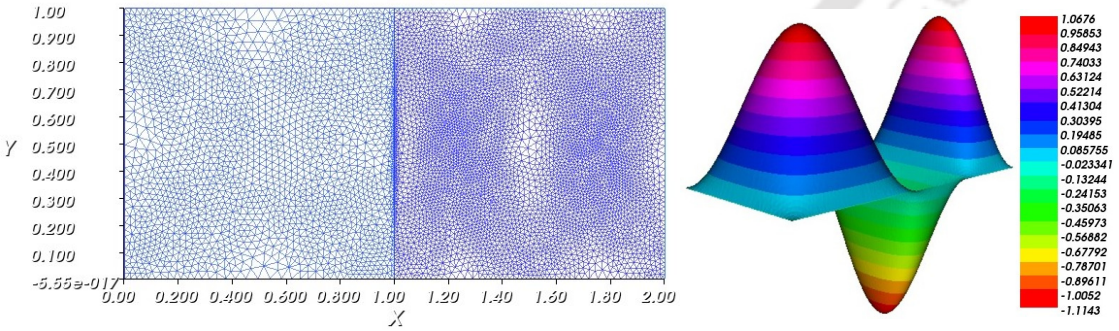

Figure 2.4: An adaptive mesh and the corresponding discrete solution at step 3.

TH-2911_136123010

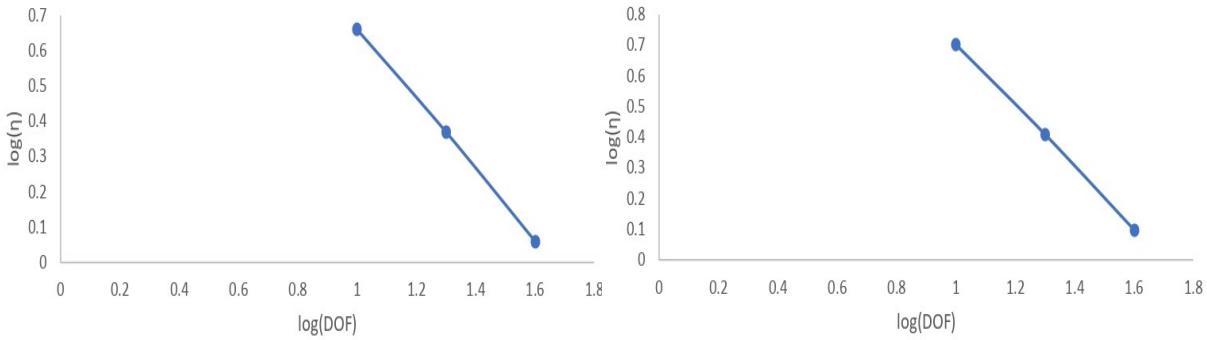

(a) (b)

Figure 2.5: Optimality of the estimator for the cases: (a) $\beta_1 = 1$, $\beta_2 = 10$ and (b) $\beta_1 = 1$, $\beta_2 = 100$. The optimal decay is observed by the line of slope -0.979 (left) and the line of slope -0.991 (right).

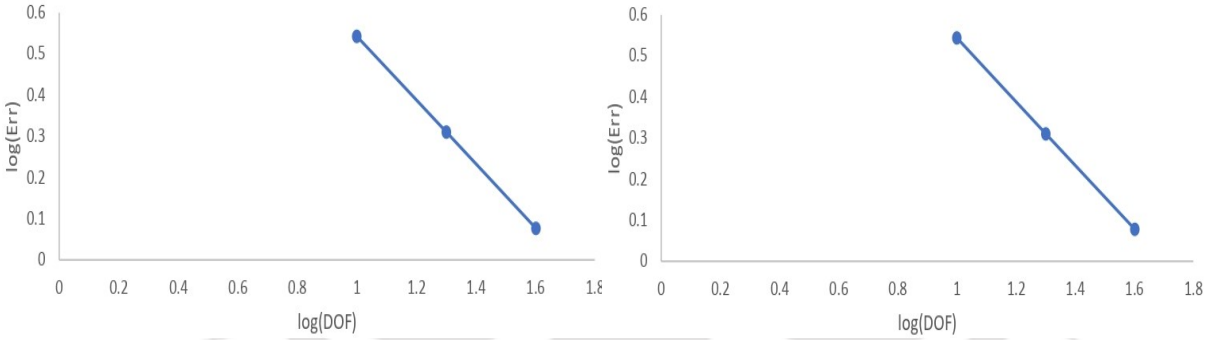

(a) (b)

Figure 2.6: Energy error versus number of degrees of freedom: (a) $\beta_1 = 1$, $\beta_2 = 10$ and (b) $\beta_1 = 1$, $\beta_2 = 100$. The quasi-optimal decay is observed by the line of slope -0.756 (left) and the line of slope -0.766 (right).

For Example 2.1, Figure 2.1 shows the uniform mesh for the computational domain Ω, where the number of triangle is 492 and the degrees of freedom is 277. For two different choices of the values of β, Table 2.1 reports the degrees of freedom (DOF), the error estimator ($\eta_{1,1}$), the energy error (Err) and the effectivity index (eff. index) for each step of adaptive mesh generation at the final time $T = 0.1$ with fixed tolerance $\epsilon = 0.019$. The adaptive mesh and the corresponding surface plot of the numerical solution (for the case $\beta_1 = 1, \beta_2 = 10$) are depicted in Figures 2.2-2.4. The plots

TH-2911_136123010

Table 2.2: The degrees of freedom (DOF), the error estimator $\eta_{1,1}$, the energy error (Err) and the effectivity index (eff. index) for different tolerances ϵ at the final time $T = 0.1$.

β	ϵ	DOF	$\eta_{1,1}$	Err	eff. index
	0.038	2001	0.126128	0.042467	2.9700
$\beta_1 = 1$	0.019	4065	0.054817	0.023802	2.3030
$\beta_2 = 10$	0.0095	8436	0.028416	0.012392	2.2931
$\beta_1 = 1$	0.038	2015	0.337125	0.042992	7.8415
$\beta_2 = 100$	0.019	4050	0.176404	0.023882	7.3865
	0.0095	8489	0.097261	0.012863	7.5613

comparing the degrees of freedom with the total error estimator for both the cases are shown in Figure 2.5. The optimal decay of the estimator is observed by the line of slope -0.979 for the choice $\beta_1 = 1, \beta_2 = 10$ (see Figure 2.5 (a)) and the line of slope -0.991 for the choice $\beta_1 = 1, \beta_2 = 100$ (see Figure 2.5 (b)). Further, in Figure 2.6, we provide plots for the energy error versus the number of degrees of freedom. For different tolerances ϵ, the degrees of freedom (DOF), the error estimator ($\eta_{1,1}$), the energy error (Err) and the effectivity index (eff. index) at the final time $T = 0.1$ are presented in Table 2.2. Table 2.2 reveals that, for a fixed time but different tolerances, both the values of the estimator and the error are reducing, and the effectivity index (eff. index) is almost constant. Figures 2.2-2.4 show that the mesh adapts very well in the neighborhood of interface Γ and higher density of the node points are distributed along the interface Γ.

Example 2.2. We consider the computational domain $\Omega = (0,1) \times (0,1) \setminus (0.5,1) \times (0.5,1)$ and the final time $T = 0.1$. The interface Γ occurs at $y = 0.5$ which divides Ω into two subdomains such that $\Omega_1 = (0, 0.5) \times (0.5, 1)$ and $\Omega_2 = (0,1) \times (0, 0.5)$. We select the functions f and g such that the exact solution of (2.1)-(2.3) is chosen as

$$u(x,y,t) = \begin{cases} -e^{-t}\sin(2\pi x)\sin(2\pi y) & \text{in } \Omega_{1,T}, \\ e^{-t}\sin(\pi x)\sin(2\pi y) & \text{in } \Omega_{2,T}, \end{cases}$$

where $\Omega_{1,T} = \Omega_1 \times [0, 0.1]$, $\Omega_{2,T} = \Omega_2 \times [0, 0.1]$.

TH-2911_136123010

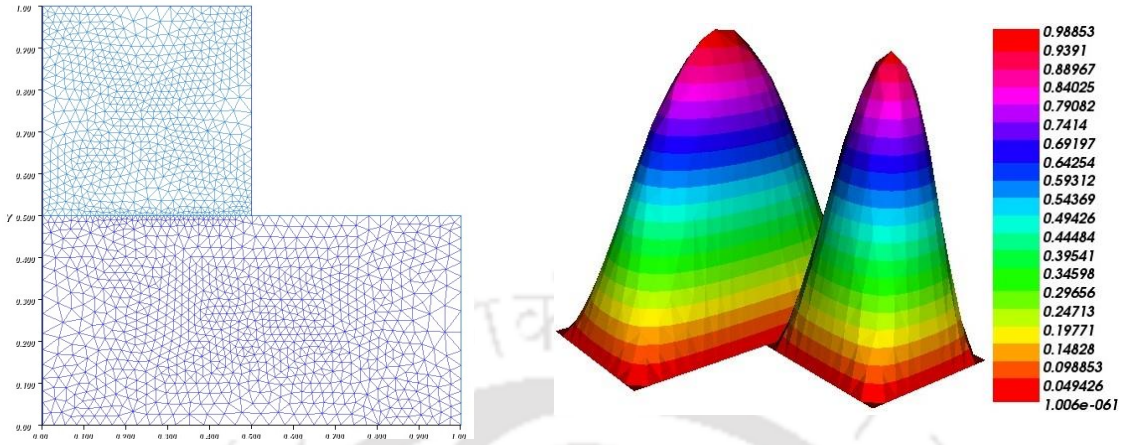

Figure 2.7: An adaptive mesh and the corresponding discrete solution at step 1.

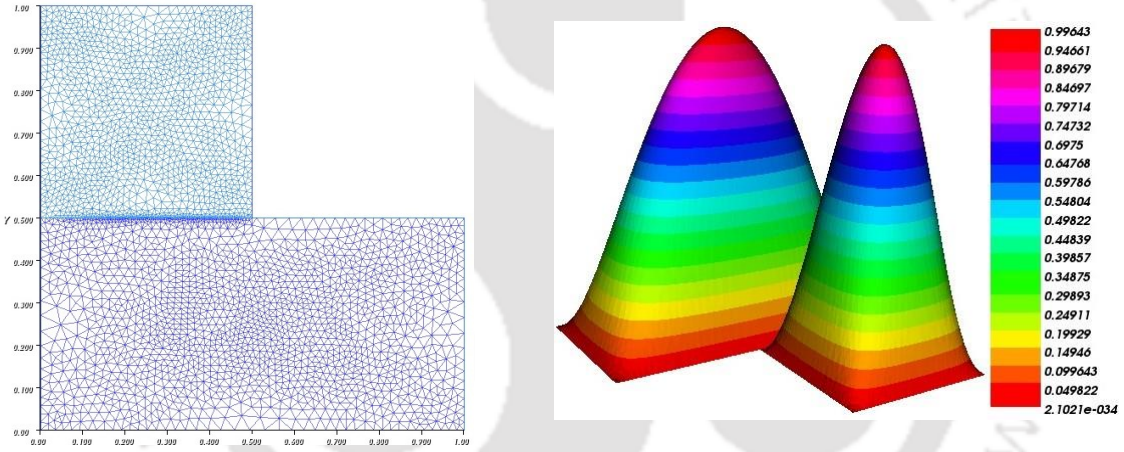

Figure 2.8: An adaptive mesh and the corresponding discrete solution at step 2.

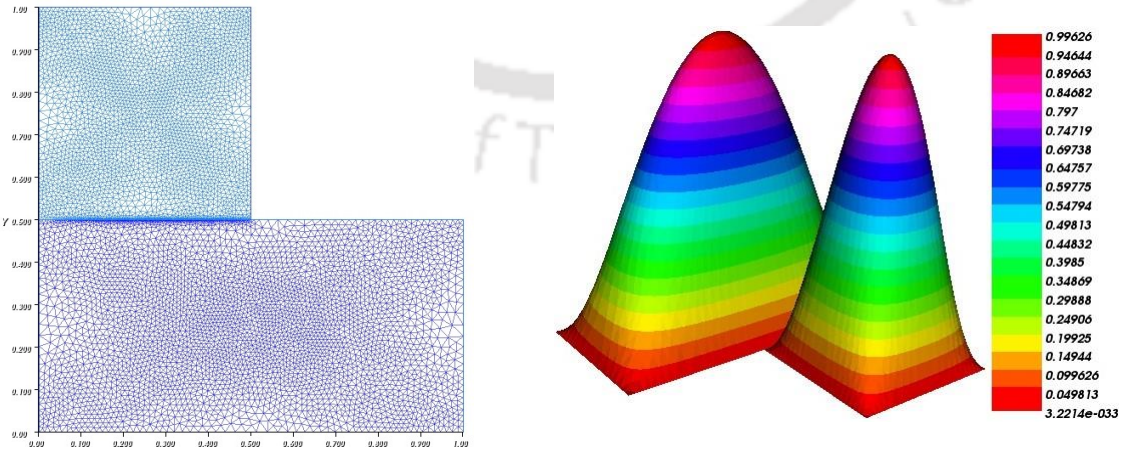

Figure 2.9: An adaptive mesh and the corresponding discrete solution at step 3.

TH-2911_136123010

Table 2.3: The degrees of freedom (DOF), the error estimator $\eta_{1,1}$, the energy error (Err) and the effectivity index (eff. index) for each step of adaptive mesh generation at the final time $T = 0.1$ with tolerance $\epsilon = 0.015$.

β	DOF	$\eta_{1,1}$	Err
$\beta_1 = 1$	836	0.377396	0.376961
$\beta_2 = 10$	1580	0.198781	0.189873
	3613	0.104103	0.095794
$\beta_1 = 1$	842	0.711163	0.069816
$\beta_2 = 100$	1620	0.362030	0.040764
	3712	0.176404	0.023882

Table 2.4: The degrees of freedom (DOF), the error estimator $\eta_{1,1}$, the energy error (Err) and the effectivity index (eff. index) for different tolerances ϵ at the final time $T = 0.1$.

β	ϵ	DOF	$\eta_{1,1}$	Err	eff. index
	0.03	1989	0.261128	0.242467	1.0769
$\beta_1 = 1$	0.015	3613	0.104103	0.095794	1.0867
$\beta_2 = 10$	0.0075	8344	0.051603	0.048346	1.0673
$\beta_1 = 1$	0.03	2012	0.337125	0.042992	2.8415
$\beta_2 = 100$	0.015	3712	0.176404	0.023882	2.3865
	0.0075	8462	0.097261	0.012863	2.5613

For Example 2.2, for two different choices of the values of β, Table 2.3 reports the degrees of freedom (DOF), the error estimator ($\eta_{1,1}$), the energy error (Err) and the effectivity index (eff. index) for each step of adaptive mesh generation at the final time $T = 0.1$ with fixed tolerance $\epsilon = 0.015$. The adaptive mesh and the corresponding surface plot of the numerical solution (for the case $\beta_1 = 1, \beta_2 = 10$) are depicted in Figures 2.7-2.9. The plots comparing the degrees of freedom with the total error estimator for

TH-2911_136123010

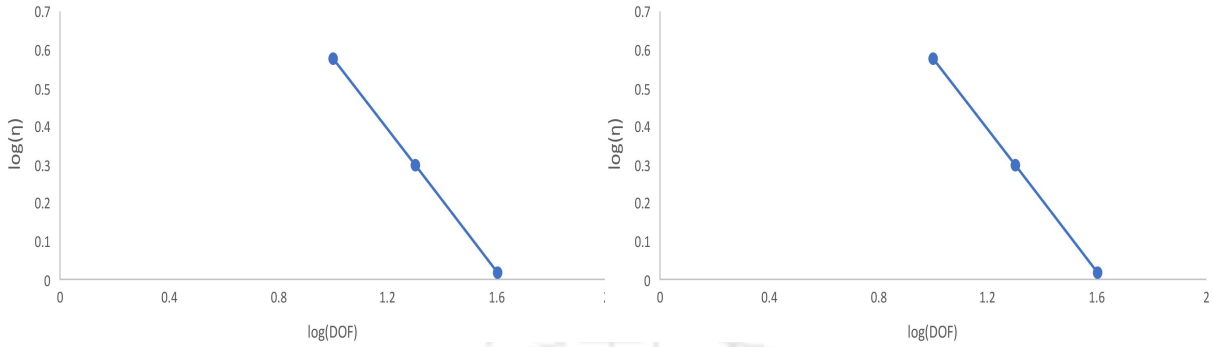

(a) (b)

Figure 2.10: Optimality of the estimator for the cases: (a) $\beta_1 = 1$, $\beta_2 = 10$ and (b) $\beta_1 = 1$, $\beta_2 = 100$. The optimal decay is observed by the line of slope -0.929 (left) and the line of slope -0.931 (right).

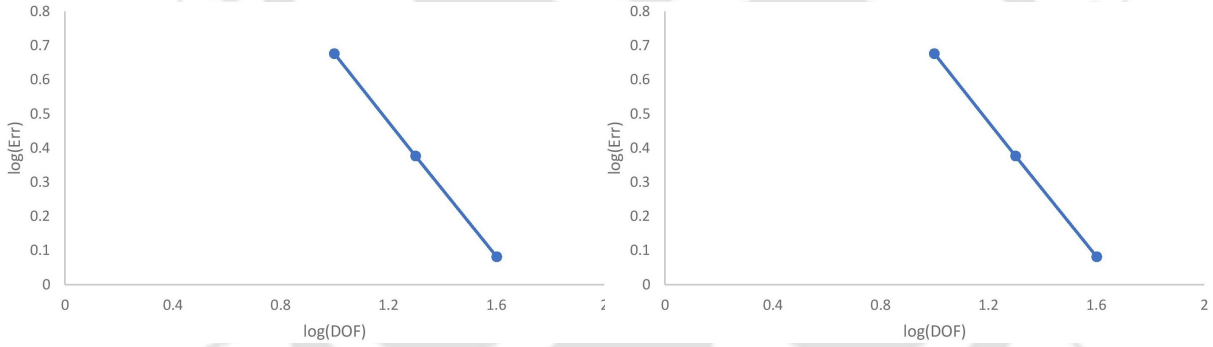

(a) (b)

Figure 2.11: Energy error versus number of degrees of freedom: (a) $\beta_1 = 1$, $\beta_2 = 10$ and (b) $\beta_1 = 1$, $\beta_2 = 100$. The quasi-optimal decay is observed by the line of slope -0.988 (left) and the line of slope -0.968 (right).

both the cases are shown in Figure 2.10. The optimal decay of the estimator is observed by the line of slope -0.929 for the choice $\beta_1 = 1, \beta_2 = 10$ (see Figure 2.10 (a)) and the line of slope -0.931 for the choice $\beta_1 = 1, \beta_2 = 100$ (see Figure 2.10 (b)). Further, in Figure 2.11, we provide plots for the energy error versus the number of degrees of freedom. For different tolerances ϵ, the degrees of freedom (DOF), the error estimator $(\eta_{1,1})$, the energy error (Err) and the effectivity index (eff. index) at the final time $T = 0.1$ are presented in Table 2.4. Table 2.4 reveals that, for a fixed time but different

TH-2911_136123010

tolerances, both the values of the estimator and the error are reducing, and the effectivity index (eff. index) is almost constant. Figures 2.7-2.9 show that the mesh adapts very well in the neighborhood of interface Γ and higher density of the node points are distributed along the interface Γ.

2.6 Concluding Remarks

(i) In this chapter, we proposed an AFEM for PIPs with nonzero flux jump. We have derived *a posteriori* upper and lower bounds for the error in the energy norm. Some new error indicators are introduced to control the error due to the discontinuous coefficients β and the nonzero flux jump g across the interface Γ. An adaptive algorithm is provided to implement the derived estimators. Our numerical experiment demonstrates that the proposed adaptive algorithm produces satisfactory numerical results.

(ii) Under suitable regularity assumptions on f, g, i.e., for $f, \frac{\partial f}{\partial t} \in L^2(0,T;L^2(\Omega))$ and $g, \frac{\partial g}{\partial t} \in L^2(0,T;L^2(\Gamma))$, starting with given solution U_h^{n-1} at t_{n-1} one can show that Algorithm 2.4.1 terminates in a finite number of iteration at each time step t_n for any given tolerances (cf. [29, Theorem 4.6]).

TH-2911_136123010

3

An AIFEM for PIPs with Nonzero Flux Jump

This chapter considers an AIFEM for solving the linear PIPs with nonhomogeneous flux jump in a two-dimensional convex polygonal domain. An unfitted finite element mesh is used to discretize the spatial domain where the grid points do not need to fit the interface. New error indicators are introduced to control the error due to unfitted meshes. We derive a global upper bound as well as a local lower bound for the error using the energy method. An adaptive algorithm for the immersed finite element method is provided using the error indicators. A numerical experiment is presented to demonstrate the behavior of the adaptive algorithm for the proposed method.

3.1 Introduction

We start with the parabolic interface problem. Let Ω be a bounded convex polygonal domain in $\mathbb{R}^2$ with Lipschitz boundary $\partial\Omega$. Let $\Omega_1 \subset \Omega$ be an open domain with C^2-smooth boundary $\partial\Omega_1 := \Gamma$. The interface Γ now divides the domain Ω into two subdomains Ω_1 and $\Omega_2 = \Omega \setminus \Omega_1$. Consider the linear parabolic interface problem of the form

$$\frac{\partial u}{\partial t} - \nabla \cdot (\beta(x)\nabla u) = f(x,t) \quad \text{in } \Omega_T \tag{3.1}$$

subject to the following initial and boundary conditions

$$u(x,0) = u_0(x) \quad \text{in} \quad \Omega; \qquad u = 0 \quad \text{on } \partial\Omega_T \tag{3.2}$$

and jump conditions across the interface Γ

$$[u] = 0, \quad \left[\beta \frac{\partial u}{\partial \mathbf{n}}\right] = g(x,t), \tag{3.3}$$

where $\Omega_T = \Omega \times (0,T]$ and $\partial\Omega_T = \partial\Omega \times [0,T]$ with $T < \infty$. The symbol $[v]$ denotes the jump of a quantity v across the interface Γ, *i.e.*, $[v](x) = v_1(x) - v_2(x)$, $x \in \Gamma$ with

TH-2911_136123010

$v_i(x) = v(x)|_{\Omega_i}$, $i = 1, 2$, and $\mathbf{n}$ denotes the unit outward normal to the boundary $\partial\Omega_1$. The discontinuous coefficient β is assumed to be positive and piecewise constant on each subdomain, *i.e.*,

$$\beta(x) = \beta_i \quad \text{for} \quad x \in \Omega_i \ (i = 1, 2).$$

The initial data u_0 is assumed to be sufficiently smooth for our purpose, and the forcing term f and the interface function g be such that

$$f \in L^2(0, T; L^2(\Omega) \quad \text{and} \quad g \in L^2(0, T; H^2(\Gamma)).$$

As a step towards finite element formulation, the weak form of the problem (3.1)-(3.3) may be stated as follows: Find the function $u : [0, T] \to H_0^1(\Omega)$ such that

$$\begin{aligned} \left(\frac{\partial u}{\partial t}, \phi\right) + (\beta(x)\nabla u, \nabla\phi) &= (f, \phi) + \langle g, \phi\rangle_\Gamma \qquad \forall \phi \in H_0^1(\Omega), \\ u(0) &= u_0, \end{aligned} \tag{3.4}$$

where $\langle \cdot, \cdot \rangle_\Gamma$ represents the scalar product of the space $L^2(\Gamma)$.

It is known that optimal or almost optimal rates of convergence can be realized if fitted finite element meshes are used, see [60, 98, 101]. In the previous chapter, we have used fitted finite element mesh by allowing mesh points to lie on the interface. However, it is difficult and time-consuming exercise to construct fitted meshes for problems involving complicated interfaces. In order to overcome this, an IFE method has been introduced by Li *et al.* in [75], and subsequently investigated by many researchers. We refer to [52, 55, 62, 64, 72, 74, 75, 78, 99] for the recent development in the *a priori* analysis of IFE methods. Some relevant work and references concerning IFE methods have been summarized in [55, 99] for elliptic interface problems, [64] for parabolic interface problems with moving interface and [78] for partially penalized finite element methods for parabolic interface problems. We refer the reader to [31] for AIFEM for elliptic equations with discontinuous coefficients and [30] for AIFEM with Lagrangian-Eulerian scheme for parabolic equations in time variable domains.

The main objective of this chapter is to develop and analyze an AIFEM for the approximation of the parabolic interface problem (3.1)-(3.3) with non-homogeneous flux jump. The main advantage of the IFE method is that it can use interface independent meshes and hence structured or even Cartesian meshes can be used to solve problems with nontrivial interface geometry. We have derived *a posteriori* error estimates for IFE method and provided an adaptive algorithm for the interface problem. The interface is assumed to be smooth and independent of time, and the finite element meshes do not necessarily lie on the interface. Some new error indicators are introduced to control the

TH-2911_136123010

error due to IFE discretization. Both global upper and local lower *a posteriori* error bounds for an IFE method are obtained using the energy method. The upper bound is bounded by the indicator for the initial error, time error indicator, space error indicator, and data approximation error indicator; while a lower bound for the local error in terms of the space error indicator is obtained following the technique of [29]. A numerical experiment is presented to illustrate the performance of the error indicators. The space mesh and time-step size adaption are carried out simultaneously to control the error due to non-body-fitted meshes.

The layout of this chapter is as follows: Section 3.2 introduces the space-time IFE discretization of the domain for (3.1)-(3.3) and recall the interface approximation property. In Section 3.3, a global upper and a local lower bounds for the error are derived. A space-time adaptive algorithm for (3.1)-(3.3) is presented in Section 3.4. In Section 3.5, numerical results are provided to demonstrate the efficiency of the proposed algorithm. Finally, a concluding remark is presented in the last section.

3.2 Space-Time IFE Discretization

This section introduces the finite element discretization where the meshes are not required to fit the interface and formulates the space-time fully discrete finite element approximations to (3.1)-(3.3).

In order to discretize the problem (3.1)-(3.3), let $\{(t_{n-1}, t_n]\}_{n=1}^N$ be a partition of $[0, T]$ with time-step size $k_n = t_n - t_{n-1}$. At each time step t_n, $n = 0, 1, \ldots, N$, let $\mathcal{T}^n$ be a regular triangulation of the domain Ω. Let h_K be the diameter of a triangle $K \in \mathcal{T}^n$. A triangle $K \in \mathcal{T}^n$ is said to be an interface triangle if the interface Γ passes through the interior of triangle K; otherwise K is called a non-interface triangle. Let $\mathcal{T}_\Gamma^n$ be the set of all interface triangles.

For each $n = 0, 1, \ldots, N$, let S^n be the H^1-conforming finite element space corresponding to the triangulation $\mathcal{T}^n$ and is defined by

$$S^n = \Big\{ v \in H^1(\Omega) : v|_K \in \mathbb{P}_1(K), \ \ \forall K \in \mathcal{T}^n \Big\},$$

where $\mathbb{P}_1(K)$ denotes the space of polynomials of degree less than or equal to 1 on K. Let $S_0^n = S^n \cap H_0^1(\Omega)$.

In order to approximate the weak formulation (3.4), we define $\beta_h(x)$ to be the approximation of the coefficient $\beta(x)$ such that $\beta_h(x) = \beta_K(x)$ for $K \in \mathcal{T}^n$, where

$$\beta_K(x) = \begin{cases} \beta(x) & \text{if } \ K \in \mathcal{T}^n \setminus \mathcal{T}_\Gamma^n, \\ \min\limits_{x \in K} \beta(x) & \text{if } \ K \in \mathcal{T}_\Gamma^n. \end{cases}$$

TH-2911_136123010

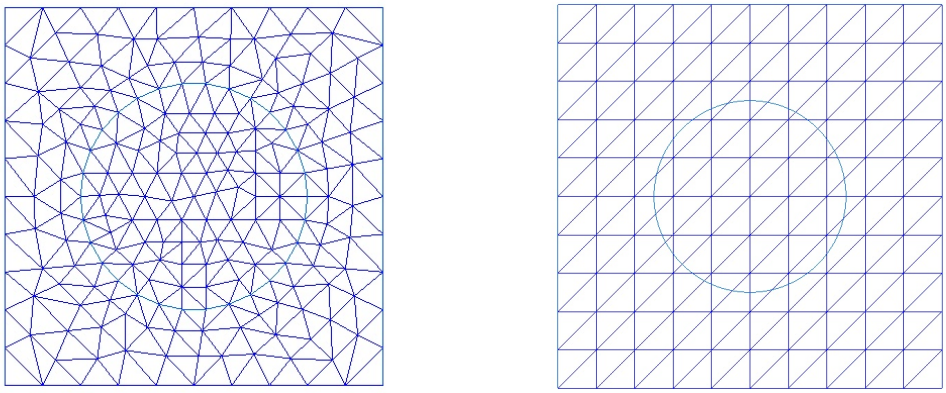

Figure 3.1: The fitted mesh (left) and unfitted mesh (right) of domain Ω.

Let Γ_h^n be a piecewise linear approximation of Γ at time t_n whose vertices are the intersection of the sides of the interface elements with Γ. Let $\bar{g}_h^n$ be the piecewise linear interpolation of g on Γ_h^n.

We now recall the following interface approximation result, see [32].

Lemma 3.2.1. *With $g \in L^2(0,T;H^2(\Gamma))$ and $\bar{g}_h^n$ as defined above, we have for all $\phi \in H_0^1(\Omega)$,*

$$\left| \int_\Gamma \bar{g}_h^n \phi \, ds - \int_{\Gamma_h^n} \bar{g}_h^n \phi \, ds \right| \leq C_{2,1} \sum_{K \in \mathcal{T}_\Gamma^n} h_K \|\bar{g}_h^n\|_{L^2(\Gamma_h^n \cap K)} \|\phi\|_{H^1(K)},$$

where the constant $C_{2,1} > 0$ depends on the minimal angle of $\mathcal{T}^n$.

Let U_h^0 be a suitable approximation of u_0 in S_0^0 over the initial mesh $\mathcal{T}^0$. The space-time finite element approximation to the problem (3.4) read as: Given U_h^0, find $U_h^n \in S_0^n$ for $1 \leq n \leq N$, such that

$$\left(\frac{U_h^n - U_h^{n-1}}{k_n}, v \right) + (\beta_h(x) \nabla U_h^n, \nabla v) = (f^n, v) + \langle \bar{g}_h^n, v \rangle_{\Gamma_h^n} \quad \forall v \in S_0^n. \tag{3.5}$$

By Lax-Milgram theorem, the discrete problem (3.5) has a unique solution $U_h^n \in S_0^n$.

3.3 A Posteriori Error Analysis

This section is devoted to the *a posteriori* error analysis for the fully discrete approximation to the problem (3.1)-(3.3). We first derive a global upper bound for the error. A local lower bound for the error in terms of the error indicators is obtained in the last part of this section.

To begin with, we need some notation. Let $\mathcal{E}^n$ be the collection of interior edges of $\mathcal{T}^n$. Let $\mathcal{E}_\Gamma^n$ be the set of all interface edges. For any $e \in \mathcal{E}^n$, let h_e be the length of

TH-2911_136123010

e, and let Ω_e be the collection of two triangles sharing the common edge e. For any triangle K, let ω_K be the set of all triangles in $\mathcal{T}^n$ that have non-empty intersection with K. For any $e \in \mathcal{E}^n$, where $e = \partial K_1 \cap \partial K_2$, ω_e denotes the union of ω_{K_1} and ω_{K_2}.

We now define two residuals for the error analysis, namely the interior residual R^n which is defined as

$$R^n := f^n - k_n^{-1}(U_h^n - U_h^{n-1}) \tag{3.6}$$

and the jump residual across $e \in \mathcal{E}^n$ is defined as

$$J_e^n := [\beta_h(x)\nabla U_h^n]_e \cdot \mathbf{n}_e = (\beta_1 \nabla U_{1h}^n|_{K_1} - \beta_2 \nabla U_{2h}^n|_{K_2}) \cdot \mathbf{n}_e, \tag{3.7}$$

where $\mathbf{n}_e$ denotes the unit vector to e points from K_2 to K_1. An integration by parts implies

$$(\beta_h(x)\nabla U_h^n, \nabla\phi) = -\sum_{e\in\mathcal{E}^n} \int_e J_e^n \phi ds \quad \forall \phi \in H_0^1(\Omega). \tag{3.8}$$

We recall some approximation properties for the Clément interpolation operator (cf. [35]) which plays a crucial role in the analysis of the adaptive immersed finite element method.

Lemma 3.3.1. *Let $\Pi^n : H_0^1(\Omega) \to S_0^n$ be the Clément interpolation operator. Then, for any $\phi \in H_0^1(\Omega)$, we have*

$$\begin{aligned} \|\phi - \Pi^n\phi\|_{L^2(K)} &\le C_{I,1}\, h_K \|\nabla\phi\|_{L^2(\omega_K)}, \quad \forall K \in \mathcal{T}^n, \\ \|\phi - \Pi^n\phi\|_{L^2(e)} &\le C_{I,2}\, h_e^{\frac{1}{2}} \|\nabla\phi\|_{L^2(\omega_e)}, \quad \forall e \in \mathcal{E}^n, \end{aligned} \tag{3.9}$$

where the positive constants $C_{I,1}, C_{I,2}$ depends only on the minimum angle of the triangulation $\mathcal{T}^n$.

3.3.1 An Upper Bound

In this section, our focus is to derive a global *a posteriori* upper bound for the error.

Let $U_h : [0, T] \to H_0^1(\Omega)$ be a continuous piecewise linear approximation in time of $u(t)$ defined by

$$U_h(t) := l_{n-1}(t)U_h^{n-1} + l_n(t)U_h^n \tag{3.10}$$

for $t \in (t_{n-1}, t_n]$, $1 \le n \le N$, where the Lagrangian functions are given by $l_{n-1}(t) = \frac{t_n - t}{k_n}$ and $l_n(t) = \frac{t - t_{n-1}}{k_n}$ $\forall t \in (t_{n-1}, t_n]$.

In the following, we present *a posteriori* upper bound for the error of the fully discrete approximation to the problem (3.1)-(3.3).

TH-2911_136123010

Theorem 3.3.1. *Let u be the solution of (3.1)-(3.3) and let U_h be its approximation defined by (3.10). Then there exists a constant $C > 0$ such that for $1 \leq m \leq N$, we have*

$$\begin{aligned}\frac{1}{2}\|u^m - U_h^m\|^2_{L^2(\Omega)} \;+\; \sum_{n=1}^{m}\int_{t^{n-1}}^{t^n} |||u - U_h^n|||^2_\Omega dt \;\leq\; C\|u_0 - U_h^0\|^2_{L^2(\Omega)} + \sum_{n=1}^{m} k_n \eta^n_{2,time} \\ + C\sum_{n=1}^{m} k_n \eta^n_{2,space} + 4\left(\sum_{n=1}^{m}\int_{t^{n-1}}^{t^n} \|f - f^n\|_{L^2(\Omega)} dt\right)^2 \\ + 4\left(\sum_{n=1}^{m}\int_{t_{n-1}}^{t_n} \|g - \bar{g}_h^n\|_{L^2(\Gamma)} dt\right)^2, \end{aligned} \tag{3.11}$$

where the constant C depends only on the minimum angle of meshes $\mathcal{T}^n$, $n = 1, \ldots, m$, and the coefficient $\beta(x)$. The time error indicator $\eta^n_{2,time}$ and the space error indicator $\eta^n_{2,space}$ are given by

$$\eta^n_{2,time} \;=\; \frac{1}{3}|||U_h^n - U_h^{n-1}|||^2_\Omega, \qquad \text{and} \qquad \eta^n_{2,space} = \sum_{K\in\mathcal{T}^n} \eta^n_{2,K}, \tag{3.12}$$

where the local error indicator $\eta^n_{2,K}$ is defined as

$$\begin{cases} \eta^n_{2,K} = \;\; h_K^2\|R^n\|^2_{L^2(K)} + \sum_{e\subset\partial K} h_e\|J_e^n\|^2_{L^2(e)}, \;\; \text{for } K \in \mathcal{T}^n \setminus \mathcal{T}^n_\Gamma, \\ \eta^n_{2,K} = \;\; h_K^2\|R^n\|^2_{L^2(K)} + \sum_{e\subset\partial K} h_e\|J_e^n\|^2_{L^2(e)} + h_K^2\|\bar{g}_h^n\|^2_{L^2(\Gamma_h^n\cap K)} \\ \qquad\qquad + \||\beta_K - \beta|^{\frac{1}{2}}\nabla U_h^n\|^2_{L^2(K)}, \qquad \text{for } K \in \mathcal{T}^n_\Gamma. \end{cases} \tag{3.13}$$

Proof. Using (3.5), (3.8) and integrating by parts, for any $\phi \in H_0^1(\Omega)$ and $v \in S_0^n$, we have

$$\begin{aligned}\left(\frac{U_h^n - U_h^{n-1}}{k_n}, \phi\right) \;+\; (\beta(x)\nabla U_h^n, \nabla\phi) \;=\; (f^n, \phi) + \langle \bar{g}_h^n, v\rangle_{\Gamma_h^n} - (R^n, \phi - v) \\ - \sum_{e\in\mathcal{E}^n}\int_e J_e^n(\phi - v)ds + \sum_{K\in\mathcal{T}^n_\Gamma}((\beta - \beta_K)\nabla U_h^n, \nabla\phi)_K. \end{aligned} \tag{3.14}$$

With an aid of (3.4), (3.10) and (3.14), for $t \in (t_{n-1}, t_n]$, we obtain

$$\begin{aligned}\left(\frac{\partial(u - U_h)}{\partial t}, \phi\right) \;+\; (\beta\nabla(u - U_h^n), \nabla\phi) \;=\; (f - f^n, \phi) + \langle g, \phi\rangle_\Gamma - \langle \bar{g}_h^n, v\rangle_{\Gamma_h^n} \\ + \;\; (R^n, \phi - v) + \sum_{e\in\mathcal{E}^n}\int_e J_e^n(\phi - v)ds + \sum_{K\in\mathcal{T}^n_\Gamma}((\beta_K - \beta)\nabla U_h^n, \nabla\phi)_K. \end{aligned}$$

TH-2911_136123010

Substituting $\phi = u - U_h$ and $v = \Pi^n \phi$ in the above equation and then using the identity

$$(\beta\nabla(u-U_h^n), \nabla(u-U_h)) = \frac{1}{2}|||u-U_h^n|||_\Omega^2 + \frac{1}{2}|||u-U_h|||_\Omega^2 - \frac{1}{2}|||U_h-U_h^n|||_\Omega^2,$$

we arrive at

$$\begin{aligned}
&\frac{1}{2}\frac{\mathrm{d}}{\mathrm{d}t}\|u-U_h\|_{L^2(\Omega)}^2 + \frac{1}{2}|||u-U_h^n|||_\Omega^2 + \frac{1}{2}|||u-U_h|||_\Omega^2 \\
= \;& \frac{1}{2}|||U_h-U_h^n|||_\Omega^2 + (f-f^n, u-U_h) + \langle g, u-U_h\rangle_\Gamma - \langle \bar{g}_h^n, \Pi^n(u-U_h)\rangle_{\Gamma_h^n} \\
&+ (R^n, (u-U_h) - \Pi^n(u-U_h)) + \sum_{e\in\mathcal{E}^n}\int_e J_e^n((u-U_h)-\Pi^n(u-U_h))ds \\
&+ \sum_{K\in\mathcal{T}_\Gamma^n}((\beta_K-\beta)\nabla U_h^n, \nabla(u-U_h))_K. \qquad (3.15)
\end{aligned}$$

Now for any $t_* \in (t_{m-1}, t_m]$, integrating (3.15) in time from 0 to t_*, $t_n \wedge t_* = \min(t_n, t_*)$ and summing over all m, we obtain

$$\begin{aligned}
&\frac{1}{2}\|(u-U_h)(t_*)\|_{L^2(\Omega)}^2 + \frac{1}{2}\sum_{n=1}^m \int_{t_{n-1}}^{t_n\wedge t_*} \left(|||u-U_h^n|||_\Omega^2 + |||u-U_h|||_\Omega^2\right) dt \\
= \;& \frac{1}{2}\|u_0-U_h^0\|_{L^2(\Omega)}^2 + \frac{1}{2}\sum_{n=1}^m\int_{t_{n-1}}^{t_n}|||U_h-U_h^n|||_\Omega^2 dt + \sum_{n=1}^m\int_{t_{n-1}}^{t_n}(f-f^n, u-U_h)dt \\
&+\sum_{n=1}^m\int_{t_{n-1}}^{t_n}\left(\langle g, u-U_h\rangle_\Gamma - \langle \bar{g}_h^n, \Pi^n(u-U_h)\rangle_{\Gamma_h^n}\right)dt \\
&+\sum_{n=1}^m\int_{t_{n-1}}^{t_n}(R^n, (u-U_h)-\Pi^n(u-U_h))dt \\
&+\sum_{n=1}^m\int_{t_{n-1}}^{t_n}\sum_{e\in\mathcal{E}^n}\int_e J_e^n((u-U_h)-\Pi^n(u-U_h))ds \\
&+\sum_{n=1}^m\int_{t_{n-1}}^{t_n}\sum_{K\in\mathcal{T}_\Gamma^n}((\beta_K-\beta)\nabla U_h^n, \nabla(u-U_h))_K dt \\
=\;& \frac{1}{2}\|u_0-U_h^0\|_{L^2(\Omega)}^2 + I_1+I_2+I_3+I_4+I_5+I_6. \qquad (3.16)
\end{aligned}$$

We now estimate the term $I_i, i = 1, \ldots, 6$, separately. For I_1, using (3.10) we have

$$\begin{aligned}
I_1 &= \frac{1}{2}\sum_{n=1}^m\int_{t_{n-1}}^{t_n}(l_{n-1}(t))^2\,|||U_h^n-U_h^{n-1}|||_\Omega^2 dt \qquad (3.17)\\
&= \frac{1}{2}\sum_{n=1}^m\frac{k_n}{3}\,|||U_h^n-U_h^{n-1}|||_\Omega^2 \;=\; \frac{1}{2}\sum_{n=1}^m k_n\eta_{2,time}^n. \qquad (3.18)
\end{aligned}$$

TH-2911_136123010

By the Cauchy-Schwarz inequality, it follows that

$$\begin{aligned} I_2 &\leq \sum_{n=1}^{m}\int_{t_{n-1}}^{t_n} \|f-f^n\|_{L^2(\Omega)}\|u-U_h\|_{L^2(\Omega)}\,dt \\ &\leq \frac{1}{8}\max_{0\leq t\leq t_*}\|u-U_h\|^2_{L^2(\Omega)} + 2\left(\sum_{n=1}^{m}\int_{t_{n-1}}^{t_n}\|f-f^n\|_{L^2(\Omega)}\,dt\right)^2. \end{aligned} \tag{3.19}$$

For I_3, we first split it into three terms as

$$\begin{aligned} I_3 &= \sum_{n=1}^{m}\int_{t_{n-1}}^{t_n}\langle g-\bar{g}_h^n, u-U_h\rangle_\Gamma\,dt + \sum_{n=1}^{m}\int_{t_{n-1}}^{t_n}\langle \bar{g}_h^n, (u-U_h)-\Pi^n(u-U_h)\rangle_\Gamma\,dt \\ &+\sum_{n=1}^{m}\int_{t_{n-1}}^{t_n}\Big(\langle \bar{g}_h^n,\Pi^n(u-U_h)\rangle_\Gamma - \langle \bar{g}_h^n,\Pi^n(u-U_h)\rangle_{\Gamma_h^n}\Big)dt. \end{aligned} \tag{3.20}$$

Now an application of the Cauchy-Schwarz inequality in (3.20) implies

$$\begin{aligned} I_3 &\leq \sum_{n=1}^{m}\int_{t_{n-1}}^{t_n}\|g-\bar{g}_h^n\|_{L^2(\Gamma)}\|u-U_h\|_{L^2(\Gamma)}dt \\ &+\sum_{n=1}^{m}\int_{t_{n-1}}^{t_n}\sum_{e\in\mathcal{E}_\Gamma^n}\|\bar{g}_h^n\|_{L^2(e)}\|(u-U_h)-\Pi^n(u-U_h)\|_{L^2(e)}dt \\ &+\sum_{n=1}^{m}\int_{t_{n-1}}^{t_n}\left(\langle \bar{g}_h^n,\Pi^n(u-U_h)\rangle_\Gamma - \langle \bar{g}_h^n,\Pi^n(u-U_h)\rangle_{\Gamma_h^n}\right)dt. \end{aligned} \tag{3.21}$$

We apply Lemma 3.3.1 and Lemma 3.2.1 to the second and third terms of (3.21) to obtain

$$\begin{aligned} I_3 &\leq \sum_{n=1}^{m}\int_{t_{n-1}}^{t_n}\|g-\bar{g}_h^n\|_{L^2(\Gamma)}\|u-U_h\|_{L^2(\Gamma)}dt \\ &+ C_{I,2}\sum_{n=1}^{m}\int_{t_{n-1}}^{t_n}\sum_{e\in\mathcal{E}_\Gamma^n}h_e^{\frac{1}{2}}\|\bar{g}_h^n\|_{L^2(e)}\|\nabla(u-U_h)\|_{L^2(\omega_e)}dt \\ &+ C_{2,1}\sum_{n=1}^{m}\int_{t_{n-1}}^{t_n}\sum_{K\in\mathcal{T}_\Gamma^n}h_K\|\bar{g}_h^n\|_{L^2(\Gamma_h^n\cap K)}\|\Pi^n(u-U_h)\|_{H^1(K)}dt. \end{aligned} \tag{3.22}$$

Utilization of Young's inequality in (3.22) leads to

$$\begin{aligned} I_3 &\leq 2\left(\sum_{n=1}^{m}\int_{t_{n-1}}^{t_n}\|g-\bar{g}_h^n\|_{L^2(\Gamma)}dt\right)^2 + \frac{1}{8}\max_{0\leq t\leq t_*}\|u-U_h\|^2_{L^2(\Omega)} \\ &+ C_{I,2}\sum_{n=1}^{m}\int_{t_{n-1}}^{t_n}\sum_{e\in\mathcal{E}_\Gamma^n}h_e^{\frac{1}{2}}\|\bar{g}_h^n\|_{L^2(e)}\|\nabla(u-U_h)\|_{L^2(\omega_e)}dt \end{aligned}$$

TH-2911_136123010

$$+ C_{2,1}\sum_{n=1}^{m}\int_{t_{n-1}}^{t_n}\sum_{K\in\mathcal{T}_\Gamma^n} h_K\|\bar{g}_h^n\|_{L^2(\Gamma_h^n\cap K)}\|u-U_h\|_{H^1(\omega_K)}dt. \tag{3.23}$$

For the remaining terms $I_i, i = 4, 5, 6$, an application of the Cauchy-Schwarz inequality and (3.9) yields

$$\begin{aligned} I_4 &\leq \sum_{n=1}^{m}\int_{t_{n-1}}^{t_n}\sum_{K\in\mathcal{T}^n}\|R^n\|_{L^2(K)}\|(u-U_h)-\Pi^n(u-U_h)\|_{L^2(K)}dt \\ &\leq C_{I,1}\sum_{n=1}^{m}\int_{t_{n-1}}^{t_n}\sum_{K\in\mathcal{T}^n} h_K\|R^n\|_{L^2(K)}\|\nabla(u-U_h)\|_{L^2(\omega_K)}dt, \end{aligned} \tag{3.24}$$

$$\begin{aligned} I_5 &\leq \sum_{n=1}^{m}\int_{t_{n-1}}^{t_n}\sum_{e\in\mathcal{E}^n}\|J_e^n\|_{L^2(e)}\|(u-U_h)-\Pi^n(u-U_h)\|_{L^2(e)}dt \\ &\leq C_{I,2}\sum_{n=1}^{m}\int_{t_{n-1}}^{t_n}\sum_{e\in\mathcal{E}^n} h_e^{\frac{1}{2}}\|J_e^n\|_{L^2(e)}\|\nabla(u-U_h)\|_{L^2(\omega_e)}dt \end{aligned} \tag{3.25}$$

and

$$\begin{aligned} I_6 &\leq \sum_{n=1}^{m}\int_{t_{n-1}}^{t_n}\sum_{K\in\mathcal{T}_\Gamma^n}\||\beta_K-\beta|^{\frac{1}{2}}\nabla U_h^n\|_{L^2(K)}\,\||\beta_K-\beta|^{\frac{1}{2}}\nabla(u-U_h))\|_{L^2(K)}dt \\ &\leq \sum_{n=1}^{m}\int_{t_{n-1}}^{t_n}\sum_{K\in\mathcal{T}_\Gamma^n}\||\beta_K-\beta|^{\frac{1}{2}}\nabla U_h^n\|_{L^2(K)}\,|||u-U_h)|||_K dt, \end{aligned} \tag{3.26}$$

respectively. Altogether these estimates and (3.16) yields

$$\begin{aligned} &\frac{1}{2}\|(u-U_h)(t_*)\|_{L^2(\Omega)}^2+\frac{1}{2}\sum_{n=1}^{m}\int_{t_{n-1}}^{t_n\wedge t_*}\left(|||u-U_h^n|||_\Omega^2+|||u-U_h|||_\Omega^2\right)dt \\ \leq\ &\frac{1}{2}\|u_0-U_h^0\|_{L^2(\Omega)}^2+\frac{1}{2}\sum_{n=1}^{m}k_n\eta_{2,time}^n+\frac{1}{4}\max_{0\leq t\leq t_*}\|u-U_h\|_{L^2(\Omega)}^2 \\ &+2\left(\sum_{n=1}^{m}\int_{t_{n-1}}^{t_n}\|f-f^n\|_{L^2(\Omega)}\,dt\right)^2+2\left(\sum_{n=1}^{m}\int_{t_{n-1}}^{t_n}\|g-\bar{g}_h^n\|_{L^2(\Gamma)}dt\right)^2 \\ &+C_{I,2}\sum_{n=1}^{m}\int_{t_{n-1}}^{t_n}\sum_{e\in\mathcal{E}_\Gamma^n} h_e^{\frac{1}{2}}\|\bar{g}_h^n\|_{L^2(e)}\|\nabla(u-U_h)\|_{L^2(\omega_e)}dt \\ &+C_{2,1}\sum_{n=1}^{m}\int_{t_{n-1}}^{t_n}\sum_{K\in\mathcal{T}_\Gamma^n} h_K\|\bar{g}_h^n\|_{L^2(\Gamma_h^n\cap K)}\|u-U_h\|_{H^1(\omega_K)}dt \\ &+C_{I,1}\sum_{n=1}^{m}\int_{t_{n-1}}^{t_n}\sum_{K\in\mathcal{T}^n} h_K\|R^n\|_{L^2(K)}\|\nabla(u-U_h)\|_{L^2(\omega_K)}dt \end{aligned}$$

TH-2911_136123010

$$+ C_{I,2}\sum_{n=1}^{m}\int_{t_{n-1}}^{t_n}\sum_{e\in\mathcal{E}^n} h_e^{\frac{1}{2}}\|J_e^n\|_{L^2(e)}\|\nabla(u-U_h)\|_{L^2(\omega_e)}dt$$
$$+\sum_{n=1}^{m}\int_{t_{n-1}}^{t_n}\sum_{K\in\mathcal{T}_\Gamma^n}\||\beta_K-\beta|^{\frac{1}{2}}\nabla U_h^n\|_{L^2(K)}|||u-U_h|||_K dt.$$

Using the Young's inequality the above estimate can be rewritten as

$$\begin{aligned}
&\frac{1}{2}\|(u-U_h)(t_*)\|^2_{L^2(\Omega)}+\frac{1}{2}\sum_{n=1}^{m}\int_{t_{n-1}}^{t_n\wedge t_*}\left(|||u-U_h^n|||^2_\Omega+|||u-U_h|||^2_\Omega\right)dt\\
\leq\ &\frac{1}{2}\|u_0-U_h^0\|^2_{L^2(\Omega)}+\frac{1}{2}\sum_{n=1}^{m}k_n\,\eta^n_{2,time}+\frac{1}{4}\max_{0\leq t\leq t_*}\|u-U_h\|^2_{L^2(\Omega)}\\
&+2\left(\sum_{n=1}^{m}\int_{t_{n-1}}^{t_n}\|f-f^n\|_{L^2(\Omega)}dt\right)^2+2\left(\sum_{n=1}^{m}\int_{t_{n-1}}^{t_n}\|g-\bar{g}_h^n\|_{L^2(\Gamma)}dt\right)^2\\
&+\frac{C}{2}\sum_{n=1}^{m}\int_{t_{n-1}}^{t_n}\sum_{K\in\mathcal{T}^n\setminus\mathcal{T}_\Gamma^n}\left(h_K^2\|R^n\|^2_{L^2(K)}+\sum_{e\subset\partial K}h_e\|J_e^n\|^2_{L^2(e)}\right)dt\\
&+\frac{C}{2}\sum_{n=1}^{m}\int_{t_{n-1}}^{t_n}\sum_{K\in\mathcal{T}_\Gamma^n}\left(h_K^2\|R^n\|^2_{L^2(K)}+\sum_{e\subset\partial K}h_e\|J_e^n\|^2_{L^2(e)}+\sum_{e\subset\partial K}h_K^2\|\bar{g}_h^n\|^2_{L^2(\Gamma_h^n\cap K)}\right.\\
&\left.+|||\beta_K-\beta|^{\frac{1}{2}}\nabla U_h^n\|^2_{L^2(K)}\right)dt+\frac{1}{2}\sum_{n=1}^{m}\int_{t_{n-1}}^{t_n}|||u-U_h|||^2_\Omega dt,
\end{aligned}$$

where the constant $C=\max\{C_{2,1}^2,C_{I,1}^2,C_{I,2}^2\}$. Using (3.12) and (3.13), we obtain

$$\begin{aligned}
&\frac{1}{2}\|(u-U_h)(t_*)\|^2_{L^2(\Omega)}+\frac{1}{2}\sum_{n=1}^{m}\int_{t_{n-1}}^{t_n\wedge t_*}\left(|||u-U_h^n|||^2_\Omega+|||u-U_h|||^2_\Omega\right)dt\\
\leq\ &\frac{1}{2}\|u_0-U_h^0\|^2_{L^2(\Omega)}+\frac{1}{2}\sum_{n=1}^{m}k_n\eta^n_{2,time}+\frac{1}{4}\max_{0\leq t\leq t_*}\|u-U_h\|^2_{L^2(\Omega)}\\
&+2\left(\sum_{n=1}^{m}\int_{t_{n-1}}^{t_n}\|f-f^n\|_{L^2(\Omega)}dt\right)^2+2\left(\sum_{n=1}^{m}\int_{t_{n-1}}^{t_n}\|g-\bar{g}_h^n\|_{L^2(\Gamma)}dt\right)^2\\
&+\frac{C}{2}\sum_{n=1}^{m}\int_{t_{n-1}}^{t_n}\eta^n_{2,space}dt+\frac{1}{2}\sum_{n=1}^{m}\int_{t_{n-1}}^{t_n}|||u-U_h|||^2_\Omega dt\\
\leq\ &\frac{1}{2}\|u_0-U_h^0\|^2_{L^2(\Omega)}+\frac{1}{2}\sum_{n=1}^{m}k_n\eta^n_{2,time}+\frac{1}{4}\max_{0\leq t\leq t_*}\|u-U_h\|^2_{L^2(\Omega)}\\
&+2\left(\sum_{n=1}^{m}\int_{t_{n-1}}^{t_n}\|f-f^n\|_{L^2(\Omega)}dt\right)^2+2\left(\sum_{n=1}^{m}\int_{t_{n-1}}^{t_n}\|g-\bar{g}_h^n\|_{L^2(\Gamma)}dt\right)^2\\
&+\frac{C}{2}\sum_{n=1}^{m}k_n\eta^n_{2,space}+\frac{1}{2}\sum_{n=1}^{m}\int_{t_{n-1}}^{t_n}|||u-U_h|||^2_\Omega dt.
\end{aligned}$$

TH-2911_136123010

Now by throwing back the third term on the right the desired estimate (3.11) follows and this completes the proof. □

Remark 3.3.1. *Observe that the term* $\||\beta_K - \beta|^{\frac{1}{2}}\nabla U_h^n\|^2_{L^2(K)}$ *appearing in the a posteriori error indicator (3.13) for the interface triangle* K *controls the error due to the approximation of coefficients* $\beta(x)$.

3.3.2 A Lower Bound

The main focus of this section to derive a lower bound for the error in terms of the local space error indicators. For this purpose, let us consider the following auxiliary problem.

Let $U_*^n \in H_0^1(\Omega)$ be the solution of

$$\left(\frac{U_*^n - U_h^{n-1}}{k_n}, \phi\right) + (\beta_h \nabla U_*^n, \nabla\phi) = (f^n, \phi) + \langle \bar{g}_h^n, \phi\rangle_{\Gamma_h^n} \quad \forall \phi \in H_0^1(\Omega). \tag{3.27}$$

For any $K \in \mathcal{T}^n$ and $\phi \in L^2(\Omega)$, we define the average of ϕ over the triangle K by

$$\mathcal{P}_K\phi = \frac{1}{|K|}\int_K \phi\, dx.$$

For $n = 1, 2, \ldots$, we choose the constants

$$\hat{\mathcal{C}}_n = \max_{K\in\mathcal{T}^n}\left\{\frac{h_K^2}{k_n} : h_K = \text{diam}(K)\right\}. \tag{3.28}$$

The crucial part is to handle the oscillation of the residual R^n which changes at each refinement stage. Define the oscillation of any function $\phi \in L^2(\Omega)$ over the mesh $\mathcal{T}^n$ by

$$\text{osc}(\phi, \mathcal{T}^n) = \left(\sum_{K\in\mathcal{T}^n} h_K^2 \|\phi - \mathcal{P}_K\phi\|^2_{L^2(K)}\right)^{\frac{1}{2}} \tag{3.29}$$

and the weighted norm $\|\cdot\|_{k_n,\Omega}$ of $H^1(\Omega)$ with the parameter $k_n > 0$ by

$$\|\phi\|_{k_n,\Omega} = \left(\frac{1}{k_n}\|\phi\|^2_{L^2(\Omega)} + |||\phi|||^2_\Omega\right)^{\frac{1}{2}}. \tag{3.30}$$

Remark 3.3.2. *Notice that by modifying time-step size* k_n *in (3.5) we are controlling the error between* $u^n = u(x, t_n)$ *and* U_h^n. *The purpose of introducing the auxiliary problem (3.27) is basically to control the error between* U_h^n *and* U_*^n, *not between* U_h^n *and the exact solution* u. *These two facts play a vital role in deriving a lower bound for the space error indicator.*

Following the ideas of [29, 31, 104], we now derive another main result of this chapter. The technical tool uses in the following theorem is the properties of bubble functions and the Cauchy-Schwarz inequality.

TH-2911_136123010

Theorem 3.3.2. *Let U_h^n and U_*^n be the solutions of (3.5) and (3.27), respectively. Then, for $K \in \mathcal{T}^n \setminus \mathcal{T}_\Gamma^n$, we have*

$$\begin{aligned}\eta_{2,K}^n &\leq C_{2,7}\sum_{K\in\Omega_e} h_K^2\|R^n-\mathcal{P}_K R^n\|_{L^2(K)}^2 \\ &\quad + C_{2,8}\hat{\mathcal{C}}_n\sum_{K\in\Omega_e}\left(\frac{1}{k_n}\|U_*^n-U_h^n\|_{L^2(K)}^2+|||U_*^n-U_h^n|||_K^2\right) \end{aligned} \tag{3.31}$$

and for $K \in \mathcal{T}_\Gamma^n$, we have

$$\begin{aligned}\eta_{2,K}^n &\leq C_{2,7}\sum_{K\in\Omega_e^\Gamma} h_K^2\|R^n-\mathcal{P}_K R^n\|_{L^2(K)}^2 \\ &\quad + C_{2,8}\,\hat{\mathcal{C}}_n\sum_{K\in\Omega_e^\Gamma}\left(\frac{1}{k_n}\|U_*^n-U_h^n\|_{L^2(K)}^2+|||U_*^n-U_h^n|||_K^2\right) \\ &\quad + C_{2,9}\sum_{e\subset\partial K} h_e\|\bar{g}_h^n\|_{L^2(e)}^2 + C_{2,7}\sum_{K\in\Omega_e^\Gamma}\||\beta_K-\beta|^{1/2}\nabla U_h^n\|_{L^2(K)}^2, \end{aligned} \tag{3.32}$$

where the constant $C_{2,i}>0$ $(i=7,8,9)$ depends only on the minimal angle of $\mathcal{T}^n$ and the coefficient $\beta(x)$.

Proof. To begin with, we first introduce the element bubble function. For any $K \in \mathcal{T}^n$, let $\psi_K = 27\lambda_1\lambda_2\lambda_3$ be the element bubble function, where λ_i's, $(i=1,2,3)$, are the barycentric coordinate functions. Using the properties of the bubble function, we have the following inf-sup inequality:

$$\inf_{v_h\in\mathbb{P}_1(K)}\sup_{\varphi_h\in\mathbb{P}_1(K)}\frac{\int_K v_h\varphi_h\psi_K}{\|\varphi_h\|_{L^2(K)}\|v_h\|_{L^2(K)}} \geq \gamma_0,$$

where the constant $\gamma_0(>0)$ depends only on the minimum angle of the triangle $K \in \mathcal{T}^n$. Let $\varphi^n \in \mathbb{P}_1(K)$ be such that $\|\varphi^n\|_{L^2(K)}=1$. Putting $v_h = \mathcal{P}_K R^n$ in the inf-sup relation and using (3.27), for $K \in \mathcal{T}^n \setminus \mathcal{T}_\Gamma^n$, we obtain

$$\begin{aligned}\gamma_0\|\mathcal{P}_K R^n\|_{L^2(K)} &\leq \int_K(\mathcal{P}_K R^n)\psi_K\varphi^n dx \\ &= \int_K(\mathcal{P}_K R^n - R^n)\psi_K\varphi^n dx + \int_K\left(\bar{f}^n-\frac{U_h^n-U_h^{n-1}}{k_n}\right)\psi_K\varphi^n dx \\ &= \int_K(\mathcal{P}_K R^n - R^n)\psi_K\varphi^n dx + \int_K\left(\frac{U_*^n-U_h^n}{k_n}\right)\psi_K\varphi^n dx \\ &\quad + (\beta_h\nabla U_*^n,\nabla\psi_K\varphi^n)_K. \end{aligned} \tag{3.33}$$

Since $U_h^n \in \mathbb{P}_1(K)$ and $\psi_K = 0$ on ∂K, an integration by parts implies $(\beta\nabla U_h^n, \nabla\psi_K\varphi^n)_K = 0$. Thus, (3.33) can be rewritten as

$$\gamma_0\|\mathcal{P}_K R^n\|_{L^2(K)} \leq \int_K(\mathcal{P}_K R^n - R^n)\psi_K\varphi^n dx + \int_K\left(\frac{U_*^n-U_h^n}{k_n}\right)\psi_K\varphi^n dx$$

TH-2911_136123010

$$+(\beta_h\nabla(U_*^n-U_h^n),\nabla\psi_K\varphi^n)_K.$$

By the Cauchy-Schwarz inequality, the above inequality gives

$$\begin{aligned}\gamma_0\|\mathcal{P}_KR^n\|_{L^2(K)} &\leq \|\mathcal{P}_KR^n-R^n\|_{L^2(K)}\|\psi_K\varphi^n\|_{L^2(K)}+\frac{1}{k_n}\|U_*^n-U_h^n\|_{L^2(K)}\|\psi_K\varphi^n\|_{L^2(K)}\\ &\quad+|||U_*^n-U_h^n|||_K\,|||\psi_K\varphi^n|||_K.\end{aligned}$$

By the inverse estimate $|||\psi_K\varphi^n|||_K\leq C_{2,2}h_K^{-1}$ and (3.28), we obtain

$$\begin{aligned}\gamma_0\|\mathcal{P}_KR^n\|_{L^2(K)} &\leq \|\mathcal{P}_KR^n-R^n\|_{L^2(K)}+\frac{1}{k_n}\|U_*^n-U_h^n\|_{L^2(K)}+C_{2,2}h_K^{-1}|||U_*^n-U_h^n|||_K\\ &\leq \|\mathcal{P}_KR^n-R^n\|_{L^2(K)}\\ &\quad+C_{2,2}\,\hat{\mathcal{C}}_n^{1/2}h_K^{-1}\left(\frac{1}{k_n}\|U_*^n-U_h^n\|_{L^2(K)}^2+|||U_*^n-U_h^n|||_K^2\right)^{1/2}.\end{aligned}\tag{3.34}$$

Again, we use the Cauchy-Schwarz inequality and (3.34) to have

$$\begin{aligned}h_K^2\|R^n\|_{L^2(K)}^2 &\leq h_K^2\,\|\mathcal{P}_KR^n-R^n\|_{L^2(K)}^2+h_K^2\,\|\mathcal{P}_KR^n\|_{L^2(K)}^2\\ &\leq C_{2,3}h_K^2\,\|R^n-\mathcal{P}_KR^n\|_{L^2(K)}^2\\ &\quad+C_{2,3}\,\hat{\mathcal{C}}_n\left\{\frac{1}{k_n}\|U_*^n-U_h^n\|_{L^2(K)}^2+|||U_*^n-U_h^n|||_K^2\right\},\end{aligned}\tag{3.35}$$

where the constant $C_{2,3}=\max\left\{(1+1/\gamma_0^2),C_{2,2}^2/\gamma_0^2\right\}$.

For $K\in\mathcal{T}_\Gamma^n$, instead of (3.33) we will have

$$\begin{aligned}\gamma_0\|\mathcal{P}_KR^n\|_{L^2(K)} &\leq \int_K(\mathcal{P}_KR^n-R^n)\psi_K\varphi^n dx+\int_K\left(\frac{U_*^n-U_h^n}{k_n}\right)\psi_K\varphi^n dx\\ &\quad+(\beta_K\nabla U_*^n,\nabla\psi_K\varphi^n)_K-(\beta_h\nabla U_h^n,\nabla\psi_K\varphi^n)_K\\ &= \int_K(\mathcal{P}_KR^n-R^n)\psi_K\varphi^n dx+\int_K\left(\frac{U_*^n-U_h^n}{k_n}\right)\psi_K\varphi^n dx\\ &\quad+(\beta_K\nabla(U_*^n-U_h^n),\nabla\psi_K\varphi^n)_K+((\beta_K-\beta)\nabla U_h^n,\nabla\psi_K\varphi^n)_K.\end{aligned}$$

Again, using the Cauchy-Schwarz inequality and the inverse estimate $|||\psi_K\varphi^n|||_K\leq C_{2,2}h_K^{-1}$, the above inequality implies

$$\begin{aligned}\gamma_0\|\mathcal{P}_KR^n\|_{L^2(K)} &\leq \|\mathcal{P}_KR^n-R^n\|_{L^2(K)}+\frac{1}{k_n}\|U_*^n-U_h^n\|_{L^2(K)}\\ &\quad+C_{2,2}h_K^{-1}|||U_*^n-U_h^n|||_K+C_{2,2}h_K^{-1}|||\beta_K-\beta|^{\frac{1}{2}}\nabla U_h^n\|_{L^2(K)},\end{aligned}$$

which with an aid of (3.28) leads to

$$\gamma_0\|\mathcal{P}_KR^n\|_{L^2(K)} \leq \|\mathcal{P}_KR^n-R^n\|_{L^2(K)}$$

TH-2911_136123010

$$+ C_{2,2}\,\hat{\mathcal{C}}_n^{1/2} h_K^{-1}\left(\frac{1}{k_n}\|U_*^n - U_h^n\|^2_{L^2(K)} + |||U_*^n - U_h^n|||^2_K\right)^{1/2}$$

$$+ C_{2,2}\, h_K^{-1}\||\beta_K - \beta|^{\frac{1}{2}}\nabla U_h^n\|_{L^2(K)}. \tag{3.36}$$

Now using (3.36) we obtain

$$\begin{aligned} h_K^2\|R^n\|^2_{L^2(K)} &\leq C_{2,3}h_K^2\,\|R^n - \mathcal{P}_K R^n\|^2_{L^2(K)} + C_{2,3}\||\beta_K - \beta|^{\frac{1}{2}}\nabla U_h^n\|^2_{L^2(K)} \\ &\quad + C_{2,3}\,\hat{\mathcal{C}}_n\Big\{\frac{1}{k_n}\|U_*^n - U_h^n\|^2_{L^2(K)} + |||U_*^n - U_h^n|||^2_K\Big\}, \end{aligned} \tag{3.37}$$

where the constant $C_{2,3}$ is defined as above.

Let $\psi_e = 4\lambda_1\lambda_2$ be the edge bubble function for any edge $e \in \mathcal{E}^n$, where λ_i $(i = 1, 2)$ is the barycentric coordinate functions associated with the node of e. Let $\psi^n = J_e^n\psi_e \in H_0^1(\Omega)$. Then, ψ^n satisfies the following properties: For all $K \in \Omega_e$, we have

$$\|\nabla\psi^n\|_{L^2(K)} \leq C_{2,4}h_e^{-\frac{1}{2}}\|J_e^n\|_{L^2(e)} \quad \text{and} \quad \|\psi^n\|_{L^2(K)} \leq C_{2,5}h_e^{\frac{1}{2}}\|J_e^n\|_{L^2(e)}. \tag{3.38}$$

We now write

$$\sum_{e\in\mathcal{E}^n} h_e\|J_e^n\|^2_{L^2(e)} = \sum_{e\in\mathcal{E}_\Gamma^n} h_e\|J_e^n\|^2_{L^2(e)} + \sum_{e\in\mathcal{E}^n\setminus\mathcal{E}_\Gamma^n} h_e\|J_e^n\|^2_{L^2(e)}. \tag{3.39}$$

For $e \in \mathcal{E}^n \setminus \mathcal{E}_\Gamma^n$, using the fact J_e^n is constant on e, $\|\phi\|_e \leq C_{2,6}\|\psi_e^{\frac{1}{2}}\phi\|_e$, (3.27) and integration by parts, we get

$$\begin{aligned} \|J_e^n\|^2_{L^2(e)} &\leq C_{2,6}\int_e J_e^n\psi^n dx \\ &= -C_{2,6}\sum_{K\in\Omega_e}\int_K \beta_h(x)\nabla U_h^n\cdot\nabla\psi^n dx. \\ &= C_{2,6}\sum_{K\in\Omega_e}\int_K \beta_h\nabla(U_*^n - U_h^n)\cdot\nabla\psi^n dx - C_{2,6}\sum_{K\in\Omega_e}\int_K R^n\psi^n dx \\ &\leq C_{2,6}\left(\sum_{K\in\Omega_e}\|\nabla(U_*^n - U_h^n)\|_{L^2(K)}\|\nabla\psi^n\|_{L^2(K)} + \sum_{K\in\Omega_e}\|R^n\|_{L^2(K)}\|\psi^n\|_{L^2(K)}\right). \end{aligned} \tag{3.40}$$

We apply (3.38) and the Young's inequality to obtain

$$h_e\|J_e^n\|^2_{L^2(e)} \leq C_{2,6}\left(C_{2,4}^2\sum_{K\in\Omega_e}|||U_*^n - U_h^n|||^2_K + C_{2,5}^2\sum_{K\in\Omega_e}h_K^2\|R^n\|^2_{L^2(K)}\right)^{\frac{1}{2}}\times\left(h_e\|J_e^n\|^2_{L^2(e)}\right)^{\frac{1}{2}},$$

which gives

$$h_e\|J_e^n\|^2_{L^2(e)} \leq C_{2,6}^2\left(C_{2,4}^2\sum_{K\in\Omega_e}|||U_*^n - U_h^n|||^2_K + C_{2,5}^2\sum_{K\in\Omega_e}h_K^2\|R^n\|^2_{L^2(K)}\right). \tag{3.41}$$

TH-2911_136123010

For $e \in \mathcal{E}_\Gamma^n$, instead of (3.40) one obtains

$$\begin{aligned}
\|J_e^n\|_{L^2(e)}^2 &\leq -C_{2,6} \sum_{K\in\Omega_e^\Gamma} \int_K \beta_K \nabla U_h^n \cdot \nabla \psi^n dx \\
&= C_{2,6} \sum_{K\in\Omega_e^\Gamma} \int_K \beta_K \nabla (U_*^n - U_h^n) \cdot \nabla \psi^n dx - C_{2,6} \sum_{K\in\Omega_e^\Gamma} \int_K R^n \psi^n dx \\
&\quad - C_{2,6} \int_e \bar{g}_h^n \psi^n ds + C_{2,6} \sum_{K\in\Omega_e^\Gamma} \int_K (\beta_K - \beta) \nabla U_h^n \cdot \nabla \psi^n dx \\
&\leq C_{2,6} \Bigg(\sum_{K\in\Omega_e^\Gamma} \|\nabla (U_*^n - U_h^n)\|_{L^2(K)} \|\nabla \psi^n\|_{L^2(K)} + \sum_{K\in\Omega_e^\Gamma} \|R^n\|_{L^2(K)} \|\psi^n\|_{L^2(K)} \\
&\quad + \|\bar{g}_h^n\|_{L^2(e)} \|\psi^n\|_{L^2(e)} + \sum_{K\in\Omega_e^\Gamma} \||\beta_K - \beta|^{1/2} \nabla U_h^n\|_{L^2(K)} \|\nabla \psi^n\|_{L^2(K)} \Bigg).
\end{aligned}$$

Using (3.38) and the Young's inequality, a simple calculation yields

$$\begin{aligned}
h_e \|J_e^n\|_{L^2(e)}^2 &\leq C_{2,6}^2 \Bigg(C_{2,4}^2 \sum_{K\in\Omega_e^\Gamma} |||U_*^n - U_h^n|||_K^2 + C_{2,5}^2 \sum_{K\in\Omega_e^\Gamma} h_K^2 \|R^n\|_{L^2(K)}^2 \\
&\quad + h_e \|\bar{g}_h^n\|_{L^2(e)}^2 + C_{2,4}^2 \sum_{K\in\Omega_e^\Gamma} \||\beta_K - \beta|^{1/2} \nabla U_h^n\|_{L^2(K)}^2 \Bigg). \qquad (3.42)
\end{aligned}$$

Taking (3.35) and (3.41), for any $K \in \mathcal{T}^n \setminus \mathcal{T}_\Gamma^n$, we have

$$\begin{aligned}
\eta_{2,K}^n &\leq C_{2,7} \sum_{K\in\Omega_e} h_K^2 \|R^n - \mathcal{P}_K R^n\|_{L^2(K)}^2 \\
&\quad + C_{2,8} \hat{\mathcal{C}}_n \sum_{K\in\Omega_e} \left(\frac{1}{k_n} \|U_*^n - U_h^n\|_{L^2(K)}^2 + |||U_*^n - U_h^n|||_K^2 \right), \qquad (3.43)
\end{aligned}$$

where the constants $C_{2,7} = (1 + C_{2,6}^2 C_{2,5}^2) C_{2,3}$ and $C_{2,8} = \max\{C_{2,7}, C_{2,7} + C_{2,6}^2 C_{2,4}^2\}$. Again, for all $K \in \mathcal{T}_\Gamma^n$, (3.37) and (3.42) gives

$$\begin{aligned}
\eta_{2,K}^n &\leq C_{2,7} \sum_{K\in\Omega_e^\Gamma} h_K^2 \|R^n - \mathcal{P}_K R^n\|_{L^2(K)}^2 \\
&\quad + C_{2,8} \hat{\mathcal{C}}_n \sum_{K\in\Omega_e^\Gamma} \left(\frac{1}{k_n} \|U_*^n - U_h^n\|_{L^2(K)}^2 + |||U_*^n - U_h^n|||_K^2 \right) \\
&\quad + C_{2,9} \sum_{e\subset\partial K} h_e \|\bar{g}_h^n\|_{L^2(e)}^2 + C_{2,7} \sum_{K\in\Omega_e^\Gamma} \||\beta_K - \beta|^{1/2} \nabla U_h^n\|_{L^2(K)}^2, \qquad (3.44)
\end{aligned}$$

where the constants $C_{2,7}, C_{2,8}$ are defined as above and $C_{2,9} = (1 + C_{2,6}^2)$. Finally, (3.43) and (3.44) lead to the desired estimates (3.31) and (3.32). This completes the proof. □

TH-2911_136123010

Remark 3.3.3. *Taking summation over all elements $K \in \mathcal{T}^n$, from (3.43) and (3.44), we have*

$$\eta^n_{2,space} = C_{2,7}\ osc(R^n, \mathcal{T}^n) + C_{2,8}\hat{\mathcal{C}}_n \|U^n_* - U^n_h\|^2_{k_n,\Omega} + C_{2,9}\sum_{e\in\mathcal{E}^n_\Gamma} h_e \|\bar{g}^n_h\|^2_{L^2(e)} + C_{2,7}\sum_{K\in\mathcal{T}^n_\Gamma} \||\beta_K - \beta|^{1/2}\nabla U^n_h\|^2_{L^2(K)},$$

where the oscillation of residual $osc(R^n, \mathcal{T}^n)$ and the weighted norm $\|U^n_* - U^n_h\|_{k_n,\Omega}$ are defined in (3.29) and (3.30), respectively.

3.4 Adaptive Algorithm

In this section, we present an algorithm to describe the adaptive procedure for the problem (3.1)-(3.3). Let ϵ_{time} be the total tolerance for the time discretization which is a part of the *a posteriori* error estimate (3.11). Based on the error equidistribution strategy of [29, 94], from (3.11) we write

$$\begin{cases} \displaystyle\sum_{n=1}^{N} k_n \eta^n_{2,\text{time}} + 4\left(\sum_{n=1}^{N}\int_{t_{n-1}}^{t_n} \|f - f^n\|_{L^2(\Omega)}dt\right)^2 \\ \qquad + \ 4\left(\displaystyle\sum_{n=1}^{N}\int_{t_{n-1}}^{t_n} \|g - \bar{g}^n_h\|_{L^2(\Gamma)}dt\right)^2 \le \epsilon_{\text{time}}. \end{cases} \tag{3.45}$$

To get (3.45) we need to adjust the time-step size k_n such that the following holds:

$$\begin{cases} \eta^n_{2,\text{time}} \le \dfrac{\epsilon_{\text{time}}}{3T}, \qquad \dfrac{1}{k_n}\displaystyle\int_{t_{n-1}}^{t_n} \|f - f^n\|_{L^2(\Omega)}dt \le \dfrac{\sqrt{\epsilon_{\text{time}}}}{2\sqrt{3}T}, \\ \dfrac{1}{k_n}\displaystyle\int_{t_{n-1}}^{t_n} \|g - \bar{g}^n_h\|_{L^2(\Gamma)}dt \le \dfrac{\sqrt{\epsilon_{\text{time}}}}{2\sqrt{3}T}. \end{cases} \tag{3.46}$$

To control the time-step size for this problem, for any given $\delta_{\text{time}} \in (0,1)$, we have

$$\begin{cases} \eta^n_{2,\text{time}} \le \delta_{\text{time}}\dfrac{\epsilon_{\text{time}}}{3T}, \qquad \dfrac{1}{k_n}\displaystyle\int_{t_{n-1}}^{t_n} \|f - \bar{f}^n\|_{L^2(\Omega)}dt \le \dfrac{\sqrt{\delta_{\text{time}}\epsilon_{\text{time}}}}{2\sqrt{3}T}, \\ \dfrac{1}{k_n}\displaystyle\int_{t_{n-1}}^{t_n} \|g - \bar{g}^n_h\|_{L^2(\Gamma)}dt \le \dfrac{\sqrt{\delta_{\text{time}}\epsilon_{\text{time}}}}{2\sqrt{3}T}. \end{cases} \tag{3.47}$$

Let ϵ_{space} be the tolerance related to the space discretization. Then for each time step n, the stopping criterion for mesh adaptation is given by

$$\eta^n_{2,\text{space}} \le \frac{\epsilon_{\text{space}}}{T}, \tag{3.48}$$

TH-2911_136123010

which is suitable for mesh refinements but not for mesh coarsening.

Following Remark 2.4.1 of Chapter 2, we now define the coarsening error indicator

$$\eta^n_{2,coarse} = \frac{1}{k_n}\|I^n_H U^n_h - U^n_h\|^2_{L^2(\Omega)} + |||I^n_H U^n_h - U^n_h|||^2_{\Omega}, \tag{3.49}$$

where $I^n_H : C(\bar{\Omega}) \to S^n_H$ is the standard linear interpolation operator, $\mathcal{T}^n_H$ be the coarsening of the mesh $\mathcal{T}^n$, and $U^n_H \in S^n_H$ be the solutions of the discrete problem (3.5) over the meshe $\mathcal{T}^n_H$. It is observed that $\eta^n_{2,coarse}$ does not depend on U^n_H.

Inviting the refinement strategies of Dörfler [43, 44] and Morin *et al.* [83], we have the following algorithm.

Algorithm 3.4.1. (Space and time adaptive algorithm). Given tolerances ϵ_{time} and ϵ_{space}, parameters $\gamma_1 \in (0,1)$, $\gamma_2 > 1$ and $\delta_{\text{time}} \in (0,1)$. Let U^{n-1}_h be the computed value at time t_{n-1} with the time step size k_n and the mesh $\mathcal{T}^{n-1}$.

Step 1: $\mathcal{T}^n := \mathcal{T}^{n-1}$, $k_n := k_{n-1}$, $t_n := t_{n-1} + k_n$
solve the fully discrete problem (3.5) for U^n_h on $\mathcal{T}^n$
compute the error estimates on $\mathcal{T}^n$

Step 2: while (3.46) is not satisfied do
{
$k_n := \gamma_1 k_n$, $t_n := t_{n-1} + k_n$
solve the fully discrete problem (3.5) for U^n_h on $\mathcal{T}^n$
compute the error estimates on $\mathcal{T}^n$
} end while

Step 3: while ($\eta^n_{2,\text{space}} > \frac{\epsilon_{\text{space}}}{T}$) do
{
refine $\mathcal{T}^n$ to produce the modified mesh $\hat{\mathcal{T}}^n$
solve the fully discrete problem (3.5) for U^n_h on $\hat{\mathcal{T}}^n$
compute the error estimates on $\hat{\mathcal{T}}^n$
while (3.46) is not satisfied do
{
$k_n := \gamma_1 k_n$, $t_n := t_{n-1} + k_n$
solve the fully discrete problem (3.5) for U^n_h on $\hat{\mathcal{T}}^n$
compute the error on $\hat{\mathcal{T}}^n$
}end while
}end while

TH-2911_136123010

Step 4: if $(\eta^n_{2,\text{coarse}} \leq \frac{\epsilon_{\text{coarse}}}{T})$

coarsen $\mathcal{T}^n$ to produce a modified mesh $\hat{\mathcal{T}}^n$

solve the fully discrete problem (3.5) for U^n_h on $\hat{\mathcal{T}}^n$

Step 5: if (3.47) is satisfied then

$\{k_n = \gamma_2 k_n\ \}$

end

end

3.5 Numerical Experiment

This section provides numerical experiment to demonstrate the performence of the estimators derived in Theorem 3.3.1 for the problem (3.1)-(3.3). All computations are carried out using the software FreeFEM++ [65].

Example 3.1. We consider the interface problem (3.1)-(3.3) defined on $\Omega_T = \Omega \times [0,T]$, where the computational domain $\Omega = (-1,1) \times (-1,1)$ and the time $T = 0.1$. The interface Γ is chosen to be a circle centered at $(0,0)$ with radius $r_0 = \frac{\pi}{6.28}$ which divides the domain Ω into two subdomains $\Omega_1 = \{x^2 + y^2 < {r_0}^2\}$ and $\Omega_2 = \{x^2 + y^2 > {r_0}^2\}$, respectively.

We now choose the forcing term f and the flux jump g such that the exact solution is given by

$$u(x,y,t) = \begin{cases} \frac{(x^2+y^2)}{\beta_1} e^t, & \text{if } (x,y) \in \Omega_{1,T}, \\ \frac{(x^2+y^2)}{\beta_2} e^t + \left(\frac{r_0^2}{\beta_1} - \frac{r_0^2}{\beta_2}\right) e^t + \kappa(\sqrt{x^2+y^2} - r_0)e^t, & \text{if } (x,y) \in \Omega_{2,T}, \end{cases}$$

where $\Omega_{1,T} = \Omega_1 \times [0,T]$, $\Omega_{1,T} = \Omega_2 \times [0,T]$ and the positive quantity κ is chosen to be 10. Here, we consider two choices for the discontinuous coefficients β: (i) $\beta_1 = 1, \beta_2 = 10$, and (ii) $\beta_1 = 1, \beta_2 = 100$.

All the constants involved in the estimators are taken as 1. We choose the parameters $\gamma_1 = 0.5, \gamma_2 = 2$ and $\delta_{time} = 0.5$ in Algorithm 3.4.1. The tolerances $\epsilon_{time}, \epsilon_{space}, \epsilon_{coarse}$ are chosen to be equal, say ϵ. We compute the energy error

$$Err = \left(\sum_{n=1}^{N} k_n |||u - U^n_h|||^2_\Omega \right)^{1/2},$$

the error estimator $\eta_{2,1}$ which is given by

$$\eta^2_{2,1} = \sum_{n=1}^{N} k_n (\eta^n_{2,time} + \eta^n_{2,space} + \eta^n_{2,coarse}) + 4 \left(\sum_{n=1}^{m} \int_{t_{n-1}}^{t_n} \|f - f^n\|_{L^2(\Omega)} \right)^2$$

TH-2911_136123010

$$+ 4 \left(\sum_{n=1}^{m} \int_{t_{n-1}}^{t_n} \|g - \bar{g}_h^n\|_{L^2(\Gamma)} \right)^2$$

and the effectivity index (eff. index $= \eta_{2,1}/Err$) of *a posteriori* error estimate.

Table 3.1: The degrees of freedom (DOF), the error estimator $\eta_{2,1}$ and the energy error (Err) with various discontinuous coefficients β when time $t = 0.1$ and tolerance $\epsilon = 0.01$.

β	DOF	$\eta_{2,1}$	Err
$\beta_1 = 1$	694	0.351962	0.133652
$\beta_2 = 10$	1305	0.172799	0.071804
	2625	0.086004	0.036457
$\beta_1 = 1$	716	3.513145	0.132988
$\beta_2 = 100$	1408	1.730870	0.065960
	2812	0.860290	0.033543

Table 3.2: The different tolerances ϵ, the degrees of freedom (DOF), the error estimator $\eta_{2,1}$, the energy error (Err) and the effectivity index (eff. index) with various discontinuous coefficients β at time $t = 0.1$.

ϵ	β	DOF	$\eta_{2,1}$	Err	eff. index
0.01		2625	0.086004	0.036457	2.3591
0.005	$\beta_1 = 1$	4919	0.043124	0.018269	2.3605
0.0025	$\beta_2 = 10$	9898	0.023956	0.008924	2.6845
0.01		2812	0.860290	0.033543	25.6473
0.005	$\beta_1 = 1$	5027	0.429425	0.017812	24.1088
0.0025	$\beta_2 = 100$	9000	0.220412	0.008824	24.9787

The adaptive mesh and the corresponding surface plots of the numerical solution at time $t = 0.1$ with $\beta_1 = 1$ and $\beta_2 = 10$ are shown in Figures 3.2-3.4. In Table 3.1, for both the choices of β, the degrees of freedom (DOF), the error indicator ($\eta_{2,1}$), the

TH-2911_136123010

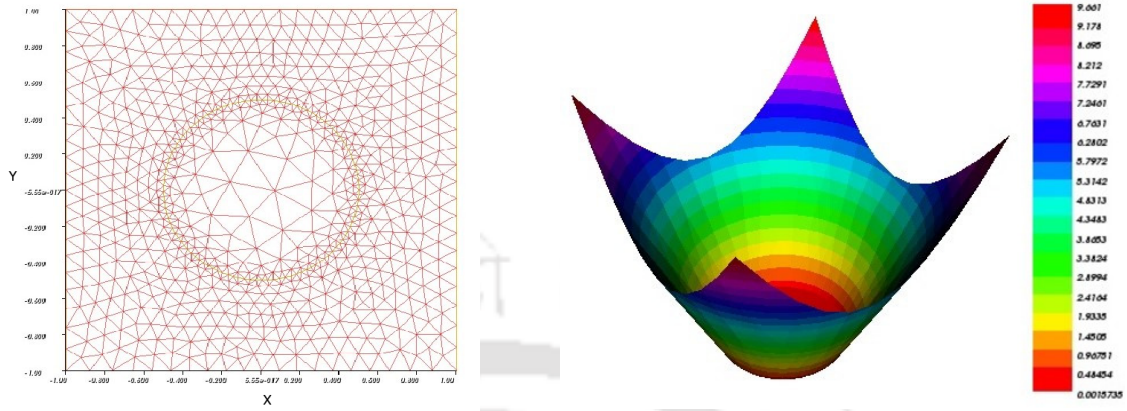

Figure 3.2: An adaptive mesh and the corresponding discrete solution at step 1.

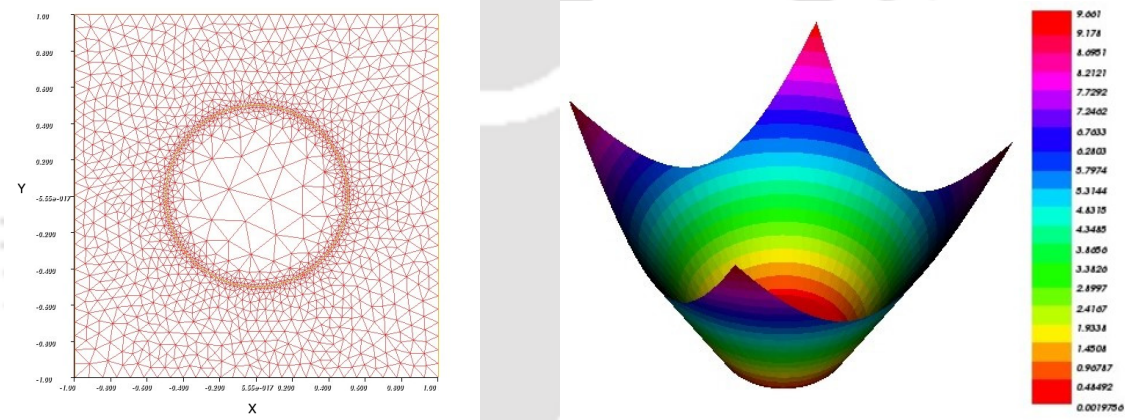

Figure 3.3: An adaptive mesh and the corresponding discrete solution at step 2.

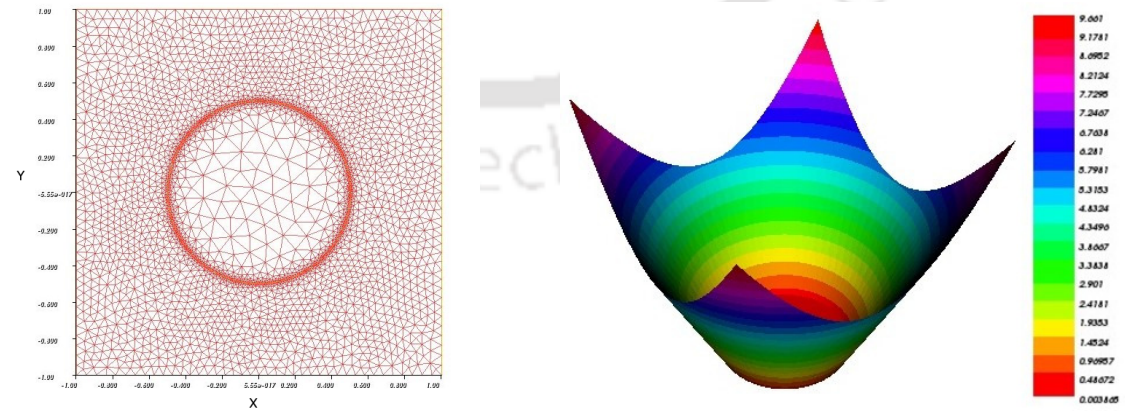

Figure 3.4: An adaptive mesh and the corresponding discrete solution at step 3.

TH-2911_136123010

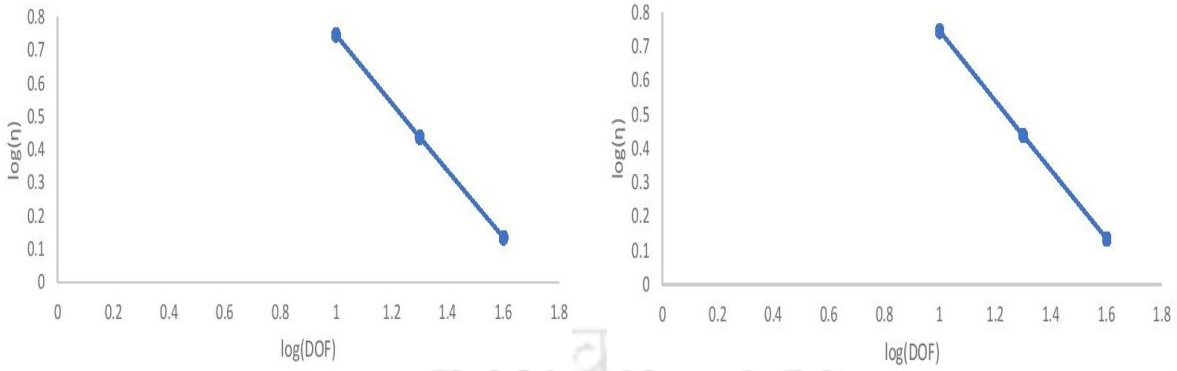

(a) (b)

Figure 3.5: Optimality of the estimator for the cases: (a) $\beta_1 = 1$, $\beta_2 = 10$ and (b) $\beta_1 = 1$, $\beta_2 = 100$. The optimal decay is observed by the line of slope -1.006 (left) and the line of slope -1.008 (right).

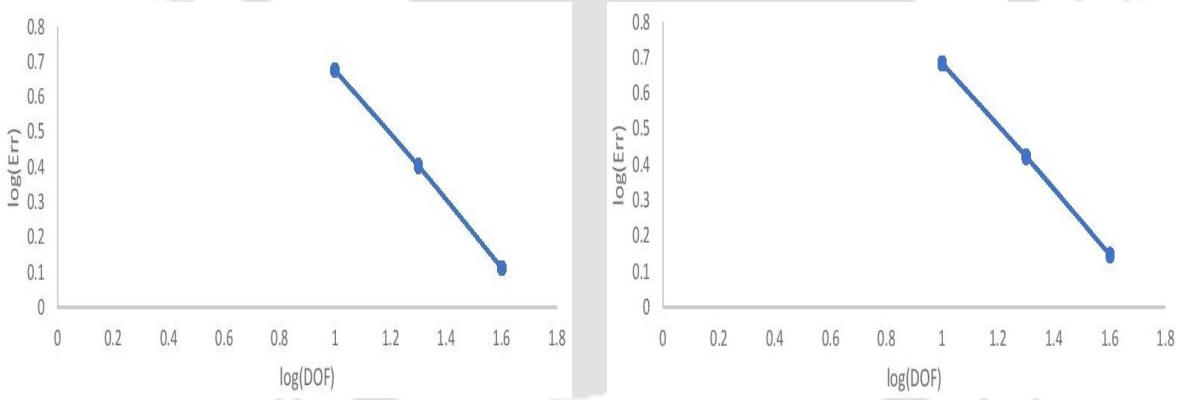

(a) (b)

Figure 3.6: Energy error versus number of degrees of freedom: (a) $\beta_1 = 1{,}0$ $\beta_2 = 10$ and (b) $\beta_1 = 1$, $\beta_2 = 100$. The quasi-optimal decay is observed by the line of slope -0.837 (left) and the line of slope -0.893 (right).

energy error (Err) and the effectivity index (eff. index) are given in each step of the adaptive mesh generation at the final time $t = 0.1$ with tolerance $\epsilon = 0.01$. At the time $t = 0.1$ for various discontinuous coefficients β with different tolerances ϵ, the degrees of freedom, the energy error, and the effectivity index are presented in Table 3.2. The plots comparing the degrees of freedom with the total error estimator for both the cases

TH-2911_136123010

are shown in Figure 3.5. The optimal decay of the estimator is observed by the line of slope -1.006 for the choice $\beta_1 = 1, \beta_2 = 10$ (see Figure 3.5 (a)) and the line of slope -1.008 for the choice $\beta_1 = 1, \beta_2 = 100$ (see Figure 3.5 (b)). Further, in Figure 3.6, we provide plots for the energy error versus the number of degrees of freedom. In Table 3.2, we observe that for a fixed time but different tolerances both the value of the indicator and the error are reducing. It is noticed that the finite element mesh away from the interface Γ is coarse due to different behavior in the subdomains and the initial mesh is adaptively refined. Figures 3.2-3.4 reveal that the finite element mesh adapts very well in the neighborhood of the interface Γ and higher density of the node points distributed along the interfacing circle.

3.6 Concluding Remarks

In this chapter, we have considered an AIFEM for solving the PIP with a nonzero flux jump. An unfitted finite element mesh is used to discretize the domain where the mesh points need not follow the interface. New error indicators are introduced to control the error due to unfitted discretization. We have derived both *a posteriori* upper and lower bounds for the error. We observe that the finite element mesh is adaptively refined and higher density of nodes along the interface Γ. It is noticed that the mesh away from the interface Γ is relatively coarser just because of different behaviors in the subdomains. Our numerical experiment indicates the effectiveness of the proposed adaptive algorithm. The present analysis extends the work of [31] from elliptic interface problems to PIPs.

TH-2911_136123010

4

An AFEM for PIPs using Nonconforming Finite Elements

This chapter is devoted to the *a posteriori* error estimates of the linear PIP using nonconforming finite elements in a convex polygonal domain. The piecewise nonconforming finite elements are used for the approximation of the spatial variables and the backward Euler method is applied for the time discretization. We derive both upper and lower bounds for the error in the energy norm. The present approach does not involve the Helmholtz decomposition while analyzing the reliability of the estimator. The constants involved in the estimators are independent of the jump of the diffusion coefficient across the interface, and the quasi-monotonocity assumption on the diffusion coefficient is relaxed. The reliability bound of the estimator consists of the element residual, the edge flux jump and the edge solution jump. An adaptive space-time algorithm is prescribed using the derived estimators. Numerical results illustrating the behavior of the estimators are provided.

4.1 Introduction

We begin by rewriting the parabolic interface problems of the form

$$\frac{\partial u}{\partial t} - \nabla \cdot (\beta(x)\nabla u) = f(x,t) \quad \text{in} \quad \Omega_T \tag{4.1}$$

with the initial and boundary conditions

$$u(x,0) = u_0(x) \quad \text{in} \quad \Omega; \qquad u = \mathcal{G}(x,t) \quad \text{on} \quad \partial\Omega_T, \tag{4.2}$$

and jump conditions across the interface Γ

$$[u] = 0, \quad \left[\beta \frac{\partial u}{\partial \mathbf{n}}\right] = 0, \tag{4.3}$$

TH-2911_136123010

where $\Omega_T = \Omega \times (0,T]$ and $\partial\Omega_T = \partial\Omega \times [0,T]$ with $T < \infty$. Here Ω is a bounded convex polygonal domain in $\mathbb{R}^2$ with a Lipschitz continuous boundary $\partial\Omega$, Ω_1 is an open and polygonal subdomain of Ω with boundary $\partial\Omega_1 := \Gamma$ (interface) and $\Omega_2 = \Omega\backslash\Omega_1$. Further, we assume that the coefficient function β is positive and piecewise constant in each subdomain, i.e.,

$$\beta(x) = \beta_i \quad \text{for} \quad x \in \Omega_i \ (i = 1, 2).$$

Here, $f \in L^2(0,T,L^2(\Omega))$, u_0 and $\mathcal{G}(x,t)$ are assumed to be smooth for our purpose.

For the purpose of finite element approximation of the problem (4.1)-(4.2) using nonconforming elements, we now introduce its weak formulation as follows: Find $u : [0,T] \to H^1_{\mathcal{G}}(\Omega)$ such that

$$\begin{aligned} \left(\frac{\partial u}{\partial t}, \phi\right) + a(u,\phi) &= (f,\phi) \quad \forall \phi \in H^1_0(\Omega), \\ u(0) &= u_0, \end{aligned} \tag{4.4}$$

where $H^1_{\mathcal{G}}(\Omega) = \{v \in H^1(\Omega) \,|\, v = \mathcal{G} \text{ on } \partial\Omega\}$. Here, $a(v,w)$ is a bilinear form on $H^1(\Omega)$ defined by $a(v,w) = (\beta\nabla v, \nabla w)$. We assume that the bilinear form $a(\cdot,\cdot)$ is continuous on $H^1(\Omega)$, i.e., there exist constants $\alpha_0 > 0$ such that

$$|a(v,w)| \le \alpha_0 \|v\|_{H^1(\Omega)} \|w\|_{H^1(\Omega)} \quad \forall v, w \in H^1(\Omega), \tag{4.5}$$

A posteriori error analysis for nonconforming finite element methods has been investigated by [4, 20, 22, 26, 37, 38, 66, 93] for elliptic problems and [84] for parabolic problems. Using the Helmholtz decomposition of the true error, the authors of [38] have established the reliability bound of the estimator for the Poisson equation which has been subsequently adopted by many researchers (cf. [4, 22, 26, 37]). The reliable estimator involves the element residual, the edge flux jump and the edge tangential derivative jump. In [13], Bernardi and Verfürth have derived the *a posteriori* error estimates under the quasi-monotone assumption on the diffusion coefficient. The idea of Helmholtz decomposition of the error was used by Nicaise and Soualem [84] to derive *a posteriori* error estimates for nonconforming finite element approximation of the heat equation. Recently, for elliptic interface problems, Cai *et al.* [20] have derived robust residual-based *a posteriori* error estimates using nonconforming elements. The reliability bound for the *a posteriori* error estimator is established without using the Helmholtz decomposition and the quasi-monotonicity assumption on the diffusion coefficient in [20]. It is known that for the conforming linear element, the degrees of freedom are the nodal values at vertices of triangles. The nodal value of the modified Clément type interpolation is defined by the average value of the function over connected elements whose corresponding diffusion coefficients are the greatest. A key advantage for

TH-2911_136123010

the nonconforming linear element is that its degrees of freedom are nodal values at the middle points of edges of triangles and that each middle point is shared by at most two triangles. A modified Clément type interpolation is constructed to satisfy the desired properties without the quasi-monotonicity assumption.

The intent of this chapter is to extend the *a posteriori* error analysis of nonconforming FEM for elliptic interface problems [20] to the parabolic interface problem (4.1)-(4.2). The interface is assumed to be time-independent. We derived both upper and lower bounds for the *a posteriori* error using energy arguments. The upper bound for the error is derived without using the Helmholtz decomposition and the quasi-monotone assumption on the diffusion coefficients; and is bounded by the element residual, the edge flux jump, and the edge solution jump. The key technical tools used in deriving the robust reliability bound include the representation of the error equation (4.25), the approximation of the modified Clément-type interpolation operator and the trace inequality. A lower bound for the local error in terms of the space error indicator is established using the strategy of [29]. A space-time adaptive algorithm is presented using the derived estimators. A numerical result is reported to illustrate the behavior of the derived estimators.

The rest of this chapter is planned as follows: Section 4.2 contains the space-time nonconforming finite element discretization. This section also introduces jump and average over edges, and error indicators. The global upper and local lower bounds for the error are derived in Section 4.3. Section 4.4 provides an adaptive space-time algorithm using derived estimators. In Section 4.5, numerical results are provided to demonstrate the behavior of the estimators. Finally, we present some concluding remarks in the last section.

4.2 Space-Time Nonconforming Finite Element Discretization

In this section, we first define the space-time nonconforming finite element spaces. For the space-time discretization, we partition the time interval $(0, T]$ into N number of subintervals $\{(t_{n-1}, t_n]\}_{n=1}^{N}$ such that $0 = t_0 < t_1 < \ldots < t_{n-1} < t_n = T$. Let $k_n = t_n - t_{n-1}$ be the time-step size of $(t_{n-1}, t_n]$. At each time step t_n, $n = 1, 2, \ldots, N$, let $\mathcal{T}_h^n$ be a regular triangulation of the domain $\bar{\Omega}$, i.e., $\forall K \in \mathcal{T}_h^n$, there exists a constant $\alpha_2 > 0$ such that $h_K \leq \alpha_2 \rho_K$, where h_K denote the diameter of the element K and ρ_K denote the diameter of the largest circle inscribed in K. A triangle $K \in \mathcal{T}_h^n$ is said to be an interface triangle if any edge or vertex of K lies on the interface Γ; otherwise K

TH-2911_136123010

is called a non-interface triangle. Let $\mathcal{T}_\Gamma^n$ denote the set of all interface triangles in $\mathcal{T}_h^n$. Let

$$\mathcal{N}_h^n = \mathcal{N}_{h,i}^n \cup \mathcal{N}_{h,b}^n \quad \text{and} \quad \mathcal{E}_h^n = \mathcal{E}_{h,i}^n \cup \mathcal{E}_{h,b}^n,$$

be the set of all vertices and edges of the triangulation $\mathcal{T}_h^n$, where

- $\mathcal{N}_{h,i}^n$ - the set of all interior vertices in $\mathcal{T}_h^n$
- $\mathcal{N}_{h,b}^n$ - the set of all vertices on the boundary $\partial\Omega$
- $\mathcal{E}_{h,i}^n$ - the set of all interior edges in $\mathcal{T}_h^n$
- $\mathcal{E}_{h,b}^n$ - the set of all edges on the boundary $\partial\Omega$.

For each $e \in \mathcal{E}_h^n$, let m_e be the mid-point of the edge e. Further, we assume that the interface $\Gamma = \partial\Omega_1 \cap \partial\Omega_2$ do not cut through any element $K \in \mathcal{T}_h^n$.

Let $S_{h,c}^n$ be the conforming finite element space on $\mathcal{T}_h^n$ defined by

$$S_{h,c}^n = \{\phi \in H^1(\Omega) : \phi|_K \in \mathbb{P}_1(K) \ \ \forall K \in \mathcal{T}_h^n\},$$

where $\mathbb{P}_1(K)$ is the space of piecewise linear polynomials of degree less than or equal to 1 on K, and

$$S_{h,\mathcal{G},c}^n = \{\phi \in S_{h,c}^n : \phi|_{\partial\Omega} = \mathcal{G}\},$$

is a subset of $S_{h,c}^n$. The nonconforming finite element space $S_{h,nc}^n$ (the Crouzeix-Raviart element [54]) associated with the triangulation $\mathcal{T}_h^n$ is given by

$$S_{h,nc}^n = \{\phi \in H^1(\Omega) : \phi|_K \in \mathbb{P}_1(K) \ \ \forall K \in \mathcal{T}_h^n, \ \phi \text{ is continuous at } m_e, \ \forall e \in \mathcal{E}_{h,i}^n\}$$

and its subset is defined by

$$S_{h,\mathcal{G},nc}^n = \{\phi \in S_{h,nc}^n : \phi(m_e) = \mathcal{G}(m_e) \ \ \forall e \in \mathcal{E}_{h,b}^n\}.$$

Let $S_{h,0,nc}^n = \{\phi \in S_{h,nc}^n : \phi(m_e) = 0 \ \ \forall e \in \mathcal{E}_{h,b}^n\}$. We now define the broken Sobolev space of degree 1 with respect to $\mathcal{T}_h^n$ by

$$H^1(\mathcal{T}_h^n) = \{\phi \in L^2(\Omega) : \phi|_K \in H^1(K), \ \forall K \in \mathcal{T}_h^n\}$$

and the corresponding bilinear form by

$$a_h(\phi, \psi) = \sum_{K \in \mathcal{T}_h^n} (\beta \nabla\phi, \nabla\psi)_K, \ \ \forall \phi, \psi \in H^1(\mathcal{T}_h^n)$$

TH-2911_136123010

equipped with the energy norm

$$|||\phi|||_\Omega = \sqrt{a_h(\phi,\phi)} = \left(\sum_{K\in\mathcal{T}_h^n} \|\beta^{\frac{1}{2}}\nabla\phi\|^2_{L^2(K)} \right)^{\frac{1}{2}}.$$

The fully discrete approximation of the exact solution $u(t)$ at $t = t_n$ in $S^n_{h,\mathcal{G},nc}$ is denoted by U^n_h. For any function ϕ continuous in $(t_{n-1}, t_n]$, let $\phi^n = \phi(\cdot, t_n)$ and $\bar{\phi}^n(\cdot) = k_n^{-1}\int_{t_{n-1}}^{t_n}\phi(\cdot,t)dt$. Let U^0_h be a suitable approximation of u_0 in the space $S^0_{h,\mathcal{G},nc}$ over the initial mesh $\mathcal{T}^0_h$.

In order to discretize the problem (4.4), we consider the piecewise linear non-confirming finite element space for the approximation of spatial variable and the backward Euler method is used for the time variable. The space-time nonconforming finite element approximation corresponding to (4.4) is stated as follows: Given $U^0_h \in S^0_{h,\mathcal{G},nc}$, find $U^n_h \in S^n_{h,\mathcal{G},nc}$ for $n = 1, 2, \cdots, N$, such that

$$\left(\frac{U^n_h - U^{n-1}_h}{k_n}, v\right) + a_h(U^n_h, v) = (\bar{f}^n, v), \quad \forall v \in S^n_{h,0,nc}. \tag{4.6}$$

4.2.1 Jump and Average

For $e \in \mathcal{E}^n_h$, let h_e be the length of edge e and let $\mathbf{n}_e$ be a unit vector normal to e. For $e \in \mathcal{E}^n_{h,b}$, let K^+_e be the boundary element with the edge e. For any $e \in \mathcal{E}^n_{h,i}$, let K^+_e and K^-_e be the two elements sharing the common edge e with

$$\beta^+_e \equiv \beta_{K^+_e} \geq \beta_{K^-_e} \equiv \beta^-_e.$$

For $e \in \mathcal{E}^n_h$, let $v|^+_e$ and $v|^-_e$ be the traces of the double valued function v over the edge e restricted on K^+_e and K^-_e, respectively. For any $\phi \in H^1(\mathcal{T}^n_h)$, which may be discontinuous across e, we define the normal flux jump by

$$[\beta\nabla\phi\cdot\mathbf{n}_e]_e := \begin{cases} (\beta\nabla\phi\cdot\mathbf{n}_e)|^+_e - (\beta\nabla\phi\cdot\mathbf{n}_e)|^-_e, & e \in \mathcal{E}^n_{h,i}, \\ 0, & e \in \mathcal{E}^n_{h,b}, \end{cases}$$

the jump over each edge $e \in \mathcal{E}^n_h$ by

$$[\phi]_e := \begin{cases} \phi|^+_e - \phi|^-_e, & e \in \mathcal{E}^n_{h,i}, \\ \phi|_e, & e \in \mathcal{E}^n_{h,b}, \end{cases}$$

TH-2911_136123010

and the average over edge $e \in \mathcal{E}_h^n$ by

$$\{\phi\}_e := \begin{cases} \frac{1}{2}(\phi|_e^+ + \phi|_e^-), & e \in \mathcal{E}_{h,i}^n, \\ \phi|_e, & e \in \mathcal{E}_{h,b}^n. \end{cases}$$

A simple calculation shows the following identity:

$$[\phi u]_e = \{\phi\}_e [u]_e + [\phi]_e \{u\}_e, \quad \forall e \in \mathcal{E}_{h,i}^n. \tag{4.7}$$

For any $v \in S_{h,0,nc}^n$, the following orthogonality property holds:

$$\int_e [v] ds = 0, \quad \forall e \in \mathcal{E}_{h,i}^n, \quad \text{and} \quad \int_e v \, ds = 0, \quad \forall e \in \mathcal{E}_{h,b}^n. \tag{4.8}$$

4.2.2 Indicators and Estimators

We now define three residuals for our present analysis namely, the element residual is defined as

$$R_K^n := \bar{f}^n - k_n^{-1}(U_h^n - U_h^{n-1}), \quad \forall K \in \mathcal{T}_h^n,$$

the numerical flux jump is defined as

$$J_{\sigma,e}^n := [\beta \nabla U_h^n \cdot \mathbf{n}_e]_e, \quad \forall e \in \mathcal{E}_h^n,$$

and the numerical solution jump is defined as

$$J_{u,e}^n := [U_h^n]_e, \quad \forall e \in \mathcal{E}_h^n.$$

For any $K \in \mathcal{T}_h^n$, let $\mathcal{N}_K^n$ and $\mathcal{E}_K^n$ denote the set of vertices and edges of K, respectively. We denote the element residual indicator by

$$\eta_{R_K,K}^n := \left(\frac{h_K^2}{\beta_K} \|R_K^n\|_{L^2(K)}^2 \right)^{\frac{1}{2}},$$

the edge flux jump indicator by

$$\eta_{J_\sigma,K}^n := \left(\sum_{e \in \mathcal{E}_K^n \cap \mathcal{E}_{h,i}^n} \frac{h_e}{2\beta_e^+} \|J_{\sigma,e}^n\|_{L^2(e)}^2 \right)^{\frac{1}{2}},$$

and the edge solution jump indicator by

$$\eta_{J_u,K}^n := \left(\sum_{e \in \mathcal{E}_K^n \cap \mathcal{E}_{h,i}^n} \frac{\beta_e^-}{2h_e} \|J_{u,e}^n\|_{L^2(e)}^2 + \sum_{e \in \mathcal{E}_K^n \cap \mathcal{E}_{h,b}^n} \frac{\beta_e}{h_e} \|J_{u,e}^n\|_{L^2(e)}^2 \right)^{\frac{1}{2}}.$$

TH-2911_136123010

Then the space error estimator associated with $\mathcal{T}_h^n$ is defined by

$$\eta_{3,space}^n := \sum_{K\in\mathcal{T}_h^n} \eta_{3,K}^n, \tag{4.9}$$

where the local space error indicator is given by

$$\eta_{3,K}^n := \left(\eta_{R_K,K}^n\right)^2 + \left(\eta_{J_\sigma,K}^n\right)^2 + \left(\eta_{J_u,K}^n\right)^2, \tag{4.10}$$

and the time error estimator is defined by

$$\eta_{3,time}^n := \frac{1}{3}\,|||U_h^n - U_h^{n-1}|||_\Omega^2. \tag{4.11}$$

The present analysis will make use of the structure of the nonconforming element which enables to bound both the element residual ($\eta_{R_K,K}^n$) and the numerical flux jump ($\eta_{J_\sigma,K}^n$) uniformly without the quasi-monotonicity. However, we are unable to do the same for the numerical solution jump ($\eta_{J_u,K}^n$). Therefore, we modify the indicator $\eta_{J_u,K}^n$ at elements where the quasi-monotonicity is not satisfied.

For each vertex $z \in \mathcal{N}_h^n$, let ω_z^n and $\mathcal{E}_z^n$, respectively, be the sets of all elements $K \in \mathcal{T}_h^n$ and all edges $e \in \mathcal{E}_h^n$ having z as a common vertex. Let

$$\widehat{\omega}_z^n = \{K \in \omega_z^n : \beta_K = \max_{K'\in\omega_z^n} \beta_{K'}\} \subset \omega_z^n$$

be the set of all elements in ω_z^n such that the corresponding diffusion coefficients are the greatest.

Definition 4.2.1 ([89]). *For any interface intersecting point $z \in \mathcal{N}_h^n$, the vertex patch ω_z^n is called quasi-monotone if for each $K \in \omega_z^n$, there exists a subset $\widehat{\omega}_{z,K}^n$ of ω_z^n such that the union of elements in $\widehat{\omega}_{z,K}^n$ is a Lipschitz domain and that the following holds:*

(i) If $z \in \mathcal{N}_h^n \setminus \mathcal{N}_{h,b}^n$, then $\{K\} \cup \widehat{\omega}_z^n \subset \widehat{\omega}_{z,K}^n$ and $\beta_K \le \beta_{K'}$, $\forall K' \in \widehat{\omega}_{z,K}^n$;

(ii) If $z \in \mathcal{N}_{h,b}^n$, then $K \in \widehat{\omega}_{z,K}^n$, $\partial\widehat{\omega}_{z,K}^n \cap \partial\Omega \neq \emptyset$ and $\beta_K \le \beta_{K'}$, $\forall K' \in \widehat{\omega}_{z,K}^n$.

Let $\mathcal{N}_\vartheta^n = \{z \in \mathcal{N}_h^n : \omega_z^n$ is not quasi-monotone$\}$ be the set of all interface intersecting points whose vertex patches are not quasi-monotone. For each triangle $K \in \mathcal{T}_h^n$, we divide it into four sub-triangles by joining the mid-points of the edges of K. Let $\mathcal{T}_{\frac{h}{2}}^n$ be the refined triangulation and $\mathcal{N}_{\frac{h}{2}}^n$ be the corresponding set of all vertices,

$$\mathcal{N}_{\frac{h}{2}}^n = \mathcal{N}_{\frac{h}{2},i}^n \cup \mathcal{N}_{\frac{h}{2},b}^n \quad\text{and}\quad \mathcal{E}_{\frac{h}{2}}^n = \mathcal{E}_{\frac{h}{2},i}^n \cup \mathcal{E}_{\frac{h}{2},b}^n,$$

where

TH-2911_136123010

- $\mathcal{N}^n_{\frac{h}{2},i}$ - the set of all interior vertices in $\mathcal{T}^n_{\frac{h}{2}}$
- $\mathcal{N}^n_{\frac{h}{2},b}$ - the set of all vertices on the boundary $\partial\Omega$
- $\mathcal{E}^n_{\frac{h}{2},i}$ - the set of all interior edges in $\mathcal{T}^n_{\frac{h}{2}}$
- $\mathcal{E}^n_{\frac{h}{2},b}$ - the set of all edges on the boundary $\partial\Omega$.

Let

$$S^n_{\frac{h}{2},\mathcal{G},c} = \{v \in H^1(\Omega) : v|_\tau \in \mathbb{P}_1(\tau) \ \ \forall \tau \in \mathcal{T}^n_{\frac{h}{2}} \text{ and } v|_{\partial\Omega} = \mathcal{G}\}$$

be the finite element space associated with the triangulation $\mathcal{T}^n_{\frac{h}{2}}$.

Let

$$\mathcal{I}^n_{\frac{h}{2}} : S^n_{h,\mathcal{G},nc} \to S^n_{\frac{h}{2},\mathcal{G},c} \tag{4.12}$$

be an interpolation operator such that for any $v \in S^n_{h,\mathcal{G},nc}$, the following holds:

(i) $(\mathcal{I}^n_{\frac{h}{2}} v)(z) = \mathcal{G}(z), \quad \forall z \in \mathcal{N}^n_{h,b},$

(ii) $(\mathcal{I}^n_{\frac{h}{2}} v)(m_e) = v(m_e), \quad \forall e \in \mathcal{E}^n_h,$

(iii) $(\mathcal{I}^n_{\frac{h}{2}} v)(z) = v|_{K_z}(z), \quad \forall z \in \mathcal{N}^n_{h,i},$

where K_z is chosen to be one element in $\widehat{\omega}^n_z$.

For each vertex $z \in \mathcal{N}^n_h$, let $\omega^n_{z,\tau}$ be the set of all elements $\tau \in \mathcal{T}^n_{\frac{h}{2}}$ with at least one vertex in $\mathcal{N}^n_\vartheta$. The indicator of the numerical solution jump $\eta^n_{J_u,K}$ is modified as follows:

$$\begin{aligned}\left(\bar{\eta}^n_{J_u,K}\right)^2 := &\sum_{z\in\mathcal{N}^n_K\setminus\mathcal{N}^n_\vartheta}\left(\sum_{e\in\mathcal{E}^n_{z,\frac{h}{2}}\cap\mathcal{E}^n_{\frac{h}{2},K}\cap\mathcal{E}^n_{\frac{h}{2},i}}\frac{\beta^-_e}{4h_e}\|J^n_{u,e}\|^2_{L^2(e)} + \sum_{e\in\mathcal{E}^n_{z,\frac{h}{2}}\cap\mathcal{E}^n_{\frac{h}{2},K}\cap\mathcal{E}^n_{\frac{h}{2},b}}\frac{\beta_e}{2h_e}\|J^n_{u,e}\|^2_{L^2(e)}\right)\\ &+ \sum_{z\in\mathcal{N}^n_K\cap\mathcal{N}^n_\vartheta}\frac{\beta_K}{2h_K}\|\mathcal{I}^n_{\frac{h}{2}}U^n_h - U^n_h\|^2_{L^2(\partial\tau_{z,K})},\end{aligned} \tag{4.13}$$

where $\tau_{K,z} = \omega^n_{z,\tau} \cap K$. Then the modified space error indicator is defined as

$$\bar{\eta}^n_{3,K} := \begin{cases}\left(\eta^n_{R_K,K}\right)^2 + \left(\eta^n_{J_\sigma,K}\right)^2 + \left(\bar{\eta}^n_{J_u,K}\right)^2, & \text{if } \mathcal{N}^n_K \cap \mathcal{N}^n_\vartheta \neq \emptyset,\\ \eta^n_{3,K}, & \text{otherwise,}\end{cases} \tag{4.14}$$

and the corresponding modified space error estimator is given by

$$\bar{\eta}^n_{3,space} = \sum_{K\in\mathcal{T}^n_h}\bar{\eta}^n_{3,K}. \tag{4.15}$$

TH-2911_136123010

Now we define

$$\widehat{\eta}^n_{J_u,K} := \left(\frac{\beta_K}{h_K}\right)^{\frac{1}{2}} \|\mathcal{I}^n_{\frac{h}{2}} U^n_h - U^n_h\|_{L^2(\partial K)} \tag{4.16}$$

and

$$\widehat{\eta}^n_{J_u} := \left(\sum_{K\in\mathcal{T}^n_h} \frac{\beta_K}{h_K}\, \|\mathcal{I}^n_{\frac{h}{2}} U^n_h - U^n_h\|^2_{L^2(\partial K)}\right)^{\frac{1}{2}}. \tag{4.17}$$

Let $\bar{\eta}^n_{J_u} = \left(\sum_{K\in\mathcal{T}^n_h} (\bar{\eta}^n_{J_u,K})^2\right)^{\frac{1}{2}}$ be the modified estimator associated with the solution jump, where

$$\left(\bar{\eta}^n_{J_u}\right)^2 = \sum_{z\in\mathcal{N}^n_h\setminus\mathcal{N}^n_\vartheta} \sum_{e\in\mathcal{E}^n_{z,h/2}} \frac{\beta^-_e}{2h_e} \|J^n_{u,e}\|^2_{L^2(e)} + \sum_{z\in\mathcal{N}^n_h\cap\mathcal{N}^n_\vartheta} \sum_{\tau\in\omega^n_{z,h/2}} \frac{\beta_\tau}{4h_\tau} \|\mathcal{I}^n_{\frac{h}{2}} U^n_h - U^n_h\|^2_{L^2(\partial\tau)}. \tag{4.18}$$

Then, the following estimate holds (cf. [20, Lemma 6.2]):

$$\widehat{\eta}^n_{J_u} \le \bar{\eta}^n_{J_u}. \tag{4.19}$$

Remark 4.2.1. *When the distribution of the diffusion coefficient is quasi-monotone i.e., $\mathcal{N}^n_\vartheta \neq \emptyset$, then $\bar{\eta}^n_{J_u,K} = \eta^n_{J_u,K}$ $\forall K \in \mathcal{T}^n_h$. Therefore, for all $K \in \mathcal{T}^n_h$, $\bar{\eta}^n_{3,K} = \eta^n_{3,K}$ and $\bar{\eta}^n_{3,space} = \eta^n_{3,space}$.*

4.3 A Posteriori Error Analysis

This section consists of *a posteriori* error analysis for the fully discrete nonconforming finite element approximation to the problem (4.1)-(4.2). We derive a global upper bound for the error and a lower bound for the error in terms of the local error indicator. Further, a lower bound for the local error in terms of the modified space error indicator is derived in the last part of this section.

We now recall from [20] the modified Clément interpolation operator defined for the nonconforming elements, which plays an important role in the error analysis. For any $K \in \mathcal{T}^n_h$, let ω^n_K be the union of triangles in $\mathcal{T}^n_h$ sharing an edge with K. For any edge $e \in \mathcal{E}^n_h$, let ω^n_e be the union of triangles in $\mathcal{T}^n_h$ having the common edge e. Let

$$\mathcal{P}_K\phi = \frac{1}{meas(K)} \int_K \phi\, dx$$

be the mean value of a given function ϕ on K and $meas(K)$ denotes the measure of K. Define

$$\pi^n_e(\phi) = \begin{cases} \mathcal{P}_{K^+_e}\phi, & \forall e \in \mathcal{E}^n_{h,i}, \\ \mathcal{P}_{K_e}\phi, & \forall e \in \mathcal{E}^n_{h,b}. \end{cases}$$

TH-2911_136123010

The modified Clément interpolation operator $\Pi_h^n : H^1(\mathcal{T}_h^n) \to S_{h,nc}^n$ be defined by

$$\Pi_h^n \phi = \sum_{e \in \mathcal{E}_h^n} (\pi_e^n \phi) \varphi_e, \tag{4.20}$$

where the nodal basis function φ_e of $S_{h,nc}^n$ is given by

$$\varphi_e = \begin{cases} 1, & \text{at mid-point } m_e, \\ 0, & \text{at mid-point of other edges.} \end{cases}$$

The following approximation properties hold (cf. [20]):

Lemma 4.3.1. Let $\Pi_h^n : H^1(\mathcal{T}_h^n) \to S_{h,nc}^n$ be the modified Clément interpolation operator defined by (4.20). Then, for any $\phi \in H^1(\mathcal{T}_h^n)$, we have

$$\|\phi - \Pi_h^n \phi\|_{L^2(K)} \leq C_{I,3} \frac{h_K}{\beta_K^{\frac{1}{2}}} \left(|||\phi|||_{\omega_K^n} + \sum_{e \in \mathcal{E}_K^n} \left(\frac{\beta_e^-}{h_e} \right)^{\frac{1}{2}} \|[\phi]\|_{L^2(e)} \right), \quad \forall K \in \mathcal{T}_h^n, \tag{4.21}$$

and

$$\|\phi|_e^+ - \pi_e \phi\|_{L^2(e)} \leq C_{I,4} \left(\frac{h_e}{\beta_e^+} \right)^{\frac{1}{2}} |||\phi|||_{L^2(K_e^+)}, \quad \forall e \in \mathcal{E}_h^n, \tag{4.22}$$

where the constants $C_{I,3}, C_{I,4}$ depend only on the shape regularity of $\mathcal{T}_h^n$.

Remark 4.3.1. *Observe that there is an extra jump term occur in (4.21) which is due to the discontinuity of the function v across the edges of $K \in \mathcal{T}_h^n$.*

In the following, we obtain an error equation which is useful to derive *a posteriori* error estimates for the fully discrete nonconforming finite element approximation to the problem (4.1)-(4.2).

4.3.1 The Error Equation

Multiplying (4.1) by a test function $v_h \in S_{h,0,nc}^n$, applying integration by parts formula and boundary condition (4.2), we have

$$\left(\frac{\partial u}{\partial t}, v_h \right) + a_h(u, v_h) = (f, v_h) + \sum_{e \in \mathcal{E}_{h,i}^n} \int_e (\beta \nabla u \cdot \mathbf{n}_e)[v_h] ds + \sum_{e \in \mathcal{E}_{h,b}^n} \int_e (\beta \nabla u \cdot \mathbf{n}_e) v_h \, ds. \tag{4.23}$$

Let $U_h : (0, T] \to S_{h,nc}^n$ be a piecewise linear approximation in time of $u(t)$ defined by

$$U_h(t) = l_{n-1}(t) U_h^{n-1} + l_n(t) U_h^n, \tag{4.24}$$

TH-2911_136123010

for $1 \le n \le N$, where $l_{n-1}(t) = \frac{t_n - t}{k_n}$ and $l_n(t) = \frac{t - t_{n-1}}{k_n}$, $\forall t \in (t_{n-1}, t_n]$ are the Lagrange hat functions. We now denote the error by $E(t) = u(t) - U_h(t)$.

The following lemma provides the error equation in terms of residual and jumps.

Lemma 4.3.2. Let u and U_h^n be the solutions of (4.4) and (4.6), respectively. With E as above, let $E_h \in S^n_{h,0,nc}$ be a suitable interpolation of E. Then, the following error equation holds:

$$\begin{aligned}\left(\frac{\partial(u-U_h)}{\partial t}, E\right) + a_h(u-U_h^n, E) &= \sum_{K\in\mathcal{T}_h^n}(R_K^n, v-v_h)_K + \sum_{K\in\mathcal{T}_h^n}(f-\bar{f}^n, E)_K \\ &- \sum_{e\in\mathcal{E}_{h,i}^n}\int_e J_{\sigma,e}^n\{E-E_h\}\,ds - \sum_{e\in\mathcal{E}_{h,i}^n\cup\mathcal{E}_{h,b}^n}\int_e\{\beta\nabla(u-U_h^n)\cdot\mathbf{n}_e\}J_{u,e}^n\,ds. \end{aligned} \tag{4.25}$$

Proof. Using (4.6), (4.23) and (4.24), we have

$$\begin{aligned}\left(\frac{\partial(u-U_h)}{\partial t}, v_h\right) + a_h(u-U_h^n, v_h) &= (f-\bar{f}^n, v_h) + \sum_{e\in\mathcal{E}_{h,i}^n}\int_e(\beta\nabla u\cdot\mathbf{n}_e)[v_h]\,ds \\ &+ \sum_{e\in\mathcal{E}_{h,b}^n}\int_e(\beta\nabla u\cdot\mathbf{n}_e)v_h\,ds, \quad \forall v_h \in S^n_{h,0,nc}. \end{aligned} \tag{4.26}$$

We now write

$$\begin{aligned}\left(\frac{\partial(u-U_h)}{\partial t}, E\right) + a_h(u-U_h^n, E) &= \left(\frac{\partial(u-U_h)}{\partial t}, E-E_h\right) + a_h(u-U_h^n, E-E_h) \\ &+ \left(\frac{\partial(u-U_h)}{\partial t}, E_h\right) + a_h(u-U_h^n, E_h) \\ &:= T_1 + T_2. \end{aligned} \tag{4.27}$$

Since $\{\beta\nabla U_h^n\cdot\mathbf{n}_e\}_e$ is a constant for all edges $e \in \mathcal{E}_h^n$, the orthogonal property (4.8) implies

$$\begin{cases}\displaystyle\int_e\{\beta\nabla U_h^n\cdot\mathbf{n}_e\}[E_h]\,ds = 0, & \forall e\in\mathcal{E}_{h,i}^n, \\ \displaystyle\int_e(\beta\nabla U_h^n\cdot\mathbf{n}_e)E_h\,ds = 0, & \forall e\in\mathcal{E}_{h,b}^n. \end{cases} \tag{4.28}$$

For the term T_1, we use integration by parts to have

$$T_1 = \left(\frac{\partial(u-U_h)}{\partial t}, E-E_h\right) - \sum_{K\in\mathcal{T}_h^n}(\nabla\cdot(\beta\nabla(u-U_h^n)), E-E_h)_K$$

TH-2911_136123010

$$
\begin{aligned}
&+\sum_{e\in\mathcal{E}_{h,i}^n}\int_e[(\beta\nabla(u-U_h^n)\cdot\mathbf{n}_e)\,(E-E_h)]ds\\
&+\sum_{e\in\mathcal{E}_{h,b}^n}\int_e(\beta\nabla(u-U_h^n)\cdot\mathbf{n}_e)\,(E-E_h)ds\\
=\;&\sum_{K\in\mathcal{T}_h^n}(R_K^n,E-E_h)_K+\sum_{K\in\mathcal{T}_h^n}(f-\bar{f}^n,E-E_h)_K\\
&+\sum_{e\in\mathcal{E}_{h,i}^n}\int_e[(\beta\nabla(u-U_h^n)\cdot\mathbf{n}_e)\,(E-E_h)]ds\\
&+\sum_{e\in\mathcal{E}_{h,b}^n}\int_e(\beta\nabla(u-U_h^n)\cdot\mathbf{n}_e)\,(E-E_h)\,ds. \qquad (4.29)
\end{aligned}
$$

Utilizing (4.7), the equation (4.29) leads to

$$
\begin{aligned}
T_1 \;=\;&\sum_{K\in\mathcal{T}_h^n}(R_K^n,E-E_h)_K+\sum_{K\in\mathcal{T}_h^n}(f-\bar{f}^n,E-E_h)_K\\
&+\sum_{e\in\mathcal{E}_{h,i}^n}\int_e[\beta\nabla(u-U_h^n)\cdot\mathbf{n}_e]\,\{E-E_h\}ds+\sum_{e\in\mathcal{E}_{h,i}^n}\int_e\{\beta\nabla(u-U_h^n)\cdot\mathbf{n}_e\}\,[E]ds\\
&-\sum_{e\in\mathcal{E}_{h,i}^n}\int_e\{\beta\nabla(u-U_h^n)\cdot\mathbf{n}_e\}\,[E_h]ds+\sum_{e\in\mathcal{E}_{h,b}^n}\int_e(\beta\nabla(u-U_h^n)\cdot\mathbf{n}_e)\,(E-E_h)ds.
\end{aligned}
$$

In the above, we use the continuity of the solution u and the normal component of the flux $(-\beta\nabla u)$, and (4.28) to obtain

$$
\begin{aligned}
T_1 \;=\;&\sum_{K\in\mathcal{T}_h^n}(R_K^n,E-E_h)_K+\sum_{K\in\mathcal{T}_h^n}(f-\bar{f}^n,E-E_h)_K-\sum_{e\in\mathcal{E}_{h,i}^n}\int_e J_{\sigma,e}^n\,\{E-E_h\}ds\\
&-\sum_{e\in\mathcal{E}_{h,i}^n\cup\mathcal{E}_{h,b}^n}\int_e\{\beta\nabla(u-U_h^n)\cdot\mathbf{n}_e\}\,J_{u,e}^n ds-\sum_{e\in\mathcal{E}_{h,i}^n}\int_e\{\beta\nabla u\cdot\mathbf{n}_e\}\,[E_h]ds\\
&-\sum_{e\in\mathcal{E}_{h,b}^n}\int_e\{\beta\nabla u\cdot\mathbf{n}_e\}\,E_h ds. \qquad (4.30)
\end{aligned}
$$

Putting $v_h = E_h$ in (4.26), the term T_2 can be expressed as

$$
T_2 = (f-\bar{f}^n,E_h) \;+\; \sum_{e\in\mathcal{E}_{h,i}^n}\int_e(\beta\nabla u\cdot\mathbf{n}_e)[E_h]\;ds+\sum_{e\in\mathcal{E}_{h,b}^n}\int_e(\beta\nabla u\cdot\mathbf{n}_e)E_h\,ds. \qquad (4.31)
$$

Substituting (4.30) and (4.31) in (4.27) gives the relation (4.25) and this completes the proof. □

TH-2911_136123010

4.3.2 An Upper Bound

This section derives a global upper bound for the error in the energy norm. We first prove the following two lemmas which will be useful to obtain the main result of this section. The first lemma is on the trace inequality and the proof uses the idea of [21, Lemma 2.1]. The second lemma provides a bound for the temporal derivative of the error in the dual norm.

Lemma 4.3.3. Let $K \in \mathcal{T}_h^n$ and $e \in \partial K$. For any $\phi \in H^{1+r}(K)$, $0 < r < \frac{1}{2}$, with $\Delta\phi \in H^{-1}(K)$, there exists a constant $C_{4,1} > 0$ independent of ϕ such that

$$\|\nabla\phi \cdot \mathbf{n}\|_{H^{r-\frac{1}{2}}(e)} \leq C_{4,1}\Big(\|\nabla\phi\|_{H^r(K)} + h_K^{1-r}\|\Delta\phi\|_{H^{-1}(K)}\Big).$$

Proof. For any $g \in H^{\frac{1}{2}-r}(e)$, there exists a lifting v_g of g such that $v_g \in H^{1-r}(K)$, $v_g|_e = g$ and $v_g|_{\partial K\setminus e} = 0$. Also, v_g satisfies the following estimate

$$\|\nabla v_g\|_{H^{-r}(K)} + h_K^{r-1}\|v_g\|_{H^1(K)} \leq C_{4,1}\|g\|_{H^{\frac{1}{2}-r}(e)}.$$

Applying Green's formula and using the above inequality, we have

$$\begin{aligned}
\langle\nabla\phi\cdot\mathbf{n}, g\rangle_e &= \langle\nabla\phi\cdot\mathbf{n}, v_g\rangle_{\partial K} \\
&= (\nabla\phi, \nabla v_g)_K + (\Delta\phi, v_g)_K \\
&\leq \|\nabla\phi\|_{H^r(K)}\|\nabla v_g\|_{H^{-r}(K)} + \|\Delta\phi\|_{H^{-1}(K)}\|v_g\|_{H^1(K)} \\
&\leq C_{4,1}\Big(\|\nabla\phi\|_{H^r(K)} + h_K^{1-r}\|\Delta\phi\|_{H^{-1}(K)}\Big)\|g\|_{H^{\frac{1}{2}-r}(e)},
\end{aligned}$$

which implies

$$\|\nabla\phi\cdot\mathbf{n}\|_{H^{r-\frac{1}{2}}(e)} = \sup_{g\in H^{\frac{1}{2}-r}(e)} \frac{\langle\nabla\phi\cdot\mathbf{n}, g\rangle_e}{\|g\|_{H^{\frac{1}{2}-r}(e)}} \leq C_{4,1}\Big(\|\nabla\phi\|_{H^r(K)} + h_K^{1-r}\|\Delta\phi\|_{H^{-1}(K)}\Big).$$

□

Remark 4.3.2. *By the Green's formula:*

$$\begin{aligned}
\int_{\partial K}(\nabla w.\mathbf{n})v ds &:= \langle\nabla w.\mathbf{n}, v\rangle \\
&= (\Delta w, v)_K + (\nabla w, \nabla v)_K \quad \forall K \in \mathcal{T}_h^n,
\end{aligned} \tag{4.32}$$

for all $w \in H^{1+r}(K)$ with $\Delta w \in L^2(K)$ and for all $v \in H^{1-r}(K)$ with $0 < r < 1/2$. By the trace theorem [56], $v|_{\partial K}$ is in $H^{1/2-r}(\partial K)$. Thus, the left hand side of (4.32) may be regarded as the duality pairing between $H^{1/2-r}(\partial K)$ and $H^{r-1/2}(\partial K)$. Since, for all edge $e \in \partial K$, the trivial extension of functions in $H^{1/2-r}(e)$ by zero to all of ∂K belongs

TH-2911_136123010

to $H^{1/2-r}(\partial K)$*, and this interpretation enable us to define the duality pairing on each edge* e *in* ∂K*,*

$$\int_e (\nabla w.\mathbf{n}) v ds := \langle \nabla w.\mathbf{n}, v\rangle_e,$$

where $(\nabla w.\mathbf{n})|_e \in H^{r-1/2}(e)$ *and* $v|_e \in H^{1/2-r}(e)$*.*

Lemma 4.3.4. *Let* u *be the solution of (4.1)-(4.2) and* U_h *be its approximation defined by (4.24). Then there exists a constant* $C_{4,2} > 0$ *depending on the shape regularity of* $\mathcal{T}_h^n$ *such that*

$$\begin{aligned}\left\|\frac{\partial(u-U_h)}{\partial t}\right\|_{H^{-1}(\Omega)} \leq\ & C_{4,2}\Bigg(\sum_{K\in\mathcal{T}_h^n}\Big(\|f-\bar{f}^n\|^2_{L^2(K)} + \|R_K^n\|^2_{L^2(K)} \\ & + \beta_K|||U_h-U_h^n|||_K^2 + \beta_K|||u-U_h^n|||_K^2\Big)\Bigg)^{\frac{1}{2}}. \end{aligned} \tag{4.33}$$

Proof. For all $\phi \in H_0^1(\Omega)$, we have

$$\begin{aligned}\left(\frac{\partial(u-U_h)}{\partial t},\phi\right) =\ & (f-\bar{f}^n,\phi) + \sum_{K\in\mathcal{T}_h^n}(R_K^n,\phi)_K + \sum_{K\in\mathcal{T}_h^n}(\beta\nabla(U_h-U_h^n),\nabla\phi)_K \\ & - \sum_{K\in\mathcal{T}_h^n}(\beta\nabla(u-U_h),\nabla\phi)_K.\end{aligned}$$

Applying the Cauchy-Schwarz inequality, the above equation implies

$$\begin{aligned}\left(\frac{\partial(u-U_h)}{\partial t},\phi\right) \leq\ & \sum_{K\in\mathcal{T}_h^n}\|f-\bar{f}^n\|_{H^{-1}(K)}\|\phi\|_{H^1(K)} + \sum_{K\in\mathcal{T}_h^n}\|R_K^n\|_{H^{-1}(K)}\|\phi\|_{H^1(K)} \\ & + \sum_{K\in\mathcal{T}_h^n}\|\beta\nabla(U_h-U_h^n)\|_{L^2(K)}\|\nabla\phi\|_{L^2(K)} \\ & + \sum_{K\in\mathcal{T}_h^n}\|\beta\nabla(u-U_h)\|_{L^2(K)}\|\nabla\phi\|_{L^2(K)} \\ \leq\ & \Bigg(\sum_{K\in\mathcal{T}_h^n}\Big(\|f-\bar{f}^n\|^2_{H^{-1}(K)} + \|R_K^n\|^2_{H^{-1}(K)} + \beta_K|||U_h-U_h^n|||_K^2 \\ & + \beta_K|||u-U_h^n|||_K^2\Big)\Bigg)^{\frac{1}{2}}\|\phi\|_{H^1(\Omega)}.\end{aligned}$$

Now,

$$\sup_{\phi\in H_0^1(\Omega)}\frac{\left(\frac{\partial(u-U_h)}{\partial t},\phi\right)}{\|\phi\|_{H^1(\Omega)}} \leq C_{4,2}\Bigg(\sum_{K\in\mathcal{T}_h^n}\Big(\|f-\bar{f}^n\|^2_{L^2(K)} + \|R_K^n\|^2_{L^2(K)}$$

TH-2911_136123010

$$+ \beta_K |||U_h - U_h^n|||_K^2 + \beta_K |||u - U_h^n|||_K^2 \Big) \Big)^{\frac{1}{2}},$$

and hence

$$\left\| \frac{\partial (u - U_h)}{\partial t} \right\|_{H^{-1}(\Omega)} \leq C_{4,2} \Bigg(\sum_{K \in \mathcal{T}_h^n} \Big(\|f - \bar{f}^n\|_{L^2(K)}^2 + \|R_K^n\|_{L^2(K)}^2 + \beta_K |||U_h - U_h^n|||_K^2 + \beta_K |||u - U_h^n|||_K^2 \Big) \Bigg)^{\frac{1}{2}}.$$

□

The upper bound for the error is presented in the following theorem.

Theorem 4.3.1. *Let u and U_h^n be the solutions of (4.4) and (4.6), respectively. Then, for any integer $1 \leq m \leq N$, there exists a constant $C > 0$ depending on the minimal angle of $\mathcal{T}_h^n$, $n = 1, 2, ..., m$, such that the following estimate hold:*

$$\|(u - U_h)(t^m)\|_{L^2(\Omega)}^2 + \sum_{n=1}^{m} \int_{t_{n-1}}^{t_* \wedge t_n} |||u - U_h^n|||_\Omega^2 dt \leq 2 \|u_0 - U_h^0\|_{L^2(\Omega)}^2 + 3 \sum_{n=1}^{m} k_n \eta_{3,time}^n + C \sum_{n=1}^{m} \int_{t_{n-1}}^{t_n} \|f - \bar{f}^n\|_{L^2(\Omega)}^2 dt + C \sum_{n=1}^{m} k_n \bar{\eta}_{3,space}^n. \tag{4.34}$$

Proof. Setting $E_h = \Pi_h^n (u - U_h)$ in (4.25), we obtain

$$\begin{aligned} & \frac{1}{2} \frac{d}{dt} \|u - U_h\|_{L^2(\Omega)}^2 + a_h(u - U_h^n, u - U_h) \\ = & \sum_{K \in \mathcal{T}_h^n} (f - \bar{f}^n, u - U_h)_K + \sum_{K \in \mathcal{T}_h^n} (R_K^n, (u - U_h) - \Pi_h^n (u - U_h))_K \\ & - \sum_{e \in \mathcal{E}_{h,i}^n} \int_e J_{\sigma,e}^n \{(u - U_h) - \Pi_h^n (u - U_h)\} ds \\ & - \sum_{e \in \mathcal{E}_{h,i}^n \cup \mathcal{E}_{h,b}^n} \int_e \{\beta \nabla (u - U_h^n) \cdot \mathbf{n}_e\} J_{u,e}^n ds \\ := & \; T_1^1 + T_2^1 + T_3^1 + T_4^1. \end{aligned} \tag{4.35}$$

For the term T_1^1, we have

$$T_1^1 \leq \sum_{K \in \mathcal{T}^n} \|f - \bar{f}^n\|_{L^2(K)} \|u - U_h\|_{L^2(K)}. \tag{4.36}$$

Using the Cauchy-Schwarz inequality and Lemma 4.3.1 for T_2^1-term, we have

$$T_2^1 \leq \sum_{K \in \mathcal{T}_h^n} \|R_K^n\|_{L^2(K)} \|(u - U_h) - \Pi_h^n (u - U_h)\|_{L^2(K)}$$

TH-2911_136123010

$$\leq C_{I,3} \sum_{K\in\mathcal{T}_h^n} \frac{h_K}{\beta_K^{\frac{1}{2}}} \|R_K^n\|_{L^2(K)} \left(|||u-U_h|||_{\omega_K^n} + \sum_{e\in\mathcal{E}_K^n} \left(\frac{\beta_e^-}{h_e}\right)^{\frac{1}{2}} \|[u-U_h]\|_{L^2(e)} \right)$$

$$\leq C_{I,3} \sum_{K\in\mathcal{T}_h^n} \eta_{R_K,K}^n \left(|||u-U_h|||_{\omega_K^n} + \sum_{e\in\mathcal{E}_K^n} \left(\frac{\beta_e^-}{h_e}\right)^{\frac{1}{2}} \|[u-U_h]\|_{L^2(e)} \right)$$

$$\leq C_{I,3} \left(\sum_{K\in\mathcal{T}_h^n} (\eta_{R_K,K}^n)^2 \right)^{\frac{1}{2}} |||u-U_h|||_\Omega. \tag{4.37}$$

To bound the term T_3^1, we first notice that

$$[(u-U_h) - \Pi_h^n(u-U_h)]_e = -[U_h^n + \Pi_h^n(u-U_h)]_e, \quad \forall e \in \mathcal{E}_{h,i}^n.$$

Since $U_h^n + \Pi_h^n(u-U_h) \in S_{h,nc}^n$ and $J_{\sigma,e}^n$ is a constant for all $e \in \mathcal{E}_h^n$, (4.8) leads to

$$\int_e J_{\sigma,e}^n \, [(u-U_h) - \Pi_h^n(u-U_h)]_e = 0, \quad \forall e \in \mathcal{E}_{h,i}^n.$$

By the properties of the nonconforming nodal basis functions $\int_{e_i} \phi_{e_j} = \delta_{ij}$, we have, for all $e \in \mathcal{E}_{h,i}^n$,

$$\begin{aligned} &\int_e \{(u-U_h) - \Pi_h^n(u-U_h)\}_e \, ds + \frac{1}{2}\int_e [(u-U_h) - \Pi_h^n(u-U_h)]_e \, ds \\ &= \int_e ((u-U_h) - \Pi_h^n(u-U_h))|_e^+ ds \; = \int_e ((u-U_h)|_e^+ - \pi_e^n(u-U_h)) ds. \end{aligned} \tag{4.38}$$

Applying (4.38) and the Cauchy-Schwarz inequality, it follows that

$$\begin{aligned} T_3^1 &= \sum_{e\in\mathcal{E}_{h,i}^n} \int_e J_{\sigma,e}^n \, \{(u-U_h) - \Pi_h^n(u-U_h)\}_e ds \\ &\quad + \frac{1}{2} \sum_{e\in\mathcal{E}_{h,i}^n} \int_e J_{\sigma,e}^n \, [(u-U_h) - \Pi_h^n(u-U_h)]_e \, ds \\ &= \sum_{e\in\mathcal{E}_{h,i}^n} \int_e J_{\sigma,e}^n \, ((u-U_h)|_e^+ - \pi_e^n(u-U_h)) ds \\ &\leq \sum_{e\in\mathcal{E}_{h,i}^n} \|J_{\sigma,e}^n\|_{L^2(e)} \, \|(u-U_h)|_e^+ - \pi_e^n(u-U_h)\|_{L^2(e)}. \end{aligned} \tag{4.39}$$

Again, using Lemma 4.3.1 to (4.39) yields

$$\begin{aligned} T_3^1 &\leq \sum_{K\in\mathcal{T}_h^n} \sum_{e\in\mathcal{E}_{h,i}^n} \|J_{\sigma,e}^n\|_{L^2(e)} \left(\frac{h_e}{\beta_e^+}\right)^{\frac{1}{2}} |||u-U_h|||_{L^2(K_e^+)} \\ &\leq C_{I,4} \left(\sum_{K\in\mathcal{T}_h^n} \sum_{e\in\mathcal{E}_K^n\cap\mathcal{E}_{h,i}^n} \frac{h_e}{2\beta_e^+} \|J_{\sigma,e}^n\|_{L^2(e)}^2 \right)^{\frac{1}{2}} \left(\sum_{K\in\mathcal{T}_h^n} |||u-U_h|||_{L^2(K_e^+)}^2 \right)^{\frac{1}{2}} \end{aligned}$$

TH-2911_136123010

$$(4.40) \qquad \leq C_{I,4}\left(\sum_{K\in\mathcal{T}_h^n}(\eta^n_{J_\sigma,K})^2\right)^{\frac{1}{2}} |||u-U_h|||_\Omega.$$

Finally, we need to bound the term T_4^1. Since the term T_4^1 contains the numerical solution jump $J^n_{u,e}$, it is not easy to bound directly over $e\in\partial K$. So, we rewrite T_4^1 in terms of integral along boundary elements. Here we note that

$$[\mathcal{I}^n_{\frac{h}{2}}U^n_h]_e=0 \ \text{ and } \ [\beta\nabla u\cdot\mathbf{n}_e]_e=0, \ \ \forall e\in\mathcal{E}^n_{h,i}, \quad \text{and} \quad \mathcal{I}^n_{\frac{h}{2}}U^n_h=0 \ \ on\ \partial\Omega.$$

Then, we rewrite T_4^1 as

$$\begin{aligned}
T_4^1 &= -\sum_{e\in\mathcal{E}^n_{h,i}\cup\mathcal{E}^n_{h,b}}\int_e\{\beta\nabla(u-U^n_h)\cdot\mathbf{n}_e\}\,J^n_{u,e}ds\\
&= \sum_{e\in\mathcal{E}^n_{h,i}\cup\mathcal{E}^n_{h,b}}\int_e\{\beta\nabla(u-U^n_h)\cdot\mathbf{n}_e\}\,[\mathcal{I}^n_{\frac{h}{2}}U^n_h-U^n_h]ds\\
&= \sum_{e\in\mathcal{E}^n_{h,i}}\int_e\{\beta\nabla(u-U^n_h)\cdot\mathbf{n}_e\}\,[\mathcal{I}^n_{\frac{h}{2}}U^n_h-U^n_h]ds\\
&\quad+\sum_{e\in\mathcal{E}^n_{h,b}}\int_e(\beta\nabla(u-U^n_h)\cdot\mathbf{n}_e)\,(\mathcal{I}^n_{\frac{h}{2}}U^n_h-U^n_h)ds.
\end{aligned}$$

By (4.7) and $[\beta\nabla u\cdot\mathbf{n}_e]_e=0$, $\forall e\in\mathcal{E}^n_{h,i}$, the above equation becomes

$$\begin{aligned}
T_4^1 &= \sum_{K\in\mathcal{T}_h^n}\int_{\partial K}(\beta\nabla(u-U^n_h)\cdot\mathbf{n}_e)\,(\mathcal{I}^n_{\frac{h}{2}}U^n_h-U^n_h)ds\\
&\quad-\sum_{e\in\mathcal{E}^n_{h,i}}\int_e[\beta\nabla(u-U^n_h)\cdot\mathbf{n}_e]\,\{\mathcal{I}^n_{\frac{h}{2}}U^n_h-U^n_h\}ds\\
&\quad-\sum_{e\in\mathcal{E}^n_{h,b}}\int_e(\beta\nabla(u-U^n_h)\cdot\mathbf{n}_e)\,(\mathcal{I}^n_{\frac{h}{2}}U^n_h-U^n_h)ds\\
&\quad+\sum_{e\in\mathcal{E}^n_{h,b}}\int_e(\beta\nabla(u-U^n_h)\cdot\mathbf{n}_e)\,(\mathcal{I}^n_{\frac{h}{2}}U^n_h-U^n_h)ds\\
&= \sum_{K\in\mathcal{T}_h^n}\int_{\partial K}(\beta\nabla(u-U^n_h)\cdot\mathbf{n}_e)\,(\mathcal{I}^n_{\frac{h}{2}}U^n_h-U^n_h)ds+\sum_{e\in\mathcal{E}^n_{h,i}}\int_e J^n_{\sigma,e}\{\mathcal{I}^n_{\frac{h}{2}}U^n_h-U^n_h\}\,ds\\
(4.41) &:= \widetilde{T}^1_{41}+\widetilde{T}^1_{42}.
\end{aligned}$$

To bound $\widetilde{T}^1_{41}$ term, using the definition of dual norm, Lemma 4.3.3, and the inverse inequality, we find that

$$\widetilde{T}^1_{41} \leq \sum_{K\in\mathcal{T}_h^n}\|\beta\nabla(u-U^n_h)\cdot\mathbf{n}_e\|_{H^{-\frac{1}{2}}(\partial K)}\,\|\mathcal{I}^n_{\frac{h}{2}}U^n_h-U^n_h\|_{H^{\frac{1}{2}}(\partial K)}$$

TH-2911_136123010

$$\leq \sum_{K\in\mathcal{T}_h^n}\Big(\|\beta\nabla(u-U_h^n)\|_{L^2(K)}+h_K\|\nabla\cdot(\beta\nabla(u-U_h^n))\|_{H^{-1}(K)}\Big)$$
$$\times\, h_K^{-\frac{1}{2}}\|\mathcal{I}_{\frac{h}{2}}^n U_h^n-U_h^n\|_{L^2(\partial K)}.$$

Now using (4.16) and (4.17), the above inequality implies

$$\begin{aligned}\widetilde{T}_{41}^1 &\leq \sum_{K\in\mathcal{T}_h^n}\Big(|||u-U_h^n|||_K+\beta_K^{-1/2}h_K\|\nabla\cdot(\beta\nabla(u-U_h^n))\|_{H^{-1}(K)}\Big)\,\widehat{\eta}_{J_u,K}^n\\ &\leq |||u-U_h^n|||_\Omega\,\widehat{\eta}_{J_u}^n+\sum_{K\in\mathcal{T}_h^n}\beta_K^{-1/2}h_K\|\nabla\cdot(\beta\nabla(u-U_h^n))\|_{H^{-1}(K)}\,\widehat{\eta}_{J_u,K}^n\\ &:= |||u-U_h^n|||_\Omega\,\widehat{\eta}_{J_u}^n+\widehat{T}_1. \qquad (4.42)\end{aligned}$$

For $\widehat{T}_1$-term, utilizing (4.4), (4.6), and the Cauchy-Schwarz inequality it follows that

$$\begin{aligned}\widehat{T}_1 &\leq \sum_{K\in\mathcal{T}_h^n}\left(\frac{h_K}{\beta_K^{1/2}}\right)\Big(\|f-\bar{f}^n\|_{L^2(K)}+\|\frac{\partial(u-U_h)}{\partial t}\|_{H^{-1}(K)}\Big)\,\widehat{\eta}_{J_u,K}^n.\\ &\leq \left(\sum_{K\in\mathcal{T}_h^n}\Big(\frac{h_K^2}{\beta_K}\Big)\Big(\|f-\bar{f}^n\|_{L^2(K)}^2+\|\frac{\partial(u-U_h)}{\partial t}\|_{H^{-1}(K)}^2\Big)\right)^{\frac{1}{2}}\widehat{\eta}_{J_u}^n.\end{aligned}$$

With an aid of Lemma 4.3.4, the above inequality leads to

$$\begin{aligned}\widehat{T}_1 &\leq \left(C_{4,2}\sum_{K\in\mathcal{T}_h^n}\Big(\frac{h_K^2}{\beta_K}\Big)\Big(\|f-\bar{f}^n\|_{L^2(K)}^2+\|R_K^n\|_{L^2(K)}^2+\beta_K|||U_h-U_h^n|||_K^2\right.\\ &\quad\left.+\,\beta_K|||u-U_h^n|||_K^2\Big)\right)^{\frac{1}{2}}\widehat{\eta}_{J_u}^n\\ &\leq C_{4,2}\Bigg(\sum_{K\in\mathcal{T}_h^n}\frac{h_K^2}{\beta_K}\|f-\bar{f}^n\|_{L^2(K)}^2+\sum_{K\in\mathcal{T}_h^n}\big(\eta_{R_K,K}^n\big)^2+\sum_{K\in\mathcal{T}_h^n}h_K^2|||U_h-U_h^n|||_K^2\\ &\quad+\sum_{K\in\mathcal{T}_h^n}h_K^2|||u-U_h^n|||_K^2\Bigg)^{\frac{1}{2}}\widehat{\eta}_{J_u}^n. \qquad (4.43)\end{aligned}$$

By (4.42) and (4.43), we have

$$\begin{aligned}\widetilde{T}_{41}^1 &\leq |||u-U_h^n|||_\Omega\,\widehat{\eta}_{J_u}^n+C_{4,2}\Bigg(\sum_{K\in\mathcal{T}_h^n}\frac{h_K^2}{\beta_K}\|f-\bar{f}^n\|_{L^2(K)}^2+\sum_{K\in\mathcal{T}_h^n}\big(\eta_{R_K,K}^n\big)^2\\ &\quad+\sum_{K\in\mathcal{T}_h^n}h_K^2|||U_h-U_h^n|||_K^2+\sum_{K\in\mathcal{T}_h^n}h_K^2|||u-U_h^n|||_K^2\Bigg)^{\frac{1}{2}}\widehat{\eta}_{J_u}^n. \qquad (4.44)\end{aligned}$$

TH-2911_136123010

For $\widetilde{T}^1_{42}$, since $J^n_{\sigma,e}$ is a constant and $[\mathcal{I}^n_{\frac{h}{2}} U^n_h] = 0$ for all $e \in \mathcal{E}^n_{h,i}$, use of orthogonal property (4.8) now yields

$$\int_e J^n_{\sigma,e}[\mathcal{I}^n_{\frac{h}{2}} U^n_h - U^n_h]\, ds = 0, \quad \forall e \in \mathcal{E}^n_{h,i}.$$

Therefore, for all $e \in \mathcal{E}^n_{h,i}$ we get

$$\begin{aligned}\int_e J^n_{\sigma,e}\,\{\mathcal{I}^n_{\frac{h}{2}} U^n_h - U^n_h\}ds &= \int_e J^n_{\sigma,e}\,\{\mathcal{I}^n_{\frac{h}{2}} U^n_h - U^n_h\}ds + \frac{1}{2}\int_e J^n_{\sigma,e}[\mathcal{I}^n_{\frac{h}{2}} U^n_h - U^n_h]ds \\ &= \int_e J^n_{\sigma,e}\,(\mathcal{I}^n_{\frac{h}{2}} U^n_h - U^n_h|^+_e)ds.\end{aligned}$$

An application of the Cauchy-Schwarz inequality implies

$$\begin{aligned}\widetilde{T}^1_{42} &= \sum_{e\in\mathcal{E}^n_{h,i}}\int_e J^n_{\sigma,e}\,(\mathcal{I}^n_{\frac{h}{2}} U^n_h - U^n_h|^+_e)ds \\ &\le \left(\sum_{K\in\mathcal{T}^n_h}\sum_{e\in\mathcal{E}^n_{h,i}}\frac{h_e}{\beta^+_e}\|J^n_{\sigma,e}\|^2_{L^2(e)}\right)^{\frac{1}{2}}\left(\sum_{K\in\mathcal{T}^n_h}\sum_{e\in\mathcal{E}^n_{h,i}}\frac{\beta^+_e}{h_e}\|\mathcal{I}^n_{\frac{h}{2}} U^n_h - U^n_h|^+_e\|^2_{L^2(e)}\right)^{\frac{1}{2}} \\ &\le \left(\sum_{K\in\mathcal{T}^n_h}\left(\eta^n_{J_{\sigma,K}}\right)^2\right)^{\frac{1}{2}}\widehat{\eta}^n_{J_u}. \qquad (4.45)\end{aligned}$$

Combining (4.41), (4.44) and (4.45), we estimate T^1_4 as

$$\begin{aligned}T^1_4 \le\ & |||u - U^n_h|||_\Omega\,\widehat{\eta}^n_{J_u} + C_{4,2}\Bigg(\sum_{K\in\mathcal{T}^n_h}\frac{h^2_K}{\beta_K}\|f - \bar{f}^n\|^2_{L^2(K)} + \sum_{K\in\mathcal{T}^n_h} h^2_K|||U_h - U^n_h|||^2_K \\ &+ \sum_{K\in\mathcal{T}^n_h}\left(\eta^n_{R_K,K}\right)^2 + \sum_{K\in\mathcal{T}^n_h} h^2_K|||u - U^n_h|||^2_K\Bigg)^{\frac{1}{2}}\widehat{\eta}^n_{J_u} + \left(\sum_{K\in\mathcal{T}^n_h}\left(\eta^n_{J_{\sigma,K}}\right)^2\right)^{\frac{1}{2}}\widehat{\eta}^n_{J_u}. \qquad (4.46)\end{aligned}$$

With an aid of the following identity

$$a_h(u - U^n_h, u - U_h) = \frac{1}{2}|||u - U_h|||^2_\Omega + \frac{1}{2}|||u - U^n_h|||^2_\Omega - \frac{1}{2}|||U_h - U^n_h|||^2_\Omega,$$

and (4.35)-(4.37), (4.40) and (4.46), we arrive at

$$\begin{aligned}&\frac{1}{2}\frac{d}{dt}\|u - U_h\|^2_{L^2(\Omega)} + \frac{1}{2}\Big(|||u - U_h|||^2_\Omega + |||u - U^n_h|||^2_\Omega\Big) \\ \le\ & \frac{1}{2}|||U_h - U^n_h|||^2_\Omega + \|f - \bar{f}^n\|_{L^2(\Omega)}\|u - U_h\|_{L^2(\Omega)} + C_{I,3}\left(\sum_{K\in\mathcal{T}^n_h}(\eta^n_{R_K,K})^2\right)^{\frac{1}{2}}|||u - U_h|||_\Omega \\ &+ C_{I,4}\left(\sum_{K\in\mathcal{T}^n_h}(\eta^n_{J_\sigma,K})^2\right)^{\frac{1}{2}}|||u - U_h|||_\Omega + |||u - U^n_h|||_\Omega\,\widehat{\eta}^n_{J_u}\end{aligned}$$

TH-2911_136123010

$$+ C_{4,2}\Bigg(\sum_{K\in\mathcal{T}_h^n} \frac{h_K^2}{\beta_K}\|f-\bar{f}^n\|^2_{L^2(K)} + \sum_{K\in\mathcal{T}_h^n} \left(\eta^n_{R_K,K}\right)^2 + \sum_{K\in\mathcal{T}_h^n} h_K^2 |||U_h - U_h^n|||_K^2$$
$$+ \sum_{K\in\mathcal{T}_h^n} h_K^2 |||u - U_h^n|||_K^2 \Bigg)^{\frac{1}{2}} \widehat{\eta}^n_{J_u} + \left(\sum_{K\in\mathcal{T}_h^n} \left(\eta^n_{J_{\sigma,K}}\right)^2 \right)^{\frac{1}{2}} \widehat{\eta}^n_{J_u}.$$

Again, an use of the Young's inequality implies

$$\begin{aligned}
&\frac{1}{2}\frac{d}{dt}\|u-U_h\|^2_{L^2(\Omega)} + \frac{1}{2}\Big(|||u-U_h|||^2_\Omega + |||u-U_h^n|||^2_\Omega\Big) \\
&\leq \frac{1}{2}|||U_h - U_h^n|||^2_\Omega + \|f-\bar{f}^n\|_{L^2(\Omega)}\|u-U_h\|_{L^2(\Omega)} + \sum_{K\in\mathcal{T}_h^n}\frac{h_K^2}{\beta_K}\|f-\bar{f}^n\|^2_{L^2(K)} \\
&\quad + C_{4,3}\Bigg(\sum_{K\in\mathcal{T}_h^n} (\eta^n_{R_K,K})^2 + \sum_{K\in\mathcal{T}_h^n} (\eta^n_{J_\sigma,K})^2 + (\widehat{\eta}^n_{J_u})^2 \Bigg) + \sum_{K\in\mathcal{T}_h^n} h_K^2 |||U_h - U_h^n|||^2_K \\
&\quad + \left(\frac{1}{4}|||u-U_h|||^2_\Omega + \sum_{K\in\mathcal{T}_h^n} h_K^2 |||u-U_h|||^2_K \right) + \frac{1}{4}|||u-U_h^n|||^2_\Omega,
\end{aligned}$$

where $C_{4,3} = \max\{C_{I,3}^2 + 1/2, C_{I,4}^2 + 1/2, \frac{1}{2}C_{4,2}^2 + 5/2\}$. Choose $\max\limits_{K\in\mathcal{T}_h^n} h_K \leq \dfrac{1}{\sqrt{2}}$ and $\max\limits_{K\in\mathcal{T}_h^n} \dfrac{h_K^2}{\beta_K} \leq \sigma < 1$, where $\sigma > 0$, such that the above inequality becomes

$$\begin{aligned}
\frac{1}{2}\frac{d}{dt}\|u-U_h\|^2_{L^2(\Omega)} + \frac{1}{4}|||u-U_h^n|||^2_\Omega \;&\leq\; \frac{3}{4}|||U_h - U_h^n|||^2_\Omega + \|f-\bar{f}^n\|_{L^2(\Omega)}\|u-U_h\|_{L^2(\Omega)} \\
&\quad + \frac{\sigma}{2}\|f-\bar{f}^n\|^2_{L^2(\Omega)} + C_{4,3}\Bigg(\sum_{K\in\mathcal{T}_h^n} \bar{\eta}^n_{3,K} \Bigg).
\end{aligned} \tag{4.47}$$

For $t_* \in (t_{m-1}, t_m]$, let $t_* \wedge t_n = \min(t_n, t_*)$. We now integrate (4.47) with respect to time from 0 to t_*, and use the Cauchy-Schwarz inequality to conclude that

$$\begin{aligned}
&\frac{1}{2}\|(u-U_h)(t_*)\|^2_{L^2(\Omega)} + \frac{1}{4}\sum_{n=1}^m \int_{t_{n-1}}^{t_*\wedge t_n} |||u-U_h^n|||^2_\Omega dt \\
&\leq \frac{1}{2}\|u_0 - U_h^0\|^2_{L^2(\Omega)} + \frac{3}{4}\sum_{n=1}^m \int_{t_{n-1}}^{t_n} |||U_h - U_h^n|||^2_\Omega \, dt + \frac{1}{4}\max_{0\leq t_*\leq t_m}\|(u-U_h)(t_*)\|^2_{L^2(\Omega)} \\
&\quad + (1+\sigma/2)\sum_{n=1}^m \int_{t_{n-1}}^{t_n} \|f-\bar{f}^n\|^2_{L^2(\Omega)} dt + C_{4,3}\sum_{n=1}^m \int_{t_{n-1}}^{t_n} \bar{\eta}^n_{3,space} dt \\
&\leq \frac{1}{2}\|u_0 - U_h^0\|^2_{L^2(\Omega)} + \frac{3}{4}\sum_{n=1}^m k_n \eta^n_{3,time} + \frac{1}{4}\max_{0\leq t_*\leq t_m}\|(u-U_h)(t_*)\|^2_{L^2(\Omega)} \\
&\quad + (1+\sigma/2)\sum_{n=1}^m \int_{t_{n-1}}^{t_n} \|f-\bar{f}^n\|^2_{L^2(\Omega)} dt + C_{4,3}\sum_{n=1}^m k_n \bar{\eta}^n_{3,space},
\end{aligned}$$

TH-2911_136123010

where $\eta^n_{3,time}$ and $\bar{\eta}^n_{3,space}$ are defined in (4.11) and (4.15), respectively. Finally, using the constant $C = \max\{2(2+\sigma), 4C_{4,3}\}$ and the standard kickback argument leads to the desired result (4.34) and this completes the proof. □

4.3.3 A Lower Bound

Our next goal is to derive a local lower bound for the error. For this, we consider the following auxiliary problem.

Let $U^n_* \in H^1_{\mathcal{G}}(\Omega)$ be the solution of

$$\left(\frac{U^n_* - U^{n-1}_h}{k_n}, \phi\right) + a_h(U^n_*, \phi) \;=\; (\bar{f}^n, \phi), \quad \forall \phi \in H^1_0(\Omega). \tag{4.48}$$

For $n = 1, 2, \ldots$, let

$$\widehat{C}^n_{nc} = \max_{K \in \mathcal{T}^n_h} \left\{ \frac{h^2_K}{\beta_K k_n} \;:\; h_K = \mathrm{diam}(K) \right\}. \tag{4.49}$$

Now we define the oscillation of any function $\phi \in L^2(\Omega)$ over $\mathcal{T}^n_h$ as

$$\mathrm{osc}(\phi, \mathcal{T}^n_h) = \left(\sum_{K \in \mathcal{T}^n_h} \frac{h^2_K}{\beta_K} \, \|\mathcal{P}_K R^n_K - R^n_K\|^2_{L^2(K)} \right)^{\frac{1}{2}} \tag{4.50}$$

and the weighted norm $\|\cdot\|_{k_n,\Omega}$ as

$$\|\phi\|_{k_n,\Omega} = \left(\frac{1}{k_n} \|\phi\|^2_{L^2(\Omega)} + |||\phi|||^2_{\Omega} \right)^{\frac{1}{2}} \quad \forall \phi \in H^1(\Omega). \tag{4.51}$$

Remark 4.3.3. *Observe that by modifying time-step size k_n in (4.6) we are basically controlling the error between $u^n = u(x, t_n)$ and U^n_h. The purpose of introducing (4.48) is essentially to control the error between U^n_h and U^n_*, not between U^n_h and the exact solution u. These two facts play a crucial role in deriving lower bound for the space error indicator.*

Theorem 4.3.2. *Let U^n_h and U^n_* be the solutions of (4.6) and (4.48), respectively. Then, for all $\mathcal{T}^n_h$, $n = 1, 2, \ldots, m$, we have*

$$\begin{aligned} \eta^n_{3,K} \;\leq\; & C_{4,11} \sum_{K \in \omega^n_K} \left(\frac{h^2_K}{\beta_K} \, \|R^n_K - \mathcal{P}_K R^n_K\|^2_{L^2(K)} \right) \\ & + C_{4,11} \widehat{C}^n_{nc} \sum_{K \in \omega^n_K} \left(\frac{1}{k_n} \|U^n_* - U^n_h\|^2_{L^2(K)} + |||U^n_* - U^n_h|||^2_K \right), \end{aligned} \tag{4.52}$$

where the positive constant $C_{4,11}$ depends only on the minimum angle of meshes $\mathcal{T}^n_h$.

TH-2911_136123010

Proof. The proof borrows the idea of Verfürth [104]. For any $K \in \mathcal{T}_h^n$, let $\psi_K = 27\lambda_1\lambda_2\lambda_3$ be the element bubble function, where $\lambda_i, i = 1, 2, 3$, are the barycentric coordinate functions. By the standard scaling argument, we have the following inf-sup relation:

$$\inf_{v_h \in \mathbb{P}_1(K)} \sup_{\varphi_h \in \mathbb{P}_1(K)} \frac{\int_K v_h \varphi_h \psi_K}{\|\varphi_h\|_{L^2(K)} \|v_h\|_{L^2(K)}} \geq \gamma_0, \tag{4.53}$$

where the constant $\gamma_0 (> 0)$ depends only on the minimum angle of triangle $K \in \mathcal{T}_h^n$. Let $\varphi^n \in \mathbb{P}_1(K)$ be a function such that $\|\varphi^n\|_{L^2(K)} = 1$. Setting $v_h = \mathcal{P}_K R_K^n$ in (4.53) and using (4.48), it gives

$$\begin{aligned}
\gamma_0 \|\mathcal{P}_K R_K^n\|_{L^2(K)} &\leq \int_K (\mathcal{P}_K R_K^n) \psi_K \varphi^n \, dx \\
&= \int_K (\mathcal{P}_K R_K^n - R_K^n) \psi_K \varphi^n \, dx + \int_K \Big(\bar{f}^n - \frac{U_h^n - U_h^{n-1}}{k_n} \Big) \psi_K \varphi^n \, dx \\
&= \int_K (\mathcal{P}_K R_K^n - R_K^n) \psi_K \varphi^n \, dx + \int_K \Big(\frac{U_*^n - U_h^n}{k_n} \Big) \psi_K \varphi^n \, dx \\
&\quad + (\beta \nabla U_*^n, \nabla(\psi_K \varphi^n))_K. \qquad (4.54)
\end{aligned}$$

Since $\psi_K = 0$ on ∂K and $U_h^n \in \mathbb{P}_1(K)$, we have $(\beta \nabla U_h^n, \nabla(\psi_K \varphi^n))_K = 0$ over K. Therefore, from (4.54), we have

$$\begin{aligned}
\gamma_0 \|\mathcal{P}_K R_K^n\|_{L^2(K)} &\leq \int_K (\mathcal{P}_K R_K^n - R_K^n) \psi_K \varphi^n \, dx + \int_K \Big(\frac{U_*^n - U_h^n}{k_n} \Big) \psi_K \varphi^n \, dx \\
&\quad + (\beta \nabla (U_*^n - U_h^n), \nabla(\psi_K \varphi^n))_K.
\end{aligned}$$

By the Cauchy-Schwarz inequality and the inverse estimate $|||\psi_K \varphi^n|||_K \leq C_{4,6} h_K^{-1}$, we have

$$\gamma_0 \|\mathcal{P}_K R_K^n\|_{L^2(K)} \leq \|\mathcal{P}_K R_K^n - R_K^n\|_{L^2(K)} + \frac{1}{k_n} \|U_*^n - U_h^n\|_{L^2(K)} + C_{4,6} \Big(\frac{\beta_K^{\frac{1}{2}}}{h_K} \Big) |||U_*^n - U_h^n|||_K.$$

The definition of $\widehat{C}_{nc}^n$ in (4.49) implies

$$\begin{aligned}
\|\mathcal{P}_K R_K^n\|_{L^2(K)} &\leq C_{4,7} \|\mathcal{P}_K R_K^n - R_K^n\|_{L^2(K)} \\
&\quad + C_{4,7} (\widehat{C}_{nc}^n)^{\frac{1}{2}} \Big(\frac{\beta_K^{\frac{1}{2}}}{h_K} \Big) \left(\frac{1}{k_n} \|U_*^n - U_h^n\|_{L^2(K)}^2 + |||U_*^n - U_h^n|||_K^2 \right)^{\frac{1}{2}}, \qquad (4.55)
\end{aligned}$$

where the constant $C_{4,7} = \max\{1/\gamma_0, C_{4,6}/\gamma_0\}$.

Now, using (4.55), we obtain

$$\frac{h_K^2}{\beta_K} \|R_K^n\|_{L^2(K)}^2 \leq \frac{h_K^2}{\beta_K} \|\mathcal{P}_K R_K^n - R_K^n\|_{L^2(K)}^2 + \frac{h_K^2}{\beta_K} \|\mathcal{P}_K R_K^n\|_{L^2(K)}^2$$

TH-2911_136123010

$$\begin{aligned} &\leq C_{4,8}\,\frac{h_K^2}{\beta_K}\,\|R_K^n - \mathcal{P}_K R_K^n\|_{L^2(K)}^2 \\ &\quad + C_{4,8}\,\widehat{C}_{nc}^n\left(\frac{1}{k_n}\|U_*^n - U_h^n\|_{L^2(K)}^2 + |||U_*^n - U_h^n|||_K^2\right), \end{aligned} \tag{4.56}$$

where the constant $C_{4,8} = \max\{(1 + C_{4,7}^2), C_{4,7}^2\}$.

Let $\psi_e = 4\lambda_1\lambda_2$ be the edge bubble function for any edge $e \in \mathcal{E}_h^n$, where λ_1 and λ_2 are the barycentric coordinate functions associated with the nodes of the edge e. Since $J_{\sigma,e}^n$ is constant on $e \in \mathcal{E}_h^n$, using (4.48) and integration by parts, we get

$$\begin{aligned} \|J_{\sigma,e}^n\|_{L^2(e)}^2 &\leq C_{4,9}\int_e [\beta\nabla U_h^n\cdot\mathbf{n}_e]J_{\sigma,e}^n\psi_e dx \\ &= -C_{4,9}\sum_{K\in\omega_e^n}\int_K \beta(x)\nabla U_h^n\cdot\nabla(J_{\sigma,e}^n\psi_e)dx \\ &= C_{4,9}\sum_{K\in\omega_e^n}\int_K \beta(x)\nabla(U_*^n - U_h^n)\cdot\nabla(J_{\sigma,e}^n\psi_e)dx \\ &\quad + C_{4,9}\sum_{K\in\omega_e^n}\int_K \Big(\frac{U_*^n - U_h^n}{k_n}\Big)(J_{\sigma,e}^n\psi_e)dx - C_{4,9}\sum_{K\in\omega_e^n}\int_K R_K^n(J_{\sigma,e}^n\psi_e)\,dx. \end{aligned}$$

Apply the Cauchy-Schwarz inequality to have

$$\begin{aligned} \|J_{\sigma,e}^n\|_{L^2(e)}^2 &\leq C_{4,9}\Bigg(\sum_{K\in\omega_e^n}\beta_K^{\frac{1}{2}}|||U_*^n - U_h^n|||_K\|\nabla(J_{\sigma,e}^n\psi_e)\|_{L^2(K)} \\ &\quad + \sum_{K\in\omega_e^n}\frac{1}{k_n}\|U_*^n - U_h^n\|_{L^2(K)}\|J_{\sigma,e}^n\psi_e\|_{L^2(K)} + \sum_{K\in\omega_e^n}\|R_K^n\|_{L^2(K)}\|J_{\sigma,e}^n\psi_e\|_{L^2(K)}\Bigg). \end{aligned} \tag{4.57}$$

Now using the fact, for all $K \in \omega_e^n$,

$$\|\nabla(J_{\sigma,e}^n\psi_e)\|_{L^2(K)} \leq C_{4,10}\,h_e^{-\frac{1}{2}}\,\|J_{\sigma,e}^n\|_{L^2(e)} \quad\text{and}\quad \|J_{\sigma,e}^n\psi_e\|_{L^2(K)} \leq C_{4,10}\,h_e^{\frac{1}{2}}\,\|J_{\sigma,e}^n\|_{L^2(e)}$$

in (4.57), it follows that

$$\begin{aligned} \|J_{\sigma,e}^n\|_{L^2(e)}^2 &\leq C_{4,9}C_{4,10}\Bigg(\sum_{K\in\omega_e^n}\beta_K^{\frac{1}{2}}|||U_*^n - U_h^n|||_K h_e^{-\frac{1}{2}}\|J_{\sigma,e}^n\|_{L^2(e)} \\ &\quad + \sum_{K\in\omega_e^n}\frac{1}{k_n}\|U_*^n - U_h^n\|_{L^2(K)}\,h_e^{\frac{1}{2}}\|J_{\sigma,e}^n\|_{L^2(e)} + \sum_{K\in\omega_e^n}\|R_K^n\|_{L^2(K)}h_e^{\frac{1}{2}}\|J_{\sigma,e}^n\|_{L^2(e)}\Bigg), \end{aligned}$$

and hence,

$$\|J_{\sigma,e}^n\|_{L^2(e)}^2 \leq C_{4,9}C_{4,10}\Bigg(\sum_{K\in\omega_e^n}|||U_*^n - U_h^n|||_K^2 + \sum_{K\in\omega_e^n}\frac{h_K^2}{\beta_K k_n^2}\|U_*^n - U_h^n\|_{L^2(K)}^2$$

TH-2911_136123010

$$+\sum_{K\in\omega_e^n}\frac{h_K^2}{\beta_K}\|R_K^n\|^2_{L^2(K)}\Bigg)^{\frac{1}{2}}\times\left(\frac{\beta_e^+}{h_e}\|J^n_{\sigma,e}\|^2_{L^2(e)}\right)^{\frac{1}{2}}.$$

Thus,

$$\begin{aligned}\left(\frac{h_e}{\beta_e^+}\right)\|J^n_{\sigma,e}\|^2_{L^2(e)} &\leq C^2_{4,9}C^2_{4,10}\widehat{C}^n_{nc}\sum_{K\in\omega_e^n}\left(|||U^n_*-U^n_h|||^2_K+\frac{1}{k_n}\|U^n_*-U^n_h\|^2_{L^2(K)}\right)\\ &\quad + C^2_{4,9}C^2_{4,10}\sum_{K\in\omega_e^n}\frac{h_K^2}{\beta_K}\|R^n_K\|^2_{L^2(K)}. \qquad (4.58)\end{aligned}$$

For any $e\in\mathcal{E}_h^n$ and $\mathbf{n}_e=(n_1,n_2)^t$, let $\nu_e=(-n_2,n_1)^t$ denote the unit vector tangent to the edge e. Let $J^n_{\nu,e}=[\nabla U^n_h\cdot\nu_e]$ be the jump of the tangential derivative of the numerical solution U^n_h along the edge e. By the continuity of U^n_h at the mid-point m_e, we have

$$\|J^n_{u,e}\|_{L^2(e)}=\frac{1}{\sqrt{12}}h_e\|J^n_{\nu,e}\|_{L^2(e)}\quad\forall e\in\mathcal{E}^n_I. \qquad (4.59)$$

For a scalar valued function w, denote the operator $\nabla^\perp$ by

$$\nabla^\perp w=\Big(\frac{\partial w}{\partial y},-\frac{\partial w}{\partial x}\Big).$$

We apply integration by parts formula and (4.48) to have

$$\begin{aligned}\|J^n_{\nu,e}\|^2_{L^2(e)} &\leq C_{4,9}\int_e[\nabla U^n_h\cdot\tau_e]J^n_{\nu,e}\psi_e\,ds\\ &= -C_{4,9}\sum_{K\in\omega_e^n}\int_{\partial K}(\nabla U^n_h\cdot\tau_e)J^n_{\nu,e}\psi_e\,ds\\ &= C_{4,9}\sum_{K\in\omega_e^n}\int_K\nabla U^n_h\cdot\nabla^\perp(J^n_{\nu,e}\psi_e)dx\\ &= C_{4,9}\sum_{K\in\omega_e^n}\int_K\nabla(U^n_*-U^n_h)\cdot\nabla^\perp(J^n_{\nu,e}\psi_e)dx\\ &\quad + C_{4,9}\sum_{K\in\omega_e^n}\int_K\Big(\frac{U^n_*-U^n_h}{k_n}\Big)(J^n_{\nu,e}\psi_e)dx-C_{4,9}\sum_{K\in\omega_e^n}\int_K R^n_K(J^n_{\nu,e}\psi_e)\,dx.\end{aligned}$$

Apply the Cauchy-Schwarz inequality to have

$$\begin{aligned}\|J^n_{\nu,e}\|^2_{L^2(e)} &\leq C_{4,9}\Bigg(\sum_{K\in\omega_e^n}\|\nabla(U^n_*-U^n_h)\|_{L^2(K)}\|\nabla^\perp(J^n_{\nu,e}\psi_e)\|_{L^2(K)}\\ &\quad+\sum_{K\in\omega_e^n}\frac{1}{k_n}\|U^n_*-U^n_h\|_{L^2(K)}\|J^n_{\nu,e}\psi_e\|_{L^2(K)}+\sum_{K\in\omega_e^n}\|R^n_K\|_{L^2(K)}\|J^n_{\nu,e}\psi_e\|_{L^2(K)}\Bigg). \qquad (4.60)\end{aligned}$$

TH-2911_136123010

Now, use of the inequalities

$$\|\nabla^{\perp}(J^n_{\nu,e}\psi_e)\|_{L^2(K)} \leq C_{4,10}\, h_e^{-\frac{1}{2}} \|J^n_{\nu,e}\|_{L^2(e)} \quad \text{and} \quad \|J^n_{\nu,e}\psi_e\|_{L^2(K)} \leq C_{4,10}\, h_e^{\frac{1}{2}} \|J^n_{\nu,e}\|_{L^2(e)}, \quad \text{for } K \in \omega^n_e$$

in (4.60) to have

$$\begin{aligned} \|J^n_{\nu,e}\|^2_{L^2(e)} \;\leq\; & C_{4,9}C_{4,10}\Bigg(\sum_{K\in\omega^n_e} \beta_K^{-\frac{1}{2}} |||U^n_* - U^n_h|||_K \; h_e^{-\frac{1}{2}} \|J^n_{\nu,e}\|_{L^2(e)} \\ & + \sum_{K\in\omega^n_e} \frac{1}{k_n} \|U^n_* - U^n_h\|_{L^2(K)}\, h_e^{\frac{1}{2}} \|J^n_{\nu,e}\|_{L^2(e)} + \sum_{K\in\omega^n_e} \|R^n_K\|_{L^2(K)}\, h_e^{\frac{1}{2}} \|J^n_{\nu,e}\|_{L^2(e)} \Bigg). \end{aligned} \tag{4.61}$$

An application of the Young's inequality in (4.61) implies

$$\begin{aligned} \|J^n_{\nu,e}\|^2_{L^2(e)} \;\leq\; & C_{4,9}C_{4,10}\Bigg(\sum_{K\in\omega^n_e} |||U^n_* - U^n_h|||^2_K + \sum_{K\in\omega^n_e} \frac{h_K^2}{\beta_K k_n^2} \|U^n_* - U^n_h\|^2_{L^2(K)} \\ & + \sum_{K\in\omega^n_e} \frac{h_K^2}{\beta_K} \|R^n_K\|^2_{L^2(K)} \Bigg)^{\frac{1}{2}} \times \left(\beta_K^{-1} h_e^{-1} \|J^n_{\nu,e}\|^2_{L^2(e)} \right)^{\frac{1}{2}}, \end{aligned}$$

and hence

$$\begin{aligned} \beta_e h_e \|J^n_{\nu,e}\|^2_{L^2(e)} \;\leq\; & C^2_{4,9}C^2_{4,10}\widehat{C}^n_{nc} \sum_{K\in\omega^n_e} \left(|||U^n_* - U^n_h|||^2_K + \frac{1}{k_n} \|U^n_* - U^n_h\|^2_{L^2(K)} \right) \\ & + C^2_{4,9}C^2_{4,10} \sum_{K\in\omega^n_e} \frac{h_K^2}{\beta_K} \|R^n_K\|^2_{L^2(K)}, \end{aligned}$$

which combine with (4.59) yields

$$\begin{aligned} \frac{\beta^-_e}{h_e} \|J^n_{u,e}\|^2_{L^2(e)} \;\leq\; & \frac{C^2_{4,9}C^2_{4,10}\widehat{C}^n_{nc}}{12} \sum_{K\in\omega^n_e} \left(|||U^n_* - U^n_h|||^2_K + \frac{1}{k_n} \|U^n_* - U^n_h\|^2_{L^2(K)} \right) \\ & + \frac{C^2_{4,9}C^2_{4,10}}{12} \sum_{K\in\omega^n_e} \frac{h_K^2}{\beta_K} \|R^n_K\|^2_{L^2(K)}. \end{aligned} \tag{4.62}$$

Putting (4.56), (4.58) and (4.62) together, the standard error indicator (4.10) leads to

$$\begin{aligned} \eta^n_{3,K} \;\leq\; & \left(1 + \frac{13C^2_{4,9}C^2_{4,10}}{12}\right) \sum_{K\in\omega^n_K} \left(\frac{h_K^2}{\beta_K} \|R^n_K\|^2_{L^2(K)} \right) \\ & + \frac{13C^2_{4,9}C^2_{4,10}\widehat{C}^n_{nc}}{12} \sum_{K\in\omega^n_K} \left(|||U^n_* - U^n_h|||^2_K + \frac{1}{k_n} \|U^n_* - U^n_h\|^2_{L^2(K)} \right) \\ \leq\; & C_{4,11} \sum_{K\in\omega^n_K} \left(\frac{h_K^2}{\beta_K} \|R^n_K - \mathcal{P}_K R^n_K\|^2_{L^2(K)} \right) \end{aligned}$$

TH-2911_136123010

$$+ C_{4,11}\widehat{C}^n_{nc}\sum_{K\in\omega^n_K}\Big(|||U^n_* - U^n_h|||^2_K + \frac{1}{k_n}\|U^n_* - U^n_h\|^2_{L^2(K)}\Big), \tag{4.63}$$

where $C_{4,11} = \max\{C_{4,8}(1+13C^2_{4,9}C^2_{4,10}/12), C_{4,8}(1+13C^2_{4,9}C^2_{4,10}/12)+13C^2_{4,9}/12\}$. This completes the proof. □

Remark 4.3.4. *Taking summation over all $K \in \mathcal{T}^n_h$, (4.9) yields*

$$\begin{aligned}\eta^n_{3,space} &\leq C_{4,11}\sum_{K\in\mathcal{T}^n_h}\sum_{K\in\omega^n_K}\left(\frac{h^2_K}{\beta_K}\,\|R^n_K - \mathcal{P}_K R^n_K\|^2_{L^2(K)}\right)\\ &\quad + C_{4,11}\widehat{C}^n_{nc}\sum_{K\in\mathcal{T}^n_h}\sum_{K\in\omega_K}\Big\{\frac{1}{k_n}\|U^n_* - U^n_h\|^2_{L^2(K)} + |||U^n_* - U^n_h|||^2_K\Big\}\\ &= C_{4,11}\ osc(R^n_K, \mathcal{T}^n_h)^2 + C_{4,11}\widehat{C}^n_{nc}\,\|U^n_* - U^n_h\|^2_{k_n,\Omega}. \end{aligned}\tag{4.64}$$

We now proceed to obtain a local lower bound using the modified indicator $\bar{\eta}^n_{3,K}$. For this purpose, the following lemma is proved to be convenient. For a proof, see [20].

Lemma 4.3.5. Let U^n_h be the solution of (4.6). Let $K \in \mathcal{T}^n_h$ be a triangle whose at least one vertex $z \in \mathcal{N}^n_\vartheta$ and let $\tau_{z,K} = K \cap \omega^n_{z,\tau}$. Let $\mathcal{I}^n_{\frac{h}{2}}$ be an interpolation operator defined in (4.12) with $K_z \in \widehat{\omega}^n_{z,\frac{h}{2},K}$. Then, we have

$$\frac{\beta_K}{h_K}\|\mathcal{I}^n_{\frac{h}{2}}U^n_h - U^n_h\|^2_{L^2(\partial\tau_{z,K})} \leq 2C^n_{z,K}\sum_{e\in\mathcal{E}^n_{z,\frac{h}{2}}}\frac{\beta^-_e}{h_e}\|[U^n_h]\|^2_{L^2(e)},$$

where $C^n_{z,K} = \max\limits_{\tau\in\widehat{\omega}^n_{z,\frac{h}{2},K}}\dfrac{\beta_K}{\beta_\tau}$.

Remark 4.3.5. *If ω^n_z is quasi-monotone, then $C^n_{z,K} = 1$, $\forall K \in \omega^n_z$.*

Remark 4.3.6. *Let us denote $\bar{\eta}^n_{J_u} = \left(\sum\limits_{K\in\mathcal{T}^n_h}(\bar{\eta}^n_{J_u,K})^2\right)^{\frac{1}{2}}$ to be the modified estimator associated with the solution jump, where*

$$(\bar{\eta}^n_{J_u})^2 = \sum_{z\in\mathcal{N}^n_h\setminus\mathcal{N}^n_\vartheta}\sum_{e\in\mathcal{E}^n_{z,h/2}}\frac{\beta^-_e}{2h_e}\|J_{u,e}\|^2_{L^2(e)} + \sum_{z\in\mathcal{N}^n_h\cap\mathcal{N}^n_\vartheta}\sum_{\tau\in\omega^n_{z,h/2}}\frac{\beta_\tau}{4h_\tau}\|\mathcal{I}^n_{\frac{h}{2}}U^n_h - U^n_h\|^2_{L^2(\partial\tau)}. \tag{4.65}$$

Then, the following estimate holds (cf. [20, Lemma 6.2]):

$$\widehat{\eta}^n_{J_u} \leq \bar{\eta}^n_{J_u}. \tag{4.66}$$

In the following, we provide a lower bound for the error in terms of the modified indicator $\bar{\eta}^n_{3,K}$ defined in (4.15).

TH-2911_136123010

Theorem 4.3.3. *Let U_h^n and U_*^n be the solutions of (4.6) and (4.48), respectively. Then, for all $K \in \mathcal{T}_h^n$, $n = 1, 2, \ldots, m$, we have*

$$\begin{aligned}\bar{\eta}_{3,K}^n \;\leq\; & \widehat{C}_{4,11} \max_{z\in\mathcal{N}_K^n} \widehat{C}_z^n \sum_{K\in\omega_K^n} \left(\frac{h_K^2}{\beta_K} \, \|R_K^n - \mathcal{P}_K R_K^n\|_{L^2(K)}^2 \right) \\ & + \widehat{C}_{4,11}\widehat{C}_{nc}^n \max_{z\in\mathcal{N}_K^n} \widehat{C}_z^n \sum_{K\in\omega_K^n} \left(\frac{1}{k_n} \|U_*^n - U_h^n\|_{L^2(K)}^2 + |||U_*^n - U_h^n|||_K^2 \right), \end{aligned} \tag{4.67}$$

where the constants $\widehat{C}_{4,11}$ depending only on the minimum angle of the triangulation $\mathcal{T}_h^n$, and $\widehat{C}_z^n = \max\limits_{z\in\mathcal{N}_K^n} C_{z,K}^n$.

Proof. For any $K \in \mathcal{T}_h^n$, let $z \in \mathcal{N}_h^n$ with $z \notin \mathcal{N}_h^n \cap \mathcal{N}_\vartheta^n$. A similar argument as (4.63) leads to the estimate for $\bar{\eta}_K^n$.

When $z \in \mathcal{N}_h^n \cap \mathcal{N}_\vartheta^n$, for each $\tau \in \omega_{z,\tau}^n$ we argue as (4.56) and (4.58) to bound the element residual $\eta_{R_\tau,\tau}^n$ and the edge flux jump $\eta_{J_\sigma,\tau}^n$ by

$$\begin{aligned}\frac{h_\tau^2}{\beta_\tau} \, \|R_\tau^n\|_{L^2(\tau)}^2 \;\leq\; & C_{4,8} \, \frac{h_\tau^2}{\beta_\tau} \, \|R_\tau^n - P_\tau R_\tau^n\|_{L^2(\tau)}^2 \\ & + C_{4,8}\widehat{C}_{nc}^n \left(\frac{1}{k_n} \|U_*^n - U_h^n\|_{L^2(\tau)}^2 + |||U_*^n - U_h^n|||_\tau^2 \right), \end{aligned} \tag{4.68}$$

and for each $e \in \mathcal{E}_{z,h/2}^n$ (i.e., the set of all edges in $\mathcal{T}_{h/2}^n$ having z as a common vertex),

$$\begin{aligned}\left(\frac{h_e}{\beta_e^+}\right) \|J_{\sigma,e}^n\|_{L^2(e)}^2 \;\leq\; & C_{4,9}^2 C_{4,10}^2 \sum_{\tau\in\omega_e^n} \frac{h_\tau^2}{\beta_\tau} \, \|R_\tau^n\|_{L^2(\tau)}^2 \\ & + C_{4,9}^2 C_{4,10}^2 \widehat{C}_{nc}^n \sum_{\tau\in\omega_e^n} \left(|||U_*^n - U_h^n|||_\tau^2 + \frac{1}{k_n} \|U_*^n - U_h^n\|_{L^2(\tau)}^2 \right). \end{aligned} \tag{4.69}$$

It now remains to bound of the modified numerical solution jump $\bar{\eta}_{J_u,K}^n$ defined in (4.65). To bound the first term on the right hand side of (4.65), we use the similar argument as (4.62). For the second term, we use Lemma 4.3.5. Then for each $\tau \in \omega_{z,\tau}^n$ and $e \in \mathcal{E}_{z,h/2}^n$, we have

$$\begin{aligned}\frac{\beta_e^-}{h_e} \|J_{u,e}^n\|_{L^2(e)}^2 \;\leq\; & \frac{C_{4,9}^2 C_{4,10}^2}{12} \sum_{\tau\in\omega_e^n} \frac{h_\tau^2}{\beta_\tau} \, \|R_\tau^n\|_{L^2(\tau)}^2 \\ & + \frac{C_{4,9}^2 C_{4,10}^2 \widehat{C}_{nc}^n}{12} \sum_{\tau\in\omega_e^n} \left(|||U_*^n - U_h^n|||_\tau^2 + \frac{1}{k_n} \|U_*^n - U_h^n\|_{L^2(\tau)}^2 \right), \end{aligned} \tag{4.70}$$

and

$$\frac{\beta_K}{h_K} \, \|\mathcal{I}_{\frac{h}{2}}^n U_h^n - U_h^n\|_{L^2(\partial\tau)}^2 \;\leq\; \frac{C_{4,9}^2 C_{4,10}^2}{6} \, C_{z,K}^n \sum_{e\in\mathcal{E}_{z,\frac{h}{2}}^n} \left(\frac{h_\tau^2}{\beta_\tau} \, \|R_\tau^n\|_{L^2(\omega_e^n)}^2 \right)$$

TH-2911_136123010

$$+\frac{C_{4,9}^2C_{4,10}^2\widehat{C}_{nc}^n}{6}\,C_{z,K}^n\sum_{e\in\mathcal{E}^n_{z,\frac{h}{2}}}\left(|||U_*^n-U_h^n|||_{\omega_e^n}^2+\frac{1}{k_n}\|U_*^n-U_h^n\|^2_{L^2(\omega_e^n)}\right). \tag{4.71}$$

Combining (4.68)-(4.71) and using (4.14) we obtain the following estimate

$$\begin{aligned}\bar{\eta}_{3,K}^n &\leq \sum_{z\notin\mathcal{N}_h^n\cap\mathcal{N}_\vartheta^n}\sum_{\tau\subset K}\bar{\eta}_\tau^n+\sum_{z\in\mathcal{N}_\vartheta^n}\sum_{\tau\subset K}\bar{\eta}_\tau^n\\ &\leq \widehat{C}_{4,11}\widehat{C}_z^n\sum_{K\in\omega_K^n}\left(\frac{h_K^2}{\beta_K}\,\|R_K^n-\mathcal{P}_KR_K^n\|^2_{L^2(K)}\right)\\ &\quad+\widehat{C}_{4,11}\widehat{C}_{nc}^n\widehat{C}_z^n\sum_{K\in\omega_K^n}\left(\frac{1}{k_n}\|U_*^n-U_h^n\|^2_{L^2(K)}+|||U_*^n-U_h^n|||_K^2\right)\end{aligned} \tag{4.72}$$

with $\widehat{C}_{4,11}=\max\{C_{4,8}+7C_{4,8}C_{4,9}^2C_{4,10}^2/12, C_{4,8}+13C_{4,9}^2C_{4,10}^2/12+13C_{4,8}C_{4,9}^2C_{4,10}^2/12\}$, and this completes the proof. □

Remark 4.3.7. *Taking summation over all $K\in\mathcal{T}_h^n$, (4.72) yields*

$$\begin{aligned}\bar{\eta}_{3,space}^n &\leq \sum_{K\in\mathcal{T}_h^n}\widehat{C}_{4,11}\widehat{C}_z^n\sum_{K\in\omega_K^n}\left(\frac{h_K^2}{\beta_K}\,\|R_K^n-\mathcal{P}_KR_K^n\|^2_{L^2(K)}\right)\\ &\quad+\sum_{K\in\mathcal{T}_h^n}\widehat{C}_{4,11}\widehat{C}_{nc}^n\widehat{C}_z^n\sum_{K\in\omega_K^n}\left(\frac{1}{k_n}\|U_*^n-U_h^n\|^2_{L^2(K)}+|||U_*^n-U_h^n|||_K^2\right)\\ &= \widehat{C}_{4,11}\;osc(R_K^n,\mathcal{T}_h^n)^2+\widehat{C}_{4,11}\widehat{C}_{nc}^n\widehat{C}_z^n\,\|U_*^n-U_h^n\|^2_{k_n,\Omega}.\end{aligned} \tag{4.73}$$

Remark 4.3.8. *The efficiency bound for the local error ensures that over refinement will not occur for the refinement strategy based on the space error indicator (4.14).*

4.4 Adaptive Algorithm

This section provides a space-time adaptive algorithm for the parabolic interface problem (4.1)-(4.2). Let ϵ_{time} be the total tolerance related to the time discretization. Based on the error equidistribution strategy [94], from (4.34), we write

$$3\sum_{n=1}^N k_n\eta_{3,\text{time}}^n+\sum_{n=1}^N\int_{t_{n-1}}^{t_n}\|f-\bar{f}^n\|^2_{L^2(\Omega)}dt\leq\epsilon_{\text{time}}. \tag{4.74}$$

To obtain (4.74) we have to adjust the time-step size k_n such that the following conditions are satisfied:

$$\eta_{3,\text{time}}^n\leq\frac{\epsilon_{\text{time}}}{6T},\qquad\int_{t_{n-1}}^{t_n}\|f-\bar{f}^n\|^2_{L^2(\Omega)}dt\leq\frac{\epsilon_{\text{time}}}{2T}. \tag{4.75}$$

TH-2911_136123010

The following conditions can be used to control the time-step size: For any given $\delta_{\text{time}} \in (0,1)$,

$$\eta^n_{3,\text{time}} \leq \delta_{time}\frac{\epsilon_{\text{time}}}{6T}, \qquad \int_{t_{n-1}}^{t_n} \|f - \bar{f}^n\|^2_{L^2(\Omega)}dt \leq \frac{\delta_{time}\epsilon_{\text{time}}}{2T}. \tag{4.76}$$

Let ϵ_{space} be the tolerance related to the space discretization. Then for each time step n, the stopping criterion for mesh adaptation is given by

$$\eta^n_{3,\text{space}} \leq \frac{\epsilon_{\text{space}}}{T}, \tag{4.77}$$

which is suitable for mesh refinements.

We now use the similar arguments of Remark 2.4.1, Chapter 2 to introduce the coarsening error indicator:

$$\eta^n_{3,\text{coarse}} = \frac{1}{k_n}\|I^n_H U^n_h - U^n_h\|^2_{L^2(\Omega)} + |||I^n_H U^n_h - U^n_h|||^2_\Omega, \tag{4.78}$$

where $I^n_H : C(\bar{\Omega}) \to S^n_H$ is the standard linear interpolation operator; $\mathcal{T}^n_H$ is the coarsening of the mesh $\mathcal{T}^n$, and $U^n_H \in S^n_H$ is the discrete problem (4.6) over meshes $\mathcal{T}^n_H$.

The following algorithm incorporates this idea and presents for one single time step (cf., [29, 94]).

Algorithm 4.4.1. *(Space and time adaptive algorithm).* Given tolerances ϵ_{time}, ϵ_{space} and ϵ_{coarse}, parameters $\gamma_1 \in (0,1)$ and $\gamma_2 > 1$. Let U^{n-1}_h be the computed value at time t_{n-1} with the time step size k_n and the mesh $\mathcal{T}^{n-1}_h$.

Step 1: $\mathcal{T}^n_h := \mathcal{T}^{n-1}_h$, $k_n := k_{n-1}$, $t_n := t_{n-1} + k_n$
solve the fully discrete problem (4.6) for U^n_h on $\mathcal{T}^n_h$
compute the error estimates on the mesh $\mathcal{T}^n_h$

Step 2: while (4.75) is not satisfied
do
{
$k_n := \gamma_1 k_n$, $t_n := t_{n-1} + k_n$
solve the fully discrete problem (4.6) for U^n_h on $\mathcal{T}^n_h$
compute the error estimates on the mesh $\mathcal{T}^n_h$
}
end

Step 3: while $\left(\eta^n_{3,space} > \frac{\epsilon_{space}}{T}\right)$ do
{

TH-2911_136123010

refine mesh $\mathcal{T}_h^n$ to produce a modified mesh $\hat{\mathcal{T}}_h^n$
solve the fully discrete problem (4.6) for U_h^n on $\hat{\mathcal{T}}_h^n$
compute the error estimates on $\hat{\mathcal{T}}_h^n$
while (4.75) is not satisfied
goto step 2
}
end

Step 4: if $(\eta_{3,coarse}^n \leq \frac{\epsilon_{coarse}}{T})$
coarsening $\mathcal{T}^n$ to produce a modified mesh $\check{\mathcal{T}}^n$
solve the fully discrete problem for U_h^n on $\check{\mathcal{T}}^n$

Step 5: if (4.76) is satisfied then
{ $k_n := \gamma_2 k_n$ }
end

4.5 Numerical Experiment

This section reports numerical results to illustrate the behavior of the derived error estimators in in Theorem 4.3.1 and 4.3.2 for the problem (4.1)-(4.2). All computations are carried out using the software FreeFEM++ (cf. [65]).

Example 4.1. We consider the problem (4.1)-(4.2) with the computational domain $\Omega = (0,2)\times(0,1)$. The interface Γ occurs at $x = 1$ which divides Ω into two subdomains such that $\Omega_1 = (0,1)\times(0,1)$ and $\Omega_2 = (1,2)\times(0,1)$. We choose the exact solution of (4.1)-(4.2) as

$$u(x,y,t) = \begin{cases} e^{\sin t}\sin(\pi x)\sin(\pi y) & \text{in } \Omega_{1,T}, \\ -e^{\sin t}\sin(2\pi x)\sin(\pi y) & \text{in } \Omega_{2,T}. \end{cases}$$

We choose the discontinuous coefficient β as $\beta_1 = 1$ and $\beta_2 = \frac{1}{2}$ such that u satisfies the jump condition (4.3) across the interface Γ.

We now compute the energy error $Err := \left(\sum_{n=1}^N k_n |||u - U_h^n|||_\Omega^2\right)^{1/2}$, the error estimator $\eta_{3,1}$ is defined by

$$\eta_{3,1}^2 = \sum_{n=1}^N k_n(\eta_{3,space}^n + \eta_{3,coarse}^n + 3\eta_{3,time}^n) + \sum_{n=1}^m \int_{t_{n-1}}^{t_n} \|f - \bar{f}^n\|_{L^2(\Omega)}^2 dt,$$

TH-2911_136123010

and the effectivity index which is defined by eff. index $= \eta_{3,1}/Err$. Here we compute our numerical results at time $T = 0.1$. All the constants involved in the estimators are taken as 1, and tolerances $\epsilon_{time}, \epsilon_{space}$ are chosen to be equal, say, ϵ and $\epsilon_{coarse} = 0.5\,\epsilon_{space}$. The parameters are chosen as $\gamma_1 = 0.5, \gamma_2 = 2$, and $\delta_{time} = 0.5$.

Table 4.1: The degrees of freedm (DOF), the error indicator $\eta_{3,1}$, the energy error (Err) and the effectivity index (eff. index) at time $t = 0.1$ and tolerance $\epsilon = 0.03$

DOF	$\eta_{3,1}$	Err
845	0.150911	0.102192
1496	0.086228	0.059237
2776	0.049396	0.033048

Table 4.2: The tolerances ϵ, the degrees of freedm (DOF), the error estimator $\eta_{3,1}$, the energy error (Err) and the effectivity index (eff. index) at time $t = 0.1$.

ϵ	DOF	$\eta_{3,1}$	Err	eff. index
0.03	2776	0.049396	0.033048	1.4946
0.015	5571	0.029546	0.024219	1.2199
0.0075	8831	0.016528	0.013235	1.2473

For fixed time $t = 0.1$, in Figures 4.1-4.3, adaptive meshes are shown at three different steps. For a fixed time $t = 0.1$ and tolerance $\epsilon = 0.03$, Table 4.1 reports the degrees of freedm (DOF) , the error indicator ($\eta_{3,1}$), the total energy error (Err) and the effectivity index (eff. index) in each step of adaptive mesh generation. We provide the graphs for the optimality decay of the estimators in Figure 4.4(a) and the energy error versus the number of degrees of freedom in Figure 4.4(b). At a fixed time $t = 0.1$ but different tolerances ϵ, the degrees of freedom, the error indicator, the energy error and the effectivity index are shown in Table 4.2. The results in Table 4.2 reveal that for a fixed time but different tolerances, the error is decreasing and the effectivity index is almost constant. From Figures 4.1-4.3, it is observed that the meshes are refined as expected near the interface Γ and higher density of the node points are distributed along the interface line $x = 1$. Our experiment for the test problem indicates that the

TH-2911_136123010

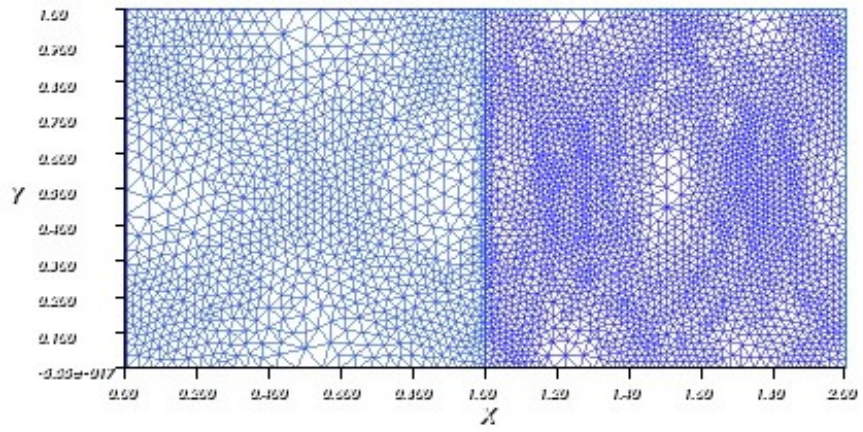

Figure 4.1: Adaptive mesh at step 1 when $t = 0.1$.

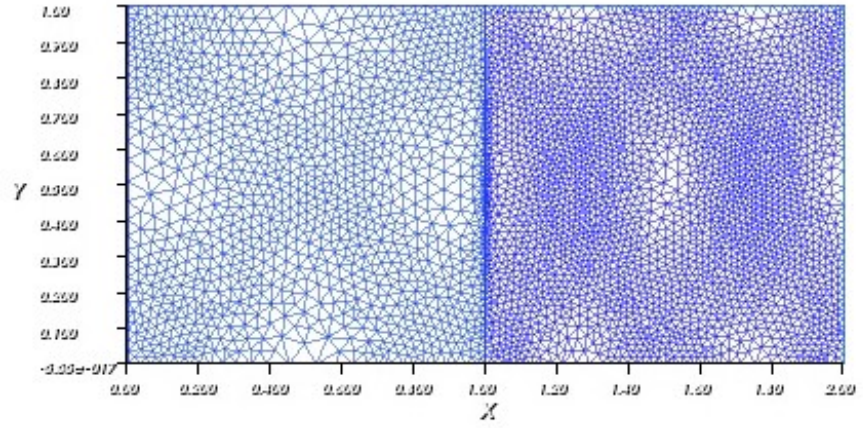

Figure 4.2: Adaptive mesh at step 2 when $t = 0.1$.

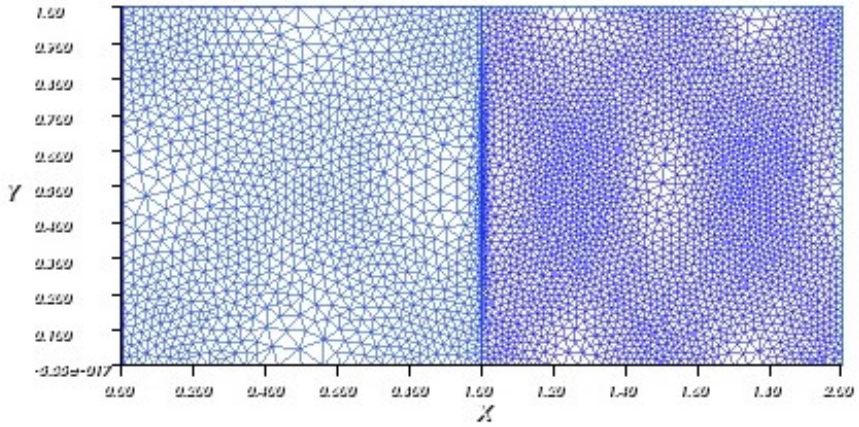

Figure 4.3: Adaptive mesh at step 3 when $t = 0.1$.

TH-2911_136123010

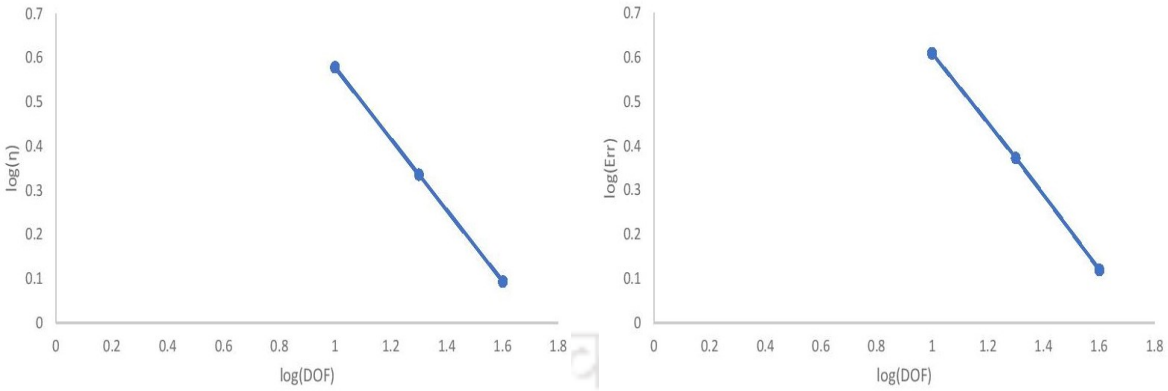

(a) (b)

Figure 4.4: (*a*) Optimality of the estimator and the optimal decay is observed by the line of slope -0.938; (*b*) The quasi-optimal decay is observed by the line of slope -0.814.

estimators derived in this paper are providing promising numerical results.

4.6 Concluding Remarks

In this chapter, we have considered a residual-based *a posteriori* error estimates for the PIP using nonconforming finite elements. Both the upper and lower bounds for the error are derived. The reliability of the estimator is derived without using the Helmholtz decomposition technique. In contrast to the existing estimators which consist of the element residual, the edge flux jump, and the edge tangential derivative jump due to Helmholtz decomposition, our estimators replace the edge tangential derivative jump by the edge solution jump. A space-time adaptive algorithm based on our error estimator is proposed. In our numerical experiment, the finite element meshes are adaptively refined around the interface Γ which supports the validity of our proposed algorithm.

TH-2911_136123010

5

An AFEM for PIPs using Noncoforming Immersed Finite Elements

In this chapter, we study *a posteriori* error analysis for PIPs using nonconforming IFE method in a two-dimensional convex polygonal domain. The finite element discretization is such that mesh points need not fit the interface. We use the piecewise linear finite elements to approximate the spatial variable, whereas the backward Euler method is used for the time discretization. The basic idea of the IFE method is to modify the basis functions which satisfy the natural jump conditions across the interface. Some new error indicators are introduced to control the error due to non-body fitted mesh. For the adaptive mesh refinement procedure, the residual-based *a posteriori* error estimates are derived using energy arguments. A global upper and a local lower bounds for the error are established. Numerical results are reported to illustrate the performance of the derived error indicators using the proposed adaptive algorithm.

5.1 Introduction

We now recall the PIP of the following form

$$\frac{\partial u}{\partial t} - \nabla \cdot (\beta(x)\nabla u) = f(x,t) \quad \text{in} \quad \Omega_T \tag{5.1}$$

subject to the initial and boundary conditions

$$u(x,0) = u_0(x) \quad \text{in} \quad \Omega; \qquad u = \mathcal{G}(x,t) \quad \text{on} \quad \partial\Omega_T, \tag{5.2}$$

and the homogeneous jump conditions

$$[u] = 0, \quad \left[\beta \frac{\partial u}{\partial \mathbf{n}}\right] = 0 \quad \text{across} \quad \Gamma, \tag{5.3}$$

TH-2911_136123010

where $\Omega_T = \Omega \times (0, T]$ and $\partial\Omega_T = \partial\Omega \times [0, T]$ with $T < \infty$. Here Ω is a bounded convex polygonal domain in $\mathbb{R}^2$ with Lipschitz boundary $\partial\Omega$. The interface Γ is assumed to be C^2-smooth which divides Ω into two subdomains Ω_1 and Ω_2 such that $\Gamma = \bar{\Omega}_1 \cap \bar{\Omega}_2$ with $\partial\Omega_1 = \Gamma$. The symbol $[v]$ denotes the jump of a quantity v across the interface Γ, *i.e.*, $[v](x) = v_1(x) - v_2(x)$, $x \in \Gamma$ with $v_i(x) = v(x)|_{\Omega_i}$, $i = 1, 2$, and $\mathbf{n}$ denotes the unit outward normal to the boundary Γ. Assume that the coefficient function β is positive and piecewise constant on each subdomain, i.e.,

$$\beta(x) = \beta_i \quad \text{for} \quad x \in \Omega_i \ (i = 1, 2).$$

Further, we assume that the source function $f \in L^2(0, T; L^2(\Omega))$, the initial data $u_0 \in H^1(\Omega)$ and the function $\mathcal{G}(x, t)$ is assumed to be smooth for our purpose.

For the nonconforming IFE approximation of the problem (5.1)-(5.3), we first introduce its weak formulation as follows: Seek a function $u : [0, T] \to H^1_{\mathcal{G}}(\Omega)$ such that

$$\begin{aligned} \left(\frac{\partial u}{\partial t}, \phi\right) + (\beta(x)\nabla u, \nabla\phi) &= (f, \phi) \quad \forall \phi \in H^1_0(\Omega), \\ u(0) &= u_0, \end{aligned} \tag{5.4}$$

where $H^1_{\mathcal{G}}(\Omega) = \{v \in H^1(\Omega) \ : \ v = \mathcal{G} \text{ on } \partial\Omega\}$.

For the interface problem, due to the low global regularity and the irregular geometry of the interface, usually the body-fitted meshes are used to achieve the optimal or almost optimal convergence, see [60, 98, 101]. It is technically difficult to construct good body-fitted meshes for problems involving geometrically complicated interfaces. To overcome this difficulty, Li *et al.* have first introduced immersed finite element (IFE) method in [75]. The basic idea of the IFE method is to locally modify basis functions on interface triangles to fit the interface jump condition (5.3). For the relevant literature on the IFE method, we refer to [12, 16, 55, 57, 62, 72, 78, 99] for elliptic and parabolic interface problems for the *a priori* error analysis, [58, 64, 111] for the parabolic moving interface problems and the references cited therein. Further, we refer to [59, 77] for nonconforming IFE method for elliptic interface problems and the reference cited therein.

The adaptive IFE method for parabolic and elliptic problems are described in [30, 31, 108]. In [31], Chen *et al.* have presented adaptive IFE methods for elliptic and Maxwell interface problems using conforming finite elements. The authors of [30] have introduced an adaptive IFE method for purely parabolic problems in time-variable domains together with arbitrary Lagrangian-Eulerian time discretization scheme. An adaptive mesh refinement technique for elliptic interface problems using the nonconforming IFE method has been recently studied by Wu *et al.* in [108].

TH-2911_136123010

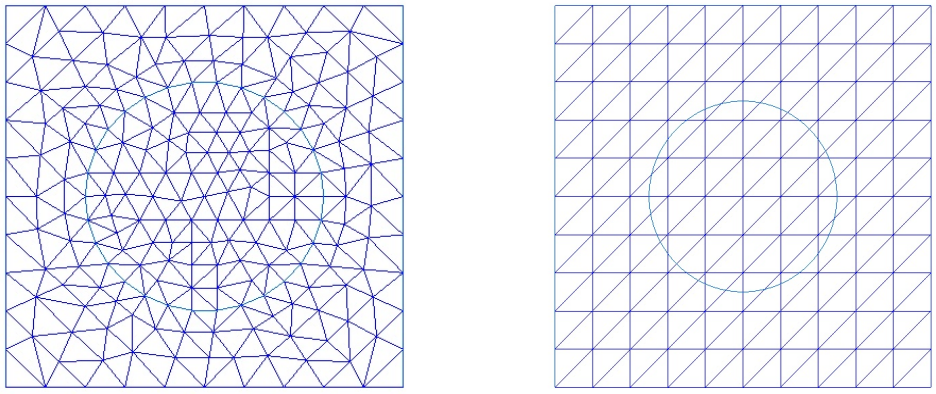

(a) (b)

Figure 5.1: (a) The fitted mesh and (b) the unfitted mesh of domain Ω.

The purpose of this chapter is to study *a posteriori* error analysis and develop an adaptive algorithm for the PIP (5.1)-(5.3) using the nonconforming IFE method. The use of interface independent meshes is the main advantage of the proposed method and hence structured or even Cartesian meshes can be used to solve interface problems. Some new error indicators are introduced to control the error due to non-body fitted mesh. We derive global *a posteriori* upper bound for the error using the energy method which is bounded by the element residual and the jump residual. A lower bound for the local error in terms of the space error indicator is also derived using the idea of [29]. A space-time adaptive algorithm is presented which is based on the refinement strategy of Dörfler [43], [83] and [29]. A numerical experiment is performed to implement the derived error indicators. In our study, it is assumed that the interface is independent of time and the finite element mesh whose vertices do not necessarily lie on the interface.

The layout of this chapter is as follows: Section 5.2 introduces the space-time nonconforming IFE discretization. The global upper and local lower bounds for the error are derived in Section 5.3. In Section 5.4, an adaptive algorithm for the proposed method is presented. Numerical results are provided to illustrate the behavior of the derived estimators in Section 5.6. Finally, a concluding remark is given in the last section.

5.2 Nonconforming IFE discretization

This section first introduce an IFE discretization and the corresponding nonconforming finite element space for our analysis. The space-time finite element formulation for the problem (5.1)-(5.3) is also described.

For the space-time nonconforming IFE space, we first divide the time interval $(0, T]$

TH-2911_136123010

into N number of subintervals $\{(t_{n-1}, t_n]\}_{n=1}^{N}$. Let $k_n = t_n - t_{n-1}$ be the time-step size of the subinterval $(t_{n-1}, t_n]$. At each time step t_n, $n = 1, \ldots, N$, let $\mathcal{T}^n$ be a regular triangulation of the domain Ω. Assume that $\mathcal{T}^n$ satisfies the usual admissibility, and compatibility conditions. A triangle $K \in \mathcal{T}^n$ is said to be an interface triangle if the interface Γ passes through the interior of triangle K; otherwise, K is called a non-interface triangle. Let $\mathcal{T}_\Gamma^n$ be the set of all interface triangles and the set of non-interface triangles be $\mathcal{T}^n \setminus \mathcal{T}_\Gamma^n$. Without loss of generality, we assume that the triangulation $\mathcal{T}^n$ satisfies the following conditions (cf.[18, 34]):

A1. $\bar{\Omega} = \cup_{K \in \mathcal{T}^n} K$.

A2. If $K_1, K_2 \in \mathcal{T}^n$ and $K_1 \neq K_2$, then either $\bar{K_1} \cap \bar{K_2} = \emptyset$ or $\bar{K_1} \cap \bar{K_2}$ is a common vertex or an edge of both triangles.

A3. If the interface Γ meets one edge of a triangle at more than two points, then the edge is part of Γ.

A4. For any triangle $K \in \mathcal{T}_\Gamma^n$, if Γ intersects K at two points, then these two points must be on different edges of the triangle K.

A5. The segment of the interface Γ in a triangle $K \in \mathcal{T}^n$ is defined by a piecewise C^2 function and the function space $C^2(K)$ is dense in $H^2(K)$.

For any $K \in \mathcal{T}^n$, let h_K be the diameter of a triangle K, and ∂K denotes the set of edges of the triangle K. Let $\mathcal{N}^n$ be the set of all vertices in $\mathcal{T}^n$, and $\mathcal{N}_K^n$ denotes the set of vertices of a triangle K. For any $K \in \mathcal{T}^n$, let ω_K^n be the set of all triangles in $\mathcal{T}^n$ having nonempty intersection with K, i.e., $\omega_K^n = \cup_{K' \cap K \in \partial K} K'$.

Associated with the triangulation $\mathcal{T}^n$, let K be an interface triangle in $\mathcal{T}^n$ with vertices A, B and C. The interface Γ passes through the interior of K and intersect two edges of K at the points D and E (see Fig. 5.2). Let the arc DME be $\Gamma_K = K \cap \Gamma$. Now we approximate Γ_K by the line segment $\overline{DE}$ and is denoted by Γ_K^h. The line segment $\overline{DE}$ divides K into two parts $\mathcal{K}_1 = \triangle CDE$ and $\mathcal{K}_2 = K - \mathcal{K}_1$ such that $K = \mathcal{K}_1 \cup \mathcal{K}_2 \cup \overline{DE}$. Let

$$\widetilde{K} = K - (\Omega_1 \cap \mathcal{K}_1) - (\Omega_2 \cap \mathcal{K}_2) \tag{5.5}$$

be such that $meas(\widetilde{K}) = O(h_K^3)$ (cf. [32]). This indicates that the interface is perturbed in a magnitude of $O(h_K^2)$.

Following [75, 108], we now construct the local basis functions on each triangle $K \in \mathcal{T}^n$ as follows. For any non-interface triangle $K \in \mathcal{T}^n \setminus \mathcal{T}_\Gamma^n$, let $S_{h,nc}^n(K)$ denote the

TH-2911_136123010

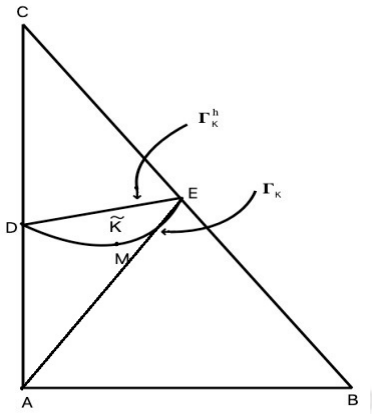

Figure 5.2: An interface triangle K.

space of all piecewise linear functions span by the standard nodal basis function of K. Our attention is only for an interface triangle $K \in \mathcal{T}_\Gamma^n$. We consider a reference interface triangle $K \in \mathcal{T}_\Gamma^n$ whose pictorial representation is given in Fig.5.2. Let the coordinates of A, B, C, D and E be

$$(0,0),\ \ (h_K,0),\ \ (0,h_K),\ \ (0,y_1)\ \text{ and }\ (h_K-y_2,y_2),$$

with $0 \le y_1, y_2 \le h_K$. The nodal basis function ϕ defined on $K \in \mathcal{T}_\Gamma^n$ as

$$\phi = \begin{cases} \phi_1 := a_0 + a_1 x + a_2(y - h_K), & \text{if } (x,y) \in \mathcal{K}_1, \\ \phi_2 := b_0 + b_1 x + b_2 y, & \text{if } (x,y) \in \mathcal{K}_2, \end{cases} \tag{5.6}$$

$$\phi_1(D) = \phi_2(D), \quad (\mathbf{n}_t \cdot \nabla\phi_1)(E) = (\mathbf{n}_t \cdot \nabla\phi_2)(E), \quad \beta_1 \frac{\partial \phi_1}{\partial \mathbf{n}} = \beta_2 \frac{\partial \phi_2}{\partial \mathbf{n}}, \tag{5.7}$$

where the coefficients $a_i, b_i \in \mathbb{R}$ $(i = 0, 1, 2)$ and $\mathbf{n}_t$ denotes the unit tangent of the approximated interface Γ_K^h.

The local finite element space on each triangle $K \in \mathcal{T}^n$ is then defined by

$$S_{h,nc}^n(K) = \begin{cases} \{\phi : \phi \text{ is linear on } K\}, & \text{if } K \in \mathcal{T}^n \setminus \mathcal{T}_\Gamma^n, \\ \{\phi : \phi \text{ is defined by (5.6)} - \text{(5.7)}\}, & \text{if } K \in \mathcal{T}_\Gamma^n. \end{cases}$$

Thus, the dimension of $S_{h,nc}^n(K)$ is also three for all K in $\mathcal{T}^n$. Let $S_h^n(\Omega)$ be the piecewise linear polynomial space on Ω at time t_n. The nonconforming IFE space on the domain Ω is defined by

$$S_{h,nc}^n(\Omega) = \Big\{\phi :\ \phi|_K \in S_{h,nc}^n(K),\ \ \forall K \in \mathcal{T}^n,\ \text{and}\ \ \phi|_K(z) = \phi|_{K'}(z)$$

TH-2911_136123010

$$\text{for } z \in \mathcal{N}_K^n \cap \mathcal{N}_{K'}^n,\ K' \in \omega_K^n\Big\},$$

and its subspace by

$$S_{h,nc,0}^n(\Omega) = \big\{\phi \in S_{h,nc}^n(\Omega) : \phi(x) = 0,\ \ \forall x \in \mathcal{N}^n \cap \partial\Omega\big\}.$$

Remark 5.2.1. *The degrees of freedom are defined as the average values over edges:*

$$(DOF)_K = \{\frac{1}{|e_i|}\int_{e_i} \phi\, ds,\ i = 1,2,3:\ \forall \textit{ nodal basis function } \phi\},$$

where $e_i, i = 1,2,3$, are the edges of triangle K. In addition, let M_i be the midpoint of the edge e_i, $i = 1,2,3$. The local basis functions $\phi_i, i = 1,2,3$, satisfies

$$\frac{1}{|e_i|}\int_{e_i} \phi_i ds = \delta_{ij}, \quad i,j = 1,2,3,$$

where δ_{ij} is the Kronecker delta function.

For the space-time nonconforming IFE approximation, we consider the piecewise linear finite element for the spatial variable and the backward Euler approximation for the time derivative. Let U_h^0 be a suitable approximation of u_0 in the space $S_{h,nc}^0$ over the initial mesh $\mathcal{T}^0$. Further, we define $\beta_h(x)$ to be the approximation of the coefficient $\beta(x)$ such that $\beta_h(x) = \beta_K(x)$ for $K \in \mathcal{T}^n$, where

$$\beta_K(x) = \begin{cases} \beta(x) & \text{if } K \in \mathcal{T}^n \setminus \mathcal{T}_\Gamma^n, \\ \min\limits_{x\in K} \beta(x) & \text{if } K \in \mathcal{T}_\Gamma^n. \end{cases}$$

The space-time nonconforming IEF approximation to the problem (5.4) is stated as follows: Given $U_h^0 \in S_{h,nc}^0(\Omega)$, find $U_h^n \in S_{h,nc}^n(\Omega)$ for $n = 1,2,\ldots,N$, such that

$$\left(\frac{U_h^n - U_h^{n-1}}{k_n}, v\right) + (\beta_h \nabla U_h^n, \nabla v) \ = \ (\bar{f}^n, v) \quad \forall v \in S_{h,nc,0}^n(\Omega), \tag{5.8}$$

where $\bar{f}^n := \frac{1}{k_n}\int_{t_{n-1}}^{t_n} f(x,t)\, dt$. The discrete problem (5.8) has a unique solution by Lax-Milgram theorem.

5.3 A Posteriori Error Analysis

This section concerns *a posteriori* error analysis for the space-time nonconforming IFE approximation to the problem (5.1)-(5.3). We derive both global upper and local lower bounds for the error in terms of error indicators.

TH-2911_136123010

We now introduce some additional notation. Let $\mathcal{E}^n = \cup_{K\in\mathcal{T}^n}\partial K$ be the set of all edges in $\mathcal{T}^n$, and let $\mathcal{E}_\Gamma^n$ be the set of all edges intersect with the interface Γ. Let h_e be the length of an edge e. For any edge $e \in \mathcal{E}^n$, let $\mathcal{N}_e^n$ be the set of vertices of an edge e, and let Ω_e denote the collection of two triangles sharing the common edge e. For any $K \in \mathcal{T}^n$ and $e \in \mathcal{E}^n$, let $\omega_e^n = \cup_{\mathcal{N}_K^n\cap\mathcal{N}_e^n\neq\theta}K'$. For each $e \in \mathcal{E}^n$, we denote K_1 and K_2 be two triangles sharing common edge e and let $\beta_e = \max\limits_{e=\partial K_1\cap\partial K_2}\{\beta_{K_1}, \beta_{K_2}\}$.

In this aspect, we will have two residual functions associated with (5.8), namely, the interior residual and the jump residual.

The interior residual R^n is defined as

$$R^n := \bar{f}^n - k_n^{-1}(U_h^n - U_h^{n-1}) + \nabla\cdot(\beta_h\nabla U_h^n) \tag{5.9}$$

and the jump residual J_e^n across $e \in \mathcal{E}^n$ is defined as

$$J_e^n := [\beta_h\nabla U_h^n]_e\cdot\mathbf{n}_e = \big((\beta_h\nabla U_h^n)|_{K_1} - (\beta_h\nabla U_h^n)|_{K_2}\big)\cdot\mathbf{n}_e, \tag{5.10}$$

where $\mathbf{n}_e$ denotes the unit vector to e points from K_2 to K_1.

Following [13], we recall the approximation properties of the quasi-interpolation operator which plays a crucial role in the present analysis. We now introduce the following notation.

For each vertex $z \in \mathcal{N}^n$, let ω_z^n denote the patch having common vertex z and let φ_z be the nodal basis function. For each $z \in \mathcal{N}^n$, we consider that

- z is contained in the subdomain $\bar{\Omega}_{i,z}$, $i = 1, 2$, and
- $\beta_{i,z}$ is maximal among all β_i such that $\bar{\Omega}_i$, $i = 1, 2$, contains z.

Let

$$\mathcal{P}_K\phi = \frac{1}{meas(K)}\int_K \phi\, dx$$

be the mean value of a given function ϕ on K and $meas(K)$ denotes the measure of K. Let π_z^n be the L^2 orthogonal projection onto the piecewise linear function space in ω_z^n and be defined by

$$\pi_z^n(\phi) = \begin{cases} \mathcal{P}_{\omega_z^n\cap\Omega_{i,z}}\phi, & \text{if } z \in \Omega, \\ 0, & \text{if } z \in \partial\Omega, \end{cases}$$

and let the quasi-interpolation operator $I_\pi^n : H_{\mathcal{G}}^1(\Omega) \to S_h^n(\Omega)$ be defined by

$$I_\pi^n\phi = \sum_{z\in\mathcal{N}^n}(\pi_z^n\phi)\varphi_z. \tag{5.11}$$

We now have the following approximation results (cf. [13]).

TH-2911_136123010

Lemma 5.3.1. *Let $I_\pi^n : H^1_{\mathcal{G}}(\Omega) \to S_h^n(\Omega)$ be the quasi-interpolation operator. Then, for any $\phi \in H_0^1(\Omega)$, we have*

$$\begin{aligned} \|\phi - I_\pi^n\phi\|_{L^2(K)} &\leq C_{I,5} h_K \beta_K^{-\frac{1}{2}} |||\phi|||_{\omega_K^n}, \quad \forall K \in \mathcal{T}^n, \\ \|\phi - I_\pi^n\phi\|_{L^2(e)} &\leq C_{I,6} h_e^{\frac{1}{2}} \beta_e^{-\frac{1}{2}} |||\phi|||_{\omega_e^n}, \quad \forall e \in \mathcal{E}^n, \end{aligned} \tag{5.12}$$

where the constants $C_{I,j} > 0, (j = 5, 6)$, depend only on the minimum angle of the triangulation $\mathcal{T}^n$.

5.3.1 An Upper Bound

The goal of this section is to derive a global *a posteriori* upper bound for the error. We need the following notation for the rest of the analysis.

Let $U_h : [0, T] \to H^1_{\mathcal{G}}(\Omega)$ be a continuous piecewise linear approximation in time of $u(t)$ defined by

$$U_h(t) := l_{n-1}(t)U_h^{n-1} + l_n(t)U_h^n \tag{5.13}$$

for $t \in (t_{n-1}, t_n]$, $1 \leq n \leq N$, where $l_{n-1}(t) = \frac{t_n - t}{k_n}$ and $l_n(t) = \frac{t - t_{n-1}}{k_n}$ are the Lagrangian functions.

The following theorem presents an upper bound for the error in the energy norm.

Theorem 5.3.1. *Let u be the solution of (5.1)-(5.3), and let U_h^n be its approximation defined by (5.8). Then, there exists a constant $C > 0$ independent of the coefficient $\beta(x)$ such that for $1 \leq m \leq N$, we have*

$$\begin{aligned} \frac{1}{2}\|u^m - U_h^m\|^2_{L^2(\Omega)} \;+\; \sum_{n=1}^{m} \int_{t_{n-1}}^{t_n} |||u - U_h^n|||^2_\Omega dt \;\leq\; \|u_0 - U_h^0\|^2_{L^2(\Omega)} + \sum_{n=1}^{m} k_n \eta^n_{4,time} \\ +\; 2C \sum_{n=1}^{m} k_n \eta^n_{4,space} + 2\left(\sum_{n=1}^{m} \int_{t_{n-1}}^{t_n} \|f - \bar{f}^n\|_{L^2(\Omega)} dt \right)^2, \end{aligned} \tag{5.14}$$

where the time error indicator $\eta^n_{4,time}$ and the space error indicator $\eta^n_{4,space}$ are given by

$$\eta^n_{4,time} \;=\; \frac{1}{3}|||U_h^n - U_h^{n-1}|||^2_\Omega, \quad \text{and} \quad \eta^n_{4,space} = \sum_{K \in \mathcal{T}^n} \eta^n_{4,K}, \tag{5.15}$$

respectively, and the local error indicator $\eta^n_{4,K}$ is given as follows: For $K \in \mathcal{T}^n \setminus \mathcal{T}^n_\Gamma$,

$$\eta^n_{4,K} = h_K^2 \beta_K^{-1} \|R^n\|^2_{L^2(K)} + \frac{1}{2} \sum_{e \subset \partial K} h_e \beta_K^{-1} \|J_e^n\|^2_{L^2(e)}, \tag{5.16}$$

TH-2911_136123010

and for $K \in \mathcal{T}_\Gamma^n$ *with* $K = \mathcal{K}_1 \cup \mathcal{K}_2$,

$$\eta_{4,K}^n = \sum_{K' \in \{\mathcal{K}_1, \mathcal{K}_2\}} h_{K'}^2 \beta_{K'}^{-1} \|R^n\|_{L^2(K')}^2 + \frac{1}{2} \sum_{e' \in \{\partial\mathcal{K}_1, \partial\mathcal{K}_2\}} h_{e'} \beta_{e'}^{-1} \|J_e^n\|_{L^2(e')}^2, \tag{5.17}$$

where $\beta_{e'} = \begin{cases} \beta_1, & \text{if } e' \in \partial_1 K, \\ \beta_2, & \text{if } e' \in \partial_2 K, \end{cases}$ *and* $\partial_i K$ $(i = 1, 2)$ *denote the set of boundary line segments of the triangle* $K \in \mathcal{T}_\Gamma^n$, *which belongs to the set* $\partial\mathcal{K}_i \setminus \Gamma$ $(i = 1, 2)$.

Proof. Let $\phi = u - U_h$ and $I_\pi^n \phi$ be the quasi-interpolation of ϕ in $S_{h,\mathcal{G}}^n(\Omega)$. Then, there exists $\mathcal{J}_h^n \phi \in S_{h,nc,\mathcal{G}}^n(\Omega)$, where $\mathcal{J}_h^n : H_{\mathcal{G}}^1(\Omega) \to S_{h,nc,\mathcal{G}}^n(\Omega)$, such that

$$\mathcal{J}_h^n \phi(z) = I_\pi^n \phi(z) \quad \forall z \in \cup_{K \in \mathcal{T}_*^n} \mathcal{N}_K^n. \tag{5.18}$$

With the help of (5.4) and (5.8), for $t \in (t_{n-1}, t_n]$, it follows that

$$\begin{aligned} \Big(\frac{\partial(u - U_h)}{\partial t}, \phi\Big) + \big(\beta\nabla(u - U_h^n), \nabla\phi\big) &= \sum_{K \in \mathcal{T}^n} (f - \bar{f}^n, \phi)_K + \sum_{K \in \mathcal{T}^n} (R^n, \phi - \mathcal{J}_h^n \phi)_K \\ &\quad + \sum_{e \in \mathcal{E}^n} \int_e J_e^n (\phi - \mathcal{J}_h^n \phi)\, \mathrm{d}s. \end{aligned} \tag{5.19}$$

Using the identity

$$\big(\beta\nabla(u - U_h^n), \nabla(u - U_h)\big) = \frac{1}{2}|||u - U_h^n|||_\Omega^2 + \frac{1}{2}|||u - U_h|||_\Omega^2 - \frac{1}{2}|||U_h - U_h^n|||_\Omega^2,$$

we arrive at

$$\begin{aligned} &\frac{1}{2}\frac{\mathrm{d}}{\mathrm{d}t}\|u - U_h\|_{L^2(\Omega)}^2 + \frac{1}{2}|||u - U_h^n|||_\Omega^2 + \frac{1}{2}|||u - U_h|||_\Omega^2 = \frac{1}{2}|||U_h - U_h^n|||_\Omega^2 \\ &+ \sum_{K \in \mathcal{T}^n} (f - \bar{f}^n, u - U_h)_K + \sum_{K \in \mathcal{T}^n} \big(R^n, (u - U_h) - \mathcal{J}_h^n(u - U_h)\big)_K \\ &+ \sum_{e \in \mathcal{E}^n} \int_e J_e^n((u - U_h) - \mathcal{J}_h^n(u - U_h)) ds. \end{aligned} \tag{5.20}$$

Now for any $t_* \in (t_{m-1}, t_m]$, let $t_n \wedge t_* = \min(t_n, t_*)$. Integrating (5.20) in time from 0 to t_* and summing over all m, we get

$$\begin{aligned} &\frac{1}{2}\|(u - U_h)(t_*)\|_{L^2(\Omega)}^2 + \frac{1}{2}\sum_{n=1}^m \int_{t_{n-1}}^{t_n \wedge t_*} \Big(|||u - U_h^n|||_\Omega^2 + |||u - U_h|||_\Omega^2\Big) dt \\ = \;& \frac{1}{2}\|u_0 - U_h^0\|_{L^2(\Omega)}^2 + \frac{1}{2}\sum_{n=1}^m \int_{t_{n-1}}^{t_n} |||U_h - U_h^n|||_\Omega^2 dt \end{aligned}$$

TH-2911_136123010

$$
\begin{aligned}
&+\sum_{n=1}^{m}\int_{t_{n-1}}^{t_n}\sum_{K\in\mathcal{T}^n}(f-\bar{f}^n,u-U_h)_K dt\\
&+\sum_{n=1}^{m}\int_{t_{n-1}}^{t_n}\sum_{K\in\mathcal{T}^n}\left(R^n,(u-U_h)-\mathcal{J}_h^n(u-U_h)\right)_K dt\\
&+\sum_{n=1}^{m}\int_{t_{n-1}}^{t_n}\sum_{e\in\mathcal{E}^n}\int_e J_e^n((u-U_h)-\mathcal{J}_h^n(u-U_h))ds\\
&= \frac{1}{2}\|u_0-U_h^0\|^2_{L^2(\Omega)}+I_1+I_2+I_3+I_4. \qquad (5.21)
\end{aligned}
$$

We now estimate the term $I_i, i=1,\ldots,4$ separately. For I_1, we use (5.13) to have

$$
\begin{aligned}
I_1 &= \frac{1}{2}\sum_{n=1}^{m}\int_{t_{n-1}}^{t_n}(l_{n-1}(t))^2\,|||U_h^n-U_h^{n-1}|||^2_\Omega dt\\
&= \frac{1}{2}\sum_{n=1}^{m}\frac{k_n}{3}\,|||U_h^n-U_h^{n-1}|||^2_\Omega \;=\; \frac{1}{2}\sum_{n=1}^{m}k_n\eta^n_{4,time}.
\end{aligned}
$$

By the Cauchy-Schwarz inequality, it follows that

$$
\begin{aligned}
I_2 &\le \sum_{n=1}^{m}\int_{t_{n-1}}^{t_n}\|f-\bar{f}^n\|_{L^2(\Omega)}\|u-U_h\|_{L^2(\Omega)}dt\\
&\le \frac{1}{4}\max_{0\le t\le t_*}\|u-U_h\|^2_{L^2(\Omega)}+\left(\sum_{n=1}^{m}\int_{t_{n-1}}^{t_n}\|f-\bar{f}^n\|_{L^2(\Omega)}dt\right)^2.
\end{aligned}
$$

To estimate I_3, we first split it as

$$
\begin{aligned}
I_3 &= \sum_{n=1}^{m}\int_{t_{n-1}}^{t_n}\sum_{K\in\mathcal{T}^n}\left(R^n,(u-U_h)-I_\pi^n(u-U_h)\right)_K dt\\
&\quad+\sum_{n=1}^{m}\int_{t_{n-1}}^{t_n}\sum_{K\in\mathcal{T}^n}\left(R^n,I_\pi^n(u-U_h)-\mathcal{J}_h^n(u-U_h)\right)_K dt\\
&=: I_3^1+I_3^2. \qquad (5.22)
\end{aligned}
$$

An application of the Cauchy-Schwarz inequality and Lemma 5.3.1 yields

$$
\begin{aligned}
I_3^1 &\le \sum_{n=1}^{m}\int_{t_{n-1}}^{t_n}\sum_{K\in\mathcal{T}^n}\|R^n\|_{L^2(K)}\|(u-U_h)-I_\pi^n(u-U_h)\|_{L^2(K)}dt\\
&\le C_{I,5}\sum_{n=1}^{m}\int_{t_{n-1}}^{t_n}\sum_{K\in\mathcal{T}^n}h_K\beta_K^{-\frac{1}{2}}\|R^n\|_{L^2(K)}|||u-U_h|||_{\omega_K^n}dt. \qquad (5.23)
\end{aligned}
$$

Again, use of the Cauchy-Schwarz inequality for the term I_3^2 implies

$$
I_3^2 \le \sum_{n=1}^{m}\int_{t_{n-1}}^{t_n}\sum_{K\in\mathcal{T}^n}\|R^n\|_{L^2(K)}\|I_\pi^n(u-U_h)-\mathcal{J}_h^n(u-U_h)\|_{L^2(K)}dt. \qquad (5.24)
$$

TH-2911_136123010

Now, application of the usual homogenization arguments, (5.18), inverse estimate, and Lemma 5.3.1 leads to

$$\begin{aligned}
&\|I_\pi^n(u-U_h)-\mathcal{J}_h^n(u-U_h)\|_{L^2(K)} \le h_K\|I_\pi^n(u-U_h)-\mathcal{J}_h^n(u-U_h)\|_{H^1(K)}\\
&\le C_\rho h_K\|\nabla I_\pi^n(u-U_h)\|_{L^2(K)}\\
&\le C_\rho h_K\Big(\|\nabla\big(I_\pi^n(u-U_h)-(u-U_h)\big)\|_{L^2(K)}+\|\nabla(u-U_h)\|_{L^2(K)}\Big)\\
&\le C_\rho\Big(\|I_\pi^n(u-U_h)-(u-U_h)\|_{L^2(K)}+\beta_K^{-\frac{1}{2}}h_K|||u-U_h|||_{\omega_K^n}\Big)\\
&\le C_\rho(C_{I,5}+1)h_K\beta_K^{-\frac{1}{2}}|||u-U_h|||_{\omega_K^n}, \qquad (5.25)
\end{aligned}$$

where the constant $C_\rho = O(\max\{\rho, 1/\rho\})$ with $\rho = \beta_1/\beta_2$. Thus, (5.24) and (5.25) implies

$$I_3^2 \le C_\rho(C_{I,5}+1)\sum_{n=1}^{m}\int_{t_{n-1}}^{t_n}\sum_{K\in\mathcal{T}^n}\beta_K^{-\frac{1}{2}}h_K\|R^n\|_{L^2(K)}|||u-U_h|||_{\omega_K^n}. \qquad (5.26)$$

Combining (5.22), (5.23) and (5.26), we have

$$I_3 \le C_{5,1}\sum_{n=1}^{m}\int_{t_{n-1}}^{t_n}\sum_{K\in\mathcal{T}^n}\beta_K^{-\frac{1}{2}}h_K\|R^n\|_{L^2(K)}|||u-U_h|||_{\omega_K^n}, \qquad (5.27)$$

where the constant $C_{5,1} = C_\rho + C_{I,5}(1+C_\rho)$. It remains to bound the term I_4. First, we rewrite I_4 as

$$\begin{aligned}
I_4 &= \sum_{n=1}^{m}\int_{t_{n-1}}^{t_n}\sum_{e\in\mathcal{E}^n}\int_e J_e^n\big((u-U_h)-\mathcal{I}_\pi^n(u-U_h)\big)dt\\
&\quad+\sum_{n=1}^{m}\int_{t_{n-1}}^{t_n}\sum_{e\in\mathcal{E}^n}\int_e J_e^n\big(\mathcal{I}_\pi^n(u-U_h)-\mathcal{J}_h^n(u-U_h)\big)dt\\
&=: I_4^1+I_4^2. \qquad (5.28)
\end{aligned}$$

For the term I_4^1, the Cauchy-Schwarz inequality and Lemma 5.3.1 gives

$$\begin{aligned}
I_4^1 &\le \sum_{n=1}^{m}\int_{t_{n-1}}^{t_n}\sum_{e\in\mathcal{E}^n}\|J_e^n\|_{L^2(e)}\|(u-U_h)-\mathcal{I}_\pi^n(u-U_h)\|_{L^2(e)}dt\\
&\le C_{I,6}\sum_{n=1}^{m}\int_{t_{n-1}}^{t_n}\sum_{e\in\mathcal{E}^n}h_e^{\frac{1}{2}}\beta_e^{-\frac{1}{2}}\|J_e^n\|_{L^2(e)}|||u-U_h|||_{\omega_e^n}dt.
\end{aligned}$$

Arguing as (5.25), for I_4^2, apply trace inequality to have

$$\|I_\pi^n(u-U_h)-\mathcal{J}_h^n(u-U_h)\|_{L^2(e)} \le C_\rho h_e^{\frac{1}{2}}\beta_e^{-\frac{1}{2}}|||u-U_h|||_{\omega_e^n}, \qquad (5.29)$$

TH-2911_136123010

where the constant $C_\rho = O(\max\{\rho, 1/\rho\})$ with $\rho = \beta_1/\beta_2$. Now, using (5.29), we have

$$I_4^2 \leq C_\rho(C_{I,6}+1)\sum_{n=1}^{m}\int_{t_{n-1}}^{t_n}\sum_{e\in\mathcal{E}^n} h_e^{\frac{1}{2}}\beta_e^{-\frac{1}{2}}\|J_e^n\|_{L^2(e)}|||u-U_h|||_{\omega_e^n}dt.$$

Estimates of I_4^1 and I_4^2 together with (5.28) imply

$$I_4 \leq C_{5,2}\sum_{n=1}^{m}\int_{t_{n-1}}^{t_n}\sum_{e\in\mathcal{E}^n} h_e^{\frac{1}{2}}\beta_e^{-\frac{1}{2}}\|J_e^n\|_{L^2(e)}|||u-U_h|||_{\omega_e^n}dt, \tag{5.30}$$

where the constant $C_{5,2} = C_\rho + C_{I,6}(1+C_\rho)$. Putting the above estimates together in (5.21) we obtain

$$\begin{aligned}
&\frac{1}{2}\|(u-U_h)(t_*)\|_{L^2(\Omega)}^2 + \frac{1}{2}\sum_{n=1}^{m}\int_{t_{n-1}}^{t_n\wedge t_*}\Big(|||u-U_h^n|||_\Omega^2 + |||u-U_h|||_\Omega^2\Big)dt\\
\leq\ &\frac{1}{2}\|u_0-U_h^0\|_{L^2(\Omega)}^2 + \frac{1}{2}\sum_{n=1}^{m}k_n\eta_{4,time}^n + \frac{1}{4}\max_{0\leq t\leq t_*}\|u-U_h\|_{L^2(\Omega)}^2 + \left(\sum_{n=1}^{m}\int_{t_{n-1}}^{t_n}\|f-\bar{f}^n\|_{L^2(\Omega)}dt\right)^2\\
&+\ C_{5,1}\sum_{n=1}^{m}\int_{t_{n-1}}^{t_n}\sum_{K\in\mathcal{T}^n} h_K\beta_K^{-\frac{1}{2}}\|R^n\|_{L^2(K)}|||u-U_h|||_{\omega_K^n}dt\\
&+ C_{5,2}\sum_{n=1}^{m}\int_{t_{n-1}}^{t_n}\sum_{e\in\mathcal{E}^n} h_e^{\frac{1}{2}}\beta_e^{-\frac{1}{2}}\|J_e^n\|_{L^2(e)}|||u-U_h|||_{\omega_e^n}dt.
\end{aligned}$$

After separating the triangles, the above estimate can be rewritten as

$$\begin{aligned}
&\frac{1}{2}\|(u-U_h)(t_*)\|_{L^2(\Omega)}^2 + \frac{1}{2}\sum_{n=1}^{m}\int_{t_{n-1}}^{t_n\wedge t_*}\Big(|||u-U_h^n|||_\Omega^2 + |||u-U_h|||_\Omega^2\Big)dt\\
\leq\ &\frac{1}{2}\|u_0-U_h^0\|_{L^2(\Omega)}^2 + \frac{1}{2}\sum_{n=1}^{m}k_n\eta_{4,time}^n + \frac{1}{4}\max_{0\leq t\leq t_*}\|u-U_h\|_{L^2(\Omega)}^2\\
&+\left(\sum_{n=1}^{m}\int_{t_{n-1}}^{t_n}\|f-\bar{f}^n\|_{L^2(\Omega)}dt\right)^2 + \frac{1}{2}\sum_{n=1}^{m}\int_{t_{n-1}}^{t_n}|||u-U_h|||_\Omega^2 dt\\
&+C\sum_{n=1}^{m}\int_{t_{n-1}}^{t_n}\sum_{K\in\mathcal{T}^n\setminus\mathcal{T}_\Gamma^n}\Big(h_K^2\beta_K^{-1}\|R^n\|_{L^2(K)}^2 + \frac{1}{2}\sum_{e\subset\partial K}h_e\beta_e^{-1}\|J_e^n\|_{L^2(e)}^2\Big)dt\\
&+C\sum_{n=1}^{m}\int_{t_{n-1}}^{t_n}\sum_{K\in\mathcal{T}_\Gamma^n}\Big(h_K^2\beta_K^{-1}\|R^n\|_{L^2(K)}^2 + \frac{1}{2}\sum_{e\subset\partial K}h_e\beta_e^{-1}\|J_e^n\|_{L^2(e)}^2\Big)dt,
\end{aligned}$$

where the constant $C = \max\{C_{5,1}^2, C_{5,2}^2\}$.
With the help of (5.16) and (5.15), we find that

$$\frac{1}{2}\|(u-U_h)(t_*)\|_{L^2(\Omega)}^2 + \frac{1}{2}\sum_{n=1}^{m}\int_{t_{n-1}}^{t_n\wedge t_*}\Big(|||u-U_h^n|||_\Omega^2 + |||u-U_h|||_\Omega^2\Big)dt$$

TH-2911_136123010

$$\leq \frac{1}{2}\|u_0 - U_h^0\|^2_{L^2(\Omega)} + \frac{1}{2}\sum_{n=1}^{m} k_n \eta^n_{4,time} + \frac{1}{4}\max_{0\leq t\leq t_*}\|u - U_h\|^2_{L^2(\Omega)}$$

$$+ \left(\sum_{n=1}^{m}\int_{t_{n-1}}^{t_n}\|f - \bar{f}^n\|_{L^2(\Omega)}dt\right)^2 + \frac{1}{2}\sum_{n=1}^{m}\int_{t_{n-1}}^{t_n}|||u - U_h|||^2_{\Omega}dt + C\sum_{n=1}^{m}\int_{t_{n-1}}^{t_n}\eta^n_{4,space}dt$$

$$\leq \frac{1}{2}\|u_0 - U_h^0\|^2_{L^2(\Omega)} + \frac{1}{2}\sum_{n=1}^{m} k_n \eta^n_{4,time} + \frac{1}{4}\max_{0\leq t\leq t_*}\|u - U_h\|^2_{L^2(\Omega)}$$

$$+ \left(\sum_{n=1}^{m}\int_{t_{n-1}}^{t_n}\|f - \bar{f}^n\|_{L^2(\Omega)}dt\right)^2 + \frac{1}{2}\sum_{n=1}^{m}\int_{t_{n-1}}^{t_n}|||u - U_h|||^2_{\Omega}dt + C\sum_{n=1}^{m} k_n\eta^n_{4,space}.$$

Finally, taking maximum over $t_* \in [t_{m-1}, t_m]$, using the fact $\|(u-U_h)(t_m)\|^2_{L^2(\Omega)} \leq \|(u-U_h)(\bar{t})\|^2_{L^2(\Omega)}$, where $\|(u-U_h)(\bar{t})\|^2_{L^2(\Omega)} = \max_{t_*\in[t_{m-1},t_m]}\|(u-U_h)(t_*)\|^2_{L^2(\Omega)}$ and the standard kickback argument, the required inequality (5.14) follows. This completes the proof. □

5.3.2 A Lower Bound

This section focuses on deriving a lower bound for the local error which is essential for the refinement/coarsening strategy for the mesh adaption. For this, we first consider the following auxiliary problem.

Let $U^n_* \in H^1_{\mathcal{G}}(\Omega)$ be the solution of

$$\left(\frac{U^n_* - U^{n-1}_h}{k_n}, \phi\right) + (\beta_h \nabla U^n_*, \nabla\phi) = (\bar{f}^n, \phi) \quad \forall \phi \in H^1_0(\Omega). \tag{5.31}$$

The purpose of considering (5.31) is basically to control the error between U^n_h and U^n_*, not between U^n_h and the exact solution $u^n = u(x, t_n)$ for fixed time-step size k_n and by adapting the mesh $\mathcal{T}^n$. Further, a crucial part is to handle the oscillation of the residual R^n which changes at each refinement stage. Define the oscillation of any function $\phi \in L^2(\Omega)$ over the mesh $\mathcal{T}^n$ by

$$\mathrm{osc}(\phi, \mathcal{T}^n) = \left(\sum_{K\in\mathcal{T}^n} h_K^2 \beta_K^{-1}\|\phi - \mathcal{P}_K\phi\|^2_{L^2(K)}\right)^{\frac{1}{2}} \tag{5.32}$$

and the weighted norm $\|\cdot\|_{k_n,\Omega}$ of $H^1(\Omega)$ with the parameter $k_n > 0$ by

$$\|\phi\|_{k_n,\Omega} = \left(\frac{1}{k_n}\|\phi\|^2_{L^2(\Omega)} + |||\phi|||^2_{\Omega}\right)^{\frac{1}{2}}. \tag{5.33}$$

For any $n = 1, 2, \ldots$, we set

$$\hat{\mathcal{C}}_n = \max_{K\in\mathcal{T}^n}\left\{\frac{h_K^2}{\beta_K k_n} : h_K = \mathrm{diam}(K)\right\}. \tag{5.34}$$

TH-2911_136123010

We borrow the idea from [29, 31, 105] to prove another main result of this chapter. The key ingredients used to derive a local lower bound in the following theorem includes the properties of bubble functions and the Cauchy-Schwarz inequality.

Theorem 5.3.2. *Let U_h^n and U_*^n be the solutions of (5.8) and (5.31), respectively. Then, for $K \in \mathcal{T}^n \setminus \mathcal{T}_\Gamma^n$, we have*

$$\begin{aligned}\eta_{4,K}^n &\leq C_{5,9} \sum_{K\in\Omega_e} h_K^2 \beta_K^{-1} \|R^n - \mathcal{P}_K R^n\|_{L^2(K)}^2 \\ &\quad + C_{5,10}\hat{\mathcal{C}}_n \sum_{K\in\Omega_e} \left(\frac{1}{k_n}\|U_*^n - U_h^n\|_{L^2(K)}^2 + |||U_*^n - U_h^n|||_K^2 \right), \end{aligned} \tag{5.35}$$

and for $K \in \mathcal{T}_\Gamma^n$, we have

$$\begin{aligned}\eta_{4,K}^n &\leq C_{5,9} \sum_{K'\in\{\mathcal{K}_1,\mathcal{K}_2\}} h_{K'}^2 \beta_{K'}^{-1} \|R^n - \mathcal{P}_K R^n\|_{L^2(K')}^2 \\ &\quad + C_{5,10}\,\hat{\mathcal{C}}_n \sum_{K'\in\{\mathcal{K}_1,\mathcal{K}_2\}} \left(\frac{1}{k_n}\|U_*^n - U_h^n\|_{L^2(K')}^2 + |||U_*^n - U_h^n|||_{K'}^2 \right), \end{aligned} \tag{5.36}$$

where the constants $C_{5,9}, C_{5,10}(>0)$ depend only on the minimal angle of $\mathcal{T}^n$.

Proof. The proof proceeds with the introduction of element bubble function. With every element $K \in \mathcal{T}^n$, let $\psi_K = 27\prod_{z\in\mathcal{N}^n}\varphi_z$ be the element bubble function, where φ_z is the linear nodal basis function for each vertex $z \in \mathcal{N}^n$. Using the properties of the bubble function, we have the following inf-sup inequality:

$$\inf_{v_h\in\mathbb{P}_1(K)} \sup_{\varphi_h\in\mathbb{P}_1(K)} \frac{\int_K v_h\varphi_h\psi_K}{\|\varphi_h\|_{L^2(K)}\|v_h\|_{L^2(K)}} \geq \gamma_0,$$

where the constant $\gamma_0(>0)$ depending only on the minimum angle of triangle $K \in \mathcal{T}^n$. Let $\varphi^n \in \mathbb{P}_1(K)$ be such that $\|\varphi^n\|_{L^2(K)} = 1$, where $\mathbb{P}_1(K)$ is the space of polynomials of degree less than equal to 1 on K. Putting $v_h = \mathcal{P}_K R^n$ in the inf-sup relation and using (5.31), for any $K \in \mathcal{T}^n \setminus \mathcal{T}_\Gamma^n$, we obtain

$$\begin{aligned}\gamma_0\|\mathcal{P}_K R^n\|_{L^2(K)} &\leq \int_K (\mathcal{P}_K R^n)\psi_K\varphi^n dx \\ &= \int_K (\mathcal{P}_K R^n - R^n)\psi_K\varphi^n dx + \int_K \left(\frac{U_*^n - U_h^n}{k_n}\right)\psi_K\varphi^n dx \\ &\quad + (\beta_h\nabla U_*^n, \nabla(\psi_K\varphi^n))_K. \end{aligned} \tag{5.37}$$

Since $U_h^n \in \mathbb{P}_1(K)$ and $\psi_K = 0$ on ∂K, an integration by parts implies $(\beta_h\nabla U_h^n, \nabla\psi_K\varphi^n)_K = 0$. Thus, (5.37) can be rewritten as

$$\gamma_0\|\mathcal{P}_K R^n\|_{L^2(K)} \leq \int_K (\mathcal{P}_K R^n - R^n)\psi_K\varphi^n dx + \int_K \left(\frac{U_*^n - U_h^n}{k_n}\right)\psi_K\varphi^n dx$$

TH-2911_136123010

$$+ (\beta_h \nabla(U_*^n - U_h^n), \nabla(\psi_K \varphi^n))_K.$$

By the Cauchy-Schwarz inequality and the inverse estimate $|||\psi_K \varphi^n|||_K \leq C_{5,3} h_K^{-1}$, we get

$$\begin{aligned}\gamma_0 \|\mathcal{P}_K R^n\|_{L^2(K)} &\leq \|\mathcal{P}_K R^n - R^n\|_{L^2(K)} \\ &\quad + \frac{1}{k_n}\|U_*^n - U_h^n\|_{L^2(K)} + C_{5,3} h_K^{-1} \beta_K^{\frac{1}{2}} |||U_*^n - U_h^n|||_K.\end{aligned}$$

Using (5.34), the above inequality implies

$$\begin{aligned}\gamma_0 \|\mathcal{P}_K R^n\|_{L^2(K)} &\leq \|R^n - \mathcal{P}_K R^n\|_{L^2(K)} \\ &\quad + C_{5,3} \hat{\mathcal{C}}_n^{\frac{1}{2}} \left\{ \frac{1}{k_n}\|U_*^n - U_h^n\|_{L^2(K)}^2 + |||U_*^n - U_h^n|||_K^2 \right\}^{\frac{1}{2}}. \qquad (5.38)\end{aligned}$$

Hence, from (5.38), it follows that

$$\begin{aligned}h_K^2 \beta_K^{-1} \|R^n\|_{L^2(K)}^2 &\leq h_K^2 \beta_K^{-1} \|\mathcal{P}_K R^n - R^n\|_{L^2(K)}^2 + h_K^2 \beta_K^{-1} \|\mathcal{P}_K R^n\|_{L^2(K)}^2 \\ &\leq C_{5,4} h_K^2 \beta_K^{-1} \|R^n - \mathcal{P}_K R^n\|_{L^2(K)}^2 \\ &\quad + C_{5,4} \hat{\mathcal{C}}_n \left\{ \frac{1}{k_n}\|U_*^n - U_h^n\|_{L^2(K)}^2 + |||U_*^n - U_h^n|||_K^2 \right\}, \qquad (5.39)\end{aligned}$$

where the constant $C_{5,4} = \max\left\{\left(1 + \frac{1}{\gamma_0^2}\right), \frac{1}{\gamma_0^2}, \frac{C_{5,3}^2}{\gamma_0^2}\right\}$.

For $K \in \mathcal{T}_\Gamma^n$ with $K = \mathcal{K}_1 \cup \mathcal{K}_2$, instead of (5.37) we will have

$$\begin{aligned}\gamma_0 \|\mathcal{P}_K R^n\|_{L^2(K)} &\leq \sum_{K' \in \{\mathcal{K}_1, \mathcal{K}_2\}} \left(\int_{K'} (\mathcal{P}_K R^n - R^n) \psi_{K'} \varphi^n dx + \int_{K'} \left(\frac{U_*^n - U_h^n}{k_n} \right) \psi_{K'} \varphi^n dx \right. \\ &\quad \left. + \ (\beta_h \nabla(U_*^n - U_h^n), \nabla(\psi_{K'} \varphi^n))_{K'} \right) \\ &\leq \sum_{K' \in \{\mathcal{K}_1, \mathcal{K}_2\}} \left(\|\mathcal{P}_K R^n - R^n\|_{L^2(K')} + \frac{1}{k_n}\|U_*^n - U_h^n\|_{L^2(K')} \right. \\ &\quad \left. + \ C_{5,3} h_{K'}^{-1} \beta_{K'}^{\frac{1}{2}} |||U_*^n - U_h^n|||_{K'} \right). \qquad (5.40)\end{aligned}$$

Arguing as above, for $K \in \mathcal{T}_\Gamma^n$, we obtain

$$\begin{aligned}h_K^2 \beta_K^{-1} \|R^n\|_{L^2(K)}^2 &\leq C_{5,4} \sum_{K' \in \{\mathcal{K}_1, \mathcal{K}_2\}} h_{K'}^2 \beta_{K'}^{-1} \|R^n - \mathcal{P}_K R^n\|_{L^2(K')}^2 \\ &\quad + C_{5,4} \hat{\mathcal{C}}_n \sum_{K' \in \{\mathcal{K}_1, \mathcal{K}_2\}} \left\{ \frac{1}{k_n}\|U_*^n - U_h^n\|_{L^2(K')}^2 + |||U_*^n - U_h^n|||_{K'}^2 \right\}, \qquad (5.41)\end{aligned}$$

TH-2911_136123010

where the constant $C_{5,4}$ is defined as above.

For every $e \in \mathcal{E}^n$, let $\psi_e = 4\prod_{z\in\mathcal{N}_e^n}\varphi_z$ be the edge bubble function, where φ_z is the linear nodal basis function for each vertex $z \in \mathcal{N}^n$. Let $\psi^n = J_e^n\psi_e$. Then, ψ^n satisfies the following properties (cf. [13]):

$$\begin{aligned} &\|\nabla\psi^n\|_{L^2(K)} \le C_{5,5}h_e^{-\frac{1}{2}}\|J_e^n\|_{L^2(e)} \quad \forall K\in\Omega_e,\\ &\|\psi^n\|_{L^2(K)} \le C_{5,6}h_e^{\frac{1}{2}}\|J_e^n\|_{L^2(e)} \quad \forall K\in\Omega_e. \end{aligned} \tag{5.42}$$

Next it remains to bound $\|J_e^n\|_{L^2(e)}$. We now write

$$\sum_{e\in\mathcal{E}^n} h_e\|J_e^n\|^2_{L^2(e)} = \sum_{e\in\mathcal{E}_\Gamma^n} h_e\|J_e^n\|^2_{L^2(e)} + \sum_{e\in\mathcal{E}^n\setminus\mathcal{E}_\Gamma^n} h_e\|J_e^n\|^2_{L^2(e)}. \tag{5.43}$$

For any $e \in \mathcal{E}^n$, we know that J_e^n is constant on e. When $e \in \mathcal{E}^n \setminus \mathcal{E}_\Gamma^n$, an integration by parts, (5.9) and (5.31) yields

$$\begin{aligned} \|J_e^n\|^2_{L^2(e)} &\le C_{5,7}\int_e J_e^n\psi^n dx\\ &= -C_{5,7}\sum_{K\in\Omega_e}\int_K \beta_h\nabla U_h^n\cdot\nabla\psi^n dx + C_{5,7}\sum_{K\in\Omega_e}\int_K \nabla\cdot(\beta_h\nabla U_h^n)\psi^n dx\\ &= C_{5,7}\sum_{K\in\Omega_e}\int_K \beta_h\nabla(U_*^n - U_h^n)\cdot\nabla\psi^n dx + C_{5,7}\sum_{K\in\Omega_e}\int_K\left(\frac{U_*^n-U_h^n}{k_n}\right)\psi^n dx\\ &\quad - C_{5,7}\sum_{K\in\Omega_e}\int_K R^n\psi^n dx. \end{aligned}$$

Applying the Cauchy-Schwarz inequality, it gives

$$\begin{aligned} \|J_e^n\|^2_{L^2(e)} &\le C_{5,7}\sum_{K\in\Omega_e}\beta_e^{\frac{1}{2}}\|\beta_e^{\frac{1}{2}}\nabla(U_*^n-U_h^n)\|_{L^2(K)}\|\nabla\psi^n\|_{L^2(K)}\\ &+ C_{5,7}\sum_{K\in\Omega_e}\frac{1}{k_n}\|U_*^n-U_h^n\|_{L^2(K)}\|\psi^n\|_{L^2(K)} + C_{5,7}\sum_{K\in\Omega_e}\|R^n\|_{L^2(K)}\|\psi^n\|_{L^2(K)}. \end{aligned} \tag{5.44}$$

We apply (5.42) and the Young's inequality to obtain

$$\begin{aligned} h_e\|J_e^n\|^2_{L^2(e)} \le C_{5,7}\Bigg(&C_{5,5}^2\sum_{K\in\Omega_e}|||U_*^n-U_h^n|||_K^2 + C_{5,6}^2\sum_{K\in\Omega_e}\frac{h_e^2}{\beta_e k_n^2}\|U_*^n-U_h^n\|^2_{L^2(K)}\\ &+\sum_{K\in\Omega_e}h_K^2\beta_e^{-1}\|R^n\|^2_{L^2(K)}\Bigg)^{\frac{1}{2}}\times\left(h_e\beta_e\|J_e^n\|^2_{L^2(e)}\right)^{\frac{1}{2}}. \end{aligned}$$

With an aid of (5.34), it follows that

$$h_e\beta_e^{-1}\|J_e^n\|^2_{L^2(e)} \le C_{5,8}\hat{\mathcal{C}}_n\sum_{K\in\Omega_e}\left(|||U_*^n-U_h^n|||_K^2 + \frac{1}{k_n}\|U_*^n-U_h^n\|^2_{L^2(K)}\right)$$

TH-2911_136123010

$$+ C_{5,7} \sum_{K\in\Omega_e} h_K^2 \beta_e^{-1} \|R^n\|^2_{L^2(K)}, \tag{5.45}$$

where the constant $C_{5,8} = \max\{C_{5,7}C_{5,5}^2, C_{5,7}C_{5,6}^2\}$.

Similarly, when $e \in \mathcal{E}_\Gamma^n$ and $e \in \partial\mathcal{K}_1 \cap \partial\mathcal{K}_2$, we have

$$\begin{aligned}
\|J_e^n\|^2_{L^2(e)} &\leq C_{5,7} \int_e J_e^n \psi^n dx \\
&= -C_{5,7} \sum_{K'\in\{\mathcal{K}_1,\mathcal{K}_2\}} \int_{K'} \beta_{K'} \nabla U_h^n \cdot \nabla\psi^n dx + C_{5,7} \sum_{K'\in\{\mathcal{K}_1,\mathcal{K}_2\}} \int_{K'} \nabla\cdot(\beta_h \nabla U_h^n)\psi^n dx \\
&= C_{5,7} \sum_{K'\in\{\mathcal{K}_1,\mathcal{K}_2\}} \int_{K'} \beta_{K'} \nabla(U_*^n - U_h^n)\cdot\nabla\psi^n dx \\
&+ C_{5,7} \sum_{K'\in\{\mathcal{K}_1,\mathcal{K}_2\}} \int_{K'} \left(\frac{U_*^n - U_h^n}{k_n}\right)\psi^n dx - C_{5,7} \sum_{K'\in\{\mathcal{K}_1,\mathcal{K}_2\}} \int_{K'} R^n\psi^n dx.
\end{aligned}$$

Arguing as above and using (5.42), a simple calculation leads to

$$\begin{aligned}
h_e\beta_e^{-1}\|J_e^n\|^2_{L^2(e)} &\leq C_{5,8}\hat{\mathcal{C}}_n \left(\sum_{K'\in\{\mathcal{K}_1,\mathcal{K}_2\}} |||U_*^n - U_h^n|||^2_{K'} + \frac{1}{k_n}\|U_*^n - U_h^n\|^2_{L^2(K')} \right) \\
&+ C_{5,7} \sum_{K'\in\{\mathcal{K}_1,\mathcal{K}_2\}} h_{K'}^2 \beta_{e'}^{-1} \|R^n\|^2_{L^2(K')}.
\end{aligned} \tag{5.46}$$

Combining (5.39) and (5.45), for any $K \in \mathcal{T}^n \setminus \mathcal{T}_\Gamma^n$, we have

$$\begin{aligned}
\eta_{4,K}^n &\leq C_{5,9} \sum_{K\in\Omega_e} h_K^2 \beta_K^{-1} \|R^n - \mathcal{P}_K R^n\|^2_{L^2(K)} \\
&+ C_{5,10}\hat{\mathcal{C}}_n \sum_{K\in\Omega_e} \left(\frac{1}{k_n}\|U_*^n - U_h^n\|^2_{L^2(K)} + |||U_*^n - U_h^n|||^2_K \right),
\end{aligned} \tag{5.47}$$

where the constants $C_{5,9} = (1 + C_{5,7})C_{5,4}$ and $C_{5,10} = (1 + C_{5,7})C_{5,4} + C_{5,8}$.

Again, for all $K \in \mathcal{T}_\Gamma^n$, (5.41) and (5.46) gives

$$\begin{aligned}
\eta_{4,K}^n &\leq C_{5,9} \sum_{K'\in\{\mathcal{K}_1,\mathcal{K}_2\}} h_{K'}^2 \beta_{K'}^{-1} \|R^n - \mathcal{P}_K R^n\|^2_{L^2(K')} \\
&+ C_{5,10}\hat{\mathcal{C}}_n \sum_{K'\in\{\mathcal{K}_1,\mathcal{K}_2\}} \left(\frac{1}{k_n}\|U_*^n - U_h^n\|^2_{L^2(K')} + |||U_*^n - U_h^n|||^2_{K'} \right).
\end{aligned} \tag{5.48}$$

Finally, together (5.47) and (5.48) gives the required estimates (5.37) and (5.36), respectively and this completes the proof. □

TH-2911_136123010

Remark 5.3.1. *Taking summation over all elements $K \in \mathcal{T}^n$, from (5.47) and (5.48), we have*

$$\begin{aligned}\eta^n_{4,space} &= \sum_{K\in\mathcal{T}^n_\Gamma} \eta^n_{4,K} + \sum_{K\in\mathcal{T}^n\setminus\mathcal{T}^n_\Gamma} \eta^n_{4,K} \\ &\leq C_{5,9}\, osc(R^n,\mathcal{T}^n) + C_{5,10}\,\hat{\mathcal{C}}_n \|U^n_* - U^n_h\|^2_{k_n,\Omega},\end{aligned}$$

where the oscillation of residual $osc(R^n,\mathcal{T}^n)$ and the weighted norm $\|U^n_* - U^n_h\|_{k_n,\Omega}$ are defined in (5.32) and (5.33), respectively.

5.4 Adaptive Algorithm

This section provides a space-time adaptive algorithm to describe the adaptive procedure for parabolic interface problem (5.1)-(5.3). For various adaptive mesh refinement techniques and their implementation, we refer the reader to [29, 43, 52, 83, 94].

Based on the error equidistribution strategy of [94], the time discretization error is equally distributed to each time interval $(t_{n-1}, t_n]$, $n = 1,\ldots,N$. Let ϵ_{time} be the total tolerance for the time discretization which is a part of *a posteriori* error estimate (5.14). Thus,

$$\sum_{n=1}^{N} k_n \eta^n_{4,\text{time}} + 2\left(\sum_{n=1}^{N}\int_{t_{n-1}}^{t_n} \|f - \bar{f}^n\|_{L^2(\Omega)} dt\right)^2 \leq \epsilon_{\text{time}}, \tag{5.49}$$

which can be achieved by adapting the time-step size k_n such that

$$\eta^n_{4,\text{time}} \leq \frac{\epsilon_{\text{time}}}{2T}, \qquad \frac{1}{k_n}\int_{t_{n-1}}^{t_n} \|f - \bar{f}^n\|_{L^2(\Omega)} dt \leq \frac{\sqrt{\epsilon_{\text{time}}}}{2T} \tag{5.50}$$

hold. Now, for any given $\delta_{\text{time}} \in (0,1)$, we have

$$\eta^n_{4,\text{time}} \leq \delta_{\text{time}}\frac{\epsilon_{\text{time}}}{2T}, \qquad \frac{1}{k_n}\int_{t_{n-1}}^{t_n} \|f - \bar{f}^n\|_{L^2(\Omega)} dt \leq \frac{\sqrt{\delta_{\text{time}}\epsilon_{\text{time}}}}{2T} \tag{5.51}$$

which can be used to control the time-step size.

Let ϵ_{space} be the tolerance related to the space discretization. Then, for each time step n, the stopping criterion for mesh adaptation reads

$$\eta^n_{4,\text{space}} \leq \frac{\epsilon_{\text{space}}}{T} \tag{5.52}$$

which is appropriate for mesh refinements but not for mesh coarsening.

Following [29, Theorem 3.1], define the coarsening error indicator

$$\eta^n_{4,coarse} = \frac{1}{k_n}\|I^n_H U^n_h - U^n_h\|^2_{L^2(\Omega)} + |||I^n_H U^n_h - U^n_h|||^2_\Omega, \tag{5.53}$$

TH-2911_136123010

where $I_H^n : C(\bar{\Omega}) \to S_H^n$ is the standard linear interpolation operator, $\mathcal{T}_H^n$ is the coarsening of the mesh $\mathcal{T}^n$ and the corresponding solution is $U_H^n \in S_H^n$. Here the estimator $\eta_{4,coarse}^n$ does not depend on U_H^n, the solution of the coarsened problem.

Algorithm 5.4.1. *(Space and time adaptive algorithm).* Given tolerances ϵ_{time} and ϵ_{space}, and parameters $\gamma_1 \in (0,1)$, $\gamma_2 > 1$ and $\delta_{\text{time}} \in (0,1)$. Let U_h^{n-1} be the computed value at time t_{n-1} with the time step size k_n over the mesh $\mathcal{T}^{n-1}$.

Step 1: $\mathcal{T}^n := \mathcal{T}^{n-1}$, $k_n := k_{n-1}$, $t_n := t_{n-1} + k_n$
solve the fully discrete problem (5.8) for U_h^n on $\mathcal{T}^n$
compute the error estimates on $\mathcal{T}^n$

Step 2: while (5.50) is not satisfied do
$k_n := \gamma_1 k_n$, $t_n := t_{n-1} + k_n$
solve the fully discrete problem (5.8) for U_h^n on $\mathcal{T}^n$
compute the error estimates on $\mathcal{T}^n$

Step 3: while ($\eta_{4,\text{space}}^n > \frac{\epsilon_{\text{space}}}{T}$) do
refine all triangle $K \in \mathcal{T}^n$
solve the fully discrete problem (5.8) for U_h^n on refined mesh $\mathcal{T}^n$
compute the error estimates on the refined mesh $\mathcal{T}^n$
while (5.50) is not satisfied
go to step 2

Step 4: if ($\eta_{4,\text{coarse}}^n \leq \frac{\epsilon_{\text{coarse}}}{T}$)
coarsening $\mathcal{T}^n$ to produce a modified mesh $\check{\mathcal{T}}^n$
solve the fully discrete problem (5.8) for U_h^n on $\check{\mathcal{T}}^n$

Step 5: if (5.51) is satisfied then
{ $k_n := \gamma_2 k_n$ }
end

5.5 Numerical Experiment

In this section, a numerical experiment is presented to illustrate the performance of the error indicators. All computations are carried out using the software FreeFEM++ [65].

Example 5.1. We consider the interface problem (5.1)-(5.3) defined on $\Omega_T = \Omega \times [0,T]$, where $\Omega = (-1,1)\times(-1,1)$ and $T = 0.1$. The interface Γ is chosen to be a circle centered

TH-2911_136123010

at $(0,0)$ with radius $r_0 = \frac{\pi}{6.28}$, i.e., $\Gamma := \{(x,y) \in \mathbf{R}^2 : x^2 + y^2 = {r_0}^2\}$ and it divides the domain Ω into two subdomains Ω_1 and Ω_2 with $\Omega_1 = \{x^2 + y^2 \leq {r_0}^2\}$. Select the forcing term f and the boundary condition $\mathcal{G}$ such that the exact solution u is as follows:

$$u(x,y,t) = \begin{cases} \frac{(x^2+y^2)}{\beta_1} e^t, & \text{if } (x,y) \in \Omega_{1,T}, \\ \frac{(x^2+y^2)}{\beta_2} e^t + \left(\frac{r_0^2}{\beta_1} - \frac{r_0^2}{\beta_2}\right) e^t, & \text{if } (x,y) \in \Omega_{2,T}, \end{cases}$$

where $\Omega_{1,T} = \Omega_1 \times [0,T]$ *and* $\Omega_{2,T} = \Omega_2 \times [0,T]$.

We compute the energy error $Err = \left(\sum_{n=1}^{N} k_n |||u - U_h^n|||_\Omega^2 \right)^{\frac{1}{2}}$, the error estimator $\eta_{4,1}$ is given by

$$\eta_{4,1}^2 = \sum_{n=1}^{N} k_n (\eta_{4,time}^n + \eta_{4,space}^n + \eta_{4,coarse}^n) + 2 \left(\sum_{n=1}^{m} \int_{t_{n-1}}^{t_n} \|f - \bar{f}^n\|_{L^2(\Omega)} dt \right)^2$$

and the effectivity index (eff. index $= \eta_{4,1}/Err$) of the *a posteriori* error estimate. All the constants involved in the estimators are taken as 1. The tolerances $\epsilon_{time}, \epsilon_{space}$ are chosen to be equal.

Table 5.1: The degrees of freedom (DOF), the error estimator $\eta_{4,1}$ and the energy error (Err) at time $t = 0.1$ with tolerance $\epsilon = 0.005$.

β	DOF	$\eta_{4,1}$	Err
	1220	0.196212	0.187321
$\beta_1 = 1$	2443	0.092250	0.091261
$\beta_2 = 10$	4437	0.054525	0.047863
	1248	2.516940	0.197260
$\beta_1 = 1$	2497	1.370790	0.099681
$\beta_2 = 100$	4502	0.522680	0.048601

We have carried out the experiment for two different choices of the discontinuous coefficient β across the interface Γ. We first take $\beta_1 = 1$, $\beta_2 = 10$, and then $\beta_1 = 1$, $\beta_2 = 100$. To generate the adaptive meshes, we use the bisection algorithm and take the parameter $\gamma_1 = 0.5$. The three different steps of adaptive meshes are shown in Figures

TH-2911_136123010

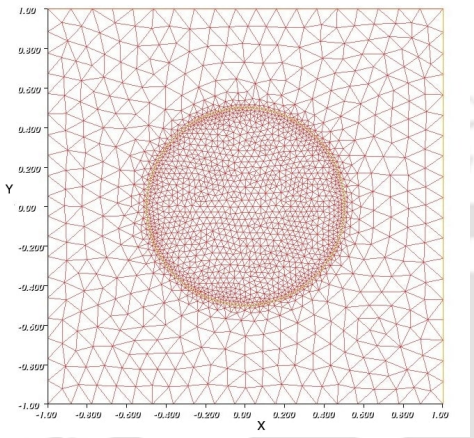

(a) Adaptive mesh at step 1.

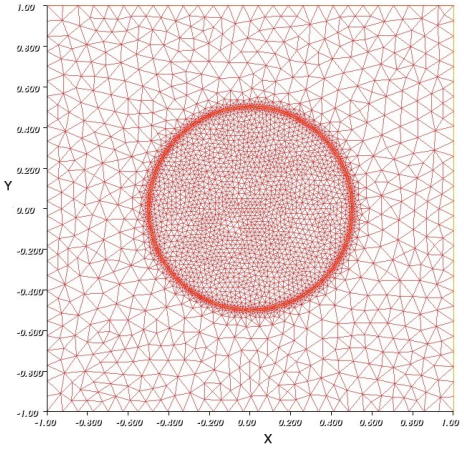

(b) Adaptive mesh at step 2.

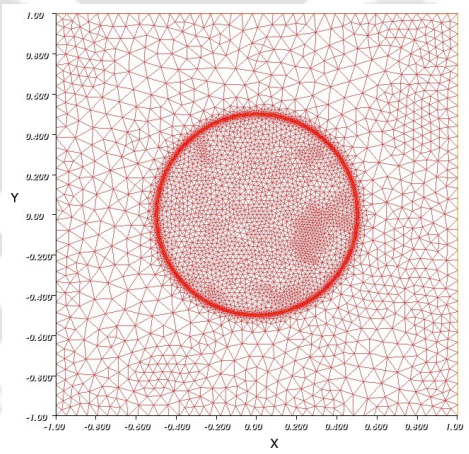

(c) Adaptive mesh at step 3.

Figure 5.3: An adaptive mesh at three different steps when $\beta_1 = 1, \beta_2 = 10$ at $t = 0.1$.

TH-2911_136123010

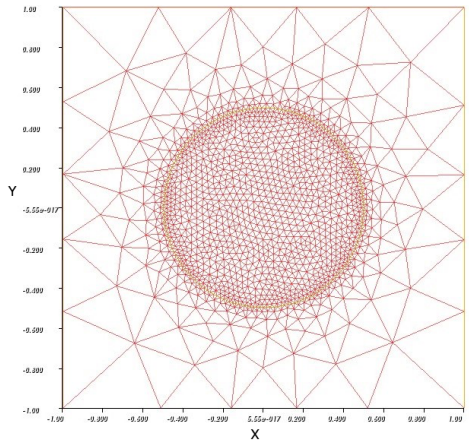

(a) Adaptive mesh at step 1.

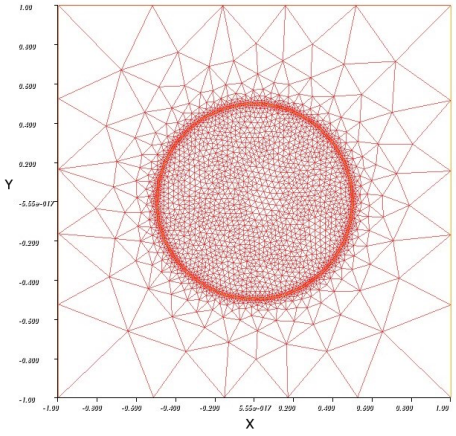

(b) Adaptive mesh at step 2.

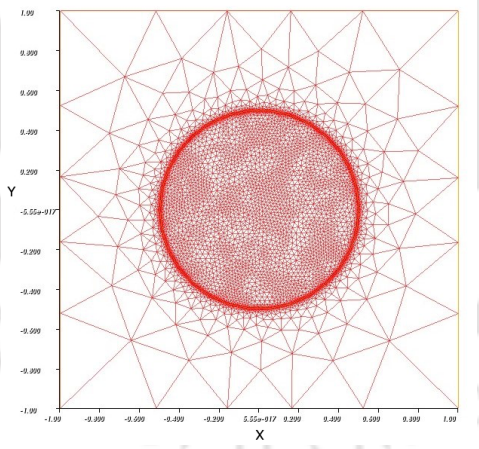

(c) Adaptive mesh at step 3.

Figure 5.4: An adaptive mesh at three different steps $\beta_1 = 1, \beta_2 = 100$ at $t = 0.1$.

TH-2911_136123010

Table 5.2: For different tolerances ϵ, the degrees of freedom (DOF), the error estimator $\eta_{4,1}$, the total energy error (Err) and the effectivity index (eff. index) at time $t = 0.1$.

β	ϵ	DOF	$\eta_{4,1}$	Err	eff. index
	0.01	2245	0.092201	0.084125	1.0960
$\beta_1 = 1$	0.005	4437	0.054525	0.047863	1.1392
$\beta_2 = 10$	0.0025	8999	0.024109	0.023241	1.0373
	0.01	2260	1.135360	0.089121	12.7395
$\beta_1 = 1$	0.005	4502	0.522680	0.048601	10.7545
$\beta_1 = 100$	0.0025	9000	0.259140	0.024812	10.4441

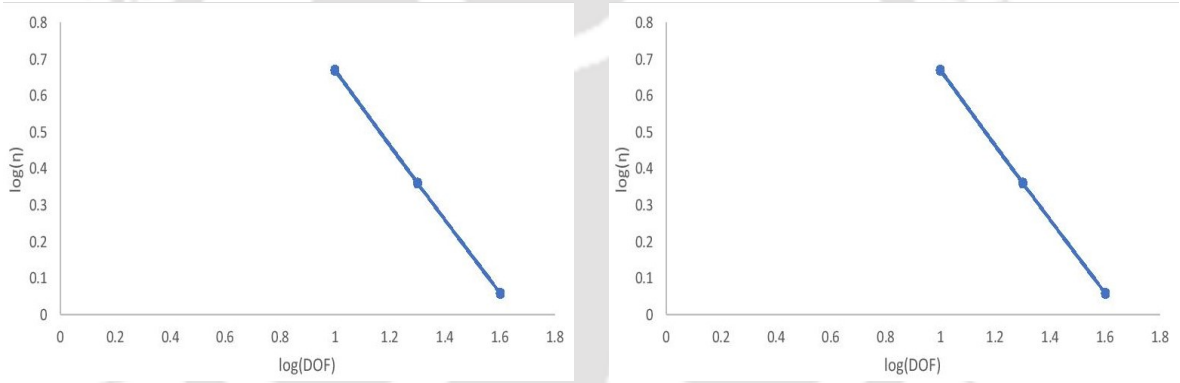

(a) (b)

Figure 5.5: Optimality of the estimator for the cases: (a) $\beta_1 = 1$, $\beta_2 = 10$ and (b) $\beta_1 = 1$, $\beta_2 = 100$. The optimal decay is observed by the line of slope -0.966 (left) and the line of slope -0.976 (right).

5.3 and 5.4. Figure. 5.3 corresponds to the choice $\beta_1 = 1$, $\beta_2 = 10$ and Figure 5.4 refers to the choice $\beta_1 = 1$, $\beta_2 = 100$.

In Table 5.1, the degrees of freedom (DOF), the error indicator $\eta_{4,1}$ and the energy error Err are presented in each step of adaptive mesh generation at final time $t = 0.1$ with tolerance $\epsilon = 0.005$ for two different set of values of β. The plots comparing the degrees of freedom with the total error estimator for both the cases are shown in Figure 5.5. The optimal decay of the estimator is observed by the line of slope -0.966 for

TH-2911_136123010

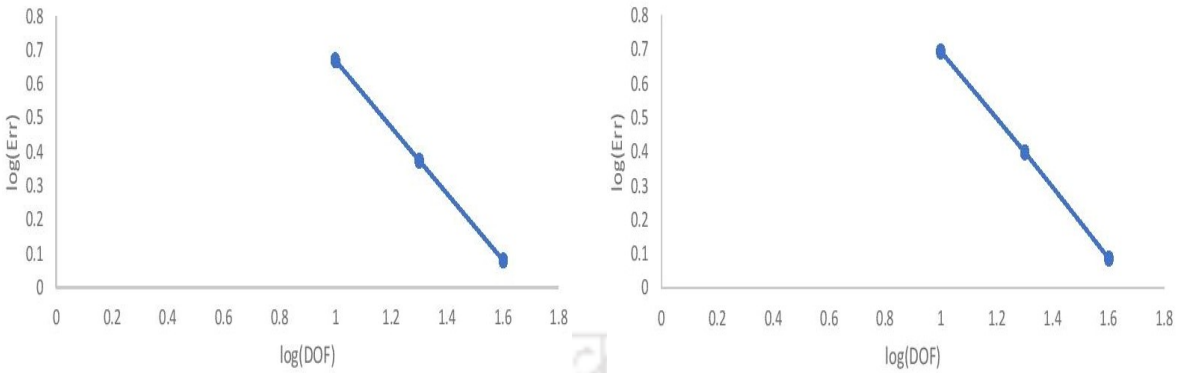

(a) (b)

Figure 5.6: Energy error versus number of degrees of freedom: (a) $\beta_1 = 1{,}0$ $\beta_2 = 10$ and (b) $\beta_1 = 1$, $\beta_2 = 100$. The quasi-optimal decay is observed by the line of slope -0.884 (left) and the line of slope -0.877 (right).

the choice $\beta_1 = 1, \beta_2 = 10$ (see Figure 5.5 (a)) and the line of slope -0.976 for the choice $\beta_1 = 1, \beta_2 = 100$ (see Figure 5.5 (b)). Further, in Figure 5.6, we provide plots for the energy error versus the number of degrees of freedom. For different tolerances ϵ, the number of nodes, the energy error and the effectivity index at $t = 0.1$ are given in Table 5.2 for two different values of β. Further in Table 5.2, we observe that both the value of the indicator and the error are reducing. Figures 5.3 and 5.4 reveals that the finite element mesh changes away from the interface Γ due to different behavior in subdomains and the initial mesh is adaptively refined. Also, we see that the finite element mesh adapts very well in the neighborhood of the interface Γ and higher density of the node points are distributed along the interface circle.

5.6 Concluding Remarks

In this chapter, we have presented *a posteriori* error analysis for the space-time immersed finite element approximation for the parabolic interface problem using non-conforming finite elements. We derived both global upper and local lower bounds for the error. New error indicators are provided to control the error due to the non-body-fitted mesh. An adaptive algorithm is presented to generate the adaptive mesh for any geometrically complicated interface. The numerical experiment is performed to illustrate the performance of the error indicators. Further, we observe that the finite element mesh adopts very well in the neighborhood of the interface Γ and the nodes are very

TH-2911_136123010

dense along the interface circle.

TH-2911_136123010

6

An AFEM for Semilinear PIPs with Nonzero Flux Jump

This chapter presents and analyzes the AFEM for a semilinear PIP subject to nonzero flux jump in a two-dimensional bounded convex polygonal domain. The forcing term is considered to be nonlinear and is assumed to satisfy the Lipschitz condition with respect to the solution variable u. We use the continuous piecewise linear finite elements for the approximation of spatial variable and the backward Euler difference is used for the time variable. Our strategy is to avoid solving the nonlinear system by considering a modified linearized fully discrete scheme. The residual-based *a posteriori* upper and lower bounds for the error are derived using energy arguments. An adaptive algorithm is constructed using the derived error estimators. The theory presented is complemented by numerical experiments to illustrate the proposed algorithm.

6.1 Introduction

We shall proceed by introducing the semilinear parabolic interface problem. Let Ω be a bounded convex polygonal domain in $\mathbb{R}^2$ with Lipschitz boundary $\partial\Omega$. Further, let $\Omega_1 \subset \Omega$ be an open domain with polygonal interface $\partial\Omega_1 := \Gamma$ and $\Omega_2 = \Omega \backslash \Omega_1$. We consider the following model problem:

$$\frac{\partial u}{\partial t} - \nabla \cdot (\beta(x)\nabla u) = f(x,t,u) \quad \text{in } \Omega_T, \tag{6.1}$$

$$u(x,0) = u_0(x) \quad \text{in } \Omega; \quad u = 0 \quad \text{on } \partial\Omega_T, \tag{6.2}$$

subject to the jump conditions across the interface Γ

$$[u] = 0, \quad \left[\beta \frac{\partial u}{\partial \mathbf{n}}\right] = g(x,t), \tag{6.3}$$

TH-2911_136123010

where $\Omega_T = \Omega \times (0,T]$ and $\partial\Omega_T = \partial\Omega \times [0,T]$ with $T < \infty$. The notation $[v]$ defines the jump of a quantity v across the interface Γ and is given by $[v](x) = v_1(x) - v_2(x)$ with $v_i(x) = v(x)|_{\Omega_i}$, $i = 1, 2$, and the symbol $\mathbf{n}$ denotes the unit outward normal to the boundary $\partial\Omega_1$. The flux jump across Γ is assumed to be nonzero, i.e., $g \neq 0$ and the diffusion coefficient $\beta(x)$ across the interface Γ is such that

$$\beta(x) = \beta_i \quad \text{for} \quad x \in \Omega_i \ (i = 1, 2),$$

where $\beta_i \in \mathbb{R}^+$. Further, we assume that the initial function $u_0(x) \in H^1(\Omega)$ and $g, \frac{\partial g}{\partial t} \in L^2(0,T; L^2(\Gamma))$. The source function $f : \bar{\Omega} \times [0,T] \times \mathbb{R} \to \mathbb{R}$ satisfies the Lipschitz condition with respect to the third argument, i.e., there exists a constant $C_L > 0$ such that

$$|f(x,t,w_1) - f(x,t,w_2)| \leq C_L |w_1 - w_2| \qquad \forall w_1, w_2 \in \mathbb{R}. \tag{6.4}$$

Hereafter, we write $f(u)$ in place of $f(x,t,u)$ for the subsequent analysis.

For the purpose of finite element approximation, we first recall the bilinear form $a(\cdot,\cdot) : H_0^1(\Omega) \times H_0^1(\Omega) \to \mathbb{R}$ defined by

$$a(v,w) = (\beta(x)\nabla v, \nabla w) \quad \forall v, w \in H_0^1(\Omega).$$

Further, we assume that the bilinear form $a(\cdot,\cdot)$ is continuous and coercive on $H_0^1(\Omega)$, i.e., there exist constants $\alpha_0, \alpha_1 > 0$ such that

$$|a(v,w)| \ \leq \ \alpha_0 \|v\|_{H^1(\Omega)} \|w\|_{H^1(\Omega)} \quad \forall v, w \in H_0^1(\Omega) \tag{6.5}$$

and

$$a(v,v) \ \geq \ \alpha_1 \|v\|^2_{H^1(\Omega)} \quad \forall v \in H_0^1(\Omega). \tag{6.6}$$

Thus the weak formulation of (6.1)-(6.3) is stated as follows: For $t \in (0,T]$, find $u(t) \in H_0^1(\Omega)$ such that

$$\begin{aligned} \left(\frac{\partial u}{\partial t}, \phi\right) + a(u,\phi) &= (f(u),\phi) + \langle g, \phi\rangle, \quad \forall \phi \in H_0^1(\Omega), \\ u(0) &= u_0, \end{aligned} \tag{6.7}$$

where and $\langle\cdot,\cdot\rangle$ denotes the scalar product for the space $L^2(\Gamma)$. Concerning the existence and uniqueness of the solution of the semilinear parabolic interface problem, we refer the reader to [51].

A *posteriori* error analysis for the semilinear PIP with homogeneous flux jump have been studied by Sen Gupta and Sinha in [95]. The authors of [95] have derived *a posteriori* upper bound in the $L^\infty(L^2)$-norm using the energy technique combined with elliptic

TH-2911_136123010

reconstruction approach. The goal of this chapter is to extend our previous methodology for linear PIP (2.1)-(2.3) to treat the semilinear PIP (6.1)-(6.3) with nonzero flux jump. We have derived both *a posteriori* upper and lower bounds for the error. A global upper bound for the error, which is bounded by the element residual and interior jump residual, is derived whereas a lower bound for the error in terms of local error indicator is established. The crucial technical tools used in the error analysis include the energy argument, the Clément interpolation approximation properties and the bubble function technique. The treatment of the oscillation of the residual which changes at each refinement procedure is crucial in the refinement/coarsening strategy. A space-time adaptive algorithm is provided which is based on the refinement strategy of Dörfler [43], Morin, Nochetto and Siebert [83], and Chen and Feng [29]. Finally, two numerical experiments are performed to illustrate the performance of the derived estimators.

The rest of this chapter is organized as follows: Section 6.2 contains the space-time discretization of the domain and the backward Euler approximation. In Section 6.3, *a posteriori* global upper and local lower bounds for the error are derived. The space-time adaptive algorithm based on the error equidistribution strategy is presented in Section 6.4. Numerical assessments of the proposed algorithm are presented to support the derived theoretical results in Section 6.6 . Finally, the last section contains the concluding remarks.

6.2 Space-Time Discretization

In this section, we shall first recall the finite element discretization of the domain. Let $\{(t_{n-1}, t_n]\}_{n=1}^N$ be a partition of $[0, T]$ with N number of sub-intervals $(t_{n-1}, t_n]$. Let $k_n = t_n - t_{n-1}$ be the time-step size of $(t_{n-1}, t_n]$. At each time level $n = 1, 2, \ldots, N$, let $\mathcal{T}^n$ be a regular triangulation of the domain $\bar{\Omega}$ which satisfies the conditions described in Chapter 2.

For $n = 1, \ldots, N$, let S^n be the finite element space corresponding to the triangulation $\mathcal{T}^n$ and be defined by

$$S^n = \big\{v \in H_0^1(\Omega) : v|_K \in \mathbb{P}_1(K) \ \ \forall K \in \mathcal{T}^n\big\},$$

where $\mathbb{P}_1(K)$ denotes the space of polynomials of degree less than or equal to 1 over the triangle K. For any continuous function ϕ defined in $(t_{n-1}, t_n]$, set $\phi^n = \phi(\cdot, t_n)$ and $\bar{\phi}^n = \frac{1}{k_n}\int_{t_{n-1}}^{t_n} \phi(\cdot, t)dt$.

For the discretization of (6.7), we now use the continuous piecewise linear finite elements for the approximation of the spatial variable while the backward Euler method is used for the time discretization. Let U_h^0 be a suitable approximation of the initial

TH-2911_136123010

data u_0 in the space S^0 over the initial mesh $\mathcal{T}^0$.

The backward Euler approximation: The fully discrete backward Euler approximation to (6.7) reads: Given $U_h^0 \in S^0$, find $U_h^n \in S^n$ for $1 \leq n \leq N$, such that

$$\left(\frac{U_h^n - U_h^{n-1}}{k_n}, v\right) + a(U_h^n, v) \quad = (f^n(U_h^n), v) + \langle \bar{g}^n, v\rangle \quad \forall v \in S^n. \tag{6.8}$$

Let $\{\varphi_i\}_{i=1}^{N_{dof}}$, where $N_{dof} = \dim(S^n)$, be the nodal basis functions for the finite element space S^n and satisfy the property

$$\varphi_i(x_j) := \delta_{ij} \quad \forall\ 1 \leq i, j \leq N_{dof}.$$

Then the solution U_h^n can be expressed as $U_h^n = \sum_{i=1}^{N_{dof}} c_i^n \varphi_i$ and (6.8) can be written in the matrix form as

$$\mathcal{A}\frac{c^n - c^{n-1}}{k_n} + \mathcal{B}c^n = \mathcal{F}(c^n) + \mathcal{D}$$

with $c^0 = \Upsilon$, where c^n is the unknown vector, $\mathcal{A} = (a_{ij})$ is the mass matrix with $a_{ij} = (\varphi_i, \varphi_j)$, $\mathcal{B} = (b_{ij})$ is the stiffness matrix with $b_{ij} = (\beta(x)\nabla\varphi_i, \nabla\varphi_j)$, $\mathcal{F}(c^n) = (f_j^n(c^n))$ is the vector with entries $f_j^n(c^n) = (f^n(\sum_{i=n}^{N_{dof}} c_i^n\varphi_i), \varphi_j)$, the vector $\mathcal{D} = (\bar{g}_j^n)$ with the entries $\bar{g}_j^n = (\bar{g}^n, \varphi_j)$ and Υ is the vector of nodal values of u_0. The above equation may be expressed as

$$\begin{aligned} (\mathcal{A} + k_n\mathcal{B})c^n &= \mathcal{A}c^{n-1} + k_n\mathcal{F}(c^n) + k_n\mathcal{D} \quad \text{for } t_n \in (0, T], \\ c^0 &= \Upsilon, \end{aligned} \tag{6.9}$$

where the matrices $\mathcal{A}$ and $\mathcal{B}$ are positive definite, and $\mathcal{F}(c^n)$ is Lipschitz continuous on $\mathbb{R}^{N_{dof}}$. Thus (6.9) gives a system of nonlinear equations. The disadvantage of the above method is that at each time level one has to solve a nonlinear system of algebraic equations due to the presence of the term $\mathcal{F}(c^n)$ in (6.8). To avoid this difficulty we modify (6.8) to a linearized fully discrete backward Euler approximation replacing the term $f^n(U_h^n)$ by $f^n(U_h^{n-1})$ (cf. [102]).

The modified backward Euler approximation: The modified linearized fully discrete backward Euler approximation to (6.7) reads as: Given $U_h^0 \in S^0$, find $U_h^n \in S^n$ for $1 \leq n \leq N$, such that

$$\left(\frac{U_h^n - U_h^{n-1}}{k_n}, v\right) + a(U_h^n, v) \quad = (f^n(U_h^{n-1}), v) + \langle \bar{g}^n, v\rangle \quad \forall v \in S^n. \tag{6.10}$$

Like the above, (6.10) can be expressed in matrix form as

$$(\mathcal{A} + k_n\mathcal{B})c^n \quad = \mathcal{A}c^{n-1} + k_n\mathcal{F}(c^{n-1}) + k_n\mathcal{D} \quad \text{for } t_n \in (0, T], \tag{6.11}$$

where the matrices $\mathcal{A}$, $\mathcal{B}$, $\mathcal{F}(c^{n-1})$ and $\mathcal{D}$ are defined as earlier. The equation (6.11) yields the system of linear equations in c^n, which has a unique solution.

TH-2911_136123010

6.3 A Posteriori Error Analysis

This section begins with the *a posteriori* error analysis for the fully discrete approximation to the problem (6.1)-(6.3). We first introduce the interior residual and jump residual, and then derive both upper and lower bounds for the error.

Let $\mathcal{E}^n$ be the collection of interior edges of triangle $K \in \mathcal{T}^n$, and let h_e be the length of edge e. We divide $\mathcal{E}^n$ into three sets $\mathcal{E}_\Gamma^n$, $\mathcal{E}_1^n$ and $\mathcal{E}_2^n$, respectively, where $\mathcal{E}_\Gamma^n$ denotes the set of all edges of the interface Γ, and $\mathcal{E}_i^n$ denotes the set of all edges of the triangulation $\mathcal{T}_i^n$, for $i = 1, 2$, respectively.

Now we define the following two residuals which will be used frequently for the rest of the analysis of this chapter.

The interior residual is defined by

$$R^n := f^n(U_h^{n-1}) - k_n^{-1}(U_h^n - U_h^{n-1}), \tag{6.12}$$

and the jump residual across $e \in \mathcal{E}^n$ is defined by

$$J_e^n := \begin{cases} [\beta \nabla U_h^n \cdot \mathbf{n}_e], & \text{if } e \in \mathcal{E}^n \setminus \mathcal{E}_\Gamma^n, \\ \bar{g}^n - [\beta \nabla U_h^n \cdot \mathbf{n}_e], & \text{if } e \in \mathcal{E}_\Gamma^n, \end{cases} \tag{6.13}$$

respectively, where $[\beta \nabla U_h^n \cdot \mathbf{n}_e] = (\beta_1 \nabla U_h^n|_{K_1} \cdot \mathbf{n}_e - \beta_2 \nabla U_h^n|_{K_2} \cdot \mathbf{n}_e)$, $\forall e \in \partial K_1 \cap \partial K_2$ and $\mathbf{n}_e$ denotes the unit normal vector to e points from K_2 to K_1. Using integration by parts, we have for all $\phi \in H_0^1(\Omega)$,

$$a(U_h^n, \phi) = -\sum_{e \in \mathcal{E}^n} \int_e J_e^n \phi ds. \tag{6.14}$$

The equation (6.10) can be written as

$$a(U_h^n, v) - (R^n, v) - \langle \bar{g}^n, v \rangle = 0 \quad \forall v \in S^n. \tag{6.15}$$

We now recall the following local approximation property for the Clément interpolation operator from Chapter 2 (cf. Lemma 2.3.1) which is crucial for our *a posteriori* error analysis.

Lemma 6.3.1. *Let $\Pi^n : H_0^1(\Omega) \to S^n$ be the Clément interpolation operator. Then, for $\phi \in H_0^1(\Omega)$, we have*

$$\begin{aligned} \|\phi - \Pi^n \phi\|_{L^2(K)} + h_K \|\nabla(\phi - \Pi^n \phi)\|_{L^2(K)} &\leq C_{I,1}\, h_K \|\nabla \phi\|_{L^2(\omega_K)}, \\ \|\phi - \Pi^n \phi\|_{L^2(e)} &\leq C_{I,2}\, h_e^{\frac{1}{2}} \|\nabla \phi\|_{L^2(\omega_e)}, \end{aligned} \tag{6.16}$$

where ω_K and ω_e denote the patch of triangles and edges in $\mathcal{T}^n$, respectively; the constants $C_{I,1}, C_{I,2}$ depend on the minimum angle of mesh $\mathcal{T}^n$, $n = 1, \ldots, N$.

TH-2911_136123010

6.3.1 An Upper Bound

In this section, we derive a global upper bound for the *a posteriori* error estimate. For this, we need the following notations. Let $U_h : [0,T] \to H_0^1(\Omega)$ be a continuous piecewise linear approximation in time of $u(t)$ defined by

$$U_h(t) = l_{n-1}(t)U_h^{n-1} + l_n(t)U_h^n \tag{6.17}$$

for $t \in (t_{n-1}, t_n]$, $1 \le n \le N$, where the Lagrange hat functions are given by $l_{n-1}(t) = \frac{t_n - t}{k_n}$ and $l_n(t) = \frac{t - t_{n-1}}{k_n}$, respectively.

The main result of this section is stated in the following theorem.

Theorem 6.3.1. *Let u be the exact solution of (6.1)-(6.3) and let U_h^n be its approximation defined by (6.10). Then for $g \in L^2(0,T;L^2(\Gamma))$, there exists a positive constant C such that for $1 \le m \le N$, we have*

$$\begin{aligned}\frac{1}{4}\|u^m - U_h^m\|^2_{L^2(\Omega)} + \sum_{n=1}^{m}\int_{t_{n-1}}^{t_n} |||u - U_h^n|||^2_{\Omega} dt \;\le\; & \|u_0 - U_h^0\|^2_{L^2(\Omega)} + 2\sum_{n=1}^{m} k_n \eta^n_{5,time} \\ & + C\sum_{n=1}^{m} k_n \eta^n_{5,space} + 4\left(\sum_{n=1}^{m}\int_{t_{n-1}}^{t_n} \|f(U_h) - f^n(U_h)\|_{L^2(\Omega)} dt\right)^2 \\ & + 4\left(\sum_{n=1}^{m}\int_{t_{n-1}}^{t_n} \|g - \bar{g}^n\|_{L^2(\Gamma)} dt\right)^2, \end{aligned} \tag{6.18}$$

where the constant C depends on the minimum angle of meshes $\mathcal{T}^n$, $n = 1, 2, \ldots, m$, and the coefficient $\beta(x)$. The time error indicator $(\eta^n_{5,time})$ and the space error indicator $(\eta^n_{5,space})$, respectively, are given by

$$\eta^n_{5,time} \;=\; \frac{1}{3}|||U_h^n - U_h^{n-1}|||^2_{L^2(\Omega)}, \quad \eta^n_{5,space} = \sum_{e \in \mathcal{E}^n} \eta^n_{5,e}$$

with the local error indicator $(\eta^n_{5,e})$ is defined as

$$\eta^n_{5,e} \;=\; \frac{1}{2}\sum_{K \in \Omega_e} h_K^2 \|R^n\|^2_{L^2(K)} + h_e \|J_e^n\|^2_{L^2(e)} + h_e \|\bar{g}_e^n\|^2_{L^2(e)}, \tag{6.19}$$

where Ω_e is the collection of two elements sharing the common edge $e \in \mathcal{E}^n$.

Proof. For any $\phi \in H_0^1(\Omega)$ and $v \in S^n$, we obtain using (6.10)

$$\left(\frac{U_h^n - U_h^{n-1}}{k_n}, \phi\right) + a(U_h^n, \phi) \;=\; \left(f^n(U_h^{n-1}), \phi\right) + \langle \bar{g}^n, v\rangle - (R^n, \phi - v)$$

TH-2911_136123010

$$+\ a(U_h^n, \phi - v). \tag{6.20}$$

From (6.7), (6.17) and (6.20), for all $t \in (t^{n-1}, t^n]$ and $v \in S^n$, we obtain

$$\begin{aligned}\left(\frac{\partial(u-U_h)}{\partial t}, \phi\right) + a(u - U_h^n, \phi) &= \big(f(u) - f^n(U_h^{n-1}), \phi\big) + \langle g, \phi\rangle - \langle \bar{g}^n, v\rangle \\ &\quad + (R^n, \phi - v) - a(U_h^n, \phi - v). \end{aligned} \tag{6.21}$$

Choose $\phi = u - U_h \in H_0^1(\Omega)$ and $v = \Pi^n \phi \in S^n$ in (6.21). Then, using the identity

$$a(u - U_h^n, u - U_h) = \frac{1}{2}|||u - U_h^n|||_\Omega^2 + \frac{1}{2}|||u - U_h|||_\Omega^2 - \frac{1}{2}|||U_h - U_h^n|||_\Omega^2,$$

we find that

$$\begin{aligned}&\frac{1}{2}\frac{d}{dt}\|u - U_h\|_{L^2(\Omega)}^2 + \frac{1}{2}|||u - U_h^n|||_\Omega^2 + \frac{1}{2}|||u - U_h|||_\Omega^2 \\ =\ &\frac{1}{2}|||U_h - U_h^n|||_\Omega^2 + \big(f(u) - f^n(U_h^{n-1}), u - U_h\big) + \langle g, u - U_h\rangle - \langle \bar{g}^n, \Pi^n(u - U_h)\rangle \\ &+ \big(R^n, (u - U_h) - \Pi^n(u - U_h)\big) + \sum_{e\in\mathcal{E}^n}\int_e J_e^n\big((u - U_h) - \Pi^n(u - U_h)\big)ds.\end{aligned}$$

Integrating the above equation with respect to t from 0 to t_*, for any $t_* \in (t_{m-1}, t_m]$ with $t_n \wedge t_* = \min(t_n, t_*)$ and summing over all m, we get

$$\begin{aligned}&\frac{1}{2}\|(u - U_h)(t_*)\|_{L^2(\Omega)}^2 + \frac{1}{2}\sum_{n=1}^m \int_{t_{n-1}}^{t_n\wedge t_*} \Big(|||u - U_h^n|||_\Omega^2 + |||u - U_h|||_\Omega^2\Big)dt \\ =\ &\frac{1}{2}\|u_0 - U_h^0\|_{L^2(\Omega)}^2 + \frac{1}{2}\sum_{n=1}^m \int_{t_{n-1}}^{t_n} |||U_h - U_h^n|||_\Omega^2 dt \\ &+ \sum_{n=1}^m \int_{t_{n-1}}^{t_n} \big(f(u) - f^n(U_h^{n-1}), u - U_h\big)dt \\ &+ \sum_{n=1}^m \int_{t_{n-1}}^{t_n} \Big(\langle g, u - U_h\rangle - \langle \bar{g}^n, \Pi^n(u - U_h)\rangle\Big)dt \\ &+ \sum_{n=1}^m \int_{t_{n-1}}^{t_n} \big(R^n, (u - U_h) - \Pi^n(u - U_h)\big)dt \\ &+ \sum_{n=1}^m \int_{t_{n-1}}^{t_n} \left(\sum_{e\in\mathcal{E}^n}\int_e J_e^n\big((u - U_h) - \Pi^n(u - U_h)\big)ds\right)dt \\ =\ &\frac{1}{2}\|u_0 - U_h^0\|_{L^2(\Omega)}^2 + I_1 + I_2 + I_3 + I_4 + I_5. \end{aligned} \tag{6.22}$$

Now, we need to estimate the terms $I_i, i = 1, \ldots, 5$ separately. Using (6.17), we have

$$I_1 = \frac{1}{2}\sum_{n=1}^m \int_{t_{n-1}}^{t_n} (l_{n-1}(t))^2\ |||U_h^n - U_h^{n-1}|||_\Omega^2 dt$$

TH-2911_136123010

$$= \frac{1}{2}\sum_{n=1}^{m}\frac{k_n}{3}|||U_h^n - U_h^{n-1}|||_\Omega^2 = \frac{1}{2}\sum_{n=1}^{m} k_n \eta_{5,\text{time}}^n. \tag{6.23}$$

By the Cauchy-Schwarz inequality, we get

$$\begin{aligned} I_2 &= \sum_{n=1}^{m}\int_{t_{n-1}}^{t_n}\big(f(u)-f(U_h),u-U_h\big)dt + \sum_{n=1}^{m}\int_{t_{n-1}}^{t_n}\big(f(U_h)-f^n(U_h),u-U_h\big)dt \\ &\quad + \sum_{n=1}^{m}\int_{t_{n-1}}^{t_n}\big(f^n(U_h)-f^n(U_h^{n-1}),u-U_h\big)dt \\ &\le \sum_{n=1}^{m}\int_{t_{n-1}}^{t_n}\|f(u)-f(U_h)\|_{L^2(\Omega)}\|u-U_h\|_{L^2(\Omega)}dt \\ &\quad + \sum_{n=1}^{m}\int_{t_{n-1}}^{t_n}\|f(U_h)-f^n(U_h)\|_{L^2(\Omega)}\|u-U_h\|_{L^2(\Omega)}dt \\ &\quad + \sum_{n=1}^{m}\int_{t_{n-1}}^{t_n}\|f^n(U_h)-f^n(U_h^{n-1})\|_{L^2(\Omega)}\|u-U_h\|_{L^2(\Omega)}dt. \end{aligned}$$

Now an application of (6.4) in the above inequality implies

$$\begin{aligned} I_2 &\le \sum_{n=1}^{m}\int_{t_{n-1}}^{t_n}\|u-U_h\|_{L^2(\Omega)}\|u-U_h\|_{L^2(\Omega)}dt \\ &\quad + \sum_{n=1}^{m}\int_{t_{n-1}}^{t_n}\|f(U_h)-f^n(U_h)\|_{L^2(\Omega)}\|u-U_h\|_{L^2(\Omega)}dt \\ &\quad + \sum_{n=1}^{m}\int_{t_{n-1}}^{t_n}\|U_h-U_h^{n-1}\|_{L^2(\Omega)}\|u-U_h\|_{L^2(\Omega)}dt. \end{aligned} \tag{6.24}$$

Again, using the Young's inequality and (6.17) in (6.24), we have

$$\begin{aligned} I_2 &\le \frac{3C_L}{2}\sum_{n=1}^{m}\int_{t_{n-1}}^{t_n}\|u-U_h\|_{L^2(\Omega)}^2dt + \frac{1}{8}\max_{0\le t\le t_*}\|u-U_h\|_{L^2(\Omega)}^2 \\ &\quad + 2\left(\sum_{n=1}^{m}\int_{t_{n-1}}^{t_n}\|f(U_h)-f^n(U_h)\|_{L^2(\Omega)}dt\right)^2 + \frac{C_L}{2}\sum_{n=1}^{m}\int_{t_{n-1}}^{t_n}\|U_h-U_h^{n-1}\|_{L^2(\Omega)}^2dt \\ &\le \frac{1}{4}\max_{0\le t\le t_*}\|u-U_h\|_{L^2(\Omega)}^2 + \frac{1}{24}\sum_{n=1}^{m}k_n\eta_{5,time}^n \\ &\quad + 2\left(\sum_{n=1}^{m}\int_{t_{n-1}}^{t_n}\|f(U_h)-f^n(U_h)\|_{L^2(\Omega)}dt\right)^2, \end{aligned} \tag{6.25}$$

where the Lipschitz constant $C_L = \frac{1}{12}$ is chosen for simplification and

$$\sum_{n=1}^{m}\int_{t_{n-1}}^{t_n}\|U_h-U_h^{n-1}\|_{L^2(\Omega)}^2dt = \frac{1}{3}\sum_{n=1}^{m}k_n\|U_h^n-U_h^{n-1}\|_{L^2(\Omega)}^2 \le \sum_{n=1}^{m}\eta_{5,time}^n.$$

TH-2911_136123010

Again, for I_3, an application of the Cauchy-Schwarz inequality and (6.16) implies

$$\begin{aligned} I_3 &= \sum_{n=1}^{m}\int_{t_{n-1}}^{t_n}\langle g-\bar{g}^n, u-U_h\rangle dt + \sum_{n=1}^{m}\int_{t_{n-1}}^{t_n}\langle \bar{g}^n, (u-U_h)-\Pi^n(u-U_h)\rangle dt \\ &\leq \sum_{n=1}^{m}\int_{t_{n-1}}^{t_n}\|g-\bar{g}^n\|_{L^2(\Gamma)}\|u-U_h\|_{L^2(\Omega)}\ dt \\ &\quad + C_{I,2}\sum_{n=1}^{m}\int_{t_{n-1}}^{t_n}\sum_{e\in\mathcal{E}_\Gamma^n} h_e^{\frac{1}{2}}\|\bar{g}^n\|_{L^2(e)}\|\nabla(u-U_h)\|_{L^2(\omega_e)}dt. \end{aligned}$$

Applying Young's inequality to the first term of the above inequality, we obtain

$$\begin{aligned} I_3 &\leq 2\left(\sum_{n=1}^{m}\int_{t_{n-1}}^{t_n}\|g-\bar{g}^n\|_{L^2(\Gamma)}dt\right)^2 + \frac{1}{8}\max_{0\leq t\leq t_*}\|u-U_h\|_{L^2(\Omega)} \\ &\quad + C_{I,2}\sum_{n=1}^{m}\int_{t_{n-1}}^{t_n}\sum_{e\in\mathcal{E}_\Gamma^n} h_e^{\frac{1}{2}}\|\bar{g}^n\|_{L^2(e)}\|\nabla(u-U_h)\|_{L^2(\omega_e)}dt. \end{aligned} \tag{6.26}$$

Similarly, for I_4 and I_5, we again apply the Cauchy-Schwarz inequality and approximation properties (6.16) to obtain

$$\begin{aligned} I_4 &\leq \sum_{n=1}^{m}\int_{t_{n-1}}^{t_n}\sum_{K\in\mathcal{T}^n}\|R^n\|_{L^2(K)}\|(u-U_h)-\Pi^n(u-U_h)\|_{L^2(K)}dt \\ &\leq C_{I,1}\sum_{n=1}^{m}\int_{t_{n-1}}^{t_n}\sum_{K\in\mathcal{T}^n} h_K\|R^n\|_{L^2(K)}\|\nabla(u-U_h)\|_{L^2(\omega_K)}dt, \end{aligned} \tag{6.27}$$

and

$$\begin{aligned} I_5 &\leq \sum_{n=1}^{m}\int_{t_{n-1}}^{t_n}\sum_{e\in\mathcal{E}^n}\|J_e^n\|_{L^2(e)}\|(u-U_h)-\Pi^n(u-U_h)\|_{L^2(e)}dt \\ &\leq C_{I,2}\sum_{n=1}^{m}\int_{t_{n-1}}^{t_n}\sum_{e\in\mathcal{E}^n} h_e^{\frac{1}{2}}\|J_e^n\|_{L^2(e)}\|\nabla(u-U_h)\|_{L^2(\omega_e)}dt, \end{aligned} \tag{6.28}$$

respectively. Taking together all the above estimates (6.23)-(6.28) and (6.22), and an application the Cauchy-Schwarz inequality, we have

$$\begin{aligned} &\frac{1}{2}\|(u-U_h)(t_*)\|_{L^2(\Omega)}^2 + \frac{1}{2}\sum_{n=1}^{m}\int_{t_{n-1}}^{t_n\wedge t_*}\Big(|||u-U_h^n|||_\Omega^2 + |||u-U_h|||_\Omega^2\Big)dt \\ \leq\ & \frac{1}{2}\|u_0-U_h^0\|_{L^2(\Omega)}^2 + \frac{13}{24}\sum_{n=1}^{m}k_n\eta_{5,time}^n + \frac{3}{8}\max_{0\leq t\leq t_*}\|u-U_h\|_{L^2(\Omega)}^2 \\ &+ 2\left(\sum_{n=1}^{m}\int_{t_{n-1}}^{t_n}\|f(U_h)-f^n(U_h)\|_{L^2(\Omega)}dt\right)^2 + 2\left(\sum_{n=1}^{m}\int_{t_{n-1}}^{t_n}\|g-\bar{g}^n\|_{L^2(\Gamma)}dt\right)^2 \end{aligned}$$

TH-2911_136123010

$$
\begin{aligned}
&+ C^{\frac{1}{2}} \sum_{n=1}^{m} \int_{t_{n-1}}^{t_n} \left(\sum_{e \in \mathcal{E}^n} \left(\frac{1}{2} \sum_{K \in \Omega_e} h_K^2 \|R^n\|_{L^2(K)}^2 + h_e \|J_e^n\|_{L^2(e)}^2 + h_e \|\bar{g}_e^n\|_{L^2(e)}^2 \right) \right)^{\frac{1}{2}} \\
&\times |||u - U_h|||_\Omega \, dt \\
\leq\ & \frac{1}{2} \|u_0 - U_h^0\|_{L^2(\Omega)}^2 + \frac{13}{24} \sum_{n=1}^{m} k_n \eta_{5,\text{time}}^n + \frac{3}{8} \max_{0 \leq t \leq t_*} \|u - U_h\|_{L^2(\Omega)}^2 \\
&+ 2 \left(\sum_{n=1}^{m} \int_{t_{n-1}}^{t_n} \|f(U_h) - f^n(U_h)\|_{L^2(\Omega)} dt \right)^2 + 2 \left(\sum_{n=1}^{m} \int_{t_{n-1}}^{t_n} \|g - \bar{g}^n\|_{L^2(\Gamma)} dt \right)^2 \\
&+ C^{\frac{1}{2}} \sum_{n=1}^{m} \int_{t_{n-1}}^{t_n} \left(\eta_{5,\text{space}}^n \right)^{\frac{1}{2}} |||u - U_h|||_\Omega dt, \qquad (6.29)
\end{aligned}
$$

where $C = \max\{C_{I,1}^2, C_{I,2}^2\}$. Finally, we apply the Young's inequality to the last term of (6.29) to obtain

$$
\begin{aligned}
&\frac{1}{2} \|(u - U_h)(t_*)\|_{L^2(\Omega)}^2 + \frac{1}{2} \sum_{n=1}^{m} \int_{t_{n-1}}^{t_n \wedge t_*} \left(|||u - U_h^n|||_\Omega^2 + |||u - U_h|||_\Omega^2 \right) dt \\
\leq\ & \frac{1}{2} \|u_0 - U_h^0\|_{L^2(\Omega)}^2 + \frac{13}{24} \sum_{n=1}^{m} k_n \eta_{5,\text{time}}^n + \frac{3}{8} \max_{0 \leq t \leq t_*} \|u - U_h\|_{L^2(\Omega)}^2 \\
&+ 2 \left(\sum_{n=1}^{m} \int_{t_{n-1}}^{t_n} \|f(U_h) - f^n(U_h)\|_{L^2(\Omega)} dt \right)^2 + 2 \left(\sum_{n=1}^{m} \int_{t_{n-1}}^{t_n} \|g - \bar{g}^n\|_{L^2(\Gamma)} dt \right)^2 \\
&+ \frac{C}{2} \sum_{n=1}^{m} \int_{t_{n-1}}^{t_n} \eta_{5,\text{space}}^n dt + \frac{1}{2} \sum_{n=1}^{m} \int_{t_{n-1}}^{t_n} |||u - U_h|||_\Omega^2 dt,
\end{aligned}
$$

A simple calculation gives the required estimate (6.18) and this completes the proof. □

6.3.2 A Lower Bound

In this section, we derive a lower bound for the local error for the *a posteriori* error indicator which plays an important role in the refinement/coarsening strategy. The treatment of the oscillation of the residual which changes at each refinement stage is crucial in deriving the lower bound.

Following [29], we consider the auxiliary problem as follows. Let $U_*^n \in H_0^1(\Omega)$ be the solution of

$$
\left(\frac{U_*^n - U_h^{n-1}}{k_n}, \phi \right) + a(U_*^n, \phi) = (f^n(U_h^{n-1}), \phi) + \langle \bar{g}^n, \phi \rangle \qquad \forall \phi \in H_0^1(\Omega). \qquad (6.30)
$$

The purpose of introducing (6.30) is to essentially control the error between U_*^n and U_h^n, not between U_h^n and the exact solution $u^n = u(x, t_n)$ for fixed time-step size k_n by adapting the mesh $\mathcal{T}^n$.

TH-2911_136123010

For any $K \in \mathcal{T}^n$ and $\phi \in L^2(\Omega)$, define

$$\mathcal{P}_K \phi = \frac{1}{|K|} \int_K \phi \, dx,$$

the average of ϕ over the triangle K. For any $n = 1, 2, \ldots$, we choose the constant

$$\hat{C}_n = \max_{K \in \mathcal{T}^n} \left\{ \frac{h_K^2}{k_n} : h_K = \operatorname{diam}(K) \right\}. \tag{6.31}$$

For a function $\phi \in L^2(\Omega)$, we define the weighted norm $\|\cdot\|_{k_n,\Omega}$ of $H^1(\Omega)$ with the parameter $k_n > 0$ by

$$\|\phi\|_{k_n,\Omega} := \left(\frac{1}{k_n} \|\phi\|^2_{L^2(\Omega)} + |||\phi|||^2_{\Omega} \right)^{\frac{1}{2}} \tag{6.32}$$

and the oscillation of the function $\phi \in L^2(\Omega)$ over the mesh $\mathcal{T}^n$ by

$$\operatorname{osc}(\phi, \mathcal{T}^n) := \left(\sum_{K \in \mathcal{T}^n} h_K^2 \|\phi - \mathcal{P}_K \phi\|^2_{L^2(K)} \right)^{\frac{1}{2}}. \tag{6.33}$$

Theorem 6.3.2. *Let U_h^n and U_*^n be the solutions of (6.10) and (6.30), respectively. Then, for $n = 1, 2, \ldots, m$, we have*

$$\begin{aligned} \eta^n_{5,e} \leq\ & C_{6,6} \hat{C}_n \sum_{K \in \Omega_e} \left\{ \frac{1}{k_n} \|U_*^n - U_h^n\|^2_{L^2(K)} + |||U_*^n - U_h^n|||^2_K \right\} \\ & + C_{6,5} \sum_{K \in \Omega_e} h_K^2 \|R^n - \mathcal{P}_K R^n\|^2_{L^2(K)} + C_{6,7} h_e \|\bar{g}^n\|^2_{L^2(e)}, \end{aligned} \tag{6.34}$$

where the constants $C_{6,j}$'s $(j = 5, 6, 7)$, depend only on the minimum angle of meshes $\mathcal{T}^n$ and the coefficient $\beta(x)$.

Proof. We borrow the idea of proof from Verfürth [104]. For any $K \in \mathcal{T}^n$, let $\psi_K = 27\lambda_1\lambda_2\lambda_3$ be the element bubble function, where λ_1, λ_2 and λ_3 are the barycentric coordinate functions. Then the following inf-sup relation satisfies

$$\inf_{v_h \in \mathbb{P}_1(K)} \sup_{\phi_h \in \mathbb{P}_1(K)} \frac{\int_K v_h \phi_h \psi_K}{\|\phi_h\|_{L^2(K)} \|v_h\|_{L^2(K)}} \geq \gamma_0,$$

where the constant $\gamma_0 > 0$ depends only on the minimum angle of $K \in \mathcal{T}^n$. Let $\phi^n \in \mathbb{P}_1(K)$ be such that $\|\phi^n\|_{L^2(K)} = 1$. Since $\psi_K = 0$ on ∂K and $U_h^n \in \mathbb{P}_1(K)$, we have $\langle \bar{g}^n, \psi_K \phi^n \rangle = 0$ on ∂K and $a(U_h^n, \psi_K \phi^n) = 0$ over K. Taking $v_h = \mathcal{P}_K R^n$ in the inf-sup relation and using (6.30), we find that

$$\gamma_0 \|\mathcal{P}_K R^n\|_{L^2(K)} \leq \int_K (\mathcal{P}_K R^n) \psi_K \phi^n dx$$

TH-2911_136123010

$$
\begin{aligned}
&= \int_K (\mathcal{P}_K R^n - R^n)\psi_K\phi^n dx + \int_K \left(f^n(U_h^{n-1}) - \frac{U_h^n - U_h^{n-1}}{k_n} \right)\psi_K\phi^n dx \\
&= \int_K (\mathcal{P}_K R^n - R^n)\psi_K\phi^n dx + \int_K \left(f^n(U_h^{n-1}) - \frac{U_*^n - U_h^{n-1}}{k_n} \right)\psi_K\phi^n dx \\
&\quad + \int_K \left(\frac{U_*^n - U_h^n}{k_n} \right)\psi_K\phi^n dx \\
&= \int_K (\mathcal{P}_K R^n - R^n)\psi_K\phi^n dx + a(U_*^n - U_h^n, \psi_K\phi^n) \\
&\quad + \int_K \left(\frac{U_*^n - U_h^n}{k_n} \right)\psi_K\phi^n dx. \qquad (6.35)
\end{aligned}
$$

By the Cauchy-Schwarz inequality, the inverse estimate $|||\psi_K\phi^n|||_K \leq C_{1,1}h_K^{-1}$ and (6.35), it follows that

$$
\gamma_0\|\mathcal{P}_K R^n\|_{L^2(K)} \leq \|\mathcal{P}_K R^n - R^n\|_{L^2(K)} + C_{1,1}h_K^{-1}|||U_*^n - U_h^n|||_K + \frac{1}{k_n}\|U_*^n - U_h^n\|_{L^2(K)}.
$$

With an aid of (6.31), it now follows that

$$
\begin{aligned}
h_K^2\|R^n\|_{L^2(K)}^2 &\leq h_K^2\|\mathcal{P}_K R^n - R^n\|_{L^2(K)}^2 + h_K^2\|\mathcal{P}_K R^n\|_{L^2(K)}^2 \\
&\leq \frac{h_K^2}{\gamma_0^2}\left\{ \frac{1}{k_n^2}\|U_*^n - U_h^n\|_{L^2(K)}^2 + \frac{C_{1,1}^2}{h_K^2}|||U_*^n - U_h^n|||_K^2 \right\} \\
&\quad + \left(1 + \frac{1}{\gamma_0^2}\right)h_K^2\|R^n - \mathcal{P}_K R^n\|_{L^2(K)}^2 \\
&\leq C_{6,3}\hat{C}_n\left\{ \frac{1}{k_n}\|U_*^n - U_h^n\|_{L^2(K)}^2 + |||U_*^n - U_h^n|||_K^2 \right\} \\
&\quad + C_{6,2}h_K^2\|R^n - \mathcal{P}_K R^n\|_{L^2(K)}^2, \qquad (6.36)
\end{aligned}
$$

where the constants $C_{6,2} = (1 + 1/\gamma_0^2)$ and $C_{6,3} = \max\{1/\gamma_0^2, C_{1,1}^2/\gamma_0^2\}$.

Let $\psi^e = 4\lambda_1\lambda_2$ be the edge bubble function for any edge $e \in \mathcal{E}^n$, where λ_1 and λ_2 are the barycentric coordinate functions associated with the node of e. Let $\psi^n = J_e^n\psi_e \in H_0^1(\Omega)$. Since J_e^n is constant on $e \in \mathcal{E}^n$, we have $\|\phi\|_{L^2(e)} \leq C_{6,4}\|\psi_e^{\frac{1}{2}}\phi\|_{L^2(e)}$. Now we use (6.30) and integrate by parts formula to obtain

$$
\begin{aligned}
\|J_e^n\|_{L^2(e)}^2 &\leq C_{6,4}\int_e J_e^n\psi^n dx = -C_{6,4}\sum_{K\in\Omega_e}\int_K \beta(x)\nabla U_h^n \cdot \nabla\psi^n dx \\
&= C_{6,4}\sum_{K\in\Omega_e}\int_K \beta(x)\nabla(U_*^n - U_h^n).\nabla\psi^n dx - C_{6,4}\sum_{K\in\Omega_e}\int_K R^n\psi^n dx \\
&\quad - C_{6,4}\int_{e;\partial K\cap\Gamma\neq\emptyset} \bar{g}^n\psi^n dx
\end{aligned}
$$

TH-2911_136123010

$$\leq C_{6,4}\Bigg(\sum_{K\in\Omega_e}\|\nabla(U_*^n-U_h^n)\|_{L^2(K)}\|\nabla\psi^n\|_{L^2(K)}$$

$$+\sum_{K\in\Omega_e}\|R^n\|_{L^2(K)}\|\psi^n\|_{L^2(K)}+\|\bar{g}^n\|_{L^2(e)}\|\psi^n\|_{L^2(e)}\Bigg). \tag{6.37}$$

Since $\|\nabla\psi^n\|_{L^2(K)}\leq C_*h_e^{-\frac{1}{2}}\|J_e^n\|_{L^2(e)}$, $\|\psi^n\|_{L^2(K)}\leq C_*h_e^{\frac{1}{2}}\|J_e^n\|_{L^2(e)}$ for all $K\in\Omega_e$, and an application of Young's inequality in (6.37) yields

$$\begin{aligned}
h_e\|J_e^n\|_{L^2(e)}^2 &\leq C_{6,4}C_*\Bigg(\sum_{K\in\Omega_e}h_e^{\frac{1}{2}}\|\nabla(U_*^n-U_h^n)\|_{L^2(K)}\|J_e^n\|_{L^2(e)}\\
&\quad+\sum_{K\in\Omega_e}h_e^{\frac{3}{2}}\|R^n\|_{L^2(K)}\|J_e^n\|_{L^2(e)}+h_e\|\bar{g}^n\|_{L^2(e)}\|J_e^n\|_{L^2(e)}\Bigg)\\
&\leq C_{6,4}C_*\Bigg(\sum_{K\in\Omega_e}|||U_*^n-U_h^n|||_K^2+\sum_{K\in\Omega_e}h_e^2\|R^n\|_{L^2(K)}^2+h_e\|\bar{g}^n\|_{L^2(e)}^2\Bigg)^{\frac{1}{2}}\\
&\quad\times\Big(h_e\|J_e^n\|_{L^2(e)}^2\Big)^{\frac{1}{2}}.
\end{aligned}$$

This implies

$$h_e\|J_e^n\|_{L^2(e)}^2 \leq C_{6,4}C_*\Bigg(\sum_{K\in\Omega_e}|||U_*^n-U_h^n|||_K^2+\sum_{K\in\Omega_e}h_e^2\|R^n\|_{L^2(K)}^2+h_e\|\bar{g}^n\|_{L^2(e)}^2\Bigg). \tag{6.38}$$

Taking together (6.19), (6.36) and (6.38) gives

$$\begin{aligned}
\eta_{5,e}^n &= \frac{1}{2}\sum_{K\in\Omega_e}h_K^2\|R^n\|_{L^2(K)}^2+h_e\|J_e^n\|_{L^2(e)}^2\\
&\leq (\frac{1}{2}+C_{6,4}C_*)C_{6,3}\hat{C}_n\sum_{K\in\Omega_e}\Bigg\{\frac{1}{k_n}\|U_*^n-U_h^n\|_{L^2(K)}^2+|||U_*^n-U_h^n|||_K^2\Bigg\}\\
&\quad+(\frac{1}{2}+C_{6,4}C_*)C_{6,2}\sum_{K\in\Omega_e}h_K^2\|R^n-\mathcal{P}_KR^n\|_{L^2(K)}^2+C_{6,4}C_*h_e\|\bar{g}^n\|_{L^2(e)}^2\\
&\leq C_{6,6}\hat{C}_n\sum_{K\in\Omega_e}\Bigg\{\frac{1}{k_n}\|U_*^n-U_h^n\|_{L^2(K)}^2+|||U_*^n-U_h^n|||_K^2\Bigg\}\\
&\quad+C_{6,5}\sum_{K\in\Omega_e}h_K^2\|R^n-\mathcal{P}_KR^n\|_{L^2(K)}^2+C_{6,7}h_e\|\bar{g}^n\|_{L^2(e)}^2,
\end{aligned}$$

where the constant $C_{6,6}=(\frac{1}{2}+C_{6,4}C_*)C_{6,3}$, $C_{6,5}=(\frac{1}{2}+C_{6,4}C_*)C_{6,2}$, $C_{6,7}=C_{6,4}C_*$. This completes the rest of the proof. □

TH-2911_136123010

Remark 6.3.1. *Summing up (6.34) for all $e \in \mathcal{E}^n$, we reach the following result*

$$\begin{aligned}\eta^n_{5,space} &\leq C_{6,6}\hat{C}_n \sum_{e\in\mathcal{E}_n}\sum_{K\in\Omega_e}\left\{\frac{1}{k_n}\|U^n_* - U^n_h\|^2_{L^2(K)} + |||U^n_* - U^n_h|||^2_K\right\} \\ &\quad + C_{6,5}\sum_{e\in\mathcal{E}^n}\sum_{K\in\Omega_e} h^2_K\|R^n - \mathcal{P}_K R^n\|^2_{L^2(K)} + C_{6,7}\sum_{e\in\mathcal{E}^n_\Gamma} h_e\|\bar{g}^n_h\|^2_{L^2(e)} \\ &= 2C_{6,6}\hat{C}_n\|U^n_* - U^n_h\|^2_{k_n,\Omega} + 2C_{6,5}\ osc(R^n,\mathcal{T}^n)^2 + C_{6,7}\sum_{e\in\mathcal{E}^n_\Gamma} h_e\|\bar{g}^n\|^2_{L^2(e)}, \qquad (6.39)\end{aligned}$$

where the weighted norm $\|U^n_* - U^n_h\|_{k_n,\Omega}$ and the oscillation of residual $osc(R^n,\mathcal{T}^n)$ are defined in (6.33) and (6.32), respectively.

6.4 Adaptive Algorithm

This section provides an algorithm to describe the adaptive procedure of the problem (6.1)-(6.3). The algorithm is based on the error equidistribution strategy [29, 94]. Let ϵ_{time} be the total tolerance related to the time discretization so that

$$\begin{cases} 2\sum_{n=1}^{N} k_n\eta^n_{5,\text{time}} + 4\left(\sum_{n=1}^{N}\int_{t_{n-1}}^{t_n}\|f(U_h) - f^n(U_h)\|_{L^2(\Omega)}dt\right)^2 \\ \quad + 4\left(\sum_{n=1}^{N}\int_{t_{n-1}}^{t_n}\|g - \bar{g}^n\|_{L^2(\Gamma)}dt\right)^2 \leq \epsilon_{\text{time}}. \end{cases} \qquad (6.40)$$

To obtain (6.40) we have to adjust the time-step size k_n such that the following relations hold:

$$\begin{cases} \eta^n_{5,\text{time}} \leq \dfrac{\epsilon_{\text{time}}}{6T}, \qquad \dfrac{1}{k_n}\displaystyle\int_{t_{n-1}}^{t_n}\|f(U_h) - f^n(U_h)\|_{L^2(\Omega)}dt \leq \dfrac{\sqrt{\epsilon_{\text{time}}}}{2\sqrt{3}T}, \\ \dfrac{1}{k_n}\displaystyle\int_{t_{n-1}}^{t_n}\|g - \bar{g}^n\|_{L^2(\Gamma)}dt \leq \dfrac{\sqrt{\epsilon_{\text{time}}}}{2\sqrt{3}T}. \end{cases} \qquad (6.41)$$

For given any $\delta_{\text{time}} \in (0,1)$, we have

$$\begin{cases} \eta^n_{5,\text{time}} \leq \delta_{\text{time}}\dfrac{\epsilon_{\text{time}}}{6T}, \qquad \displaystyle\int_{t_{n-1}}^{t_n}\|f(U_h) - f^n(U_h)\|_{L^2(\Omega)}dt \leq \dfrac{\sqrt{\delta_{\text{time}}\epsilon_{\text{time}}}}{2\sqrt{3}T}, \\ \dfrac{1}{k_n}\displaystyle\int_{t_{n-1}}^{t_n}\|g - \bar{g}^n\|_{L^2(\Gamma)}dt \leq \dfrac{\sqrt{\delta_{\text{time}}\epsilon_{\text{time}}}}{2\sqrt{3}T} \end{cases} \qquad (6.42)$$

Let ϵ_{space} be the tolerance related to the space discretization which is allowed for the part of the *a posteriori* error estimate in (6.18). Then for each time step n, the stopping criterion for mesh adaptation is to satisfy

TH-2911_136123010

$$\eta^n_{5,\text{space}} \leq \frac{\epsilon_{\text{space}}}{2}. \tag{6.43}$$

This stopping criteria is suitable for mesh refinements but not for mesh coarsening. For our analysis, we will use a coarsening error indicator $\eta^n_{5,coarse}$ (cf. [29]) which is defined by

$$\eta^n_{5,coarse} = \frac{1}{k_n}\|I^n_H U^n_h - U^n_h\|^2_{L^2(\Omega)} + |||I^n_H U^n_h - U^n_h|||^2_\Omega, \tag{6.44}$$

where I^n_H is the standard linear finite element interpolant. The indicator $\eta^n_{5,coarse}$ does not depend on the solution of the coarsened problem. Also, this property allows the mesh to coarsen only once, without checking whether the solution of the coarsened problem satisfies the stopping criteria (6.43). Using the above fact, we present the following space-time adaptive algorithm.

Algorithm 6.4.1. *(Space and time adaptive algorithm).* Given tolerances ϵ_{time}, ϵ_{space} and ϵ_{coarse}, parameters $\gamma_1 \in (0,1)$, $\gamma_2 > 1$ and $\delta_{time} \in (0,1)$. Let U^{n-1}_h be the computed value at time t^{n-1} with the time step size k_n and the mesh $\mathcal{T}^{n-1}$.

Step 1: $\mathcal{T}^n := \mathcal{T}^{n-1}$, $k_n := k_{n-1}$, $t_n := t_{n-1} + k_n$
solve the fully discrete problem (6.10) for U^n_h on $\mathcal{T}^n$
compute the error estimates on $\mathcal{T}^n$

Step 2: while (6.41) is not satisfied
do
{
$k_n := \gamma_1 k_n$, $t_n := t_{n-1} + k_n$
solve the fully discrete problem (6.10) for U^n_h on $\mathcal{T}^n$
compute the error estimates on $\mathcal{T}^n$
}
end

Step 3: while $\left(\eta^n_{5,space} > \frac{\epsilon_{space}}{T}\right)$ do
{
refine mesh $\mathcal{T}^n$ to produce a modified mesh $\hat{\mathcal{T}}^n$
solve the fully discrete problem (6.10) for U^n_h on $\hat{\mathcal{T}}^n$
compute the error estimates on $\hat{\mathcal{T}}^n$
while (6.41) is not satisfied

TH-2911_136123010

goto Step 2
}
end

Step 4: if ($\eta^n_{5,coarse} \leq \frac{\epsilon_{coarse}}{T}$)
coarsen mesh $\mathcal{T}^n$ to produce a modified mesh $\mathcal{T}^n$.
solve the fully discrete problem (6.10) for U^n_h on $\mathcal{T}^n$

Step 5: if (6.42) is satisfied then
{
$k_n := \gamma_2 k_n$
}
end

6.5 Numerical Experiment

This section is devoted to numerical experiment corresponding to the parabolic interface problem (6.1)-(6.3). We consider two test problems to validate our theoretical results. The first example consists of a straight interface whereas a polygonal interface is considered in the second example. For both the test examples, we consider two different choices of the discontinuous coefficients β: (i) $\beta_1 = 1$, $\beta_2 = 10$, and (ii) $\beta_1 = 1$, $\beta_2 = 100$. The bisection algorithm is used to generate refined meshes. We take the parameters $\gamma_1 = 0.5$ in Algorithm 6.4.1. All the constants involved in the estimators are taken as 1. The tolerances ϵ_{time} and ϵ_{space} are chosen to be equal, say ϵ, and $\epsilon_{coarse} = 0.5\epsilon$. For our numerical experiments, we have not considered the coarsening of mesh. We compute the energy error $Err := \left(\sum_{n=1}^{N} k_n |||u - U^n_h|||^2_\Omega\right)^{1/2}$ and the effectivity index of *a posteriori* error estimate which is defined as eff. index $= \eta_{5,1}/Err$, where the error estimator $\eta_{5,1}$ is given by

$$\eta^2_{5,1} = \sum_{n=1}^{N} k_n(\eta^n_{5,time} + \eta^n_{5,space} + \eta^n_{5,coarse}) + 4\left(\sum_{n=1}^{m}\int_{t_{n-1}}^{t_n} \|f(U_h) - f^n(U_h)\|_{L^2(\Omega)}\right)^2 + 4\left(\sum_{n=1}^{m}\int_{t_{n-1}}^{t_n} \|g - \bar{g}^n\|_{L^2(\Gamma)}\right)^2.$$

All computations are carried out using the software FreeFem++ (cf. [65]).

Example 6.1. We solve the problem (6.1)-(6.3) in the computational domain $\Omega = (0, 2) \times (0, 1)$. The interface Γ occur at $x = 1$ which divides the domain Ω into two

TH-2911_136123010

subdomains such that $\Omega_1 = (0,1) \times (0,1)$ and $\Omega_2 = (1,2) \times (0,1)$. Select the forcing function $f(x,y,t,u)$, the initial condition $u_0(x,y)$ and the flux jump $g(x,y,t)$ such that the exact solution $u(x,y,t)$ of (6.1)-(6.3) is of the form

$$u(x,y,t) = \begin{cases} t\sin(\pi x)\sin(\pi y) & \text{in } \Omega_1 \times (0,T], \\ -t\sin(\pi x)\sin(\pi y) & \text{in } \Omega_2 \times (0,T]. \end{cases}$$

Table 6.1: The degrees of freedom (DOF), the error estimator $\eta_{5,1}$ and the energy error (Err) at time $t = 0.01$ and tolerance $\epsilon = 0.01$

β	DOF	$\eta_{5,1}$	Err
$\beta_1 = 1$	869	0.021926	0.003161
$\beta_2 = 10$	1566	0.011494	0.002064
	3053	0.005894	0.001318
$\beta_1 = 1$	850	0.027123	0.004812
$\beta_2 = 100$	1546	0.014505	0.003323
	3025	0.007565	0.002358

Table 6.2: The different tolerances ϵ, the degrees of freedom (DOF), the error estimator $\eta_{5,1}$, the energy error (Err) and the effectivity index (eff. index) at time $t = 0.01$

β	ϵ	DOF	$\eta_{5,1}$	Err	eff. index
	0.01	3053	0.005894	0.001318	4.4719
$\beta_1 = 1$	0.005	5953	0.002127	0.001296	1.6412
$\beta_2 = 10$	0.0025	8995	0.001054	0.001024	1.0248
	0.01	3025	0.007565	0.002358	3.2082
$\beta_1 = 1$	0.005	6149	0.004525	0.001938	2.3348
$\beta_2 = 100$	0.0025	9000	0.002551	0.001598	1.5963

TH-2911_136123010

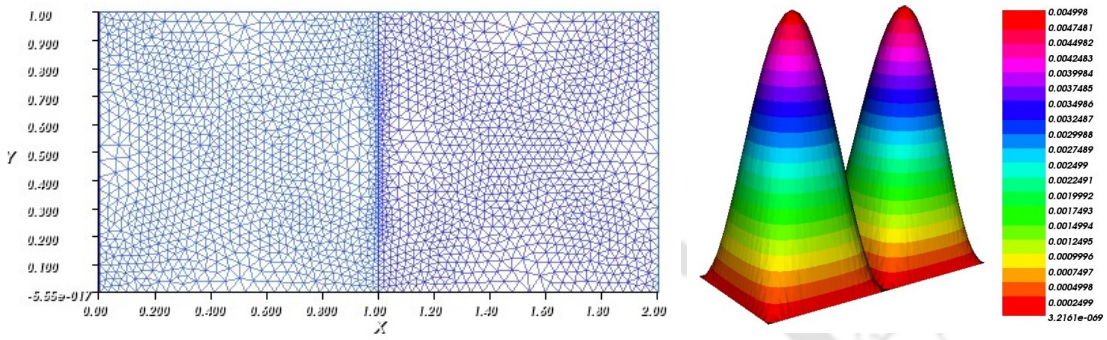

Figure 6.1: An adaptive mesh and the corresponding discrete solution at step 1.

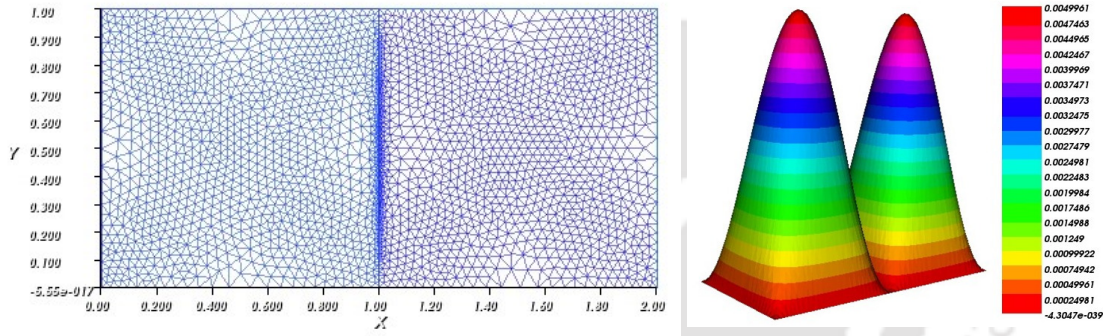

Figure 6.2: An adaptive mesh and the corresponding discrete solution at step 2

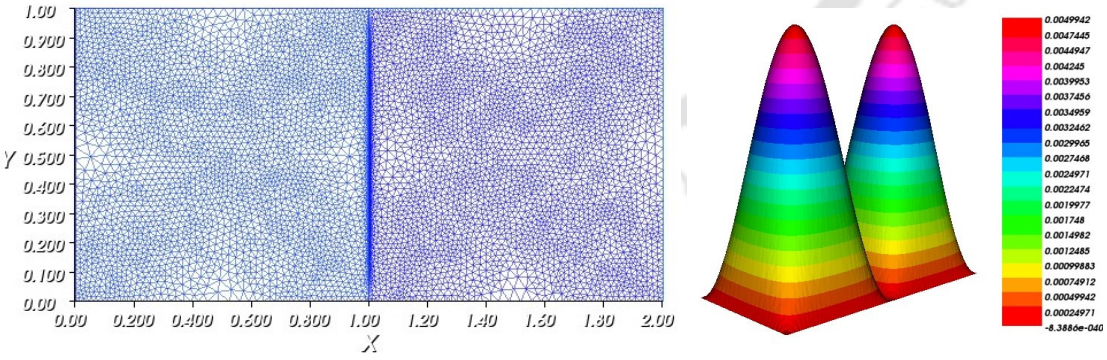

Figure 6.3: An adaptive mesh and the corresponding discrete solution at step 3.

TH-2911_136123010

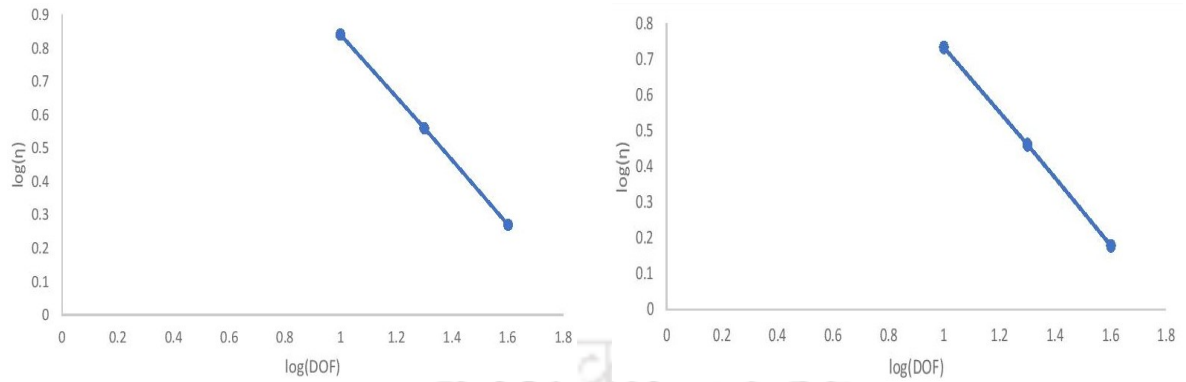

(a) (b)

Figure 6.4: Optimality of the estimator for the cases: (a) $\beta_1 = 1$, $\beta_2 = 10$ and (b) $\beta_1 = 1$, $\beta_2 = 100$. The optimal decay is observed by the line of slope -0.908 (left) and the line of slope -0.921 (right).

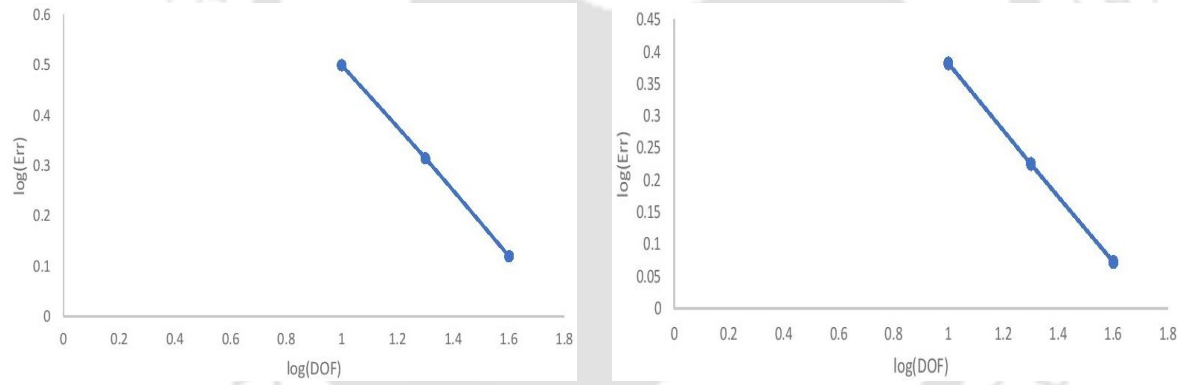

(a) (b)

Figure 6.5: Energy error versus number of degrees of freedom: (a) $\beta_1 = 1{,}0$ $\beta_2 = 10$ and (b) $\beta_1 = 1$, $\beta_2 = 100$. The quasi-optimal decay is observed by the line of slope -0.6221 (left) and the line of slope -0.6512 (right).

For Example 6.1, the adaptive mesh and the corresponding surface plots of the numerical solution at time $t = 0.01$ are given in Figures 6.1 to 6.3. In Table 6.1, for both cases of β, the degrees of freedom (DOF), the error estimator $(\eta_{5,1})$ and the energy error (Err) are given in each step of adaptive mesh generation at final time $t = 0.01$ with the given tolerance $\epsilon = 0.01$. Figure 6.4 shows the plots comparing the degrees of freedom with the total error estimator for both the cases of β. The optimal decay of

TH-2911_136123010

the estimator is observed by the line of slope -0.908 for the choice $\beta_1 = 1, \beta_2 = 10$ (see Figure 6.4 (a)) and the line of slope -0.921 for the choice $\beta_1 = 1, \beta_2 = 100$ (see Figure 6.4 (b)). Further, in Figure 6.5, we provide plots for the energy error versus the number of degrees of freedom. At fixed time $t = 0.01$ for different tolerances ϵ, the degrees of freedom (DOF), the energy error (Err) and the effectivity index (eff. index) are given in Table 6.2.

Example 6.2. In the second example, we solve the problem (6.1)-(6.3) in a computational domain $\Omega = (0,1) \times (0,1)$. We consider $\Omega_1 = (0.25, 0.75) \times (0.25, 0.75)$ and $\Omega_2 = \Omega \setminus \Omega_1$ so that the interface Γ becomes a polygonal interface. Select the functions $f(x,y,t,u)$, $u_0(x,y)$ and $g(x,y,t)$ such that the exact solution $u(x,y,t)$ is as follows:

$$u(x,y,t) = \begin{cases} t\sin(2\pi(x-0.25))\sin(2\pi(y-0.25)) & \text{in } \Omega_1 \times (0,T], \\ t\sin(4\pi x)\sin(4\pi y) & \text{in } \Omega_2 \times (0,T]. \end{cases}$$

Table 6.3: The degrees of freedom (DOF), the error estimator $\eta_{5,1}$ and the energy error (Err) at time $t = 0.01$ and tolerance $\epsilon = 0.03$

β	DOF	$\eta_{5,1}$	Err
	1850	0.4524639	0.018459
$\beta_1 = 1$	2604	0.226861	0.010273
$\beta_2 = 10$	2897	0.113658	0.005858
	1863	1.4676500	0.0193382
$\beta_1 = 1$	2732	0.5963200	0.0108444
$\beta_2 = 100$	2910	0.4552980	0.0105663

For Example 6.2, the adaptive mesh and the corresponding surface plots of the numerical solution at time $t = 0.01$ are given in Figures 6.6 to 6.8. The plots comparing the degrees of freedom with the total error estimator for both the cases are shown in Figure 6.9. The optimal decay of the estimator is observed by the line of slope -0.995 for the choice $\beta_1 = 1, \beta_2 = 10$ (see Figure 6.9 (a)) and the line of slope -0.986 for the choice $\beta_1 = 1, \beta_2 = 100$ (see Figure 6.9 (b)). Further, Figure 6.10 provide plots for the energy error versus the number of degrees of freedom. In Table 6.3, the degrees of freedom (DOF), the error estimator $(\eta_{5,1})$ and the energy error (Err) are given in each

TH-2911_136123010

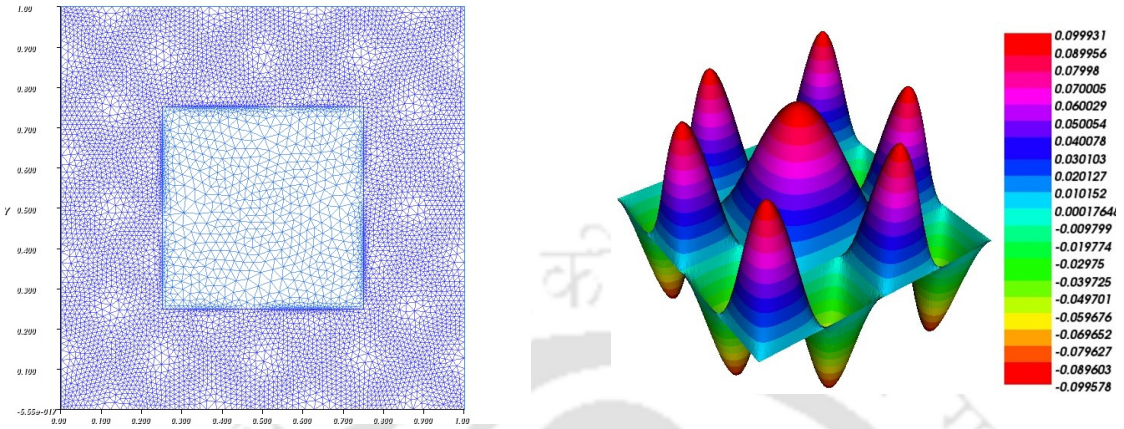

Figure 6.6: An adaptive mesh and the corresponding discrete solution at step 1.

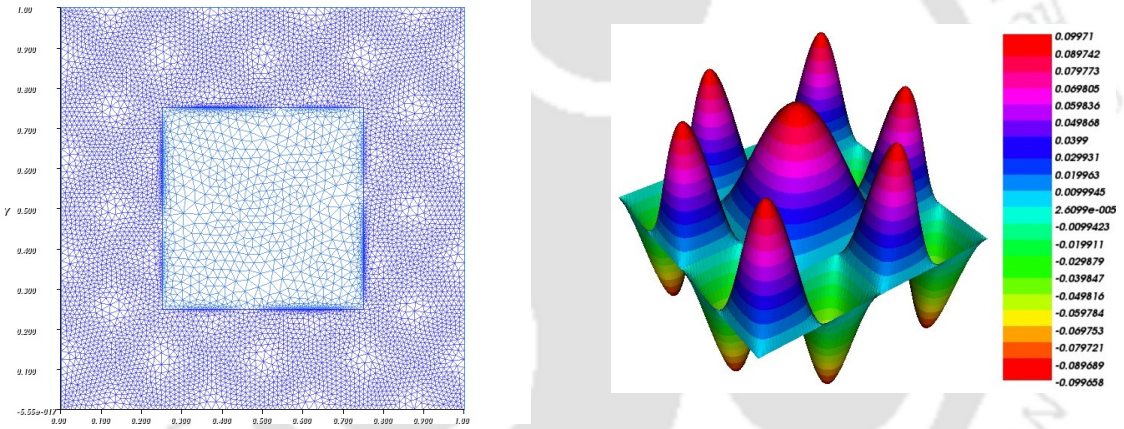

Figure 6.7: An adaptive mesh and the corresponding discrete solution at step 2.

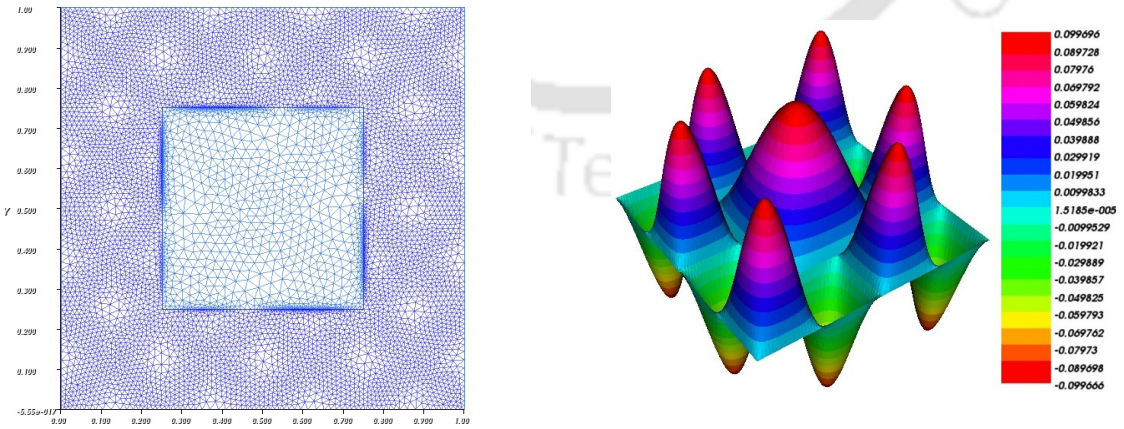

Figure 6.8: An adaptive mesh and the corresponding discrete solution at step 3.

TH-2911_136123010

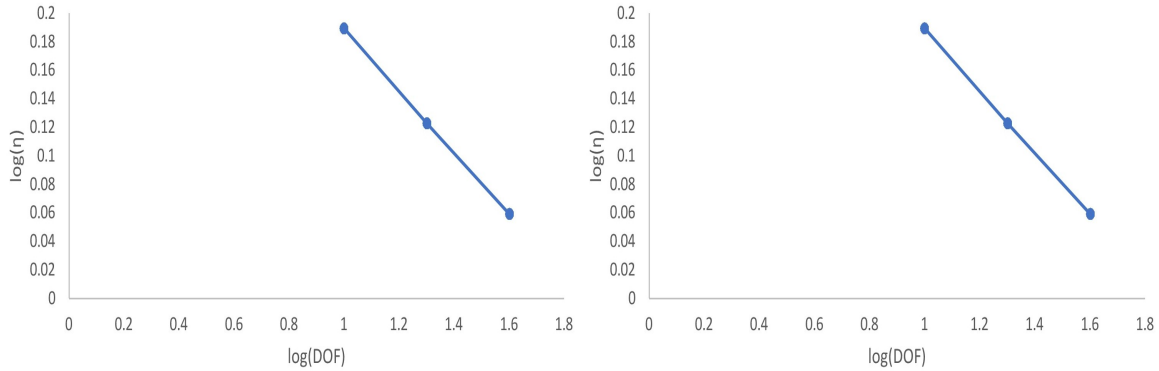

(a) (b)

Figure 6.9: Optimality of the estimator for the cases: (a) $\beta_1 = 1$, $\beta_2 = 10$ and (b) $\beta_1 = 1$, $\beta_2 = 100$. The optimal decay is observed by the line of slope -0.995 (left) and the line of slope -0.986 (right).

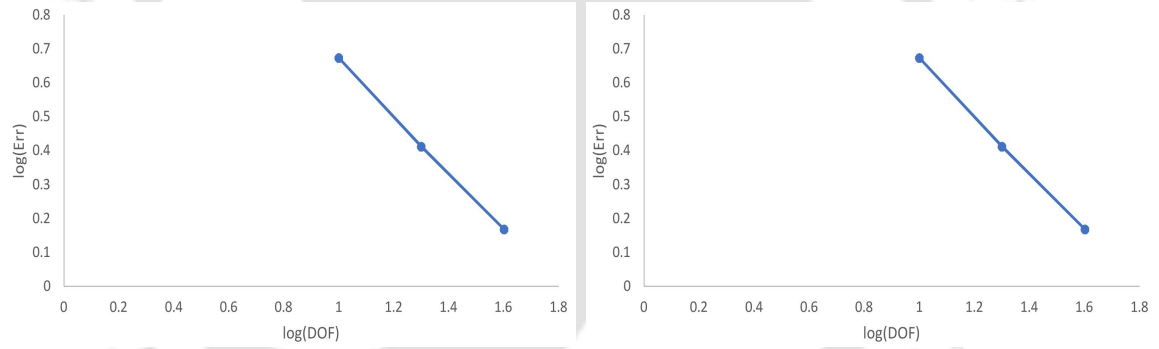

(a) (b)

Figure 6.10: Energy error versus number of degrees of freedom: (a) $\beta_1 = 1{,}0$ $\beta_2 = 10$ and (b) $\beta_1 = 1$, $\beta_2 = 100$. The quasi-optimal decay is observed by the line of slope -0.839 (left) and the line of slope -0.816 (right).

step of adaptive mesh generation at final time $t = 0.01$ with the tolerance $\epsilon = 0.03$. At fixed time $t = 0.01$, for different tolerances ϵ, the degrees of freedom (DOF), the energy error (Err) and the effectivity index (eff. index) are given in Table 6.4.

In Tables 6.1-6.2 and Tables 6.3-6.4, we observe that for a fixed time with different mesh sizes and different tolerances the value of the estimator and the error reduces. Figures 6.1 to 6.3 and Figures 6.6 to 6.8 reveal that the finite element mesh are refined

TH-2911_136123010

Table 6.4: The different tolerances ϵ, the degrees of freedom (DOF), the error estimator $\eta_{5,1}$, the energy error (Err) and the effectivity index (eff. index) at time $t = 0.01$

β	ϵ	DOF	$\eta_{5,1}$	Err	eff. index
	0.03	2897	0.113658	0.005858	19.4021
$\beta_1 = 1$	0.015	5636	0.089844	0.004909	18.3019
$\beta_2 = 10$	0.0075	8996	0.067146	0.004125	16.2778
	0.03	2200	0.4552980	0.0105663	43.0896
$\beta_1 = 1$	0.015	4665	0.3268070	0.0089378	36.5646
$\beta_2 = 100$	0.0075	8987	0.2412290	0.0077719	31.0387

very well and higher density of node points are distributed around the interface Γ.

6.6 Concluding Remarks

In this chapter, we presented an adaptive algorithm for the fully discrete finite element approximation for the semilinear parabolic interface problem with nonzero flux jump. Both global upper and local lower bounds for the error are derived. The treatment of the oscillation of the residual plays an important role in each refinement procedure. The present analysis extends the convergence analysis of AFEM for linear PIP to the semilinear PIP with nonzero flux jump across the interface. The numerical experiments reveal the behavior of the proposed algorithm with promising numerical results.

TH-2911_136123010

7

Conclusions and Extensions

This chapter presents the critical assessment of the results highlighting the contributions of the current thesis work and the technical tools used in the analysis. It also provides some information for the scope of possible extensions and future investigations.

7.1 Critical Review of the Results

In this thesis, the study was set out to explore AFEMs for both linear and semilinear PIPs in a bounded convex polygonal domain in $\mathbb{R}^2$. For some problems, the interface Γ is assumed either to be of the polygonal type or class C^2. Due to the discontinuity of the coefficient along the interface Γ, the solution of the PIP has low global regularity. AFEMs are the best suited numerical technique to enhance the efficiency and accuracy of these kinds of problems. This is because adaptivity allows local mesh refinement around the interface to achieve the desired residual bound with a few degrees of freedom as possible. However, there exists limited work on the AFEM for PIPs and this thesis has attempted to address some of the unexplored issues. In this thesis, a *posteriori* error analysis and adaptive algorithms for conforming FEM, conforming IFE method, nonconforming FEM, and nonconforming IFE method for the PIP are analyzed. The chapter-wise contributions of the thesis are as follows.

Our first problem in Chapter 2 considers an AFEM for the fully discrete finite element approximation for the linear PIP (2.1)-(2.3) in a bounded convex polygonal domain in $\mathbb{R}^2$. The space discretization uses the standard piecewise linear elements while the backward Euler scheme is used to approximate the time derivative. The residual-based *a posteriori* error estimates are derived using the energy method. Some new error indicators are introduced to control the error due to the discontinuous coefficients and nonhomogeneous flux jump across the interface. Both upper and lower bounds (Theorem 2.3.1 and Theorem 2.3.2) for the error are established. The adaptive algorithm

TH-2911_136123010

(Algorithm 2.4.1) is presented using the derived error indicators and a numerical example (Example 2.1) is reported to illustrate the theoretical analysis. Our numerical result shows that the finite element mesh adapts very well where the solution has a discontinuity and a higher density of the node points distributed around the interface. The key technical tools used include Clément type interpolation approximation properties, properties of the bubble functions, and the techniques of [29].

Chapter 3 deals with an AIFEM for the fully discrete finite element approximation for the linear PIP (3.1)-(3.3). In this chapter, the interface Γ is assumed to be of class C^2. We have introduced the space-time IFE discretization where the finite element mesh does not follow the actual interface. The standard piecewise linear finite elements are considered for the spatial discretization and the backward Euler approximation is used for the time derivative. Some new error indicators are introduced to control the error due to the non-body fitted mesh. We have derived both upper and lower bounds (Theorem 3.3.1 and Theorem 3.3.2) for the error in terms of the local error indicators. The key technical ingredients used in deriving the *a posteriori* error estimates are the interpolation approximation properties, energy arguments, and the properties of bubble function. Numerical experiment is performed to demonstrate the adaptive mesh refinement procedure.

Chapter 4 is devoted to the residual-based AFEM for the problem (4.1)-(4.2) using nonconforming finite elements. The discretization is done using the adaptive finite elements in spatial variable combining with the backward Euler approximation in time. The nonconforming finite element spaces are piecewise linear functions over the triangulation of Ω. The proposed *a posteriori* error analysis does not involve the Helmholtz decomposition while analyzing the reliability of the estimator. Both upper and lower bounds (Theorem 4.3.1 and Theorem 4.3.2) for the error are derived. In addition, a lower bound for the error in terms of the modified error indicator is also established (Theorem 4.3.3). The technical tools used in our analysis involves the modified Clément-type interpolation approximation properties, the error equation (Lemma 4.3.2), the energy argument, the properties of bubble functions and the stability properties (Lemma 4.3.3 and Lemma 4.3.4) in the energy norm. Numerical results are provided to show the effectiveness of the estimators using Algorithm 4.4.1.

In Chapter 5, we have considered *a posteriori* error estimation and adaptive mesh refinement for the problem (5.1)-(5.3) using nonconforming IFE method in a bounded convex polygonal domain in $\mathbb{R}^2$. We assumed that the interface is of class C^2 and time-independent. The nonconforming IFE discretization is introduced and the finite element meshes need not follow the interface. The key tools used to derive the residual-based *a*

TH-2911_136123010

posteriori error estimates involve interpolation approximation properties, homogenization arguments, energy argument, and properties of bubble functions. The global upper bound (Theorem 5.3.1) and a lower bound (Theorem 5.3.2) for the error in terms of the local error indicators are derived. New error indicators (5.15)-(5.17) are provided to control the error due to non-body fitted mesh. Our numerical results show the good effects of the requited estimators using the proposed Algorithm 5.4.1.

Chapter 6 is concerned with an AFEM for the semilinear PIP (6.1)-(6.3) with nonzero flux jump. The space discretization uses the continuous piecewise linear finite elements while the backward Euler approximation is considered for the time discretization. The modified linearized backward Euler method for the time discretization is also considered to avoid solving the nonlinear system of algebraic equations at each time level. The forcing term is assumed to satisfy the Lipschitz condition. We have derived *a posteriori* upper and lower bounds for the error. The upper bound (Theorem 6.3.1) of the error involves an indicator for the initial error, temporal and spatial error indicators, and indicators for data approximation error. A lower bound (Theorem 6.3.2) for the error in terms of local error indicator is established. The crucial technical tools used in our analysis involve the interpolation approximation properties, the Cauchy-Schwarz inequality, the Young's inequality, the properties of the bubble functions and energy arguments. Numerical results (Examples 6.1 and 6.2) are presented to illustrate the performance of the derived error indicators using the proposed adaptive Algorithm 6.4.1.

7.2 Future Works

The results of this thesis could be extended to the following interesting problems to be taken up in the future.

Nonlinear parabolic interface problems. Let Ω be a bounded polygonal domain in $\mathbb{R}^2$ with smooth boundary $\partial\Omega$. Let Ω_1 be a subset of Ω with smooth interface $\Gamma = \partial\Omega_1$ and let $\Omega_2 = \Omega\backslash\Omega_1$. Consider the following nonlinear PIP of the form

$$\frac{\partial u}{\partial t} + \mathbf{L}u = f(x,t) \quad \text{in } \Omega_T \tag{7.1}$$

with the initial and boundary conditions

$$u(x,0) = u_0(x) \quad \text{in} \quad \Omega; \qquad u = 0 \quad \text{on } \partial\Omega_T, \tag{7.2}$$

and jump conditions across the interface Γ

$$[u] = 0, \quad \left[\beta(x,u)\frac{\partial u}{\partial \mathbf{n}}\right] = g(x,t), \tag{7.3}$$

TH-2911_136123010

where the operator $\mathbf{L}$ is of the form

$$\mathbf{L}u = -\nabla \cdot (\beta(x,u)\nabla u) + b_0(x,u)u \tag{7.4}$$

and $\Omega_T = \Omega \times (0,T]$ and $\partial\Omega_T = \partial\Omega \times [0,T]$, $T < \infty$. The functions $\beta, b_0 : \Omega \times \mathbb{R} \to \mathbb{R}$ are such that the operator $\mathbf{L}$ is monotone and Lipschitz continuous. Further, we assume that β is of the form

$$\beta(x,u(x)) \;=\; \beta_i(x,u(x)) \quad \text{for} \quad x \in \Omega_i, \;\; u(x) \in \mathbb{R}\ (i=1,2),$$

where $\beta_i : \Omega \times \mathbb{R} \to \mathbb{R}$ is continuous.

Some investigations concerning *a priori* error analysis have been made for the elliptic interface problems [50, 110]. To the best of authors' knowledge, the AFEM for nonlinear parabolic interface problems with the smooth interface is not available in the literature. The nonlinear case is far more complicated and requires few additional efforts. It would be an interesting investigation on AFEM for the problem (7.1)-(7.3) with smooth interface based on *a posteriori* error analysis.

Parabolic integro-differential equations with interfaces. Consider the parabolic integro-differential equation of the form

$$\frac{\partial u}{\partial t} - \nabla \cdot (\beta(x)\nabla u) = f + \int_0^t B(t,s)u(s)ds \quad \text{in} \;\; \Omega_T \tag{7.5}$$

with prescribed initial and boundary conditions

$$u(x,0) = u_0(x) \quad \text{in} \quad \Omega; \qquad u = 0 \quad \text{on} \;\; \partial\Omega_T, \tag{7.6}$$

and jump conditions across the interface Γ

$$[u] = 0, \quad \left[\beta \frac{\partial u}{\partial \mathbf{n}}\right] = g, \tag{7.7}$$

where $\Omega = \Omega_1 \cup \Gamma \cup \Omega_2$ is a convex polygonal domain in $\mathbb{R}^2$ with Lipschitz boundary $\partial\Omega$, $\Omega_1 \subset \Omega$ is an open domain with C^2 smooth interface $\Gamma = \partial\Omega_1$ and $\Omega_2 = \Omega \backslash \Omega_1$. Here $\Omega_T = \Omega \times (0,T]$ and $\partial\Omega_T = \partial\Omega \times [0,T]$, $T < \infty$. Further, we assume that the coefficient β is positive and piecewise constant, i.e.,

$$\beta(x) = \beta_1 \quad \text{for} \quad x \in \Omega_1; \quad \beta(x) = \beta_2 \quad \text{for} \quad x \in \Omega_2,$$

and $B(t,s)$ is a first order partial differential operator of the form

$$B(t,s)u(s) = \sum_{j=1}^{2} b_j(x;t,s)\frac{\partial u(x,s)}{\partial x_j} + u(x,s).$$

TH-2911_136123010

Here u, f and g are functions of x and t only.

The problem (7.5)-(7.7) arises in several applications, such as heat conduction in rigid materials with memory, the compression of viscoelasticity media, nuclear reactor dynamics and the epidemic phenomena in biology ([27, 36]). Such an extension is not straightforward because of the discontinuous coefficient and the Volterra integral term. Some investigation concerning *a priori* error analysis have been made for the problem (7.5)-(7.7) with $g = 0$ ([41]). It will be very interesting and challenging task to study *a posteriori* error analysis and adaptive algorithms using both conforming and non-conforming finite elements for the problem (7.5)-(7.7).

Hyperbolic interface problems. Let Ω be a convex polygonal domain in $\mathbb{R}^2$ with boundary $\partial\Omega$. Let $\Omega_1 \subset \Omega$ be an open domain with smooth interface $\Gamma = \partial\Omega_1$ and let $\Omega_2 = \Omega \backslash \Omega_1$. Consider the hyperbolic interface problems of the form

$$\frac{\partial^2 u}{\partial t^2} - \nabla \cdot (a(x)\nabla u) + b(x)u = f(x,t) \quad \text{in} \quad \Omega_T \tag{7.8}$$

with boundary condition

$$u = 0 \quad \text{on} \quad \partial\Omega_T, \tag{7.9}$$

initial conditions

$$\begin{aligned} u(x,0) &= u_0(x) \quad \text{in} \quad \Omega, \\ \frac{\partial u}{\partial t}(x,0) &= v_0(x) \quad \text{in} \quad \Omega, \end{aligned} \tag{7.10}$$

and jump conditions across the interface Γ

$$[u] = 0, \quad \left[a(x)\frac{\partial u}{\partial \mathbf{n}}\right] = g, \tag{7.11}$$

where $\Omega_T = \Omega \times (0,T]$ and $\partial\Omega_T = \partial\Omega \times [0,T]$, $T < \infty$. The coefficient matrix β is assumed to be discontinuous across the inietface Γ but piecewise smooth in each sundomain, i.e.,

$$a(x) = a_i(x) \quad \text{for} \quad x \in \Omega_i, i = 1, 2.$$

Further, we assume that the matrix $a(x)$ is symmetric, uniformly positive definite in Ω and $b(x) > 0$. The source function f and the initial functions u_0, v_0 are assumed to be sufficiently smooth. The equation (7.8) is often used as a simple model in seismology or ocean acoustics, in which the ocean bottom is described as a multi-layered fluid medium. In this case, the coefficient represents the velocity of sound which is discontinuous between sediment layers and u is the acoustic velocity [17]. In electromagnetism,

TH-2911_136123010

the equation (7.8) corresponds to a problem in which the material occupying the interior is a dielectric rather than metal ([7]). Due to the presence of a smooth interface, the true solution to this problem has a low global regularity. It is very challenging to obtain higher-order convergence. Although a good number of articles is available concerning *a priori* and *a posteriori* error analysis for the problem (7.8)-(7.11) ([3, 40, 42]), it would be further interesting work to study an AFEM for the proposed problem (7.8)-(7.11).

Parabolic moving interface problems. Consider the model one-dimensional moving interface problem of the form

$$\frac{\partial u}{\partial t} - \frac{\partial}{\partial x}\left(\beta(x,t)\frac{\partial u}{\partial x}\right) = f(x,t), \quad x \in \Omega \times (0,\infty), \tag{7.12}$$

$$u(0,t) = 0 = u(1,t) \quad t > 0, \quad \text{and} \quad u(x,0) = u_0(x), \quad x \in \Omega, \tag{7.13}$$

$$\frac{d\alpha}{dt} = h(t,\alpha; u^-, u^+, \frac{\partial u}{\partial x}^-, \frac{\partial u}{\partial x}^+), \quad t > 0, \tag{7.14}$$

where $\Omega = [0,\alpha) \cup (\alpha, 1]$, h is a known function, $u^-, u^+, \frac{\partial u}{\partial x}^-$ and $\frac{\partial u}{\partial x}^+$ are the limiting values of $u(x,t)$ and $\frac{\partial u}{\partial x}$ from the left and right hand side of a moving interface $\alpha(t)$. The jump conditions across the interface $\alpha(t)$ are given by

$$[u] = u(\alpha^-, t) - u(\alpha^+, t) = 0, \tag{7.15}$$

$$\left[\beta\frac{\partial u}{\partial x}\right] = \beta(\alpha^+,t)\frac{\partial u}{\partial x}(\alpha^+,t) - \beta(\alpha^-,t)\frac{\partial u}{\partial x}(\alpha^-,t) = q(t). \tag{7.16}$$

The coefficient $\beta(x,t) > 0$ and the source function $f(x,t)$ are assumed to be discontinuous across the interface $\alpha(t)$. Such problems (7.12)-(7.16) occur in studying blood flow in a beating heart [86, 87]. It would be interesting and challenging to see how the analysis of Chapter 3 and Chapter 5 can be extended to derive the *a posteriori* error estimates and develop an adaptive meshing procedure for the finite element method.

TH-2911_136123010

Bibliography

[1] R. A. Adams, *Sobolev Spaces*, Academic Press, New York, 1975.

[2] R. A. Adams and J. F. Fournier, *Sobolev Spaces*, vol. 140, Academic Press, Amsterdam, 2003.

[3] M. O. Adewole, *On finite element method for linear hyperbolic interface problems*, J. Nigerian. Math. Society, 37 (2018), pp. 41–55.

[4] M. Ainsworth, *Robust a posteriori error estimation for nonconforming finite element approximation*, SIAM J. Numer. Anal., 42 (2005), pp. 2320–2341.

[5] M. Ainsworth and J. T. Oden, *A Posteriori Error Estimation in Finite Element Analysis*, Wiley-Interscience, New York, 2000.

[6] G. D. Akrivis and V. A. Dougalis, *Finite difference discretizations of some initial and boundary value problems with interface*, Math. Comp., 56 (1991), pp. 505–522.

[7] A. Aldroubi and M. Renardy, *Energy methods for a parabolic-hyperbolic interface problem arising in electromagnetism*, Z. Angew. Math. Phys., 39 (1988), pp. 931–936.

[8] I. Babuška, *The finite element method for elliptic equations with discontinuous coefficients*, Computing, 5 (1970), pp. 207–213.

[9] I. Babuška and W. C. Rheinboldt, *A-posteriori error estimates for the finite element method*, Int. J. Numer. Meth. Engrg., 12 (1978), pp. 1597–1615.

[10] ——, *A-posteriori error estimates for the finite element solutions for one dimensional problems*, SIAM J. Numer. Anal., 18 (1981), pp. 565–589.

[11] I. Babuvška and W. C. Rheinboldt, *Error estimates for adaptive finite element computations*, SIAM J. Numer. Anal., 15 (1978), pp. 736–754.

TH-2911_136123010

[12] J. W. Barrett and C. M. Elliott, *Fitted and unfitted finite-element methods for elliptic equations with smooth interfaces*, IMA J. Numer. Anal., 7 (1987), pp. 283–300.

[13] C. Bernardi and R. Verfürth, *Adaptive finite element methods for elliptic equations with non-smooth coefficients*, Numer. Math., 85 (2000), pp. 579–608.

[14] S. Berrone, *Robust a posteriori error estimates for finite element discretizations of the heat equation with discontinuous coefficients*, ESAIM: Math. Model. Numer. Anal., 40 (2006), pp. 991–1021.

[15] D. R. Bojović and B. S. Jovanović, *Convergence of a finite difference method for solving 2d parabolic interface problems*, J. Comput. Appl. Math., 236 (2012), pp. 3605–3612.

[16] J. H. Bramble and J. T. King, *A finite element method for interface problems in domains with smooth boundaries and interfaces*, Adv. Comput. Math., 6 (1996), pp. 109–138.

[17] L. M. Brekhovskikh, *Waves in layered media*, Applied Mathematics and Mechanics, 16 (1980).

[18] S. Brenner and R. Scott, *The Mathematical Theory of Finite Element Methods*, vol. 15, Texts in Applied Mathematics, Springer, New York, 2008.

[19] M. Brera, J. W. Jerome, Y. Mori, and R. Sacco, *A conservative and monotone mixed-hybridized finite element approximation of transport problems in heterogeneous domains*, Comput. Methods Appl. Mech. Engrg, 199 (2010), pp. 2709–2720.

[20] Z. Cai, C. He, and S. Zhang, *Residual-based a posteriori error estimate for interface problems: Nonconforming linear elements*, Math. Comp., 86 (2017), pp. 617–636.

[21] Z. Cai, X. Ye, and S. Zhang, *Discontinuous galerkin finite element methods for interface problems: a priori and a posteriori error estimations*, SIAM J. Numer. Anal., 49 (2011), pp. 1761–1787.

[22] Z. Cai and S. Zhang, *Recovery-based error estimators for interface problems: mixed and nonconforming finite elements*, SIAM J. Numer. Anal., 48 (2010), pp. 30–52.

[23] ——, *Robust residual- and recovery-based a posteriori error estimators for interface problems with flux jumps*, Numer. Methods Partial Differential Equations, 28 (2012), pp. 476 – 491.

TH-2911_136123010

[24] A. Cangiani, E. H. Georgoulis, and M. Jensen, *Discontinuous galerkin methods for mass transfer through semipermeable membranes*, SIAM J. Numer. Anal., 51 (2013), pp. 2911–2934.

[25] C. Carstensen, *Interface problems in viscoplasticity and plasticity*, SIAM J. Math. Anal., 25 (1994), pp. 1468–1487.

[26] C. Carstensen, S. Bartels, and S. Jansche, *A posteriori error estimates for nonconforming finite element methods*, Numer. Math., 92 (2002), pp. 233–256.

[27] C. Chen and P. G. Shih Tsimin, *Finite element methods for integro-differential equations*, London, World Scintific, 1997.

[28] Z. Chen and S. Dai, *On the efficiency of adaptive finite element methods for elliptic problems with discontinuous coefficients*, SIAM J. Sci. Comput., 24 (2002), pp. 443–462.

[29] Z. Chen and J. Feng, *An adaptive finite element algorithm with reliable and efficient error control for linear parabolic problems*, Math. Comp., 73 (2004), pp. 1167–1193.

[30] Z. Chen, Z. Wu, and Y. Xiao, *An adaptive immersed finite element method with arbitrary lagrangian-eulerian scheme for parabolic equtaions in time variable domains.*, Int. J. Numer. Anal. Model., 12 (2015), pp. 567–591.

[31] Z. Chen, Y. Xiao, and L. Zhang, *The adaptive immersed interface finite element method for elliptic and maxwell interface problems*, J. Comput. Phys., 228 (2009), pp. 5000–5019.

[32] Z. Chen and J. Zou, *Finite element methods and their convergence for elliptic and parabolic interface problems*, Numer. Math., 79 (1998), pp. 175–202.

[33] K. Chrysafinos and L. S. Hou, *Error estimates for semidiscrete finite element approximations of linear and semilinear parabolic equations under minimal regularity assumptions*, SIAM J. Numer. Anal., 40 (2002), pp. 282–306.

[34] P. G. Ciarlet, *The Finite Element Method for Elliptic Problems*, vol. 40, Society for Industrial and Applied Mathematics, 2002.

[35] P. Clément, *Approximation by finite element functions using local regularization*, RAIRO. Anal. Numer., 9 (1975), pp. 77–84.

[36] B. R. Coleman and M. E. Gurtin, *Equipresence and constitutive equations for rigid heat conductors*, Z. Angew. Math., (1967), pp. 199–208.

TH-2911_136123010

[37] E. Dari, R. Durán, and C. Padra, *Error estimators for nonconforming finite element approximations of the stokes problem*, Math. Comp., 64 (1995), pp. 1017–1033.

[38] E. Dari, R. Duran, C. Padra, and V. Vampa, *A posteriori error estimators for nonconforming finite element methods*, ESAIM: Math. Model. Numer. Anal., 30 (1996), pp. 385–400.

[39] R. Dautray and J. L. Lions, *Mathematical Analysis and Numerical Methods for Science and Technology, Evolution Problems*, vol. 5, Springer-Verlag, Berlin, 1992.

[40] B. Deka, *A posteriori error estimates for finite element approximations to the wave equation with discontinuous coefficients*, Numer. Methods PDEs., 35 (2019), pp. 1630–1653.

[41] B. Deka and R. C. Deka, *Finite element method for a class of parabolic integro-differential equations with interfaces*, Indian J. Pure Appl. Math., 44 (2013), pp. 823–847.

[42] B. Deka and R. K. Sinha, *Finite element methods for second order linear hyperbolic interface problems*, J. Appl. Math. Comp., 218 (2012), pp. 10922–10933.

[43] W. Dörfler, *A convergent adaptive algorithm for poisson's equation*, SIAM J. Numer. Anal., 33 (1996), pp. 1106–1124.

[44] ——, *A time-space adaptive algorithm for the linear time-dependent Schrödinger equation*, Numer. Math., 73 (1996), pp. 419–448.

[45] W. Dörfler and M. Rumpf, *An adaptive strategy for elliptic problems including a posteriori controlled boundary approximation*, Math. Comput., 67 (1998), pp. 1361–1382.

[46] K. Eriksson and C. Johnson, *An adaptive finite element method for linear elliptic problems*, Math. Comp., 50 (1988), pp. 361–383.

[47] ——, *Adaptive finite element methods for parabolic problems. I. A linear model problem*, SIAM J. Numer. Anal., 28 (1991), pp. 43–77.

[48] ——, *Adaptive finite element methods for parabolic problems. II. Optimal error estimates in $L_\infty(L_2)$ and $L_\infty(L_\infty)$*, SIAM J. Numer. Anal., 32 (1995), pp. 706–740.

[49] ——, *Adaptive finite element methods for parabolic problems. IV. Nonlinear problems*, SIAM J. Numer. Anal., 32 (1995), pp. 1729–1749.

TH-2911_136123010

[50] M. Feistauer and A. Ženíšek, *Finite element solution of nonlinear elliptic problems*, Numer. Math., 50 (1987), pp. 451–475.

[51] H. Feng and L. J. Shen, *The finite element method for semilinear parabolic equations with discontinuous coefficients*, J. Comput. Math., (1999), pp. 191–198.

[52] W. Feng, X. He, Y. Lin, and X. Zhang, *Immersed finite element method for interface problems with algebraic multigrid solver*, Communications Comput. Phys., 15 (2014), pp. 1045–1067.

[53] D. Gilbarg and N. S. Trudinger, *Elliptic Partial Differential Equations of Second Order*, Springer-Verlag, Berlin-New York, 1977.

[54] V. Girault and P.-A. Raviart, *Finite Element Methods for Navier-Stokes Equations*, vol. 5, Springer Series in Computational Mathematics, Springer-Verlag, Berlin, 1986.

[55] Y. Gong, B. Li, and Z. Li, *Immersed-interface finite-element methods for elliptic interface problems with nonhomogeneous jump conditions*, SIAM J. Numer. Anal., 46 (2008), pp. 472–495.

[56] P. Grisvard, *Elliptic Problems in Nonsmooth Domains*, vol. 24, Monographs and Studies in Mathematics, Pitman, Boston, MA, 1985.

[57] R. Guo, *A linear immersed finite element space defined by actual interface curve on triangular meshes*, thesis Virginia Tech, (2017).

[58] ——, *Solving parabolic moving interface problems with dynamical immersed spaces on unfitted meshes: Fully discrete analysis*, SIAM J. Numer. Anal., 59 (2021), pp. 797–828.

[59] R. Guo, T. Lin, and X. Zhang, *Nonconforming immersed finite element spaces for elliptic interface problems*, Comput. Math. Appl., 75 (2018), pp. 2002–2016.

[60] J. Guzmán, M. Sánchez, and M. Sakis, *On the accuracy of finite element approximation to a class of interface problems*, Math. Comput., 85 (2016), pp. 2071–2098.

[61] W. Hackbusch, *Elliptic Differential Equations*, vol. 18, Springer Series in Computational Mathematics, Springer-Verlag, Berlin, 1992.

[62] A. Hansbo and P. Hansbo, *An unfitted finite element method, based on nitsche's method, for elliptic interface problems*, Comput. Methods Appl. Mech. Egnrg., 191 (2002), pp. 5537–5552.

[63] G. H. Hardy, J. E. Littlewood, and G. Pólya, *Inequalities*, Cambridge University Press, Cambridge, 1952.

TH-2911_136123010

[64] X. He, T. Lin, Y. Lin, and X. Zhang, *Immersed finite element methods for parabolic equations with moving interface*, Numer. Methods Partial Differential Equations, 29 (2013), pp. 619–646.

[65] F. Hecht, *New development in freefem++*, J. Numer. Math., 20 (2012), pp. 251–266.

[66] R. H. W. Hoppe and B. Wohlmuth, *Element-oriented and edge-oriented local error estimators for nonconforming finite element methods*, ESAIM: Math. Model. Numer. Anal., 30 (1996), pp. 237–263.

[67] S. Hou and X.-D. Liu, *A numerical method for solving variable coefficient elliptic equation with interfaces*, J. Comput. Phys., 202 (2005), pp. 411–445.

[68] J. Huang and J. Zou, *Some new a priori estimates for second-order elliptic and parabolic interface problems*, J. Differential Equ., 184 (2002), pp. 570–586.

[69] B. S. Jovanović and L. G. Vulkov, *Finite difference approximation of strong solutions of a parabolic interface problem on disconnected domains.*, Publ. Inst. Math. (Beograd) (N.S.), (2008), pp. 37–48.

[70] R. B. Kellogg, *On the poisson equation with intersecting interfaces*, Applicable Anal., 4 (1974), pp. 101–129.

[71] O. A. Ladyzenskaja, V. A. Solonnikov, and N. N. Ural'ceva, *Linear and quasilinear equations of parabolic type, Translated from the Russian by S. Smith. Translations of Mathematical Monographs*, vol. 23, American Mathematical Society, USA, 1967.

[72] R. J. Leveque and Z. Li, *The immersed interface method for elliptic equations with discontinuous coefficients and singular sources*, SIAM J. Numer. Anal., 31 (1994), pp. 1019–1044.

[73] Z. Li and K. Ito, *Maximum principle preserving schemes for interface problems with discontinuous coefficients*, SIAM J. Sci. Comput., 23 (2001), pp. 339–361.

[74] ——, *The Immersed Interface Method: Numerical Solutions of PDEs Involving Interfaces and Irregular Domains*, vol. 33, Frontiers in Applied Mathematics, SIAM, Philadaelphia, PA, 2006.

[75] Z. Li, T. Lin, and X. Wu, *New cartesian grid methods for interface problems using the finite element formulation*, Numer. Math., 96 (2003), pp. 61–98.

[76] Z. Li, W. C. Wang, I. L. Chern, and M. C. Lai, *New formulations for interface problems in polar coordinates*, SIAM J. Sci. Comput., 25 (2003), pp. 224–245.

TH-2911_136123010

[77] T. Lin, D. Sheen, and X. Zhang, *A nonconforming immersed finite element methods for elliptic interface problems*, J. Sci. Comput., 79 (2019), pp. 442–463.

[78] T. Lin, Q. Yang, and X. Zhang, *Partially penalized immersed finite element methods for parabolic interface problems*, Numer. Methods Partial Differential Equations, 31 (2015), pp. 1925–1947.

[79] X.-D. Liu, R. P. Fedkiw, and M. Kang, *A boundary condition capturing method for poisson's equation on irregular domains*, J. Comput. Phys., 160 (2000), pp. 151–178.

[80] G. Lumer and L. Weis, *Evolution equations and their applications in physical and life sciences*, vol. 215, of Lecture Notes in Pure and Applied Mathematics, New York, 2001.

[81] R. C. MacCamy and M. Suri, *A time-dependent interface problem for two-dimensional eddy currents*, Quart. Appl. Math., 44 (1987), pp. 675–690.

[82] T. Miyazaki, *Water Flow in Soils*, CRC Press, 2006.

[83] P. Morin, R. H. Nochetto, and K. G. Siebert, *Data oscillation and convergence of adaptive fem*, SIAM J. Numer. Anal., 38 (2000), pp. 466–488.

[84] S. Nicaise and N. Soualem, *A posteriori error estimates for a nonconforming finite element discretization of the heat equation*, ESAIM: Math. Model. Numer. Anal., 39 (2005), pp. 319–348.

[85] B. F. Nielsen, *Finite element discretizations of elliptic problems in the presence of arbitrarily small ellipticity: An error analysis*, SIAM J. Numer. Anal., 36 (1999), pp. 368–392.

[86] C. S. Peskin, *Numerical analysis of blood flow in the heart*, J. Comput. Phys., 25 (1977), pp. 220–252.

[87] C. S. Peskin, *Lectures on mathematical aspects of physiology*, in Lectures Appl. Math., no. 19, AMS, 1981, pp. 69–107.

[88] D. Peterseim, *Composite finite elements for elliptic interface problems*, Math. Comp., 83 (2014), pp. 2657–2674.

[89] M. Petzoldt, *A posteriori error estimators for elliptic equations with discontinuous coefficients*, Adv. Comput. Math., 16 (2002), pp. 47–75.

[90] M. Picasso, *Adaptive finite elements for a linear parabolic problem*, Comput. Methods Appl. Mech. Engrg., 167 (1998), pp. 223–237.

[91] R. Rannacher, *Adaptive Galerkin finite element methods for partial differential equations*, J. Comp. Appl. Math., 128 (2001), pp. 205–233.

TH-2911_136123010

[92] A. Reusken and T. H. Nguyen, *Nitsche's method for a transport problem in two-phase incompressible flows*, J. Fourier Anal. Appl., 15 (2009), pp. 663–683.

[93] F. Schieweck, *A posteriori error estimates with post-processing for nonconforming finite elements*, ESAIM: Math. Model. Numer. Anal., 36 (2002), pp. 489–503.

[94] A. Schmidt and K. G. Siebert, *ALBERT: An adaptive hierarchical finite element toolbox*, IAM, University of Freiburg, 2000.

[95] J. Sen Gupta and R. K. Sinha, *A posteriori error analysis of semilinear parabolic interface problems using elliptic reconstruction*, Appl. Anal., 97 (2018), pp. 552–570.

[96] J. Sen Gupta, R. K. Sinha, G. M. M. Reddy, and J. Jain, *A posteriori error analysis of two-step backward differentiation formula finite element approximation for parabolic interface problems*, J. Sci. Comput., 69 (2016), pp. 406–429.

[97] ——, *New interpolation error estimates and a posteriori error analysis for linear parabolic interface problems*, Numer. Methods Partial Differential Equations, 33 (2017), pp. 570–598.

[98] R. K. Sinha and B. Deka, *Optimal error estimates for linear parabolic problems with discontinuous coefficients*, SIAM J. Numer. Anal., 43 (2005), pp. 733–749.

[99] ——, *An unfitted finite-element method for elliptic and parabolic interface problems*, IMA J. Numer. Anal., 27 (2007), pp. 529–549.

[100] ——, *Finite element methods for semilinear elliptic and parabolic interface problems*, Appl. Numer. Math., 59 (2009), pp. 1870–1883.

[101] ——, *$L^\infty(L^2)$ and $L^\infty(H^1)$ norms error estimates in finite element method for linear parabolic interface problems*, Numer. Funct. Anal. Optim., 32 (2011), pp. 267–285.

[102] V. Thomée, *Galerkin finite element methods for parabolic problems*, vol. 25, Springer Series in Computational Mathematics, Springer-Verlag, Berlin, second ed., 2006.

[103] V. Thomée and L. Wahlbin, *On Galerkin methods in semilinear parabolic problems*, vol. 12, SIAM J. Numer. Anal., 1975.

[104] R. Verfürth, *A Review of A Posteriori Error Estimates and Adaptive Mesh Refinement Technique*, Wiley-Teubner, New York, 1996.

[105] ——, *A review of a posteriori error estimation techniques for elasticity problems*, Comput. Methods Appl. Mech. Engrg., 176 (1999), pp. 419–440.

TH-2911_136123010

[106] ——, *A posteriori error estimations for finite element discretizations of the heat equation*, Calcolo, 40 (2003), pp. 195–212.

[107] H. Wei, L. Chen, Y. Huang, and B. Zheng, *Adaptive mesh refinement and superconvergence for two-dimensional interface problems*, SIAM J. Sci. Comput., 36 (2014), pp. A1478–A1499.

[108] C. T. Wu, Z. Li, and M. C. Lai, *Adaptive mesh refinement for elliptic interface problems using the non-conforming immersed finite element method*, Int. J. Numer. Anal. Model., 8 (2011), pp. 466–483.

[109] Q. Yang and X. Zhang, *Discontinuous galerkin immersed finite element methods for parabolic interface problems*, J. Comput. Appl. Math., 299 (2016), pp. 127–139.

[110] A. Ženíšek, *The finite element method for nonlinerar elliptic equations with discontinuous coefficients*, Numer. Math., 58 (1990), pp. 51–77.

[111] X. Zhang, Y. Lin, and Y. Lin, *A method of lines based on immersed finite elements for parabolic moving interface problems*, Adv. Appl. Math. Mech., 5 (2013), pp. 548–568.

TH-2911_136123010

List of published and communicated papers

Based on the work carried out in this thesis, the following are the published and communicated papers.

1. T. Ray and R. K. Sinha, *An adaptive finite element method for semilinear parabolic interface problems with nonzero flux jump*, Appl. Numer. Math., 153 (2020), pp. 381–398.

2. T. Ray and R. K. Sinha, *An adaptive finite element method for parabolic interface problems with nonzero flux jump*, Comput. Math. Appl., 82 (2021), pp. 97-112.

3. T. Ray and R. K. Sinha, *An adaptive immersed finite element method for linear parabolic interface problems with nonzero flux jump.* (Communicated)

4. T. Ray and R. K. Sinha, *An adaptive finite element method for linear parabolic interface problems using nonconforming elements.* (Communicated)

5. T. Ray and R. K. Sinha, *A posteriori error estimation and adaptive mesh refinement for parabolic interface problems using non-conforming immersed finite element method.* (Communicated)

TH-2911_136123010